prepared for:

Rijkswaterstaat-RIKZ

National Institute for Coastal and Marine Management

SILTMAN
Analysis of field measurements

semi-permanent measuring stations Maasmond area

desk study

February 1998

Z2263

WL | delft hydraulics

SILTMAN

Analysis of field measurements

semi-permanent measuring stations Maasmond area

J.C. Winterwerp

delft hydraulics

delft hydraulics

CLIENT : Rijkswaterstaat - RIKZ

TITLE : SILTMAN: Analysis of field measurements in Maasmond area

ABSTRACT :

This report describes the analysis of a series of field measurements at semi-permanent measuring stations in the Maasmond area with the use of the 1DV POINT MODEL of Delft Hydraulics. The analysis consists of two steps:

- sensitivity analyses with the model, and
- prognostic simulations for locations in between the measuring stations

From this study the following conclusions have been drawn:

1. Both for steady and tidal flow conditions a saturation concentration can be defined beyond which the flow is no longer able to carry sediment.
2. The value of this saturation concentration for tidal flow conditions is a function of the various time scales of the physical processes, and amounts to about 0.5 g/l for Maasmond conditions.
3. The effect of surface waves and salinity induced stratification on this saturation concentration is considerable, the latter effect however is not yet fully understood.
4. It is not possible to accurately simulate the data measured at the permanent measuring stations with the 1DV POINT MODEL; the main reason must probably be sought in advective processes not accounted for in a 1D model.
5. However, the suspended sediment concentrations computed with the 1DV model are in reasonable agreement with the observations for a calibrated set of physical parameters. This includes the influence of hindered settling induced by flocculation effects, which appeared to be an important parameter.
6. The 1DV simulations reveal that the measured time variations in suspended sediment concentration are caused to a large extend by a continuous cycle of deposition and resuspension.
7. Within the Maasgeul, the flow velocity decreases so much that the flow no longer can support the sediment. However, this does not result in a rapid formation of fluid mud, as the time scale for this formation is a function of the settling velocity. It is hypothesized that fluid mud layers can be formed rapidly only through the effects of sediment-induced density currents. (turbidity currents)

REFERENCES:

Rijkswaterstaat-RIKZ, contract RKZ-451, dated July 21, 1997

Contact person: dr. J.M. de Kok

REV	ORIGINATOR		DATE	REMARKS	REVIEWED BY		APPROVED BY	
0.0	J.C. Winterwerp		Oct.1, 1997	draft phase 1	R.E. Uittenbogaard			
0.1	J.C. Winterwerp		Nov. 28, 1997	final phase 1				
0.2	J.C. Winterwerp		Jan. 21, 1998	draft	R.E. Uittenbogaard			
1.0	J.C. Winterwerp		Feb. 3, 1998	final			T. Schilperoort	

KEYWORD(S)	CONTENTS	STATUS
field measurements, mud, hindered settling, saturation concentration, fluid mud formation, Maasmond	TEXT PAGES : 45 TABLES : - FIGURES : ca 70 APPENDICES : 2	☐ PRELIMINARY ☐ DRAFT ♣ FINAL
	PROJECT IDENTIFICATION: Z2263	

Summary, conclusions and recommendations

The National Institute for Coastal and Marine Management (Rijkswaterstaat, RIKZ) is commissioned by the Rijkswaterstaat departments, Directorate Zuid-Holland and Directorate Noordzee and by the "Gemeentelijk Havenbedrijf Rotterdam" (Rotterdam Harbour Authorities) to develop a modelling system for studying the sediment transport processes in the vicinity of the "Maasmond". In particular the following questions have to be addressed:

1. what is the origin of the mud encountered in the vicinity of the Maasmond,
2. what are the transport processes and what is the transport path of the mud, and
3. where and under which conditions can the mud settle in the navigational channels and harbour basins?

To answer these questions, Rijkswaterstaat initiated the SILTMAN-project. Within this framework, four semi-permanent measuring stations were installed by Rijkswaterstaat near the mouth of the Maasmond to monitor the flow velocity at 0.35 m above the sea bed, and the suspended sediment concentration at 0.15, 0.55, 2 and 7 m above the bed. During the second and third week of November 1996 suspended sediment concentrations beyond 10 g/l were measured. This report describes a detailed analysis of these measurements with the use of the 1DV POINT MODEL developed in an earlier phase of the SILTMAN-project. Two series of simulations are carried out with this model:

I A series of sensitivity analyses for Maasmond conditions to enhance our understanding of the model and the relevant physical processes and their interrelation, and

II A series of runs to simulate the actually observed suspended sediment concentration distributions to aid the analysis of the measurements (so-called prognostic simulations).

The objective of the present project is to analyze a series of field measurements in the Maasmond area with the aim to 1) further substantiate some hypotheses on the sediment transport processes and 2) establish to what extend these processes can be simulated with the three-dimensional model TRIWAQ-SLIB3D, developed for this area.

From this study the following conclusions are drawn:

I sensitivity analyses

1. A saturation concentration C_s can be defined, which represents the maximal sediment load that can be carried in suspension by the turbulent flow. At concentrations beyond this threshold value, the vertical concentration profile collapses to form a high concentrated near-bed layer.

2. Seven scaling parameters have been identified that govern the magnitude of this saturation concentration under tidal flow conditions. Three have been elaborated in this report, i.e. a bulk Richardson number, a time scale for settling and a time scale for mixing, the latter two relative to the tidal period. The other four parameters are the relative time scales for flocculation, thixotropy, consolidation and erosion (swell).

3. The saturation concentration C_s scales with $\rho u_*^3/ghW_s$ for steady flow conditions, and with $\rho U^{8/3}/ghW_s^{2/3}$ for the tidal flow conditions encountered in the Maasmond area. A typical value for C_s for Maasmond conditions amounts to about 0.5 g/l.

4. Surface waves have a significant effect on C_s, because of its enhancement of the vertical mixing. On the other hand, hindered settling, higher harmonic tidal constituents, and wind-induced surface shear stresses only have a small effect. The influence of the latter however is not properly understood.

5. Salinity-induced stratification does limit the effective mixing (water) depth. The local saturation concentration increases inversely proportional to this smaller water depth. As a result, it seems that salinity-induced stratification does not affect the total load that can be carried by the flow. Note however, that salinity induced stratification does affect the suspended sediment vertical, hence the horizontal advection of the sediment.

6. The 1DV-simulations showed that even under severe wave conditions ($H_{1/3}$ = 3 m, T = 6 s), concentrations of 200 μm sand particles do not exceed a few 100 mg/l at a few dm above the sea bed. Hence, the observed turbidities are mainly attributed to fine grained sediments.

II prognostic simulations

7. For a specific setting of the physical parameters, i.e. W_s = 0.6 mm/s and C_0 = 0.5 g/l, it is possible to obtain a reasonable resemblance between computed and observed concentration distributions. However, several peaks in the measured sediment concentration cannot be reproduced with the 1DV POINT MODEL. This is probably caused by horizontal advection effects.

8. In- or excluding waves does not significantly improve the resemblance between calculations and observations. This is probably attributed to the relative short duration of the simulations. It is highly unlikely that the observed concentration profiles are affected by water-bed exchange processes of mud (erosion of the sea bed), or by a dynamic, thin (1 dm) layer of fluid mud on the sea bed.

9. It appeared however crucial to account for the effects of hindered settling, which is accounted for through a very simple flocculation formula. Omission of this effect will result in a total collapse of the concentration profile for the conditions under consideration.

10. Though no definite proof has been obtained, the most likely picture of the sediment dynamics in the Maasmond area beyond the Maasgeul reads as follows: the concentration profile, hence the horizontal sediment transport, is the result of a continuous cycle of deposition and re-entrainment at a concentration level close to the saturation concentration, as a result of which the turbulence properties of the flow are seriously affected.

11. While passing the Maasgeul, the sediment carrying capacity of the flow reduces by almost an order of magnitude because of the increase in water depth and decrease in flow velocity.

12. Hence, in the Maasgeul the suspension becomes supersaturated, and the flow is no longer able to carry the sediment. The formation of a high-concentrated near-bed suspension or fluid mud layer in the 1DV POINT MODEL is governed by the time scale for settling, which is too large to explain the clear water conditions frequently observed in the Caland- and Beerkanaal.
    It is hypothesized that an interaction between the collapse of the concentration profile and the accompanying generation of a sediment-induced density current (turbidity current) is the

propelling agent behind the formation of fluid mud in the Maasmond area.

13. Sediment-induced stratification effects appear to be important in the Maasmond-area. As these stratification effects and turbulence mixing are not coupled in the TRIWAQ-SLIB3D code of Rijkswaterstaat, the processes described above cannot be simulated in detail with this model. However, outside the Maasgeul, i.e. beyond the area where saturation effects become important, the horizontal transport of suspended sediment may still be approximated within acceptable accuracy through a parameterization of the influence of the suspended sediment on the vertical mixing.
    Within the Maasgeul, and further upstream, other modelling tools will have to be used.

From this report a few suggestions for further research were identified:

1. The effect of salinity-induced stratification on the saturation concentration and on the actual concentration profiles seems large. It is however not fully understood, and more research is required. To quantify this effect properly, it is recommended to measure the salinity distribution at the semi-permanent measuring stations simultaneously with the other measurements.

2. The contribution of wind-induced shear stresses on the vertical mixing is not understood and should be further studied.

3. As hindered settling appeared to be a major parameter for a successful simulation of the observations, the existing flocculation model should be further developed and tested to account for a proper description of settling velocity and floc size.

4. The possibilities of a parameterization of the influence of near-saturated sediment concentrations on the vertical mixing should be studied to enable accurate sediment transport simulations for rough weather conditions with the TRIWAQ-SLIB3D code.

5. The set-up of a simple, schematized full three-dimensional model of the Maasmond area is recommended, including the sediment-induced buoyancy effects on turbulent mixing, to study the formation of fluid mud layers as a result of the interaction of a collapsing concentration profile and sediment-induced density currents.

6. The present 1DV POINT MODEL does contain a module to simulate the formation from deposition and the subsequent behaviour of fluid mud layers, which can be used to study the mobility of such fluid mud layers in the Maasmond area. However, as no practical experience with this model, nor with similar models elsewhere in the world, exists, it is recommended to calibrate this model first against laboratory experiments (fluid mud tests in the annular flume) prior to application for Maasmond conditions.

Table of contents

List of notations

C_D	drag coefficient for wind-induced stresses
C_s	depth-mean saturation concentration by mass
$C_{s,0}$	C_s for non-hindered settling conditions
c	sediment concentration by mass
c_s	local saturation concentration by mass
$c_{.\epsilon}$	coefficient in dissipation equation of k-ϵ turbulence model
c_μ	coefficient in dissipation equation of k-ϵ turbulence model
D	grain size of sediment particles
D_p	grain size of primary particles
d	depth with respect to reference plane
f_w	friction coefficient for wave-induced bed friction
g	gravity acceleration
H	wave height
H_{rms}	root mean square wave height
$H_{1/3}$	significant wave height
$\hat{H}$	characteristic wave height
h	water depth
k	turbulent kinetic energy
k	wave number
M	erosion parameter in erosion formula by Partheniades
m	coefficient in Munk-Andersen damping relation
n	coefficient in Munk-Andersen damping relation
P	turbulence production
p	pressure
Ri	gradient Richardson number
Ri_f	flux Richardson number
Ri_*	bulk Richardson number
S	salinity
T	tidal period, c.q. wave period
T_m	relative mixing time
T_p	peak wave period
T_{rel}	relaxation time in 1DV POINT MODEL
T_{rms}	wave period of root mean square wave height
T_s	relative settling time
$T_{1/3}$	wave period for significant wave height
t	time
U	depth-averaged velocity
U_m	amplitude of time-varying depth-averaged velocity
U_0	prescribed depth-averaged velocity in 1DV POINT MODEL
U_{10}	wind velocity at 10 m height
u	local horizontal flow velocity
u_*	shear velocity
u_{*b}	flow-induced shear velocity
u_{*s}	wind-induced shear velocity (at water surface)
u_{*w}	wave-induced shear velocity (at sea bed)
W_s	mean settling velocity
$W_{s,eff}$	effective mean settling velocity

w	local vertical velocity
w_s	local settling velocity
$\hat{X}_{orb}$	wave-induced orbital excursion at bed
z	vertical coordinate
z_{bc}	apparent roughness height
z_0	roughness height
α	relative sediment density
β	parameter defined in (3.13)
Γ_T	eddy diffusivity
Γ_0	eddy diffusivity for buoyant neutral conditions
Δt	time step in 1DV POINT MODEL
Δz_b	vertical grid size in 1DV POINT MODEL
δ	thickness of near-bed high concentrated layer
δ_w	thickness wave-induced boundary layer
ϵ	dissipation
ζ	water level with respect to reference plane
κ	von Kármàn constant
λ	wave length
ν	kinematic viscosity
ν_T	eddy viscosity
Π	dimensionless parameter
ρ	bulk density of fluid
ρ_s	specific density of sediment
ρ_w	specific density of water
σ_T	turbulent Prandtl-Schmidt number
τ	time scale
τ_b	effective bed shear stress (effect of flow and waves)
τ_f	flow-induced bed shear stress
τ_d	critical shear stress for deposition in deposition formula by Krone
τ_e	critical shear stress for erosion in erosion formula by Partheniades
τ_s	wind-induced shear stress at water surface
τ_w	wave-induced bed shear stress
ϕ	sediment concentration by volume
ω	wave frequency

miscellaneous

$\hat{.}$	dimensionless quantity
$.'$	turbulent fluctuating quantity

1. Introduction

The National Institute for Coastal and Marine Management (Rijkswaterstaat, RIKZ) is commissioned by the Rijkswaterstaat departments, Directorate Zuid-Holland and Directorate Noordzee and by the "Gemeentelijk Havenbedrijf Rotterdam" (Rotterdam Harbour Authorities)to develop a modelling system for studying the sediment transport processes in the vicinity of the "Maasmond". In particular the following questions have to be addressed:

1. what is the origin of the mud encountered in the vicinity of the Maasmond,
2. what are the transport processes and what is the transport path of the mud, and
3. where and under which conditions can the mud settle in the navigational channels and harbour basins?

An important reason for carrying out this study is given by the various plans for considerable alterations in the local infrastructure, among which an extension of the "Maasvlakte" and another management strategy of the "Haringvliet" sluices. All these measures will affect the hydraulic regime, hence the sediment transport in the Maasmond area. It was decided to carry out a thorough study on the mud dynamics in the form of field measurements, data regression, desk studies and mathematical model studies. These activities are carried out in the framework of the SILTMAN-project.

Verlaan and Spanhoff (1994) re-analyzed historical data and conjectured that "the most probable mechanism for the sediment transport in the coastal zone is *1)* in the form of suspended sediment transport with a more or less homogeneous concentration profile and *2)* in the form of a near bed dense layer, but *3)* not in the form of classical fluid mud layers". However, no detailed data were available to verify this hypothesis. Therefore, an extensive monitoring programme was set up by Rijkswaterstaat, consisting, amongst other things, of the deployment of four semi-permanent measuring stations and a series of so-called 13-hours measurements from measuring vessels.

Rijkswaterstaat/RIKZ commissioned Delft Hydraulics to analyze a series of data obtained at these semi-permanent stations by contract RKZ-451, dated July 21, 1997. This analysis is carried out with the help of sensitivity analyses and prognostic simulations with the 1DV POINT MODEL developed during an earlier phase of the SILTMAN-project (Winterwerp and Uittenbogaard, 1997).

> *The objective of the present project is to analyze a series of field measurements in the Maasmond area with the aim to 1) further substantiate the hypothesis on the sediment transport processes mentioned above, and 2) establish to what extent these processes can be simulated with the three-dimensional model TRIWAQ-SLIB3D, developed for this area.*

The study is carried out in two phases. In Phase I a sensitivity analysis is undertaken with the 1DV POINT MODEL to establish the relevant parameters and to assess whether the field observations can be simulated qualitatively with this model. In Phase II of the study so-called prognostic simulations are carried out with the aim to study the behaviour of the sediment suspension under various hydrodynamic conditions, as encountered in the Maasmond area. Chapter 2 contains a summary of the field measurements that are analyzed in this report. Chapter 3 gives a short description of the processes modelled and equations discretisized in the 1DV POINT MODEL. The Chapters 4 and 5 contain the results of the sensitivity analyses, and Chapter 6 finally presents the results of the prognostic simulations.

A major objective of the SILTMAN-project consists of the development of a model to simulate the transport of fine grained (cohesive) sediment for the Maasmond area with TRIWAQ-SLIB3D, as developed by Rijkswaterstaat-RIKZ. Wherever relevant, discussions of the results with respect to the modelling of the sediment transport processes in the Maasmond area with TRIWAQ-SLIB3D are therefore presented at various sections throughout the text. Note that at present the coupling of water movement and turbulence with stratification effects induced by fine-grained suspended sediment is not yet implemented in TRIWAQ-SLIB3D.

2. Description of field data

2.1 SILTMAN field measurements

In the framework of the SILTMAN-project, field measurements were carried out in the Maasmond-area, comprising of continuous measurements at the four semi-permanent stations B, G, H and I, a series of "13-hours" boat-measurements, and measurements in the Caland-canal with an instrumented fish suspended from ms Octans. The present study deals with the analysis of the data obtained from the semi-permanent stations, and uses the other data only qualitatively, where relevant.

The location of the semi-permanent stations B, G, H and I is shown in Fig. 2.1. At these stations the following measurements are carried out:

- suspended sediment concentration measurements at 0.15 and 0.55 m above the bed with a MEX turbidity sensor,
- suspended sediment concentration measurements at 2 and 7 (8) m above the bed with optical turbidity sensors mounted in the HYDROLAB measuring frames, and
- flow velocity and direction at 0.35 m above the sea bed with an UCM flow meter.

For more information, the reader is referred to OCN, 1997. Note that not all data are available at all locations (see Sections 2.3 and 2.4).

In the present study the data of November 1996 are analyzed in detail. These have been supplied by Rijkswaterstaat/RIKZ in digitized form, the turbidity data only in sensor units. The latter therefore have to be transformed into physical units [kg/m^3] using the calibration curves for the instruments. The calibration curve for the HYDROLAB sensors was supplied by RIKZ, the calibration curve for the MEX sensors is elaborated by Delft Hydraulics (Borsje, 1997). The calibration factors are summarized in Table 2.1; the sensor units have to be multiplied by this factor to obtain the suspended sediment concentration in kg/m^3.

station	file code	sensor	calibration factor	standard deviation
B	205	MEX 0.15 m	5.46	0.12
		MEX 0.55 m	5.79	0.13
G	405	MEX 0.15 m	7.23	0.16
		MEX 0.55 m	6.64	0.45
H	305	MEX 0.15 m	8.25	0.36
		MEX 0.55 m	9.59	0.72
I	105	MEX 0.15 m	3.39	0.02
		MEX 0.55 m	7.75	1.94
all		HYDROLAB 2 & 7 m	2	-

Table 2.1: Calibration factors turbidity measurements Winter 96/97.

The data for February 1996 are collected from OCN (1997) and are available in physical units.

Note that the calibration of the turbidity sensors were carried out with diatomacous ("diatomee-aarde"), and not against actual mud samples. The actual suspended sediment concentration may therefore be 50 to 100 % higher than the values obtained with the calibration factors of Table 2.1.

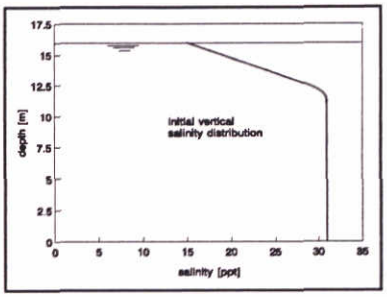

Finally, a characteristic salinity profile, used for the numerical simulations, is deduced from van 't Hart (1996), based on observations on 29 and 30 November 1995. These measurements show a persistent layer of brackish water on top of a saline water column with a thickness of the order of 3 to 5 m. Therefore, a simple linear/constant salinity profile is proposed to be used in the numerical simulations: a layer of brackish water with a linear salinity gradient from 15 ppt at the water surface till 31 ppt at 4 m below the water surface on top of a saline water column of 31 ppt salinity; the sharp kink at the intersect of the linear and constant part of the distribution is smoothed in the numerical simulations a little to suppress the largest peaks in the density gradients.

2.2 Hydro-meteorological data

The transport of cohesive sediment in the Maasmond area is governed by the availability of mud, the tidal movement, Rhine-water-induced density currents, surface waves and wind.

winddata

Data on the wind field at the station Hoek van Holland for the months February and November 1996 have been reported by Rijkswaterstaat, Directorate North Sea (1996). The actual wind speed data are plotted in the Figures 2.2 and 2.3 These values have been used in the Phase II simulations. For the Phase I simulations, the data of the period November 13 and 14 have been averaged, the result of which is presented in Table 2.2.
Note that eventually the numerical simulations are carried out for a wind speed of 15 m/s, as the effect of the actual wind speed of 7 m/s is too small to have a significant effect on the numerical results.

wave data

Data on the significant wave height $H_{1/3}$ at the station Maasgeul for the months February and November 1996 have been reported by Rijkswaterstaat, Directorate North Sea (1996). The actual $H_{1/3}$ data are also plotted in the Figures 2.2 and 2.3. The wave direction is assumed to be more or less North, as northern wind prevail during these periods.
For the present simulations of the influence of waves on the transport of suspended sediment, the averaged wave height H_{rms} is required, which follows from $H_{rms} = H_{1/3}/\sqrt{2}$ (van der Velden, 1989). The peak wave period T_p, at which the spectrum has its maximum energy, is obtained from an empirical relation by Roskam (1995), averaged for all wave directions. The period of the significant wave height $T_{1/3}$ is obtained from $T_{1/3} \approx 0.9\ T_p$. The results are summarized in Table 2.2.

mean values for Phase I simulations	
wind speed	7.0 & 15.0 m/s
wave height $H_{1/3}$	1.86 m
peak period T_p	5.9 s
wave period $T_{1/3}$	5.4 s
wave height H_{rms}	1.3 m
wave period T_{rms}	5.0 s

Table 2.2: Mean hydro-meteo data for November 13 & 14, 1996.

2.3 Results for February 1996

Winter 95/96 is characterized by exceptionally calm weather and in this period hardly any maintenance dredging had to be carried out in the Maasmond-area. During the entire period from November 1995 through April 15, when the sensors at the semi-permanent stations were in operation, suspended sediment concentrations beyond several 10 mg/l have only been recorded in the week of 13 through 20 February 1996. During this period the following data are available (OCN, 1997):

location	B	G	H	I
MEX conc. 0.15 m	*	*	*	-
MEX conc. 0.55 m	*	*	*	-
HYDROLAB conc. 2 m	*	-	-	-
HYDROLAB conc. 8 m	*	-	-	-
flow velocity 0.35 m	*	*	*	-
flow direction	*	*	*	-

Table 2.3: Available data February 1996.

The results for February 17 through 21 are presented in the Figures 2.4 through 2.7. When the wind speed exceeds 15 m/s and significant wave height 4 m, the suspended sediment concentration near the bed becomes a few g/l for a short period.

2.4 Results for November 1996.

During the month November 1996 the following data have been made available by Rijkswaterstaat:

location	B	G	H	I
MEX conc. 0.15 m	*	?	*	*
MEX conc. 0.55 m	*	*	*	*
HYDROLAB conc. 2 m	-	-	*	-
HYDROLAB conc. 7 m	-	-	*	-
flow velocity 0.35 m	*	*	-	-
flow direction	*	*	-	-

Table 2.4: Available data November 1996 (? = not reliable).

The data for various sub-periods are presented in Fig. 2.8 through 2.11.

2.5 Preliminary analysis of the field measurements

From a global inspection of the available data a series of preliminary conclusions can be drawn:

1. Note that the suspended sediment concentrations at 0.15 and 0.55 m do not show much difference. Sometimes, the concentration at 0.55 m appears even larger than at 0.15 m (Fig. 2.8b). Assuming that such unstable sediment concentration profiles, if occurring for instance during sedimentation, would vanish rapidly, this is an indication for the (in)accuracy of the data.

2. The wind speed and wave height during the period of February 17-21 and of November 12-16 are of the same order-of-magnitude. However, the suspended sediment concentrations in February are much smaller than those of November. The major difference between these two periods is the weather condition in the preceding periods. As mentioned before, winter 95/96 was exceptionally calm, whereas in autumn 96 already several storms did occur prior to the measuring period. Apparently, it takes time and a few and/or long period(s) of rough weather to increase the suspended sediment concentrations in the Dutch coastal zone of the North Sea up to values of a few g/l.

3. The general trend of the suspended sediment concentration profiles is that maximal values are measured near the bed around slack water, whereas higher in the water column minimal values are then being found. This picture indicates that these fluctuations in concentration profile are due to deposition during slack water and re-mixing over the water column at increasing flow velocities.
   Note however, that occasionally maximal values of the near bed concentration are observed at maximal flow velocity, indicating re-entrainment of a high concentrated near bed suspension

and/or the effect of horizontal advection.

4. An estimate can be made of the magnitude of the settling velocity by elaborating the mass balance for the lower 0.55 m of the water column, assuming that the increase in suspended sediment concentration is caused by settling from the water column above only:

$$\delta \frac{\Delta c}{\Delta t} = W_s c \qquad (2.1)$$

in which c is the suspended sediment concentration, δ the thickness of the control volume (0.55 m), t time and W_s the settling velocity. From the various data, W_s is estimated at $W_s \approx$ 0.3 to 0.5 mm/s. Note that (2.1) can be obtained readily by a formal integration of the mass balance over the control volume δ:

$$\int_{z=0}^{\delta} \left[\frac{\partial c}{\partial t} - W_s \frac{\partial c}{\partial z} \right] dz \qquad (2.2)$$

assuming zero-flux at the sea bed z = 0 and little vertical mixing ($W_s \approx W_{s,eff}$ and no mixing).

Note that measurements, during calm weather conditions though, in February 1996 with the CILAS (OCN, 1996) indicated a particle size of the order of 50 to 150 μm, which is well in agreement with the settling velocity estimated above (Winterwerp, 1998).

5. A final remark concerns the suspended sediment concentrations in the Beerkanaal/Calandkanaal. Preliminary measurements by Rijkswaterstaat at ebb tide during the second week of November 1996 showed virtually no sediment in the water column (concentrations of a few 10 ppm at most, Woudenberg, 1997), whereas simultaneously sediment concentrations off shore measured values up to and above 10 g/l. Apparently, all sediment entering the Maasgeul has fallen out of the water column to form a high concentrated near-bed suspension, c.q. fluid mud layer.

3. The 1DV POINT MODEL

Detailed descriptions of the 1DV POINT MODEL are presented by Uittenbogaard et al. (1996) and Winterwerp and Uittenbogaard (1997). In the following sections a brief summary of the model equations is given enabling interpretation of the numerical simulations in the next chapters. We implicitly assume that the water-sediment can be described as a single-phase fluid in which all particles follow the turbulence movements, but for their settling velocity (e.g. Uittenbogaard, 1994), and that all sediment (particles) remain part of the fluid (water) column.

3.1 The momentum equation

The sediment-water mixture is treated as a one-phase fluid. All horizontal velocity and concentration gradients are neglected and the horizontal velocity u is in one direction only (no vertical rotation, e.g. veering). The momentum equation then reads:

$$\frac{\partial u}{\partial t} + \frac{1}{\rho}\frac{\partial p}{\partial x} = \frac{\partial}{\partial z}\left\{(\nu + \nu_T)\frac{\partial u}{\partial z}\right\} \tag{3.1}$$

in which

- p = pressure,
- t = time,
- u = horizontal velocity (in x-direction),
- x = horizontal coordinate,
- z = vertical coordinate,
- ρ = bulk density of water-sediment mixture,
- ν = molecular viscosity, and
- ν_T = turbulent eddy viscosity.

The effects of wind and waves on turbulence are encountered for through a modification of ν_T.

The pressure term in (3.1) is adjusted to maintain a given, time-dependent depth-averaged velocity:

$$\frac{1}{\rho}\frac{\partial p}{\partial x} = \frac{\tau_s - \tau_b}{\rho h} + \frac{U(t) - U_o(t)}{T_{rel}} \; ; \quad U(t) = \frac{1}{h}\int_{-d+z_{bc}}^{\zeta} u(z',t)\,dz' \tag{3.2}$$

in which

- d = depth with respect to a reference plane,
- h = water depth, $h = d + \zeta(t)$,
- T_{rel} = relaxation time,
- U = actual computed depth-averaged flow velocity,
- U_o = desired depth-averaged flow velocity (i.e. user input),
- z_{bc} = apparent roughness height,
- τ_b = shear stress at bed,
- τ_s = shear stress at water surface, and
- ζ = level of water surface with respect to reference plane.

The boundary conditions for (3.1) read:

$$\tau_b = \left\{\rho(\nu+\nu_T)\frac{\partial u}{\partial z}\right\}\Big|_{z=-d+z_{bc}} \quad ; \quad \tau_s = \left\{\rho(\nu+\nu_T)\frac{\partial u}{\partial z}\right\}\Big|_{z=\zeta} \tag{3.3}$$

The bed shear stress τ_b depends on the near-bed velocity through the following quadratic friction law that satisfies the log-law of flow over a rough bed:

$$\tau_b = \rho\,|u_{*b}|u_{*b} \quad ; \quad u_{*b} = \frac{u(-d+z_{bc}+\frac{1}{2}\Delta z_b)}{\kappa\log(1+\frac{1}{2}\Delta z_b/z_{bc})} \tag{3.4}$$

In (3.4) is κ the Von Kármàn constant ($\kappa \approx 0.41$), z_{bc} the apparent bed-roughness height and the near-bed velocity $u(-d+z_{bc}+\frac{1}{2}\Delta z_b)$ is defined in the centre of the computational bed layer with thickness Δz_b. Note that the roughness height z_0 holds for a steady fully-developed turbulent flow over a flat, immobile sandy or muddy bed. This roughness height increases to the apparent z_{bc} ($z_{bc} \geq z_0$) by turbulence generated through orbital motions induced by surface waves, see Section 3.3 for further details.

3.2 The effect of wind

In (3.3) the boundary condition at the free surface follows from the projection of the wind shear stress in u-direction, and τ_s is defined by

$$\tau_s = \rho_a C_D |\underline{U}_{10}| U_{10} \tag{3.5}$$

Here ρ_a is the density of air, C_D the drag coefficient for wind over the free surface and $\underline{U}_{10}$ is the wind speed vector recorded 10 metres above the mean free-surface level with component U_{10} in u-direction. The drag coefficient C_D is given by the formulation of Smith and Banke (1975):

$$C_D = (0.63 + 0.066|\underline{U}_{10}|)\cdot 10^{-3} \tag{3.6}$$

N.B. In the KUSTSTROOK-model with algebraic turbulence model of the coastal area along the Dutch coast, the best agreement between observed and computed near surface flow velocities is obtained with a constant value of $C_D = 2\ 10^{-3}$.

3.3 The effect of waves

The effect of waves on vertical mixing is modelled through the approach by Grant and Madsen (1979) in the form of an additional boundary condition in the flow model.

According to potential theory for infinitesimal waves on a uniform current the following relations

$$\hat{X}_{orb} = \frac{\hat{H}/2}{\sinh(kh)} \quad ; \quad \hat{u}_{orb} = \omega \hat{X}_{orb} \quad ; \quad \omega^2 = gk\tanh(kh) \quad ; \quad k = \frac{2\pi}{\lambda} \tag{3.7}$$

hold for the near-bed orbital horizontal particle excursion amplitude $\hat{X}_b$ and the frequency ω of waves with wave height $\hat{H}$ and wave number k on water with depth h. The rms-value of the wave-induced bed shear stress is defined by:

$$\tau_w = \left\langle \tilde{\tau}_w^2 \right\rangle^{1/2} = \rho_w u_{*w}^2 \; ; \; u_{*w}^2 = \frac{1}{2} f_w \hat{u}_{orb}^2 \tag{3.8}$$

with friction coefficient f_w and near-bed horizontal orbital velocity magnitude $\hat{u}_{orb}$. Note that for sediment transport the mean wave height $\hat{H}_{rms}$ has to be used. The following formulation for the wave-related friction coefficient is used:

$$\begin{aligned} &\hat{X}_{orb}/z_o \geq 47.1 : \; f_w = 0.00251 \exp\left[9.94 \left(z_o/\hat{X}_{orb}\right)^{0.19}\right] \\ &\hat{X}_{orb}/z_o < 47.1 : \; f_w = 0.3 \end{aligned} \tag{3.9}$$

Grant and Madsen found the following approximation to the wave-affected boundary layer thickness:

$$\delta_w = \frac{2\kappa}{\omega} \sqrt{u_{*b}^2 + u_{*w}^2} \tag{3.10}$$

The (mean) eddy viscosity ν_T within the turbulent wave-boundary layer behaves as:

$$z_o \leq z \leq \delta_w : \; \nu_T = \kappa \left(u_{*b} + u_{*w}\right) z \tag{3.11}$$

with level $z \leq \delta_w$ above the bed and with unknown mean bed shear stress $\tau_b = \rho_w u_{*b}^2$. Note that with the constant shear stress τ_b throughout the wave-boundary, (3.11) yields a logarithmic velocity profile based on $(u_{*b} + u_{*w})$ rather than on u_{*b} only, as expected for a given $\tau_b = \rho_w u_{*b}^2$.

Above the wave-boundary layer (3.10) which is increased in thickness when a mean flow is present, the wave-induced turbulence is not notable and Grant and Madsen assume that:

$$z > \delta_w : \; \nu_T = \kappa u_{*b} z \tag{3.12}$$

in which the shear stress is kept constant and equal to the bed stress $\tau_b = \rho_w u_{*b}^2$; this is the usual assumption for a log-law flow.

The two logarithmic velocity profiles are matched at $z = \delta_w$. The wave-boundary layer contributes to the mean flow above the wave-boundary layer through an increase in effective roughness z_{bc}:

$$\delta_w \geq z_o : \; \frac{z_{bc}}{z_o} = \left(\frac{\delta_w}{z_o}\right)^{\beta} \; ; \; \beta = 1 - \sqrt{\frac{1}{1 + u_{*w}^2/u_{*b}^2}} \tag{3.13}$$

Consequently, the bed shear stress is related to the mean horizontal velocity beyond the wave-boundary layer by

$$\tau_b = \rho_w u_{*b}^2 \; ; \quad u_{*b} = \frac{u(-d + z_{bc} + \tfrac{1}{2}\Delta z_b)}{\kappa \log(1 + \tfrac{1}{2}\Delta z_b / z_{bc})} \; , \quad \text{provided} \quad \tfrac{1}{2}\Delta z_b \geq \delta_w \tag{3.14}$$

in which Δz_b is the thickness of the near-bed computational grid cell. Note that z_{bc} appears in (3.14), which depends on u_{*b} that is unknown initially; z_{bc} and u_{*b} are therefore solved iteratively.

Soulsby et al. (1993) compare various methods for the assessment of the combined effects of flow and waves on the bed shear stress and conclude that for small waves Grant and Madsen overestimate this effect considerably (by about 20 %). When wave effects become larger, the overestimation reduces to less than 10 %.
Though other methods (e.g. Fredsøe) appear to be more accurate, for the time being, we prefer the use of the Grant and Madsen approach in the present study, as this method is simple, and yet contains a clear physical background. Algorithms for other methods however are readily available at Delft Hydraulics to be implemented into the 1DV POINT MODEL.

3.4 The k-ϵ turbulence model

The k-ϵ turbulence model implemented in the 1DV POINT MODEL (neglecting horizontal advection terms) consists of a transport equation for the turbulent kinetic energy k and the turbulent dissipation ϵ:

$$\frac{\partial k}{\partial t} = \frac{\partial}{\partial z}\left\{\left(\nu + \Gamma_T^{(k)}\right)\frac{\partial k}{\partial z}\right\} - \overline{u'w'}\frac{\partial u}{\partial z} - \frac{g}{\rho}\overline{\rho'w'} - \epsilon \tag{3.15}$$

$$\frac{\partial \epsilon}{\partial t} = \frac{\partial}{\partial z}\left\{\left(\nu + \Gamma_T^{(\epsilon)}\right)\frac{\partial \epsilon}{\partial z}\right\} - c_{1\epsilon}\frac{\epsilon}{k}\overline{u'w'}\frac{\partial u}{\partial z} - c_{1\epsilon}(1 - c_{3\epsilon})\frac{\epsilon}{k}\frac{g}{\rho}\overline{\rho'w'} - c_{2\epsilon}\frac{\epsilon^2}{k} \tag{3.16}$$

in which a prime denotes turbulent fluctuations and an overbar ensemble averaging over the turbulent time scale. In the present study we have omitted the possible contribution of internal waves to the turbulence production. The turbulent transport terms are modelled as a diffusion process:

$$\overline{u'w'} = -\nu_T \frac{\partial u}{\partial z} \; ; \quad \overline{\phi'w'} = -\Gamma_T^{(\phi)} \frac{\partial \phi}{\partial z} \tag{3.17}$$

The eddy viscosity ν_T and eddy diffusivity $\Gamma_T^{(\phi)}$ are given by:

$$\nu_T = c_\mu \frac{k^2}{\epsilon} \; ; \quad \Gamma_T^{(\phi)} = \frac{\nu_T}{\sigma_T^{(\phi)}} \tag{3.18}$$

in which $\sigma_T^{(\phi)}$ is the turbulent Prandtl-Schmidt number. The various coefficients appearing in the k-ϵ model are the result of calibration to grid-generated turbulence and log-law velocity profile, which yield:

$$c_\mu = 0.09 \; ; \quad c_{1\epsilon} = 1.44 \; ; \quad c_{2\epsilon} = 1.92 \; ; \quad \sigma_T^{(k)} = 1.0 \; ; \quad \sigma_T^{(\epsilon)} = 1.3 \; ; \quad \sigma_T^{(\rho)} = 0.7 \; ;$$
$$\kappa = 0.41 \; ; \quad c_{3\epsilon} = 1 \quad \text{for} \quad \frac{\partial \rho}{\partial z} \leq 0 \; , \quad c_{3\epsilon} = 0 \quad \text{for} \quad \frac{\partial \rho}{\partial z} > 0 \tag{3.19}$$

free surface and at the bed are set to zero:

$$w_s^{(\ell)} c^{(\ell)}\Big|_{z=-d+z_{bc}} = 0 \; ; \; \Gamma_T^{(\ell)} \frac{\partial c^{(\ell)}}{\partial z}\Big|_{z=-d+z_{bc}} = 0 \quad ; \quad w_s^{(\ell)} c^{(\ell)}\Big|_{z=\zeta} = 0 \; ; \; \Gamma_T^{(\ell)} \frac{\partial c^{(\ell)}}{\partial z}\Big|_{z=\zeta} = 0 \quad (3.24)$$

Inside the computational bed layer, the deposition mass flux D_e and the erosion mass flux E are designated to the source and sink terms of (3.23) by:

$$z = \tfrac{1}{2}\Delta z_b : \; P_c^{(\ell)} = D_e^{(\ell)} \; ; \; \epsilon_c(\ell) = E^{(\ell)} \quad (3.25)$$

For cohesive sediment, the fluxes are described with the well-known Partheniades-Krone formulations:

$$E^{(\ell)} = M S\left(\frac{\tau_{bw}}{\tau_e} - 1\right) \; ; \; D_e^{(\ell)} = w_s c_b^{(\ell)} S\left(1 - \frac{\tau_{bw}}{\tau_d}\right) \; ; \; c_b^{(\ell)} = c^{(\ell)}\left(z = \tfrac{1}{2}\Delta z_b, t\right) \quad (3.26)$$

in which we use the step function $S(\alpha)$:

$$\alpha > 0 : S(\alpha) = \alpha \; and \; \alpha \le 0 : S(\alpha) = 0 \quad (3.27)$$

which is used as a switch for the erosion and deposition fluxes. This switching is controlled by the given (input) threshold values for the erosion-shear stress τ_e and deposition-shear stress τ_d compared to the total bed shear stress, the latter defined by:

$$\tau_{bw} = \rho\left(u_{*b}^2 + u_{*w}^2\right) \quad (3.28)$$

For non-cohesive sediment (e.g. sand), we apply Van Rijn's (1987) pick-up function:

$$E = 1.5 W_s \frac{D_{50}}{h} \frac{T_m^{1.5}}{D_*^{0.3}} \quad (3.29)$$

$$\text{with} \quad D_* = D_{50}\left(\frac{(\rho_s - \rho_w)g}{\rho_w \nu^2}\right)^{1/3}, \quad \text{and} \quad T_m = \frac{\tau_b - \tau_{cr}}{\tau_{cr}}$$

in which D_{50} is the median particle diameter, and τ_{cr} is the threshold value for sediment transport according to Shields.

3.7 Buoyancy effects

The bulk density of water is not only a function of salinity and temperature (Section 3.5), but also the suspended sediment concentration according to:

$$\rho(S,\theta,c^{(\ell)}) = \rho_w(S,\theta) + \sum_\ell \left(1 - \frac{\rho_w(S,\theta)}{\rho_s^{(\ell)}}\right) c^{(\ell)} \quad (3.30)$$

where $c^{(\ell)}$ is the suspended sediment concentration of fraction (ℓ), and $\rho_s^{(\ell)}$ its specific density.

4 Scaling laws for suspended sediment transport

4.1 Dimensional analysis

The dynamics of the vertical suspended sediment concentration profile are governed by the equations for the mass balance (3.23), the momentum (3.1) and the k-ϵ turbulence closure (3.15) & (3.16), neglecting horizontal advective effects. Assuming that the turbulent kinetic energy scales with the shear velocity squared u_*^2 and that the vertical eddy viscosity and diffusivity scale with the shear velocity times water depth hu_*, seven parameters can be identified that describe the suspended sediment distribution in the water column: the water depth h, the shear velocity u_*, a characteristic time scale T (for tidal flow condition T equals one quarter of the tidal period), the (constant) settling velocity of the sediment W_s, the density of the water ρ, the acceleration of gravity g, and the saturation concentration C_s. The latter is defined as the maximal depth averaged suspended sediment concentration that can be carried by the flow - for a more rigorous definition see Section 4.2. Note that grain size and sediment density are implicitly taken into account in W_s, as is the flow velocity in u_*.

Appendix A contains the details of a dimensional analysis using the Π-theorem, yielding the following functional relationship for tidal flow conditions:

$$\frac{C_s}{\rho} = f(T_s, T_m, Ri_*) \tag{4.1}$$

in which the following dimensionless parameters are defined:

$$T_s = \frac{h}{W_s T} \quad = \text{relative time scale for settling}$$

$$T_m = \frac{h}{u_* T} \quad = \text{relative time scale for vertical mixing}$$

$$Ri_* = \frac{g h C_s}{\rho u_*^2} \quad = \text{bulk Richardson number (buoyancy effects).}$$

Note that for steady flow conditions, the tidal period is no longer a parameter, and the number of dimensionless parameters reduces by one. In fact it can be shown that T_s and T_m merge to yield W_s/u_*, resulting in the following functional relationship for steady flow conditions:

$$\frac{C_s}{\rho} = g\left(\frac{W_s}{u_*}, Ri_*\right) \tag{4.2}$$

This relation was found earlier by Galland et al. (1997).

In the Maasmond area $T_s \approx 1$ (h = 16 m, $W_s \approx 0.5$ mm/s), which reduces the number of possibilities of Table A.3 by a factor 2/3.

It should be noted that the actual dynamics of fine grained cohesive sediments in the water column are governed by four more time scales. As a result of flocculation processes, sediment particles

may aggregate (or break down) as a function of the sediment concentration, turbulence intensity and their physico-chemical properties, resulting in variations in settling velocity and thixotropic processes in high-concentrated near bed layers affecting their (maximal) volumetric concentration and resistance to erosion. Together with consolidation processes, these thixotropic processes determine to what extent the sediment-water mixture can be regarded as a single-phase fluid, and whether the water-mud interface will be able to generate turbulence. Finally, the rate of erosion does determine the availability of sediment that can be carried by the flow.
These time scales should be studied in relation to the time scale of the driving forces, i.e. the tidal period. Summarizing we define four more dimensionless parameters:

$\frac{T_f}{T}$ = relative time scale for flocculation processes

$\frac{T_t}{T}$ = relative time scale for thixotropic processes

$\frac{T_c}{T}$ = relative time scale for consolidation

$\frac{T_e}{T}$ = relative time scale for erosion

These four time scales are not further elaborated in the present report, but used for some qualitative notes. The first three scaling laws, though, form a major part of the analyses in the following sections.

4.2 Stationary flow and saturated suspensions

Teisson et al. (1992) studied the numerical simulation of suspended sediment with a Reynolds stress model. In their analysis they conclude that an "upper boundary for the sediment distribution" should exist: suspended sediment concentrations cannot exceed this upper boundary. A similar conclusion is drawn by Winterwerp (1996) and Uittenbogaard et al. (1996). In the latter report this upper boundary is called the saturation concentration c_s and this terminology will be applied throughout this report.

The c_s-concept is based on the experimental observations (e.g. Turner, 1973) that beyond a critical value (about 0.15) of the flux Richardson number Ri_f, all turbulence is damped, and no matter can be kept in suspension. Ri_f follows from the turbulent kinetic energy equation and is defined as the ratio of the buoyancy and production term; the contribution of the diffusion term is neglected in the present study (Uittenbogaard et al., 1996):

$$Ri_f = -\frac{g\overline{w'\rho'}}{\rho\,\overline{u'w'}\frac{\partial u}{\partial z}} = -\frac{\alpha g\overline{w'c'}}{\rho\,\overline{u'w'}\frac{\partial u}{\partial z}} \qquad (4.3)$$

in which u', w', c' and ρ' are the turbulent fluctuations of the horizontal and vertical velocity components u and w, and the turbulent fluctuations of the suspended sediment concentration c and the water density ρ, g is the gravitational acceleration, z the vertical coordinate, α the relative

sediment density ($\alpha=(\rho_s-\rho_w)/\rho_s$), and the overbar denotes averaging over the turbulence time scale. If the sediment dynamics are evaluated starting from low concentrations, a zero-order approximation is justified, and we assume a logarithmic velocity profile (parabolic viscosity distribution) and local equilibrium:

$$\nu_T = \kappa u_* z\left(1-\frac{z}{h}\right), \qquad \frac{\partial u}{\partial z} = \frac{u_*}{\kappa z}, \quad \text{and} \quad \overline{w'c'} = -w_s c \tag{4.4}$$

in which κ is the von Kármàn constant, h the water depth and w_s the settling velocity of the sediment particles. Substitution into (4.3) for $Ri_f = 0.15$ (critical value) yields:

$$c_s = \frac{0.15\rho}{\alpha g \kappa}\frac{u_*^3}{h w_s}\left(\frac{h}{z}-1\right) \tag{4.5}$$

A depth-averaged saturation concentration C_s can be defined, scaling as:

$$C_s = \frac{1}{h}\int_0^h c_s dz \propto \frac{\rho}{g}\frac{u_*^3}{h W_s} \tag{4.6}$$

We recognize that (4.6) is a function of the scaling parameters u_*/W_s and Ri_*, defined in (4.1). As the additional assumption of local equilibrium is made, yielding $Ri_* \propto u_*/w_s$, C_s/ρ scales with only one dimensionless parameter, i.e. (4.6), e.g. Galland et al. (1997). It is remarkable that this formula strongly resembles the formula for the transport of loose grain material (e.g. sand) by Bagnold (1966). This is further elaborated in Appendix B.

Finally we can introduce the effects of hindered settling:

$$w_s \approx w_{s,0}(1-\phi)^5 \tag{4.7}$$

in which ϕ is the volumetric concentration of the particles, to be quantified with fractal theory for aggregated fragile cohesive sediment particles (e.g. Kranenburg, 1994). For a fractal dimension $n_f = 2$, ϕ becomes (e.g. Winterwerp, 1996):

$$\phi = \frac{D}{D_p}\frac{c}{\rho_s} \tag{4.8}$$

in which D is the actual diameter of the particle (mud floc) and D_p the diameter of the primary particles of the aggregate. Substitution of (4.8) into (4.7) and (4.6) for small volumetric concentrations gives:

$$C_s \propto C_{s,0}\left(1 + 5\frac{D}{D_p}\frac{\rho}{\rho_s}\frac{u_*^3}{g h W_s}\right) \tag{4.9}$$

showing that the effect of hindered settling is primarily a decrease in effective settling velocity, resulting in an increase in the saturation concentration, which is linear with the floc size for small suspended sediment concentrations.

4.3 Numerical simulations for steady flow

The scaling law (4.6) is tested with numerical experiments using the 1DV POINT MODEL. The setting of the physical/numerical parameters are presented in Table 4.1, and are used throughout this report, unless explicitly mentioned otherwise.

parameter	symbol	value	remarks
water depth	h	16 m	constant, also for tidal flow
flow velocity	U	variable	steady state
tidal velocity amplitude	U_m	variable	
bed roughness	z_o	10^{-3} m	hydraulic rough
surface roughness	z_s	0.1 m	
water density	ρ_w	1020 kg/m^3	
sediment density	ρ_s	2650 kg/m^3	
initial sediment concentration	C_o	variable	homogeneous vertical profile
settling velocity	W_s	0.5 mm/s	constant
hindered settling		no	
flocculation model		no	
water-bed exchange		no	
Prandtl-Schmidt number	$\sigma_T^{(c)}$	0.7	
wind		no	
waves		no	
salinity gradients		no	
number of layers	Δz	100	equidistant
time step	Δt	1 min	
relaxation time	T_{rel}	$2 \times \Delta t$	

Table 4.1: Reference physical/numerical parameters 1DV POINT MODEL

In the first series of numerical experiments, the flow velocity is set at a fixed value, and the homogeneous suspended sediment concentration C_0 is varied in small steps until the vertical concentration profile collapses. The simulations are run for 10 hours which exceeds the settling time $T_s = h/W_s$. As an example, the concentration profiles and turbulence parameters are plotted in Fig. 4.1 and 4.2 for a depth-averaged velocity U = 0.2 m/s in the form of isolutals (lines of

constant suspended sediment concentration, similar to the notion of isohalines for lines of constant salinity). It is shown that a small increase of C_0 from 0.023 kg/m^3 to 0.024 kg/m^3 causes an entirely different pattern: the flow becomes saturated and a high-concentrated near-bed layer is formed (Uittenbogaard et al., 1996). It is conjectured that this is an important mechanism behind the rapid formation of fluid mud in the "Maasgeul".

Fig. 4.2c through 4.2h show the temporal evolution of the computed eddy diffusivity and sediment concentration. In the period t = 50 through t = 200 a pronounced interface develops in the upper part of the water column, accompanied by a gradual decrease in eddy diffusivity in the lower part of the water column. Note the "double parabolic" diffusivity profile in Fig. 4.2e, characteristic for highly stratified flows. In between t = 200 and t = 400 the picture alters, as the vertical profiles collapse, until ultimately we observe a thin near bed layer with concentrations beyond 0.5 g/l. The diffusivity is restored slightly from its collapse around t = 1000 (Fig. 4.2g), but only up to about 10 % of its original value (Fig. 4.2c). Note that in the present modelling, the mud layer remains a viscous fluid. In nature, aggregation and consolidation will occur, resulting in a strength build-up, as a result of which turbulence may be produced again at the water-mud interface, restoring the diffusivity profile. This strength build-up does prevent the re-entrainment of the sediment by the restored diffusivity. We can conclude that the collapse is irreversible and governed by the time scales for thixotropy and consolidation.

A further series of experiments is carried out for U = 0.4 (0.2) 1.0 m/s. The initial depth-averaged concentration just prior to the collapse of the concentration profile is defined as the saturation concentration C_s. The collapse is rapid and suddenly, as anticipated in Table A.3 ($T_s << 1$). Its variation with U is plotted in Fig. 4.3a. The numerical results show that C_s scales with U^3, as deduced in Section 4.1.

Next the settling velocity was decreased to W_s = 0.1 mm/s and the experiments are repeated for U = 0.5 m/s. The simulation time is increased by a factor 5 to account for the longer settling time. The resulting saturation concentration matches the previous results properly (see Fig. 4.3a).

Because of the large sensitivity of the vertical concentration profile and turbulence properties near the saturation concentration, an additional series of numerical experiments at U = 0.6 m/s is carried out to establish the influence of time step and number of layers in the simulations: the time step is set at 0.2 and 5 min (also varying T_{rel} proportionally), maintaining 100 layers, and the number layers is decreased down to 20, maintaining a time step of 1 min. The results are also plotted in Fig. 4.3a, showing a marginal effect of these numerical parameters, and have not been altered any more.
We can draw the conclusion that the TRIWAQ-SLIB3D simulations can be carried out with 20 layers in the vertical, and probably less, as long as the sediment concentration does not become (super-) saturated[1)].

Finally the effect of hindered settling on C_s is studied. The results are presented in Fig. 4.3b, showing an increase of C_s with grain size D, i.e. with the effects of hindered settling (e.g. equ's (4.8 & 4.9)). Note that for saturated suspensions the formation of a lutocline is enhanced by the effects of hindered settling (Kranenburg, 1992), affecting C_s oppositely; this effect however is not

[1)] Note that in the case of remixing for increasing flow velocity, the concentration profile may become highly stratified and sufficient vertical resolution is required for a proper numerical simulation.

elaborated in the present study.

A last remark concerns the behaviour of the k-ϵ model. It is well known that this model collapses under highly stratified conditions, stopping to generate turbulence (e.g. Simonin et al., 1989). However, also Teisson et al. (1992) found a similar maximal sediment concentration that can be carried by the flow, using a Reynolds-stress model. As this behaviour also follows from physical analyses, we therefore conclude that the picture emerging from the preceding section is physically sound. We do recommend however, to check some of the numerical results (and those of Section 4.5) with such a Reynolds stress model, especially to verify the scaling laws deduced.

4.4 Unsteady flows

For unsteady, e.g. tidal flows the equilibrium approach outlined above cannot be used, as the dynamics of mixing and settling become important. This can be demonstrated from a global analysis of the mass balance for suspended sediment in the vertical plane:

$$\frac{\partial c}{\partial t} + \frac{\partial w_s c}{\partial z} = \frac{\partial}{\partial z}\left(\Gamma_T \frac{\partial c}{\partial z}\right) \tag{4.10}$$

in which Γ_T is the turbulent eddy diffusivity, related to the eddy viscosity through the turbulent Prandtl-Schmidt number σ_T: $\Gamma_T = \nu_T/\sigma_T$. Equ (4.10) shows that the advection term scales with h/w_s and the diffusion term with h^2/Γ_T, hence with h/u_*.

The dynamics of high concentrated sediment suspensions are governed by three time scales: the tidal time scale T (= 1/4 of tidal period), the settling time $T_s = h/W_sT$, and the time scale for vertical mixing: $T_m = 10h/u_*T$ (assuming a parabolic diffusivity profile).

Note that T_s is of the order of unity for the Maasmond conditions.

Now let us consider two extreme cases and the intermediate one (see also Appendix A, Table A.3):

I. $T_s >> T_m$

If $h/w_s >> h/u_*$, the time scale for vertical mixing is much smaller than the time scale for settling, i.e. within a tidal cycle the sediment can always be mixed entirely over the water column. In fact the advection term in equ (4.10) becomes unimportant. The saturation concentration will be determined by the maximal flow velocities occurring. In the extreme case that $w_s = 0$, equ (4.10) describes the mixing of a passive tracer over the water column.

II. $T_s << T_m$

If $h/w_s << h/u_*$, the time scale for vertical mixing is much larger than the time scale for settling. Within a tidal cycle, C_s will be determined by the minimal flow velocity, and the concentration vertical will adjust itself immediately to the velocity variations. In the case of reversing flow this would mean that the flow would only be able to carry very little sediment, i.e. $C_s \propto \min(u_*^3)$. The high-concentrated near-bed layer will first have to be eroded, decreasing the buoyancy effects, before the turbulence level is restored to carry the sediment in suspension.

It is noted that in the case of sand transport, the sediment will form a hard bed upon deposition, enabling the local production of turbulence, whence the erosion of the bed at increasing tidal velocities (i.e. in this case we have small thixotropic and consolidation time scales).

III. $T_s \approx T_m$

The case that h/w_s is of the same order as h/u_* is relevant for the Maasmond area (though u_* of course varies considerably over the tidal period) and allows a further quantitative analysis. For this purpose we introduce the following dimensionless quantities:

$$c = C_s\hat{c}\,, \quad t = \tau\hat{t}\,, \quad z = h\hat{z}\,, \quad u = U\hat{u}\,, \quad \text{and} \quad w_s = W_s\hat{w}_s \tag{4.11}$$

where a hat denotes a dimensionless quantity. Around slack tide highly stratified conditions can occur when $c \approx C_s$, decreasing the eddy diffusivity considerably. This can be accounted for through the introduction of a damping function (Karelse, 1974):

$$\Gamma_T = \frac{\Gamma_0}{(1+mRi)^n} \tag{4.12}$$

in which Γ_0 is the eddy diffusivity for neutral conditions, to be scaled with hu_*, m and n are empirical coefficients, and the gradient Richardson number Ri is defined as:

$$Ri = -\frac{g\partial\rho/\partial z}{\rho(\partial u/\partial z)^2} = -\frac{\alpha g\partial c/\partial z}{\rho(\partial u/\partial z)^2} \tag{4.13}$$

For $mRi >> 1$ the scaled mass balance reads:

$$\frac{C_s}{\tau}\frac{\partial\hat{c}}{\partial\hat{t}} + \frac{W_sC_s}{h}\frac{\partial\hat{w}_s\hat{c}}{\partial\hat{z}} = \frac{u_*U^{2n}}{h^{n-1}C_s^n}\frac{C_s}{h^2}\left(\frac{\rho}{g}\right)^n\frac{\partial}{\partial\hat{z}}\left(\hat{\Gamma}_0\frac{\partial\hat{c}}{\partial\hat{z}}\right) \tag{4.14}$$

Galland et al. (1997) apply the Munk-Anderson (1948) relation and show that the vertical eddy viscosity and diffusivity, and the suspended sediment concentration profile computed with a Reynolds stress model are well approximated by using this relation in the vertical advection-diffusion equation. It is therefore also applied in the present analysis:

$$\Gamma_T = \frac{\Gamma_0}{(1+3.3Ri)^{1.5}} \tag{4.15}$$

and we obtain the scaling law for suspended sediment concentrations under tidal conditions:

$$C_s \propto \frac{\rho}{g}\frac{U^{8/3}}{hW_s^{2/3}} \tag{4.16}$$

It is remarkable, that the powers of U and W_s for tidal conditions are close to those for steady flow, but not identical. The next section contains numerical proof of these new scaling laws.

4.5 Numerical experiments for tidal flow

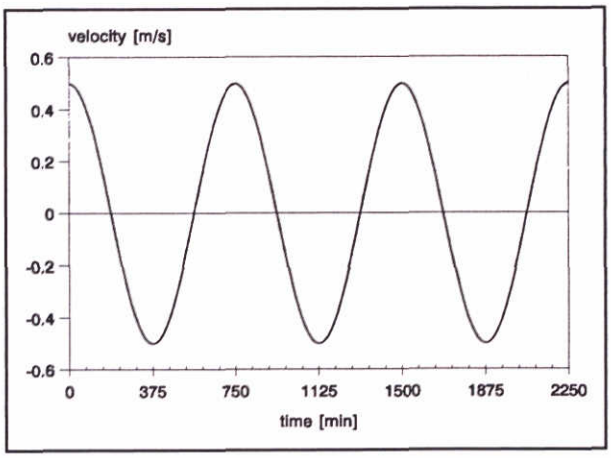

Numerical simulations are carried out for a tidal situation with an M_2-tide only, at a period of 12.5 hours; the water depth is kept constant[2]. A sketch of the tidal variation in depth-averaged velocity is given on the next page. All other parameters, given in Table 4.1 are kept constant. The experimental procedure outlined in Section 4.2 is applied again, that is, given a specific tidal amplitude, C_0 is varied until the concentration profile collapses. Because of the variation in flow velocity, hence mixing characteristics of the flow, the suspended sediment concentration varies with time, showing its steepest gradients around slack water, forming a high concentrated near bed layer. C_s is now defined as that value of C_0 beyond which this high concentrated near bed layer cannot be resuspended any more. This definition is somewhat more subjective than for steady flow conditions, as a small range in concentrations exists where the concentration profile is more or less critical before a complete collapse is observed, e.g. Table A.3. As an additional criterium, the variations of the gradient Richardson number is monitored. This is shown in Fig. 4.4 and 4.5. For C_0 = 0.13 g/l, t = 1950 min, some stratification is observed near the water surface, for C_0 = 0.15 g/l, this stratification is so strong that hardly any sediment can be carried in the upper 20 % of the water column. At increasing C_0 this pictures becomes more and more pronounced, until eventually no sediment can be carried in suspension. Note that some time later (Fig. 4.4b vs 4c) the entire concentration profile collapses, generating a high-concentrated near-bed suspension at a concentration of several g/l. It is also noted that the collapse of the concentration profile always starts near the water surface, where a lutocline is being formed caused by the settling of the sediment. Richardson numbers tend to become increasingly large, though it should be mentioned that at a sufficient large Ri, its actual value does not have a realistic meaning any more.

Figure 4.4 and 4.5 show the isolutals for the three tidal periods; continuation of the simulations give similar results for the (sub-)saturation conditions. For super-saturation no sediment can be carried in suspension eventually, as was shown earlier by Uittenbogaard et al. (1996).

The experimental results are summarized in Fig. 4.6. Fig. 4.6a presents the computed variation of C_s with U, showing that the scaling $C_s \propto U^{8/3}$ is a reasonable one. The variation of S_s with W_s, presented in Fig. 4.6b, is studied for a range from W_s = 0.001 mm/s to W_s = 1 mm/s. For larger values of W_s the saturation concentration could not be established unambiguously, as also for very small sediment concentrations the concentration gradient is very large (Rouse profile). Fig. 4.6b shows that in the range $0.1 < W_s < 1$ mm/s the scaling of $C_s \propto W_s^{-2/3}$ is reasonable. It should be noted that the agreement between the numerical results and the (4.16) is not trivial at

[2] The tidal variations in water level are small with respect to the total water depth. Moreover, a varying water level in a mass conserving 1DV model does pose interpretation problems, as this variation by itself does generate additional vertical concentration gradients.

all, as (4.16) is obtained through a different approach. At smaller values of W_s the slope becomes steeper and in agreement with the scaling for steady flow ($C_s \propto W_s^{-1}$), e.g. (4.6).

Finally, the effect of hindered settling is determined for tidal conditions. A settling velocity of W_s = 0.5 mm/s corresponds to a grain size of about 150 μm (Winterwerp, 1998). At an estimated saturation concentration of about 0.13 g/l for a tidal flow with amplitude 0.5 m/s, this would yield a volumetric concentration less than 0.002 and a reduction in settling velocity smaller than 1 %. It is envisaged that this effect will not be visible in the computational results.
Therefore a simulation with the 1DV POINT MODEL is carried out for somewhat extreme parameter settings. The model is run for a tidal velocity amplitude of 0.8 m/s, W_s = 0.5 mm/s and D = 300 μm. In that case the reduction in settling velocity is 7 %, and the 1DV POINT MODEL reveals a saturation concentration C_s = 0.60 g/l. For a condition without hindered settling C_s = 0.56 g/l. The ratio between these two values is exactly 0.93.
It can therefore be concluded that the effects of hindered settling on the values of the saturation concentration for tidal conditions are small and comparable to those for steady state conditions, i.e. just a reduction in overall settling velocity. In all other sensitivity analyses, the effect of hindered settling is therefore omitted.

From the various numerical experiments, presented in Section 4.3 and the present section it can be concluded that the scaling relations deduced in the Sections 4.2 and 4.4 are confirmed, and they will be used in the further analyses of numerical and field data in this report.

It should be emphasized that the results, hence the conclusions, presented in this Chapter are obtained for suspended sediment concentrations at or below their saturation value, and for constant settling velocity. Even for these conditions strong stratification effects occur, modifying the concentration profile, hence horizontal sediment transport, considerably. This is addressed once more in Section 5.6.

5 Sensitivity analyses for secondary effects

5.1 Sensitivity analyses for secondary effects without sediment

In the following sections the effect of seven additional actors will be studied:

1. the effect of the higher harmonic component M_4,
2. the effect of wind,
3. the effect of wind and waves,
4. the effect of a salinity-induced stratification,
5. the effect of water-bed exchanges,
6. the influence of buoyancy effects, and
7. the behaviour of sand particles.

To facilitate the interpretation of the effects 2, 3 and 4 on the sediment carrying properties of the flow, these effects are first studied without sediment. We simulate the flow for steady conditions, i.e. U = 0.5 m/s and apply the model and physical data given in Table 2.2 and 4.1, assessing the effects by comparing the values of the eddy viscosity with the reference situation, i.e. flow alone.

Fig. 5.1a shows the computed eddy viscosity ν_T for the reference situation, the situation with wind only, with waves only and with wind and waves. Fig. 5.1b show the same results, but now scaled with the reference profile. The effect of a wind velocity of 7 m/s is so small, that the wind speed has been increased up to 15 m/s. However, the effect is still an increase in ν_T by less than 2 %, except near the water surface, where the viscosity decreases to zero. At first sight this result is contrary to our intuition, as one would expect that an overall increase in "roughness" (e.g. wind friction) would increase turbulence production, hence viscosity. On the other hand, also the dissipation would increase, and it is the balance between these two that determines ν_T. However, at present it is not clear whether the computed behaviour of ν_T is correct or erroneous, and more research is required for a definite answer. As wind effects (**not** wave effects though) are expected to be small in the Maasmond area anyway, we will omit these in the further analyses of the field data.

The increase of ν_T by surface waves with a height of H_{rms} = 1.3 m and period of 5 sec is considerable, and amounts to about 20 %. This is due to an increase of the effective z_0-value from 1 10^{-3} without waves to 3.4 10^{-3} for the situation with waves, corresponding to an increase of the shear velocity u_* from 0.025 m/s to 0.029 m/s. Note that, as discussed in Chapter 3, for small waves, the effects of waves on the vertical mixing are a bit overpredicted by the Grant & Madsen approach implemented in the 1DV POINT MODEL.

Finally, the resulting eddy viscosity profile for the combined case with wind and waves is almost identical to the case of waves only, as to be expected.

The effect of salinity-induced stratification is studied through a simulation with steady flow (U = 0.5 m/s) and the initial salinity profile sketched on page 4. Note that in this simulation the initial salinity profile is kept in the so-called "diagnostic mode" (i.e. kept constant as no vertical mixing is included). Fig. 5.2 presents the computed flow and eddy viscosity profile at three different time steps, showing a continuous decrease in viscosity. This behaviour can be explained as follows: Due to the initial stratification, the eddy viscosity in the upper 25 % of the water column is nil, hence the hydraulic resistance is very small. As a result, the flow starts to concentrate in the upper part of the water column, which is exactly the picture shown in Fig. 5.2. However, this is

not a physically sound phenomenon, as the 1DV POINT MODEL does not contain the driving forces to maintain the (initial) salinity gradient.
However, physically meaningful simulations can still be carried out for tidal conditions, as the time scale for the behaviour discussed in the preceding paragraph is much larger than the time scale of the semi-diurnal tidal period. The resulting velocity and eddy viscosity profiles at various times are given in Fig. 5.3a and 3b, showing more or less parabolic viscosity profiles in the lower part of the water column. However, the actual values of ν_T are about 1/3 of the reference values (Fig. 5.1a).
As no turbulence is generated in the upper part of the water column, it is interesting to study whether an additional source in the form of wind-induced stresses does have an effect. For this purpose an additional simulation is carried out, identical to the latter one, but with a wind of 15 m/s. Resulting velocity and eddy viscosity profiles are presented in Fig. 5.4a and 4b, showing very little effect.

The simulations presented in the following sections have all been carried out with the parameter settings of Table 4.1 and a semi-diurnal tide with velocity amplitude U_m = 0.5 m/s and period T = 12.5 hrs, unless mentioned otherwise.

5.2 Effect of M_4 component

The effects of higher harmonic components on the net horizontal sediment transport is well known, and often significant. We therefore study the effects of the higher harmonic M_4-component on the vertical transport processes. Analyses by RIKZ show that $U_4 \approx 0.07\ U_2$, where U_4 is the amplitude of the M_4-velocity component, and U_2 the amplitude of the semi-diurnal velocity component. Simulations with the 1DV POINT MODEL have been carried out for a combination of conditions, summarized in Table 5.1.

	residual flow M_0 [m/s]	M_2 component		M_4 component		sat. conc. C_s [g/l]
		ampl U_2 [m/s]	phase ϕ_2 [deg]	ampl U_4 [m/s]	phase ϕ_4 [deg]	
reference	-	0.5	0.0	-	-	0.13
effect M_4	-	0.5	0.0	0.035	45	0.14
effect M_4	-	0.5	0.0	0.035	0	0.14
effect residual flow	0.035	0.5	0.0	-	-	0.14

Table 5.1: Effect higher harmonics on C_s.

Table 5.1 shows that the effect of an M_4-component on C_s is smaller than 8 %. An additional simulation was carried out for a residual current of 0.035 m/s; the effect appears similar to that of the M_4-component.

We can also estimate the effect of higher harmonics from the scaling laws, assuming $C_s \propto U^n$, 2 where n = 8/3 (or 3):

$$\frac{C_{s,1,2}}{C_{s,1}} \propto \frac{\int_0^{T/4} (U_1 \cos \omega t + U_2 \cos(2\omega t - \phi))^n dt}{\int_0^{T/4} (U_1 \cos \omega t)^n dt} \quad \left[= 1 + \frac{9\pi}{16} \frac{U_2}{U_1} + \frac{21}{10} \frac{U_2^2}{U_1^2} \quad \text{for} \quad n=3 \text{ and } \phi=0 \right] \tag{5.1}$$

in which U_1 and U_2 are the amplitudes of the main and secondary velocity component. Values for $C_{s,1,2} / C_{s,1}$ from a numerical evaluation of equ (5.1) are given in Table 5.2.

	n = 8/3	n = 3
$\phi = 0$	1.11	1.13
$\phi = 45°$	1.18	1.21

Table 5.2: Values of $C_{s,1,2} / C_{s,1}$.

The results for $\phi = 0$ are, within the accuracy of establishing C_s with the 1DV POINT MODEL, in agreement with the effects presented in Table 5.1. For $\phi = 45°$, $C_{s,1,2} / C_{s,1}$ from equ (5.1) is about 10 % larger than obtained with the 1DV POINT MODEL. This difference is probably not within the accuracy of the numerical results, and we must conclude that at present the influence of higher harmonics on C_s is not understood. Possibly, also the smaller tidal time scale of the processes attributed to the M_4-component play a role as well, though the M_4-component is small by itself.

5.3 Effect of wind and waves

The results of the simulations to assess the effect of wind are presented in Fig. 5.5a through 5.5d. As discussed in Section 5.1, the actual wind in November 13/14 was about 7 m/s, and very little effect on the turbulence characteristics is observed. Therefore, simulations with a wind speed of 15 m/s are carried out. Comparison with Fig. 4.4 and 4.5 show only small differences, as was expected from the preliminary simulations described in Section 5.1. We can anticipate that also for simulations with the TRIWAQ-SLIB3D of the Maasmond area wind-induced mixing may be neglected.

The influence of waves with H_{rms} = 1.3m, T_{rms} = 5 s is presented in Fig. 5.6a through 5.6d, showing an increase in saturation concentration up to $C_s \approx 0.23$ g/l. Note that for steady flow conditions the effect of wind yields an increase in eddy diffusivity by about 20 %. As $C_s \propto U^{8/3}$, one would expect an increase of C_s to $1.3 \times 1.2^{8/3} = 0.21$ g/l, which is close to the model value of 0.23 g/l. Comparison of Fig. 5.6b with 4.4b shows similar eddy diffusivity profiles, as expected. Contrary to the preceding paragraph, we must conclude that simulations of the sediment transport in the Maasmond area with the TRIWAQ-SLIB3D do require the inclusion of wave-induced mixing effects.

5.4 Effect of salinity induced stratification

In many estuaries and coastal zones significant vertical density gradients occur as a result of fresh water flowing over the sea water. This is also the case in the Maasmond area, as shown in Chapter 2. Such gradients do affect the turbulence properties significantly, as discussed in Section 5.1. Therefore, a series of simulations is carried out to study the effect of a fresh-saline water induced vertical density gradient; as in Section 5.1, this gradient is kept constant throughout the simulation by switching off the vertical mixing processes for salt (not for sediment, of course), except for the first time step to smoothen the steep gradient around z = 12 m.

The results are again presented in the form of isolutals in depth-time diagrams shown in Fig. 5.7a, 7c and 7d and 5.8a and 8b, and for one series in the form of vertical profiles at t = 1900 min in Fig. 5.7b. Note that, though the initial salinity induced density kink is positioned at z = 12 m, the first diffusion step is to generate a more gentle gradient across the upper half of the water column (Fig. 5.7b). As a result, sediment is mixed only over the lower half of the water column, e.g. Fig. 5.7a, 7c through 5.8b.

The saturation concentration for the case without wind and waves amounts to $C_s \approx 0.14$ kg/m^3 and with wind and waves to $C_s \approx 0.24$ kg/m^3. It is remarkable that these values are (a bit) larger than for the simulations without salinity-induced gradients; the total load however is almost identical, which would imply that homogeneous and salinity-induced stratified flow would be able to carry the same amount of sediment. Apparently, the scaling law (equ (4.6) or (4.16)) is also locally valid: a decrease in effective water (mixing) depth results in a proportional increase in C_s. Of course, we will need experimental data to verify this conclusion; these are not available at present though. For the time being we must conclude that salinity-induced stratification effects should be included in simulations with the TRIWAQ-SLIB3D of the Maasmond area.

5.5 Effect of water-bed exchanges

All simulations presented in the previous sections of this report have been carried out without water-bed exchange processes. In fact, the bed is treated as an impermeable and inert boundary. All sediment settling on this bed still forms part of the water column, behaving as a Newtonian fluid. Apart form possible non-Newtonian effects, this is a fair approach for the Maasmond conditions, as the actual seabed mainly consists of sand.

However, it is interesting to study the effects of an active bed in the sense that settling does remove sediment form the water column, and (re-)erosion of the bed may take place under favourable conditions. These bed dynamics are modelled with the classical formulae by Krone and Partheniades (equ (3.26) & (3.27)):

$$E = M\left(\frac{\tau_b}{\tau_e} - 1\right) \quad \text{for} \quad \tau_b > \tau_e \tag{5.1}$$

$$D = W_s c\left(1 - \frac{\tau_b}{\tau_d}\right) \quad \text{for} \quad \tau_b < \tau_d \tag{5.2}$$

in which E and D are the erosion and deposition rate respectively, τ_b is the actual bed shear stress,

including the possible effects of waves, M is an erosion parameter, and τ_e and τ_d are threshold values for erosion and deposition. In the present simulations, the latter three parameters have been set at an arbitrary, but reasonable value, as shown in Table 5.3.

M	0.1 10^{-3}	kg/m^2s
τ_e	0.5	Pa
τ_d	0.1	Pa

Table 5.3: Mud parameters

Note that in this approach we assume that the effect of waves is limited to an enhancement of the bed shear stress; no interbed processes, as stress accumulation, liquefaction, etc. are accounted for.

First, a series of simulations is carried out for tidal flow only, i.e. wind nor waves. The resulting isolutals are presented in Fig. 5.9 for an initial sediment concentration $\mathbf{C_0 = 5.0\ g/l}$. We observe a rapid decline of the suspended sediment concentration over the settling time scale $T_s = h/W_s \approx$ 530 min. After most of the sediment is removed from the water column, the flow is able to carry a remaining fraction of about 0.1 g/l in suspension. Relatively, the erosion rate is so small, that it does not really contribute to this picture. It was argued earlier on qualitative grounds (Winterwerp, 1996) that for (tidal) flow conditions the flow will always be able to carry sediment eroded from the bed, as the vertical mixing scales with U^3, whereas the flow-induced erosion rate scales with U^2. The picture presented in Fig. 5.9 is qualitatively identical for all initial concentrations.
Note that in this approach the sediment is immediately removed from the water column, maintaining the rigid bed characteristics relevant for the turbulence boundary conditions. This is a sound approach for sandy sediment, but not for cohesive sediment: large rates of sedimentation will result in a non-consolidated soft bed with different turbulence properties. In fact in that case the near bed sediment will remain part of the water column, an approach followed throughout this report, apart, of course, from possible non-Newtonian effects. In that case, thixotropic time scales become to play a role.

In a second series of numerical experiments, the effects of water-bed exchange processes are studied for the case with wind and waves (Table 2.1). After some trial and error the clearest presentation of these effects is achieved through a simulation with zero initial concentration. All sediment in the water column originates from erosion. The resulting isolutals are presented in Fig. 5.10 showing that initially sediment is entrained into the water column, but after about 500 min the concentration profile collapses. This is due to a continuous supply of sediment from the bed, exceeding the sedimentation processes significantly. Hence, rapidly the amount of sediment exceeds the saturation concentration, and turbulence collapses, forming a high concentrated near bed layer (fluid mud layer). This process can be regarded as a self-saturating process. Also this effect was predicted earlier (Winterwerp, 1996) on qualitative grounds, and can be understood by realizing that the mixing and erosive properties of the flow have now been separated by the addition of an independent erosion agent (e.g. waves).
Again it should be noted that this simulation can only be used for a qualitative understanding of the effect of wave-induced erosion on the concentration profile. In reality, the formation of a fluid mud layer will affect the erosive properties of the surface waves through a damping of these

waves themselves and through the protection of the underlying bed. Moreover, in many cases the sea bed will not be horizontal, and the fluid mud will/may flow away, leaving the bed again exposed to wave effects.

5.6 Influence of buoyancy effects

The influence of sediment induced buoyancy effects is studied by omitting the contribution of the suspended sediment concentration in the equation of state (equ (3.29)). The numerical results are plotted in Fig. 5.11. Comparison with those presented in Fig. 4.6a shows a large difference in vertical concentration distribution: Fig. 5.11 shows no tendency of high near bed concentrations around slack water, as observed during SILTMAN field measurements (e.g. Chapter 2).
It should be concluded that it is not possible, not even in a qualitative way, to simulate the observed high concentrated near bed mud suspensions with a model excluding sediment-induced buoyancy effects.

5.7 Behaviour of fine sand

The sea bed in the Maasmond area contains sand with a median diameter $D_{50} \approx 200$ μm. The 1DV POINT MODEL allows us to study whether this sand can be suspended to contribute (significantly) to the observed turbidity at the various semi-permanent measuring stations. For this purpose two simulations have been carried out, both for steady flow conditions (U = 0.6 m/s) and with Van Rijn's pick-up function (equ (3.29)) as boundary condition. In run 1 the effect of flow only is studied, whereas in run 2, the effect of waves with a significant wave height $H_{1/3} = 3$ is included. The results are presented in Fig. 5.12, showing that for flow only, the near-bed sediment concentration does not exceed a few 10 mg/l. Waves do increase the suspended sediment concentration considerably, but not beyond 0.5 g/l at the levels of the turbidity sensors. Hence we can conclude that it is not likely that the measurements of the suspended sediment concentrations at the semi-permanent Stations B, G, H and I are diluted by considerable amounts of 200 μm sand particles. Moreover, their contribution to the optical sensor signal will be even smaller, as the sensor was calibrated for much finer material.

A few simulations were carried out for much finer sand ($D_{50} = 50$ μm) under tidal conditions. We now allow the sediment to form a rigid bed after deposition, and apply Van Rijn's pick-up function again. In fact we now assume that the time scales for thixotropy/consolidation and erosion are very small: the near bed sediment dynamics respond instantaneous to the variations in hydrodynamics, and turbulence production is not affected by a near-bed high-concentrated suspension.
Results for two different initial conditions (i.e. $C_0 = 0$ and $C_0 = 0.5$ g/l) are presented in Fig. 5.13 and 5.14, showing identical concentration verticals after some initial time period. This, of course, is to be expected: the availability of sediment is unlimited, and no irreversible damping of turbulence occurs, as a result of which the ultimate concentration distribution is not affected by initial conditions.

5.8 Summary and discussion

The simulations with the 1DV POINT MODEL show that also for unsteady (tidal) flow conditions a saturation concentration C_s can be found, beyond which no sediment can be kept in suspension. For tidal flow conditions C_s is defined as the depth-averaged sediment concentration that can be carried by the flow in suspension during at least one small interval of the tidal period. The actual value of C_s is defined more arbitrary then for steady flow, as for tidal flow a (small) range exists before the entire concentration profile collapses. This is attributed to the specific time scales for the Maasmond area ($T_s \approx 1$). For Maasmond conditions, i.e. for the time scales relevant in the Maasmond area, C_s seems to scale with $U^{8/3}$ and $W_s^{-2/3}$.

The results of the various simulations, all carried out for tidal flow with an amplitude of U_m = 0.5 m/s, are summarized in Fig. 5.15.

The effects of a (small) M_4-component, hindered settling and a wind velocity up to 15 m/s are small. The small effect of a higher harmonic is not entirely understood; it may be related to the time scale of the M_4-period. The effect of hindered settling is mainly a decrease in effective settling velocity, and as such does cause a (small) increase in C_s.

Waves appear to increase C_s considerably, though it should be borne in mind that the present Grant & Madsen formulation does overestimate wave-induced mixing effects. However, the effect is so large that the increase in effective hydraulic roughness, hence turbulence production, should be accounted for in simulating the transport of near-saturated sediment suspensions, hence in TRIWAQ-SLIB3D.

The effect of salinity induced stratification is a reduction of the effective mixing depth. Apparently, the scaling laws are also locally applicable, and the decrease in effective water depth results in a proportional increase in the local saturation concentration. As a consequence, the total load that can be carried by the flow is not affected by such salinity stratification.
The vertical distribution of the suspended sediment, though, hence its horizontal transport, of course, is affected by the salinity effects and should therefore be accounted for in TRIWAQ-SLIB3D-simulations of the Maasmond area.

The simulations with water-bed exchange processes do not include the effects of these processes on the bed properties (hydraulic roughness, damping of waves, etc.), and can therefore only be regarded as indicative. An interesting conclusion though is that, in contrast to flow-induced bed erosion, in the case of wave-induced erosion, self-saturation of the flow can occur.

The influence of sediment-induced buoyancy effects on the concentration profile is large, as shown from a simulation omitting the contribution of sediment concentration to the equation of state. In that case a more or less Rouse-like profile is computed, and no near bed high concentrated mud suspensions are found.

Medium grained sand (D_{50} = 200 μm) cannot be brought in suspension to a degree that the turbidity measurements are seriously diluted by the presence of sand particles.

From these results a series of preliminary conclusions can be drawn with respect to the dynamics of the concentration profiles observed at the semi-permanent measuring stations B, G, H and I. The data in Fig. 2.8 and 2.9 indicate a tidal amplitude of about 0.6 - 0.9 m/s, hence a saturation

concentration of about C_s = 0.3 to 0.8 g/l (for U_m = 0.8 m/s, C_s = 0.56 g/l) at a settling velocity of 0.5 mm/s. Waves could enhance these C_s-values considerably.
The simulations for U_m = 0.8 m/s, C_0 = 0.56 g/l, and no initial salinity-induced density gradients show near bed concentrations values up to 15 g/l.
Hence we can conclude that, for the parameters selected, the sensitivity analyses yield suspended sediment concentrations similar to those observed at the semi-permanent measuring stations. These will therefore be used in the simulations of Chapter 6.

6. Calibration, analyses and prognostic simulations

6.1 General

The simulations described in this chapter are carried out for the hydro-meteo conditions measured during November 13 & 14 and November 20 & 21, 1996, as during these days large suspended sediment concentrations were measured, and, equally important, a consistent set of field data are available. The main part of the simulations is carried out for station B, as both velocity and concentration are available here, and station B is still relatively unaffected by the presence of the Maasgeul. More details on these periods can be found in Chapter 2 of this report.

The observed wave climate at the Maasgeul station is schematisized in a series of constant and with time linearly varying wave heights, as shown in Fig. 6.1. The relevant mean wave heights H_{rms} and corresponding wave periods T_{rms} have been established with the procedure outlined in Section 2.2, but now we assume that the waves are primarily from NNW-direction. The actual wave parameters used for the simulations are summarized in Table 6.1.

date	time [min]	H_{rms} [m]	T_{rms} [s]	ω [s^{-1}]
Nov. 13 & 14, 00:00 hr	0	2.6	6.4	1.0
	130	2.6	6.4	1.0
	430	1.6	5.6	1.1
	1530	1.6	5.6	1.1
	1820	1.0	5.1	1.2
	2300	1.0	5.1	1.2
	2560	0.6	4.8	1.3
	2880	0.6	4.8	1.3
Nov. 21 & 22, 00:00 hr	0	2.3	6.1	1.0
	1090	1.5	5.5	1.1
	1860	1.5	5.5	1.1
	2270	2.2	6.2	1.0
	2280	2.0	5.9	1.1

Table 6.1: Schematisized wave climate.

Though simulations have been carried out both with and without waves, all simulations were done without wind-induced shear stresses at the water surface.

The flow velocity was measured at 0.35 m height above the bed. To obtain the representative depth-averaged velocity U, a logarithmic velocity profile is assumed. For a Chézy coefficient of

65 $m^{1/2}/s$ and a water depth h = 16 m, we find $U = 1.54 \times u_{z=0.35m}$ The observed data have been multiplied with this value after manually removing a few of the most extreme peaks in the measured velocities. Next, the data set is smoothed by averaging the velocity over three neighbouring points. This procedure is done twice. The resulting data file is presented in Fig. 6.2 and 6.3, together with the original data.

Finally, a positive/negative sign was added to the data to account for the variation in flow direction - the results of this latter procedure are shown in Fig. 6.4 and 6.5.

All simulations are carried out for the 48 hours covered by the data, plus 22 hours before. The latter was done to obtain a realistic concentration profile at the start of the actual simulations, as only vertically homogeneous concentration profiles can be entered into the 1DV POINT MODEL. During these 22 hours, the velocity profile of the first simulation day is repeated, and the wave height is set at the value at the start of the 48-hour-simulation.

Tidal variations in water level are not taken into account because, as $\Delta h/h$ is small. This also avoids difficulties in interpretation arising from such water level variations.

A last remark concerns the HYDROLAB-data at 2 and 7 m height above the bed. These are available only for station H (see Chapter 2) but still have been included in the graphs in the next sections, as their trend is expected to be similar for all four measuring stations. It should be borne in mind though that the flow conditions at station H will differ from the other locations; in particular it is expected that the flow velocities will be substantially higher than at for instance station B.

6.2 Calibration of the 1DV POINT MODEL and analysis of the data

The simulations have all, but one, been carried out with a constant settling velocity. However, quite early during the calibration process it became clear that the effects of hindered settling have to be accounted for somehow, otherwise the observed concentration profiles could not be simulated at all. Though a full flocculation model is implemented in the 1DV POINT MODEL (Winterwerp and Uittenbogaard, 1997), a simple approximation is applied here, reading:

$$W_s = W_{s,0}(1 - \alpha c)^5 \tag{6.1}$$

in which α is a measure for the floc size. Note that $\alpha = 0.1$ corresponds to a floc size of about 1 mm (Winterwerp, 1998).

To facilitate the analyses of the results, the computed bed shear stresses for the simulation periods of 13 & 14 and 21 & 22 November are plotted in Fig. 6.4 and 6.5, together with the computed depth-averaged flow velocity. Note that the bed shear stress always exceeds the threshold value for deposition of about 0.1 Pa, from which it can be concluded that no sedimentation of mud can take place during these periods.

Table 6.2 gives a summary of all simulations presented in this chapter.

Fig. 6.7 through 6.10 show the large effect of hindered settling. If this effect is not, or only partly taken into account, sediment concentrations, hence their gradients near the bed, become too large

to resuspend the sediment, and a (thin) layer of hyper-concentrated sediment is then being formed. Vice versa, when α is too large, the settling velocity will be reduced too much, and no high-concentrated near-bed suspensions are found at all (Fig. 6.10).
The large value of α also prevents the formation of fluid mud ($c \approx 100$ g/l). For the present simulations this is acceptable, as the time scale for such formation is too large to be realized during slack tide conditions. This implies that a full flocculation model is required to include the effects of fluid mud formation.

run	Fig.	simulation time in November	W_s [mm/s]	floc model*)	α (6.1)	C_0 [g/l]	special features
P02	6.7	13/14	0.6	no	0	0.5	surface waves
P18	6.8	13/14	0.6	A	0.05	0.5	surface waves
P04	6.9	13/14	0.5	B	0.1	0.5	surface waves
P05	6.10	13/14	0.5	C	0.2	0.5	surface waves
P12	6.11	13/14	0.5	B	0.1	0.5	surface & internal waves
P11	6.12	13/14	0.5	B	0.1	0.5	surface waves and erosion
P13	6.13	13/14	0.6	B	0.1	0.5	surface waves: **reference parameters**
P16	6.14	13/14	0.6	B	0.1	0.3	surface waves
P14	6.15	13/14	1.0	B	0.1	0.3	surface waves
P15	6.16	13/14	0.6	B	0.1	0.5	surface waves and salinity
P17	6.17	13/14	0.6	B	0.2	0.5	no surface waves
F04	6.18	13/14		full model		0.5	surface & internal waves
P21	6.19	13/14	0.6	B	0.1	0.5	surface waves and positive U only
P19	6.20	21/22	0.6	B	0.1	0.5	surface waves
P20	6.21	21/22	0.6	B	0.1	0.3	surface waves

Table 6.2: Summary of calibration runs (*) refers to code in figures).

Note that $\alpha = 0.05$ in equ (6.1) corresponds to a particle diameter of about $D_{max} \approx 0.5$ mm and a maximal possible concentration in the 1DV-simulations of $c_{max} \approx 20$ g/l. The latter value is still in the range of the observed data as the calibration may be off by a factor 2 (e.g. Section 2.1). This stresses again the great need to carry out a detailed calibration of turbidity sensors, especially when they are deployed for such a long time.

Surprisingly, the major effect of including the mixing by internal waves on the concentration profile is found higher in the water column; their effect on the near-bed concentrations is fairly small, e.g. Fig. 6.11. This will be discussed below.

Inspection of Fig. 6.9 shows that the computed sediment concentrations near the bed are of the same order of magnitude as observed values. However, several peaks in these observations are not predicted; some of them occurring at large flow velocities. Therefore the possible contribution of erosion is investigated, using the erosion formula by Partheniades:

$$E = M\left(\frac{\tau_b}{\tau_e} - 1\right) \quad \text{for} \quad \tau_b > \tau_e \tag{6.2}$$

in which the following parameter settings have been used: M = 10^{-5} kg/m^{2}s and τ_e = 0.5 Pa. The results, presented in Fig. 6.12, show a gradual increase in sediment concentration especially higher in the water column, which will continue until the flow becomes fully saturated after which the concentration profile collapses, as predicted in Section 5.5.

It should be noted though, that it is not very likely that the sea bed will contain large quantities of mud that can be resuspended, as in simulation P12, because no conditions favourable for deposition were met prior to the simulation time, e.g. Fig. 6.4 (τ_d > 0.1 Pa). We conclude therefore that the peaks in the concentration distribution cannot be attributed to erosion of mud from the sea bed.
Moreover, it is not likely that these peaks are due to sand particles, brought in suspension by the flow or waves. Hence, it must be concluded that the peaks in the observed sediment concentrations must be due to advective effects.

The best agreement between observations and simulations is obtained for the parameter setting of run P13 - see Fig. 6.13. Therefore, the numerical results are analyzed in detail for these conditions with the use of Fig. 6.13*. Around t = 1800 the simulations and observations agree well, and the sediment dynamics are analyzed for six times, referred to as t = a through t = f. At t = a, when slack water occurs, we observe an increase in sediment concentration at z = 0.15 m, but hardly any changes higher in the water column. This increase is apparently caused by deposition. It continues until the flow velocity has exceeded some threshold value at t = b, after which a reverse trend is observed caused by a remixing of the sediment. Only at t = c, approximately 1 hr later, the concentration starts to rise at z = 0.55 m, which agrees with the extremely small eddy diffusivity at that time (see below). Again some time later at t = d, the concentration at z = 2 m starts to increase, with a simultaneous decrease of the concentration at z = 0.15 and z = 0.55 m. Note that also at z = 7 m the concentration now starts to decrease. Only at t = e, the concentration at z = 7 m starts to increase, at the cost of the concentration at z = 2 m. Then at t = f this process repeats again, starting with a decrease of the concentration high in the water column, and an increase near the bed.
Note that though the wave activity decreases sharply around t = 1440, no spectacular effect on the concentration profile is observed.

This picture is qualitatively observed at other times as well, with an asymmetrical trend because of the positive velocities are larger than the negative ones. For some later time span, vertical details of the flow have been plotted in Fig. 6.13a through 13f. At t = 3150 and t = 3200 we observe two interfaces, one around z = 0.3 m, and a second near z = 12 m. The concentration near the bed cannot exceed c $\approx$ 10 g/l because of α = 0.1 in the hindered settling formula. Note the extreme small values of the eddy diffusivity two to three orders of magnitude smaller than the values for non stratified conditions: $\Gamma_{max} \approx 0.06$ m^2/s. At t = 3300 the flow velocity has increased so much that the suspension is being remixed. In the mean time the second interface is still lowering, indicating that during the 1.5 hrs monitored here, the water column can be divided in three more or less independently behaving parts. This is further substantiated by the large

values of the gradient Richardson number Ri at the two interfaces, and explains the influence of internal waves higher in the water column. At t = 3400 just one interface is observed and the lower part of the water column carries all the sediment. However, a new deposition phase has already started.
As a result of the larger positive velocities, mixing is more rapid during this phase of the tide. At t = 3600, a 2 m thick high-concentrated near-bed layer is observed. At t = 3700, the whole mass of sediment is mixed entirely over the water column, and a logarithmic velocity profile is restored with an almost parabolic diffusivity profile.

Simulations at a considerable smaller initial sediment concentration of C_0 = 0.3 g/l show an almost homogeneous concentration vertical (Fig. 6.14), as expected, as this value is substantially smaller than the saturation concentration.
A simultaneous increase of the settling velocity up to W_s = 1 mm/s shows a picture (Fig. 6.15) comparable to that of Fig. 6.13, though with more variation in the concentration peaks. The concentration higher in the water column though becomes smaller, and during a major part of the tidal period the flow is not able to carry sediment at z = 7 m. The decrease in concentration at z = 7 m corresponds to an increase in concentration at z = 2 m.

Simulations including the effect of salinity-induced stratification have also been carried out. From the analyses in Section 5.4 it was concluded that salinity stratification merely limits the effective water (mixing) depth, whereas the flow is still able to carry the same load. The results, presented in Fig. 6.16 still resemble those of Fig. 6.13 qualitatively, though the temporal variations of the sediment concentration are more pronounced. Given the fact that actual salinity information is not available, and that the salinity distribution probably will vary considerable with the phasing of the tide, no further simulations with salinity-induced stratification have been carried out.

Exclusion of the mixing effects by surface waves has a fairly small influence - compare Fig. 6.17 with 6.13. This seems to contradict our earlier conclusions that these effects do contribute significantly to the value of C_s. The explanation for this apparent paradox is twofold:

1. The sediment suspension around Station B is probably still sub-saturated,
2. The simulations are relatively short, and a collapse of the concentration profile takes considerable time (e.g. Section 6.3).

Because of the large effect of flocculation, c.q. hindered settling, a few simulations were carried out with the full flocculation model implemented in the 1DV POINT MODEL. The initial parameter settings were identical to those presented by Winterwerp and Uittenbogaard (1997). After some trial and error though the parameters were set at the values found for Ems mud (Winterwerp, 1998). The results are presented in Fig. 6.18, showing no resemblance with the observations at all. The main reason for this anomaly is that the settling velocity near the interface becomes far too large in the model; more realistic values would require a further tuning of the model parameters. More research is needed to cope with this problem and the important time scale for flocculation.

Finally, a run is carried out in which the depth-mean flow velocity is kept positive only, as in the original data set. The result is given in Fig. 6.19. Comparison with Fig 6.13 shows large differences. We believe that simulations with only positive depth-mean velocity are not realistic, as this approach does violate the harmony between flow reversal and advective effects. In fact, the simulations of run P21 showed such weird vertical velocity distributions, that the results cannot be trusted at all.

From the preceding analyses a new insight on the behaviour of the concentration distribution has emerged. This picture suggests that the concentration distribution and the subsequent sediment transport is governed by a cycle of deposition and resuspension (mixing) at a concentration level that affects the turbulence mixing characteristics significantly, i.e. the concentration is close to the saturation level. The major question now of course arises as to whether this behaviour observed in the simulations represents physical reality. First we note that the measured peaks at z = 0.15 and z = 0.55 m always occur simultaneously (e.g. Fig. 6.13). Hence a possible cycle of deposition and remixing cannot be deduced from these data. The hypothesis that a thin layer of fluid mud below z = 0.15 m is cyclically entrained and formed again, provides a possible explanation for the observed data. Given a depth-mean concentration of the order of 0.5 g/l, a fluid mud layer of thickness 0.1 m would yield a concentration of about 50 to 100 g/l. This is a reasonable value for fluid mud layers. However, experimental and theoretical studies (Kranenburg and Winterwerp, 1996 and Winterwerp and Kranenburg, 1996) show that entrainment rates for the conditions at station B would amount to at least a few dm per hour. Hence, such a fluid mud layer cannot be stable, and this hypothesis should therefore be rejected.
We observe, however, a reverse trend in increasing/decreasing concentrations near the bed and higher in the water column. Though the concentrations at z = 2 and 7 m were measured at station H, this station is so close to station B, that the variations in time should be more or less similar. Such a reverse trend strongly indicates a cycle of deposition and remixing.
The observation that the peaks, which are not simulated by the 1DV POINT MODEL, occur at relative large flow velocity suggest horizontal advective effects, because erosional effects are not likely, as explained above. Another explanation of this difference might be sought in the effects of a non-homogeneous sediment mixture, including possibly the contribution of (fine) sand.
Summarizing these arguments we can conclude that we have no definite proof that the picture predicted with the 1DV POINT MODEL accurately describes the physical processes in the Maasmond area during storm conditions, but that no likely alternative picture can be hypothesized. Therefore, for the time being, we anticipate that the concentration distribution measured at the semi-permanent measurement station B, and the subsequent sediment transport, is governed by a cycle of deposition and resuspension at a concentration level that affects the turbulence mixing characteristics significantly, i.e. close the saturation level.

With the parameter settings for run P13, a simulation has been carried out for the hydro-meteo conditions of November 21 and 22, the results of which are shown in Fig. 6.20. Apparently, the computed concentrations are too high, which may be caused by an overestimation of the volume of sediment in the water column. Therefore, a second run was made with an initial depth-averaged concentration of C_0 = 0.3 g/l - see Fig. 6.21. The concentration values are a bit low now, however.
It is remarkable that the measured concentrations higher in the water column do exceed the computed values considerably, contrary to the simulations for November 13 & 14. At present, no explanation was found for this difference, except for a possible smaller settling velocity. However, no data are available to confirm this hypothesis.

6.3 Prognostic simulations

In this chapter a series of simulations is presented for conditions expected in the Maasgeul off shore, and in between the breakwaters. As actual measurements of velocity nor suspended sediment concentration have been carried out here, an estimate has been made of the velocity field. The measurements at station B are included in the graphs for comparison with the earlier

simulations.

For simulating the changes in suspended sediment concentration, while advected horizontally from shallow (Station B) to deeper water in the Maasgeul, the 1DV POINT MODEL was used in a Langrangian fashion by increasing water depth and decreasing flow velocity with travel time. First the effect of a deepening of the water depth from 16 m at station B to 24 m within the Maasgeul is studied. For this purpose the water depth is increased by a factor 1.5 immediately, whereas the flow velocity is decreased by the same factor, but only at t = 1320 min (start of actual 48-hours-simulation). The result is presented in Fig. 6.22 showing a gradual collapse of the concentration profile, initiated in the upper part of the water column. It should be noted that the time scale of this collapse, hence the forming of a fluid mud layer, is governed by the time scale for settling, which is by far insufficient to explain the absence of considerable volumes sediment in the water column in between the breakwaters, as measured by Rijkswaterstaat. It is hypothesized that the formation of fluid mud layers is governed by the interaction of a collapse of the concentration profile caused by exceeding the saturation level, together with the generation of a sediment-driven density current.

Next a series of simulations is carried out for hypothetical hydro-meteo conditions with a sinusoidal tide and the initial salinity profile given on this page, as measured on April 8, 1997. Maximal ebb velocity amounts to 0.5 m/s and the maximal flood velocity to 0.8 m/s, and a significant wave height $H_{1/3}$ = 3 m is applied. The conditions for the three simulations are summarized in Table 6.3. Initial conditions are identical to those of reference run P13 (Table 6.2).

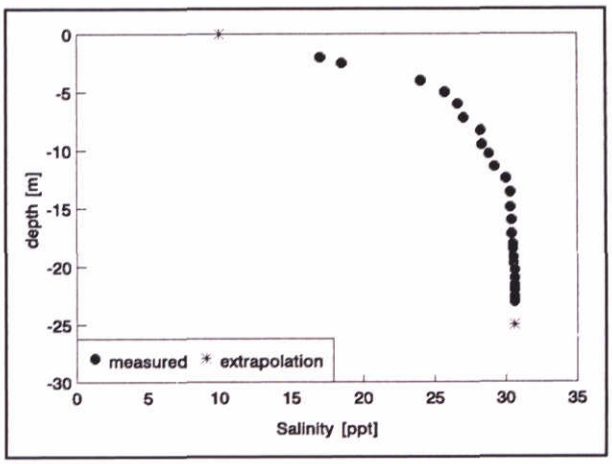

The results of the simulations are presented in Fig. 6.23 through 6.25. Fig. 6.23a shows the isolutals for simulation Q04 with conditions characteristic for outside the Maasgeul; time series at h = 0.15, 0.55, 2 and 7 m above the bed are shown in Fig. 6.23b. The concentrations in the lower part of the water column are similar to those of run P13 (Fig. 6.13), at the two upper stations they are a bit smaller. In the upper half of the water column no sediment can be carried by the flow because of the salinity-induced stratification. These results suggest that for Q04-conditions, the flow is able to carry the sediment in suspension.

Fig. 6.24 shows the results for the conditions off shore (run Q05), but within the Maasgeul. We observe that the concentration distribution near the bed is identical to that of run Q04. Only higher in the water column differences are found: the water-mud interface for run Q05 is lower than for run Q04. The explanation for this behaviour near the bed is the use of the hindered settling formulation (6.1), which limits the maximal near-bed concentration. Fig. 6.24a shows a gradual decrease in the thickness of the near-bed layer: eventually all sediment will settle into the near-bed layer and cannot be resuspended any more.

	run Q04	run Q05	run Q06
	off shore outside Maasgeul	off shore inside Maasgeul	in between breakwaters
h	17 m	25 m	25 m
U	$U = 0.15 + 0.65\cos\frac{2\pi t}{T}$		
$H_{1/3}$	3 m		-
H_{rms}	2.1 m		-
T_{rms}	6.3 s		-
C_0	0.6 g/l		
W_s	0.5 mm/s		
salinity profile	yes		

Table 6.3: Parameters for prognostic simulations.

The difference with simulation Q06 (no waves) is very small and limited to the upper station. The reason for this small difference is that the effect of 3 m waves at a depth of 25 m is small anyway: the wave-induced bed shear stress is of the same order as the flow-induced bed shear stress. Also run Q06 will eventually show a total collapse of the concentration profile.

The results of the runs Q04 through Q06 should be considered in the light that:

1. The velocity for the three runs is kept constant - this certainly will not be the case in the Maasmond area - whereas the concentration distribution is highly sensitive to the flow velocity.
2. The salinity distribution is kept constant throughout the simulations. In reality, this distribution will also alter throughout the tidal period.
3. The hindered settling effects and the dynamics of the near-bed high-concentrated sediment layer are only marginally accounted for; the actual dynamics are much more complicated and a more sophisticated description is required.

From our scaling laws we deduce that the sediment carrying capacity of the flow, while passing the Maasgeul, reduces to about 10 to 20 % because of an increase in water depth from 16 to 24 m and a decrease in flow velocity by 2/3. Moreover, the contribution of surface waves to the vertical mixing processes vanishes, yielding an additional reduction by about 20 %. This analysis is confirmed by the results of the prognostic simulations, especially the one presented in Fig. 6.22, showing a rapid collapse of the sediment concentration profile.

references

Borsje, P, 1997, "Overdrachtsfactoren sensoren", Delft Hydraulics letter VM360/97 (B420), d.d. May 26, 1997.

Eckart, 1958, "Properties of water, part II. The equation of state of water and sea water at low-temperature and pressures". Am.J..Sc., vol. 256, pp. 225-240.

Galland, J.-C., Laurence, D. and Teisson, C., 1997, "Simulating turbulent vertical exchange of mud with a Reynolds stress model", Proceedings of the 4th Nearshore and Estuarine Cohesive Sediment Transport Conference INTERCOH'94, Wallingford, UK, John Wiley & Sons, pp 439-448.

Grant, W.D. and Madsen, O.S., 1979, "Combined wave and current interaction with a rough bottom", J. Geophys. Res., vol. 84, no. C4, pp. 1797-1808.

Hart, W.I.J., van 't, 1996, "Meetverslag ms. Holland week 48a, 1995", Rijkswaterstaat, Directorate North Sea, SILTMAN project.

Karelse, M., 1974, "Vertical exchange coefficient in stratified flows", Delft Hydraulics, Report R880 (ed. H.C.N. Breusers).

Kranenburg, C., 1992, "Hindered settling and consolidation of mud - analytical results", Delft University of Technology, Department of Civil Engineering, Report 11-92.

Kranenburg, C., 1994, "On the fractal structure of cohesive sediment aggregates", Estuarine, Coastal and Shelf Science, Vol. 39, pp 451-460.

Kranenburg, C. and Winterwerp, J.C., 1997, "Erosion of fluid mud layers. I: entrainment model", ASCE, Journal of Hydraulic Engineering, Vol 123, No 6, pp 504-511.

Munk W.H. and Anderson, E.R., 1948, "Notes on a theory of the thermocline", Journal of Marine Research, Vol.1, pp 276-295.

OCN, The Oceanographic Company of the Netherlands, 1996, "SILTMAN (2) - Eindrapportage in-situ metingen", referentie 127.01.

OCN, The Oceanographic Company of the Netherlands, July 1997, "Maasmond Wintermeting 1995/1996", CD-rom Ref. 216.21.

Rijkswaterstaat, Directorate North Sea, Hydro Meteo Centrum Rijnmond, 1996, "Maandbulletin t.b.v. vaalgeulbeheer, Februari 1996 en November 1996" (in Dutch).

Rijn, L.C. van, 1987, "Mathematical modelling of morhological processes in the case of suspended sediment transport", PhD thesis, Delft University of Technology, also Delft Hydraulics Communications No 382.

Smith, S.D. and Banke, E.G., 1975, "Variation of the sea surface drag coefficient with wind-speed", Quarterly Journal of the Royal Meteorological Society, Vol 101, pp 665-673.

Roskam, B., 1995, "Golfklimaten bij EUR en LEG t.b.v. Maasvlakte", MER werkdocument RWS-RIKZ, Rapport RIKZ/OS-95.111x (in Dutch).

Simonin, O., Uittenbogaard, R.E., Baron, F. and Viollet, P.L., 1989, "Possibilities and limitations to simulate turbulence fluxes of mass and momentum, measured in a steady stratified mixing layer", Proceedings of the XXIII IAHR Congress, Ottawa, August 21-25, published by National Ressearch Council Canada, pp A55-A62.

Soulsby, R.L., Hamm, L., Klopman, G., Myrhaug, D., Simons, R.R. and Thomas, G.P., 1993, "Wave-current interaction within and outside the bottom boundary layer", Coastal Engineering, vol. 21, pp. 41-69.

Teisson, C., Simonin, O., Galland, J.-C. and Laurence, D., 1992, "Turbulence and mud simulation: a Reynolds stress model and a two-phase flow model", Proceedings of the 23nd International Conference on Coastal Engineering, Venice, pp 2853-2866.

Turner, J.S., 1973, "Buoyancy effects in fluids", Cambridge at the University Press.

Uittenbogaard, R.E., 1994, "Physics of turbulence; technical report on subtask5.2", MAST-VERIPARSE-project, Delft Hydraulics, Report Z649.

Uittenbogaard, R.E., Winterwerp, J.C., Kester, J.A.Th.M. van and Leepel, H., 1996, "3D Cohesive Sediment Transport; a preparatory study about implementation in DELFT3D", Delft Hydraulics, report Z1022.

Velden, E.T.J.M. van der, 1990, "Coastal Engineering, Volume II", Delft University of Technology, Department of Civil Engineering, lecture series f7.

Verlaan, P. and Spanhoff, R, 1994, "Siltation in the Maasmond, Inventory and re-analysis", OCN, July 1994. (in Dutch)

Winterwerp, J.C., 1996, "HCBS, High Concentrated Benthic Suspensions; SILTMAN prepatory study", Delft Hydraulics, Report Z1013 (in Dutch).

Winterwerp, J.C. and Uittenbogaard, R.E., 1997, "Sediment transport and fluid mud flow; Physical mud properties and parameterization of vertical transport processes SILTMAN - set-up of a POINT-MUD MODEL", Delft Hydraulics, Report Z2005.

Winterwerp, J.C. and Kranenburg, C., 1997, "Erosion of fluid mud layers. II: experiments and model validation", ASCE, Journal of Hydraulic Engineering, Vol 123, No 6, pp 512-519.

Winterwerp, J.C., 1998, "A simple model for turbulence induced flocculation of cohesive sediment", Journal of Hydraulic Research, scheduled for publication February 1998.

Woudenberg, C. van, 1997, "First results of preliminary measurements in the Calandkanaal/Beerkanaal", oral information.

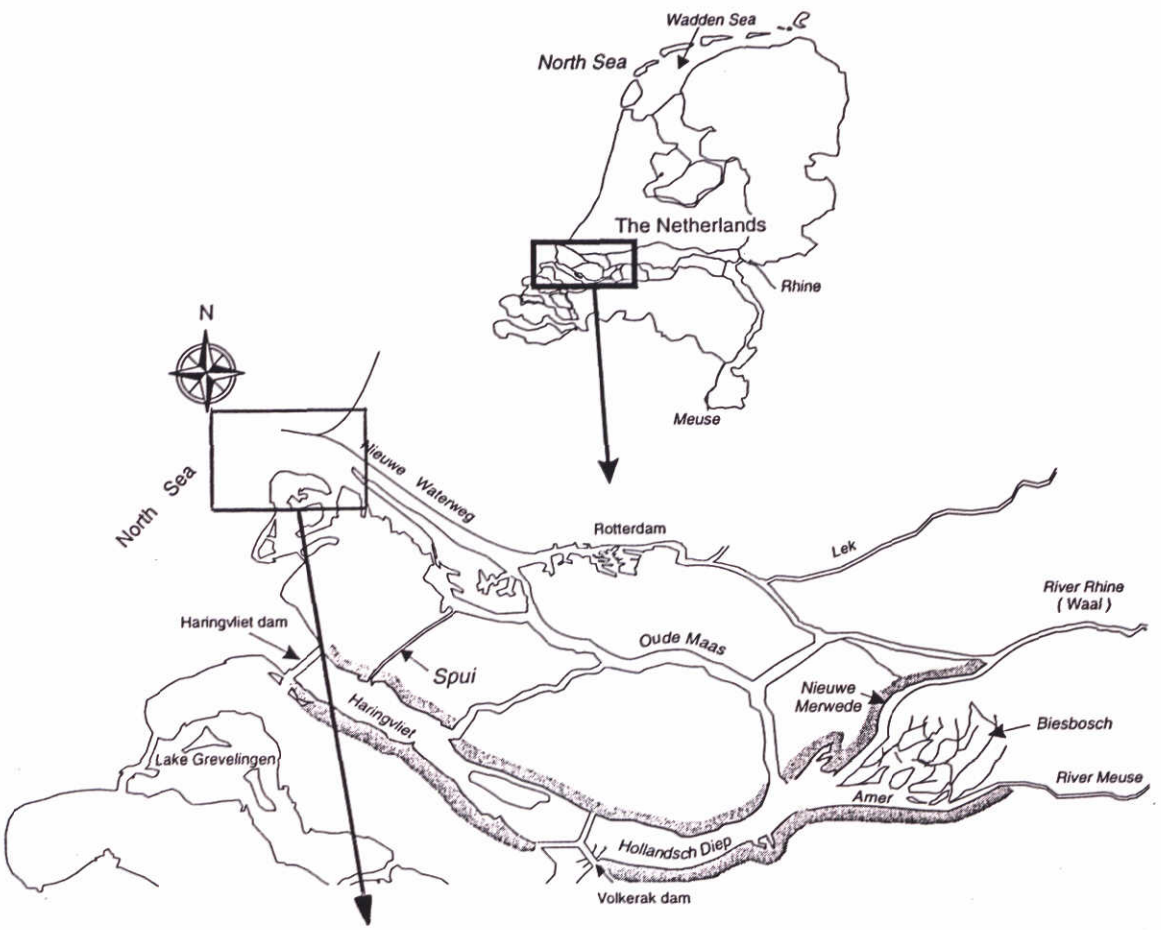

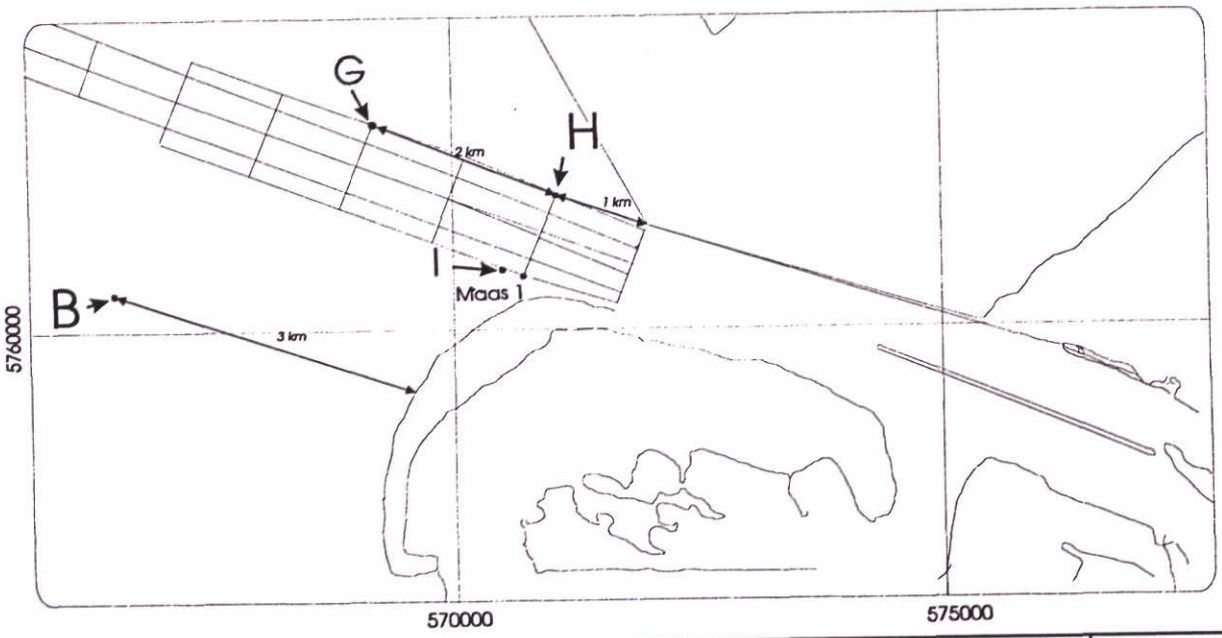

Location of permanent measuring stations A, G, H and I		Sept. 1997
	SILTMAN	
DELFT HYDRAULICS	Proj: Z2263	Fig. 2.1

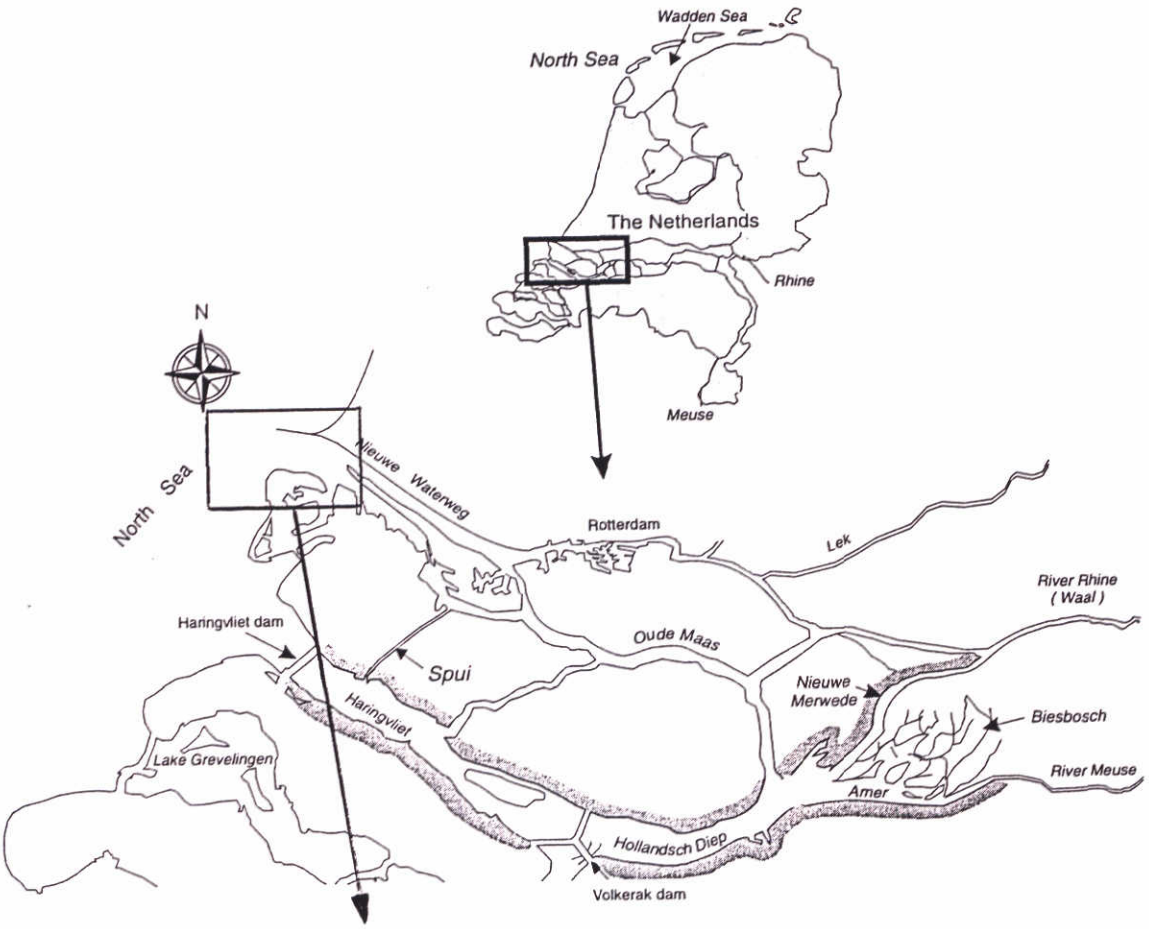

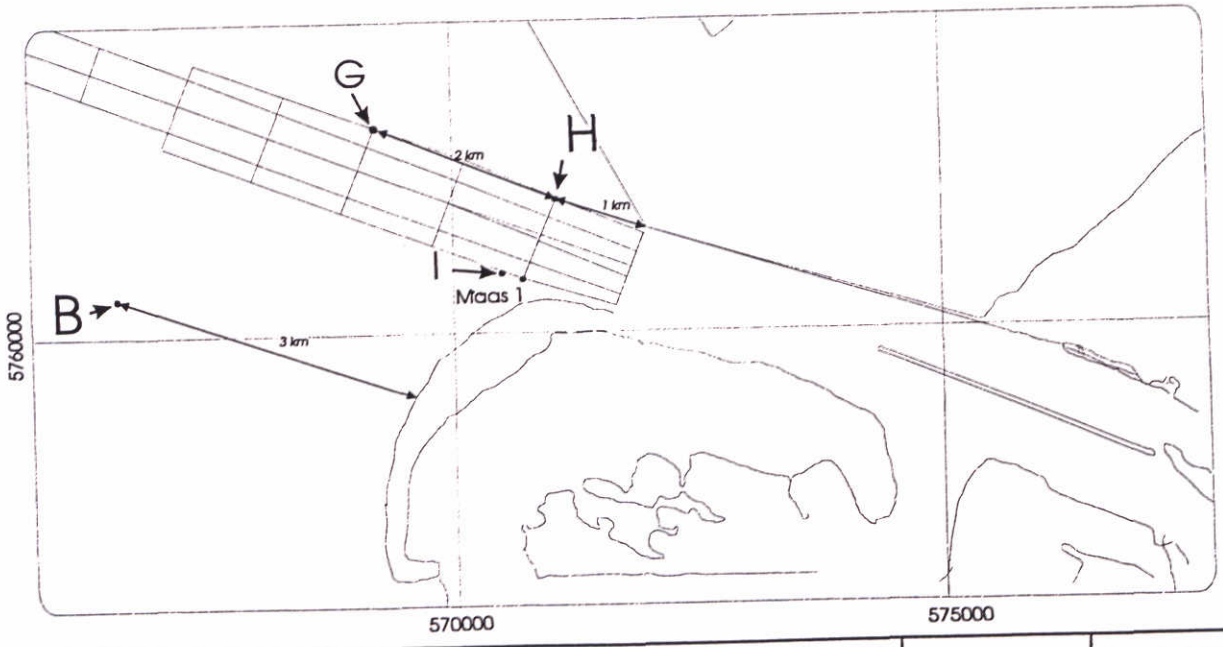

Location of permanent measuring stations A, G, H and I		Sept. 1997
	SILTMAN	
DELFT HYDRAULICS	Proj: Z2263	Fig. 2.1

Wind speed and direction at Hoek van Holland
and significant wave height Maasgeul

february 1996

DELFT HYDRAULICS

Z-2263

Fig. 2.2

Wind speed and direction at Hoek van Holland
and significant wave height Maasgeul

november 1996

DELFT HYDRAULICS

Z-2263

Fig. 2.3

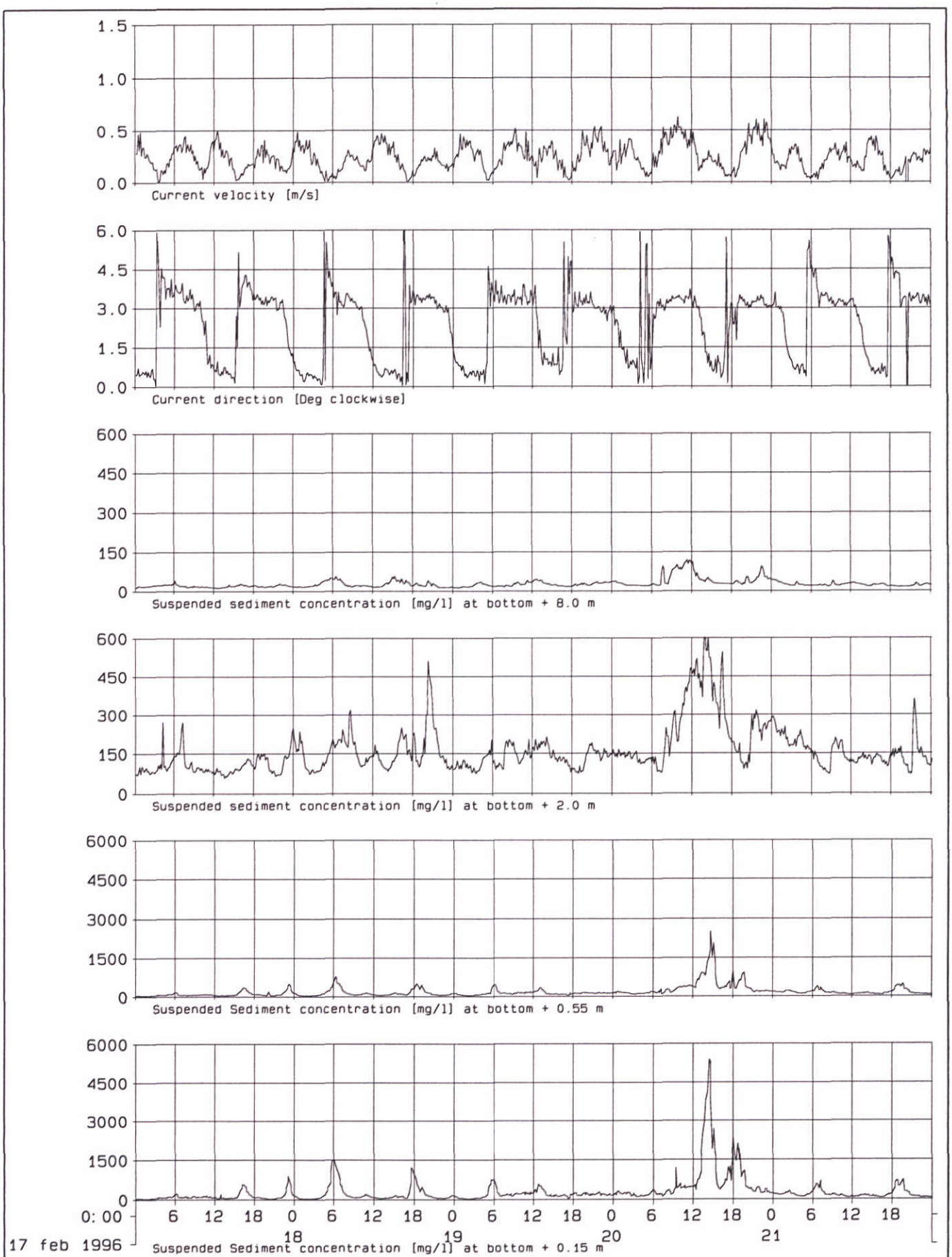

Flow velocity and sediment concentration measured during Feb 1996.

Station B

SILTMAN

DELFT HYDRAULICS

Proj: Z2263 | Fig: 2.4

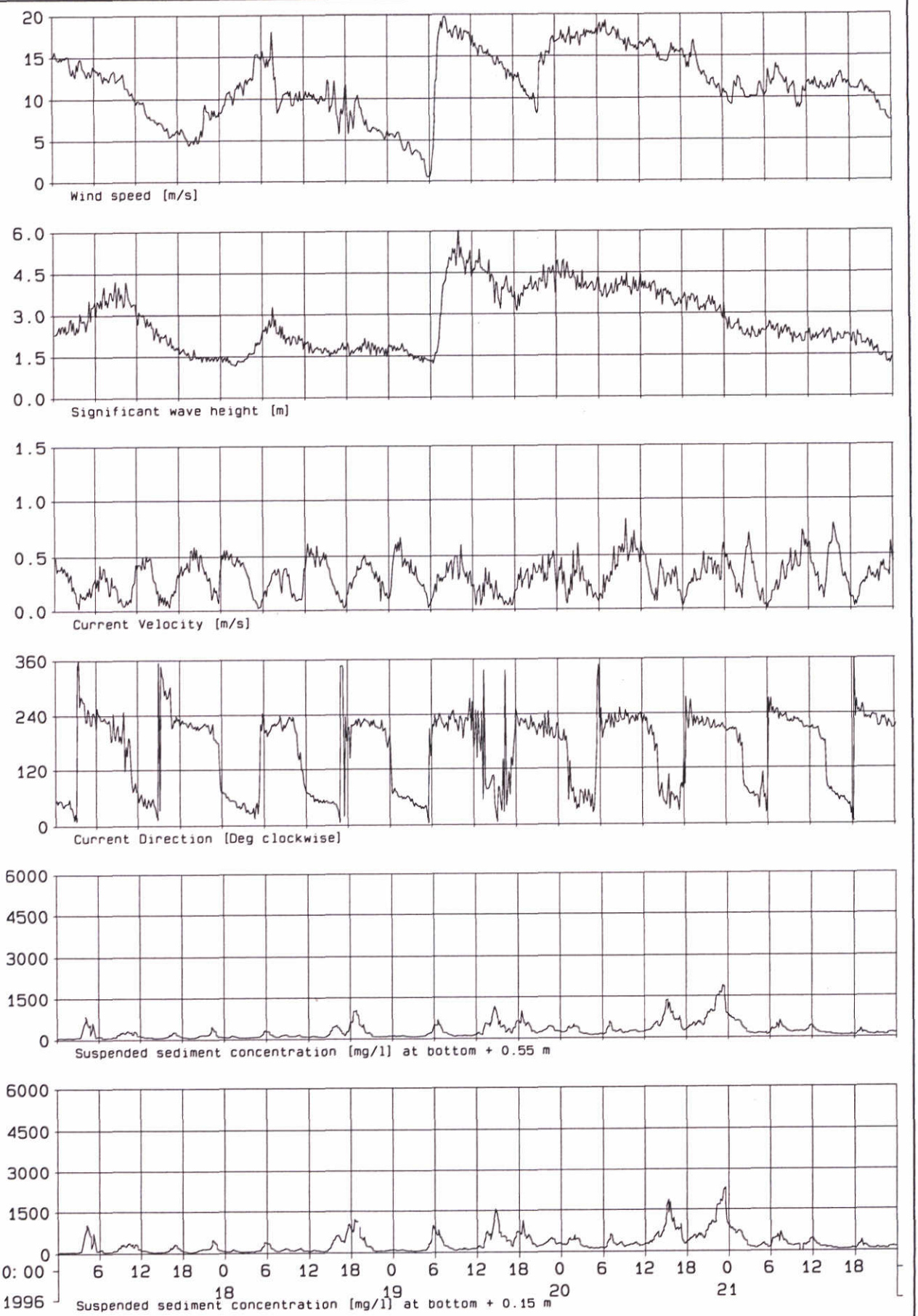

Wind speed (Hoek van Holland), significant wave height (Maasgeul), flow velocity and suspended sediment concentration measured during Feb 1996.

Station G

SILTMAN

D E L F T H Y D R A U L I C S

Proj: Z2263 | Fig: 2.5

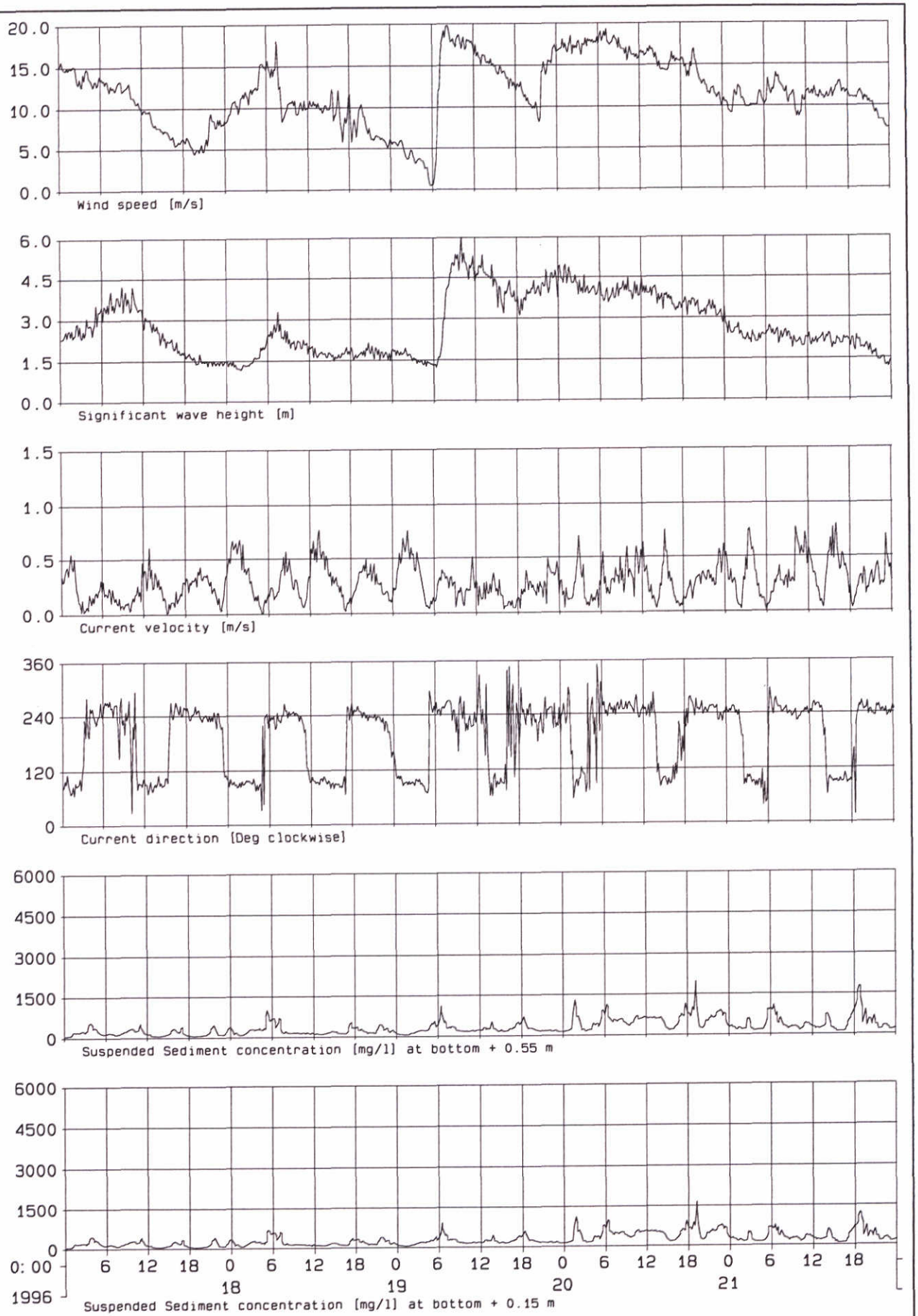

Wind speed (Hoek van Holland), significant wave height (Maasgeul), flow velocity and suspended sediment concentration measured during Feb 1996.	Station H	
	SILTMAN	
DELFT HYDRAULICS	Proj: Z2263	Fig: 2.6

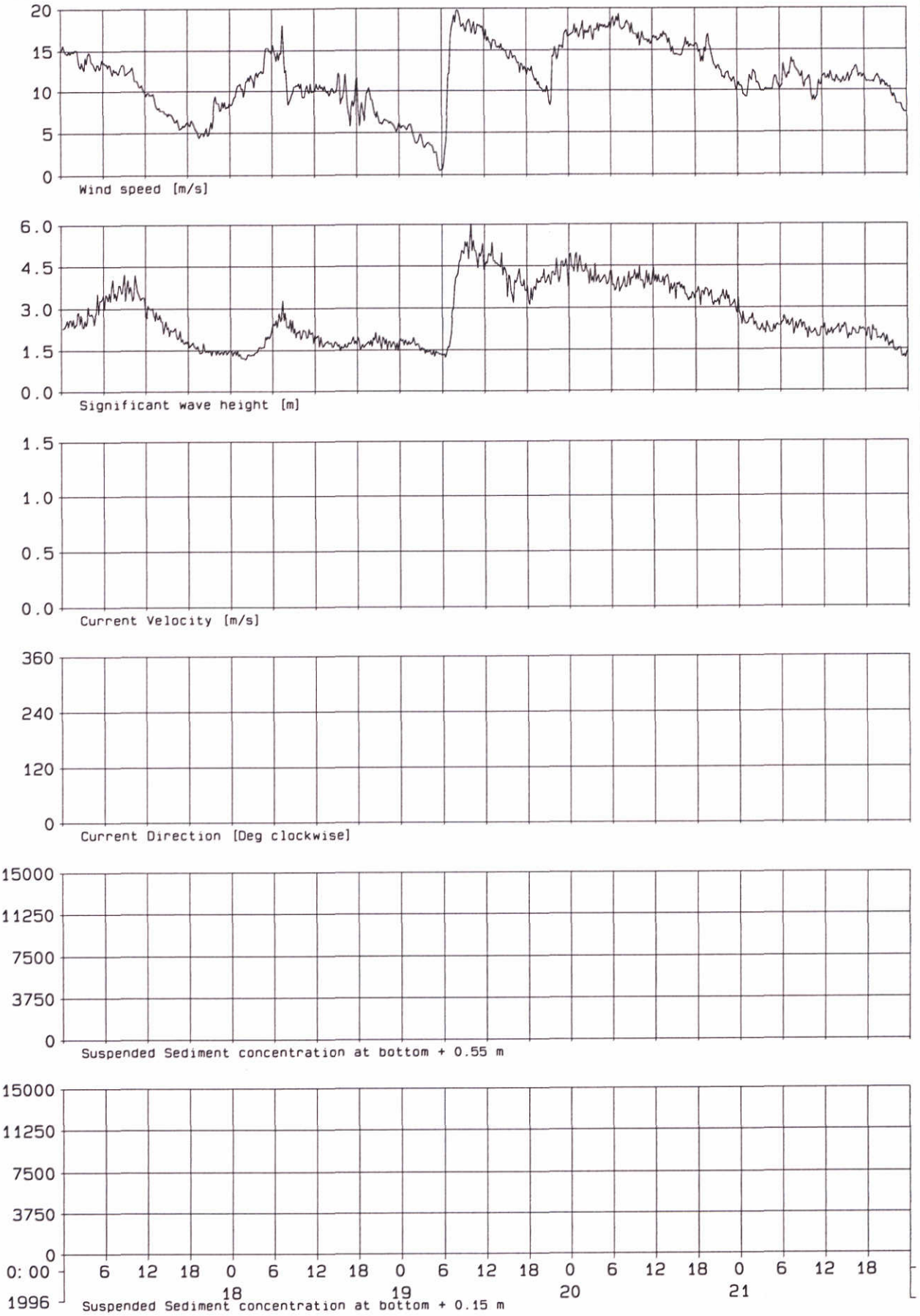

Wind speed (Hoek van Holland), significant wave height (Maasgeul), flow velocity and suspended sediment concentration measured during Feb 1996.	Station I	
	SILTMAN	
DELFT HYDRAULICS	Proj: Z2263	Fig: 2.7

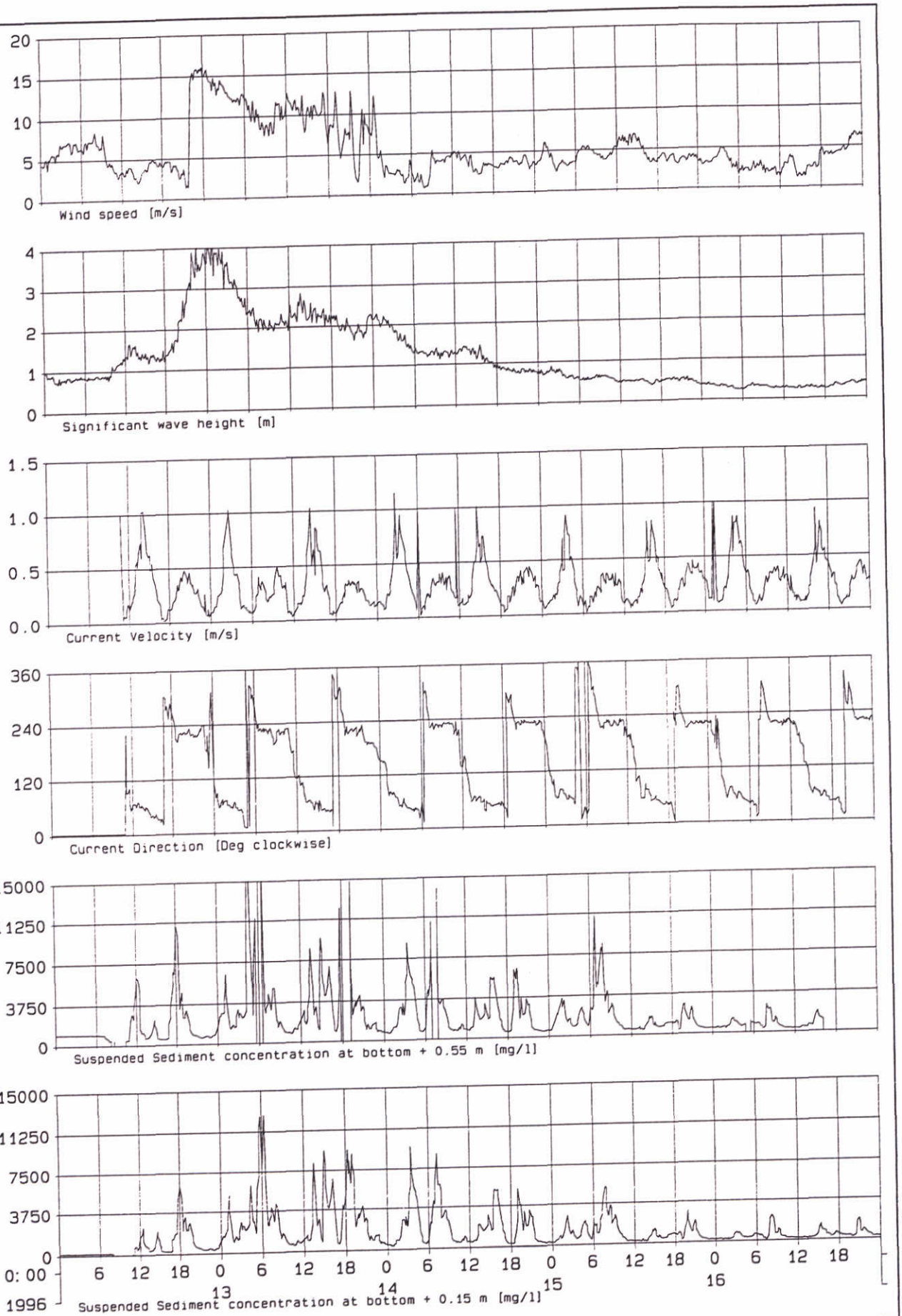

Wind speed (Hoek van Holland), significant wave height (Maasgeul), flow velocity and suspended sediment concentration measured during Nov 1996.

Station B

SILTMAN

DELFT HYDRAULICS

Proj: Z2263 | Fig: 2.8a

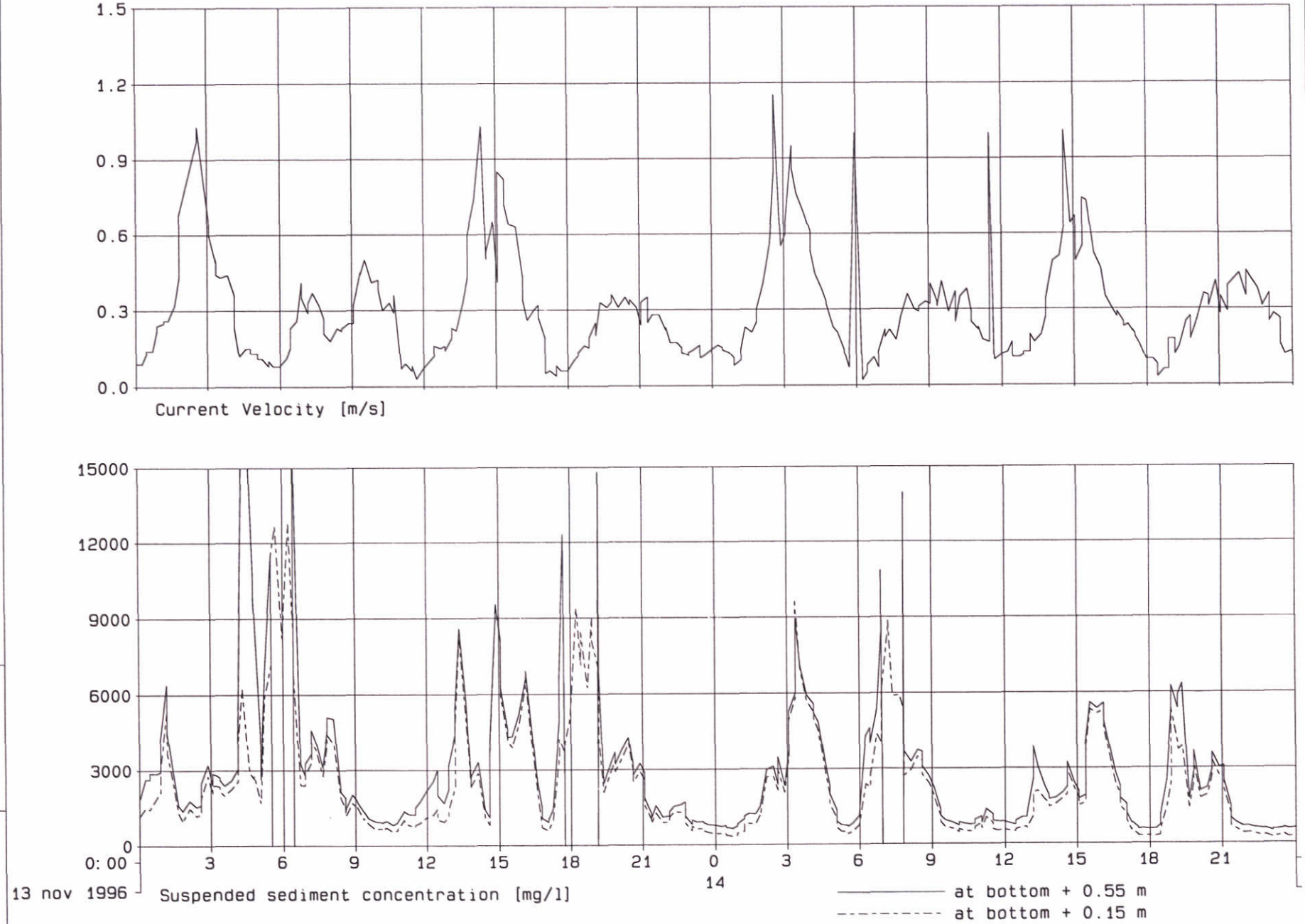

Flow velocity and suspended sediment concentration, measured during November 1996.

Station B

SILTMAN

Proj: Z2263

Fig: 2.8b

DELFT HYDRAULICS

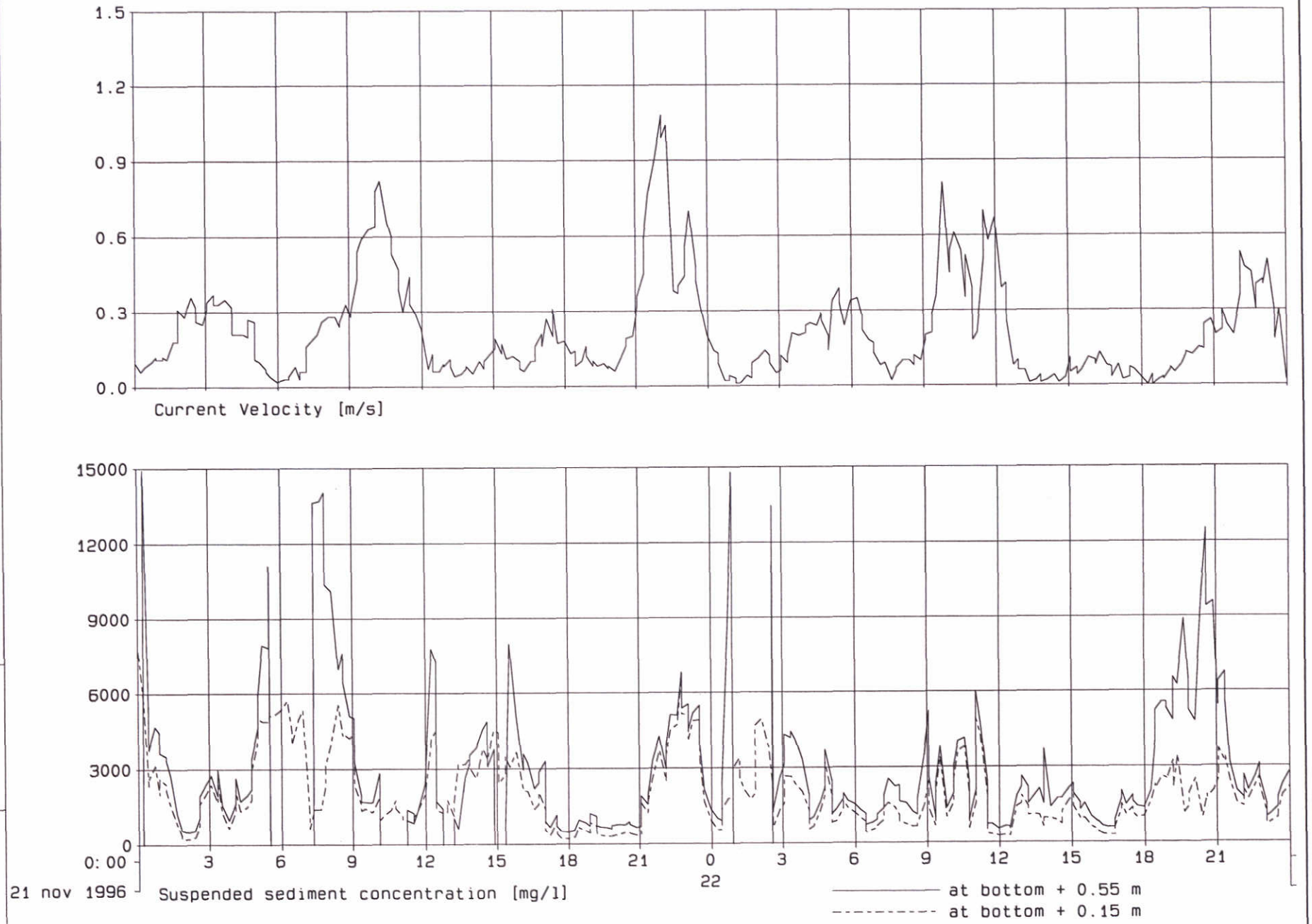

Flow velocity and suspended sediment concentration, measured during November 1996.

Station B

SILTMAN

Proj: Z2263 Fig: 2.8c

DELFT HYDRAULICS

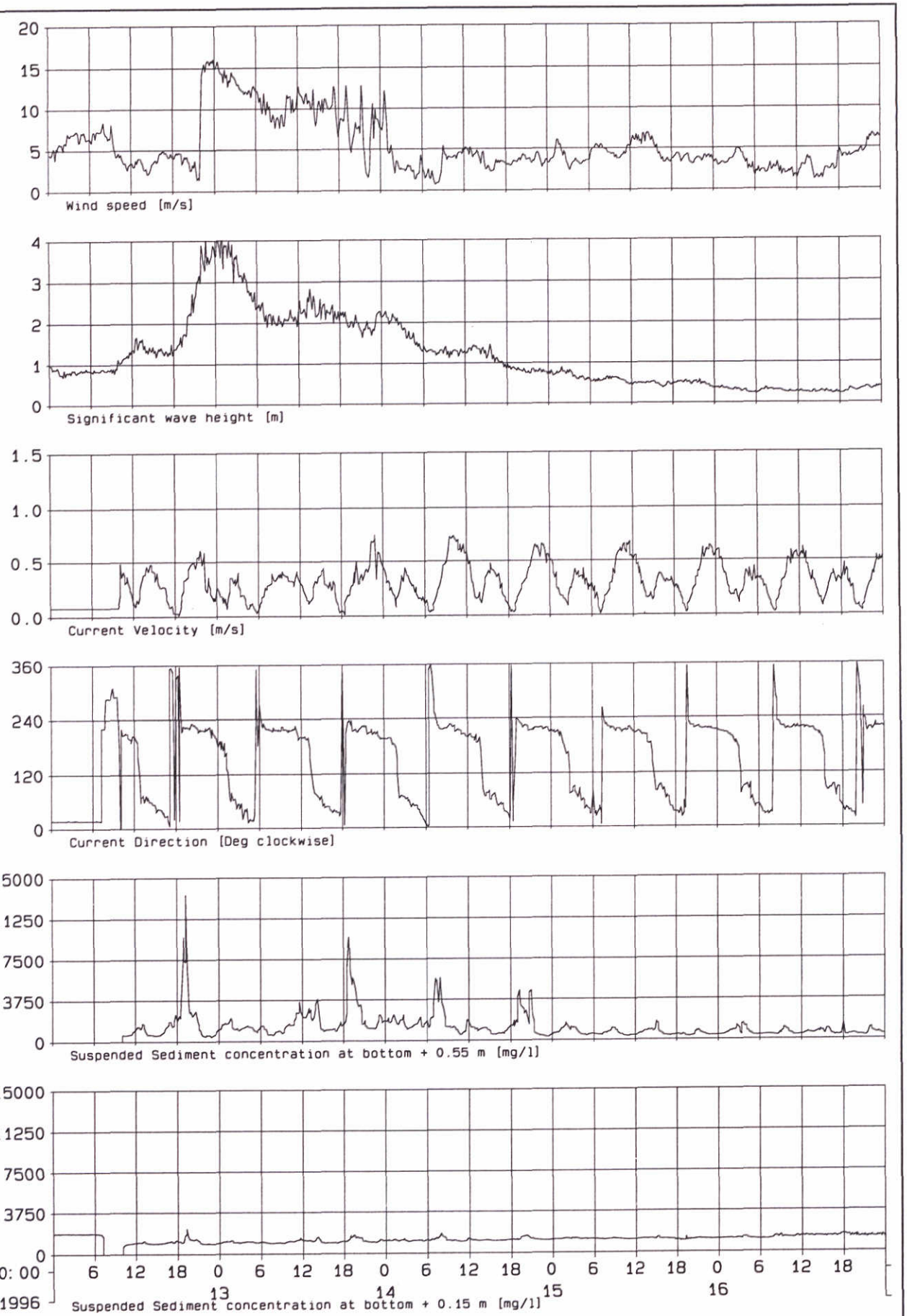

Wind speed (Hoek van Holland), significant wave height (Maasgeul), flow velocity and suspended sediment concentration measured during Nov 1996.	Station G	
	SILTMAN	
DELFT HYDRAULICS	Proj: Z2263	Fig: 2.9a

Flow velocity and
suspended sediment concentration,
measured during November 1996.

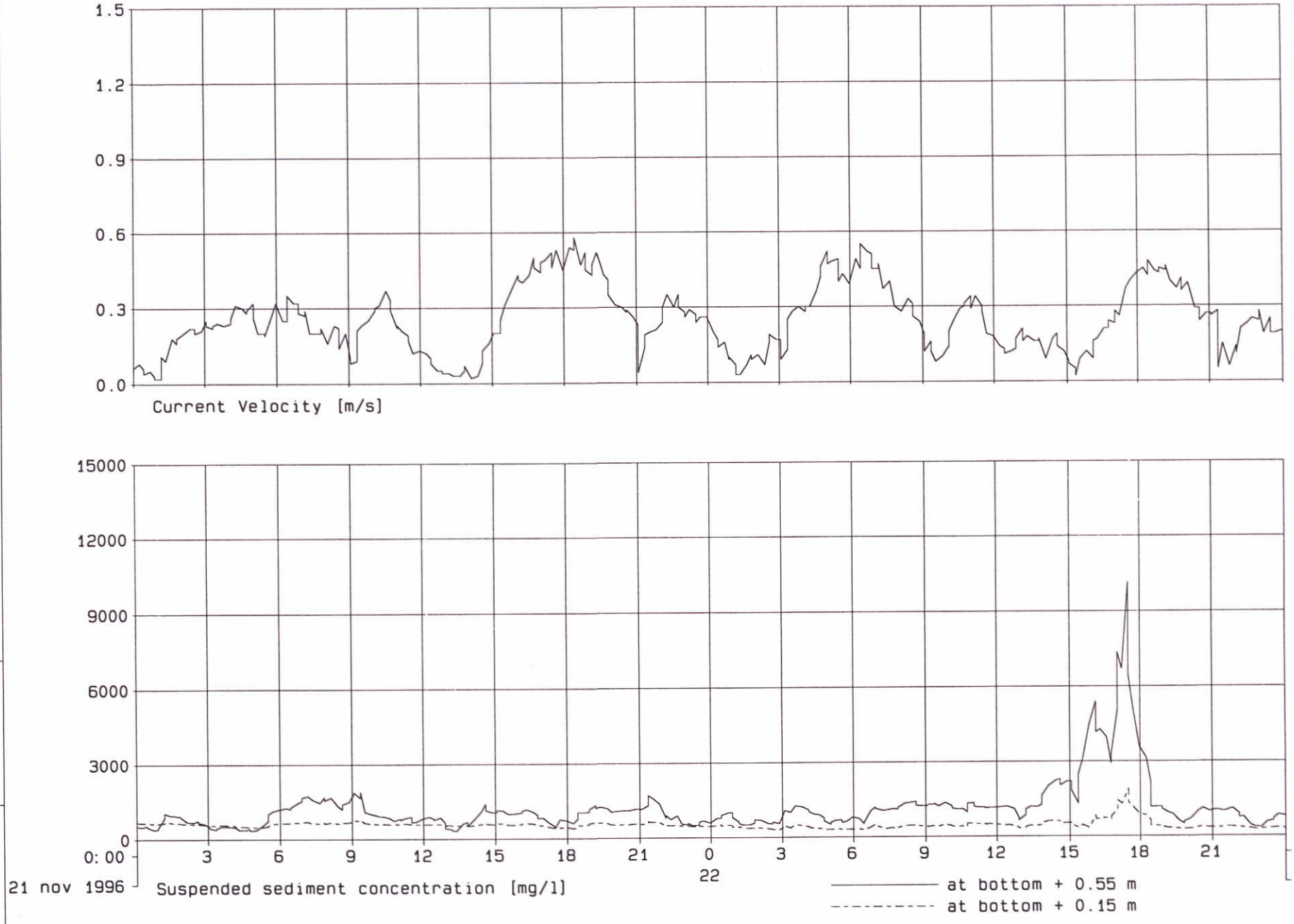

DELFT HYDRAULICS

Station G	
SILTMAN	
Proj: Z2263	Fig: 2.9c

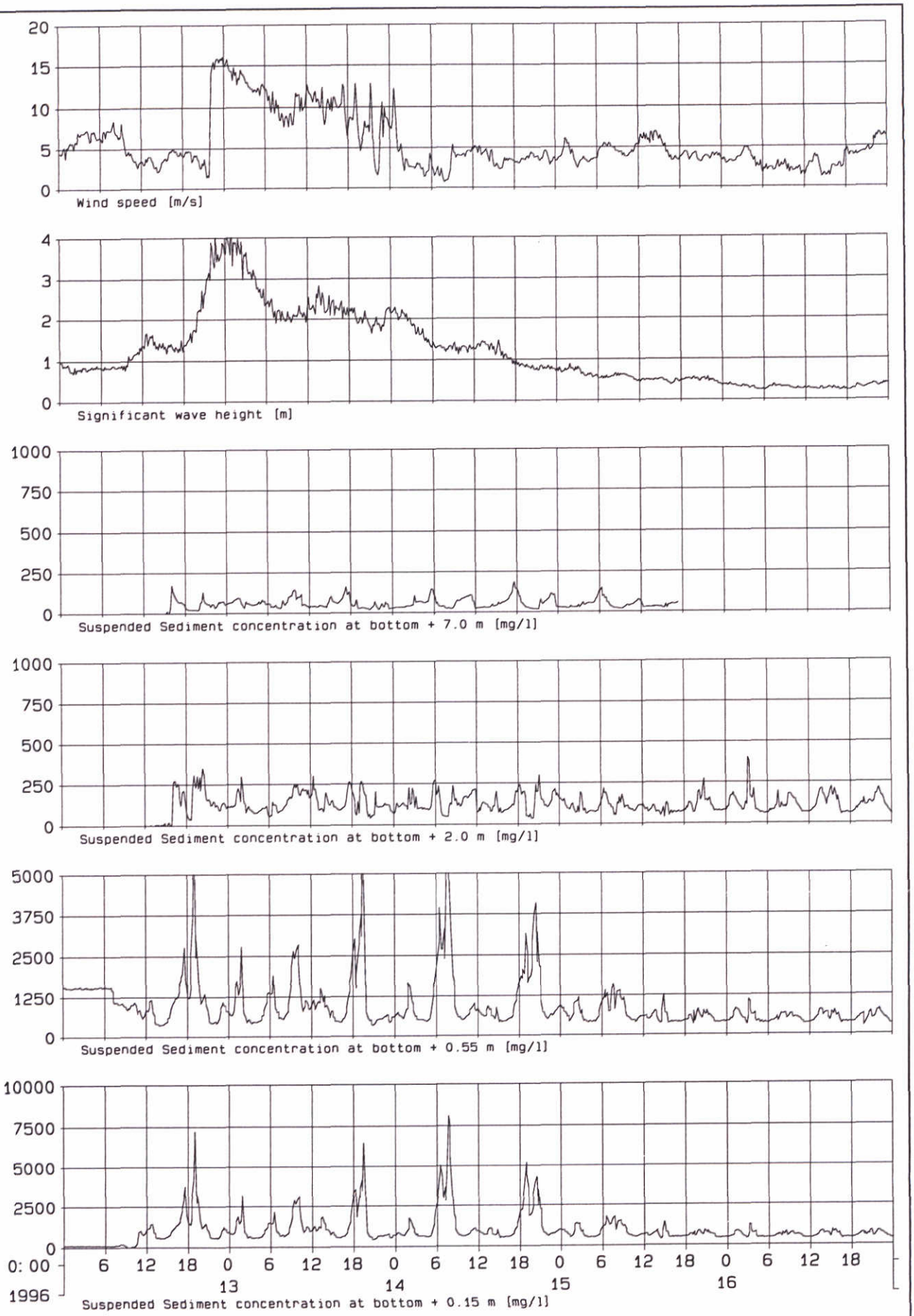

Wind speed (Hoek van Holland), significant wave height (Maasgeul), flow velocity and suspended sediment concentration measured during Nov 1996.

Station H

SILTMAN

DELFT HYDRAULICS

Proj: Z2263 | Fig: 2.10a

Flow velocity and suspended sediment concentration, measured during November 1996.	Station H	
	SILTMAN	
DELFT HYDRAULICS	Proj: Z2263	Fig: 2.10b

Flow velocity and suspended sediment concentration, measured during November 1996.	Station H	
	SILTMAN	
DELFT HYDRAULICS	Proj: Z2263	Fig: 2.10c

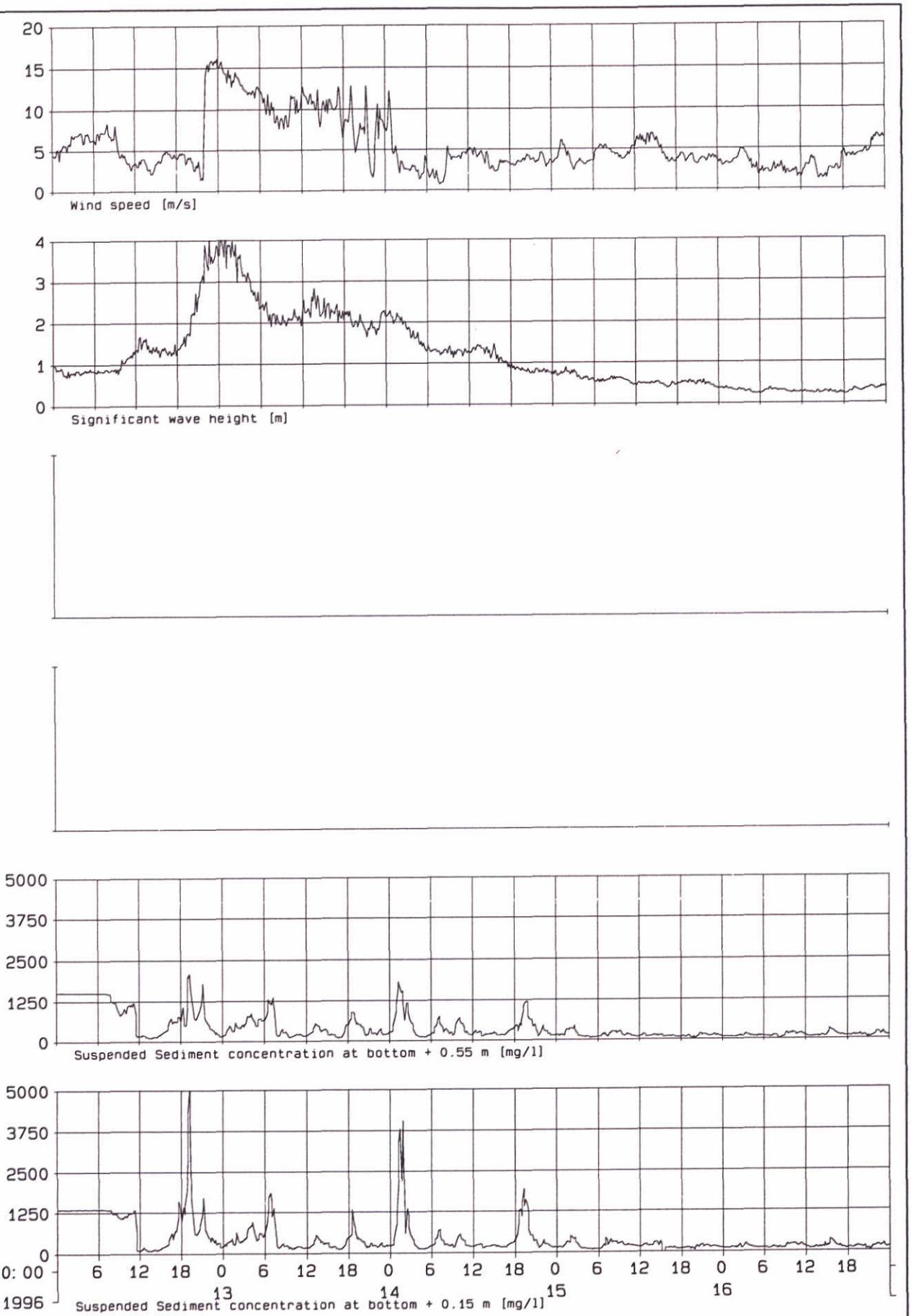

Wind speed (Hoek van Holland), significant wave height (Maasgeul), flow velocity and suspended sediment concentration measured during Nov 1996.	Station I	
	SILTMAN	
D E L F T H Y D R A U L I C S	Proj: Z2263	Fig: 2.11a

Flow velocity and
suspended sediment concentration,
measured during November 1996.

Station I

SILTMAN

DELFT HYDRAULICS

Proj: Z2263 | Fig: 2.11b

Flow velocity and
suspended sediment concentration,
measured during November 1996.

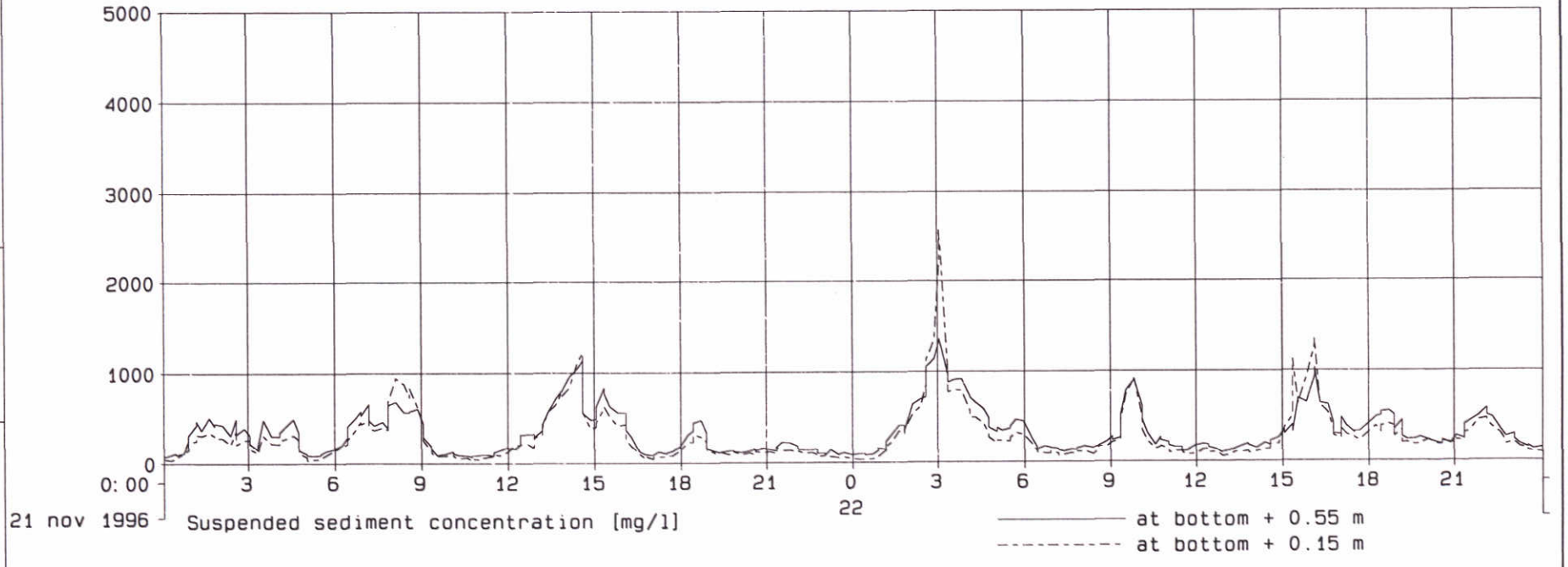

DELFT HYDRAULICS

SILTMAN

Station I

Proj: Z2263

Fig: 2.11c

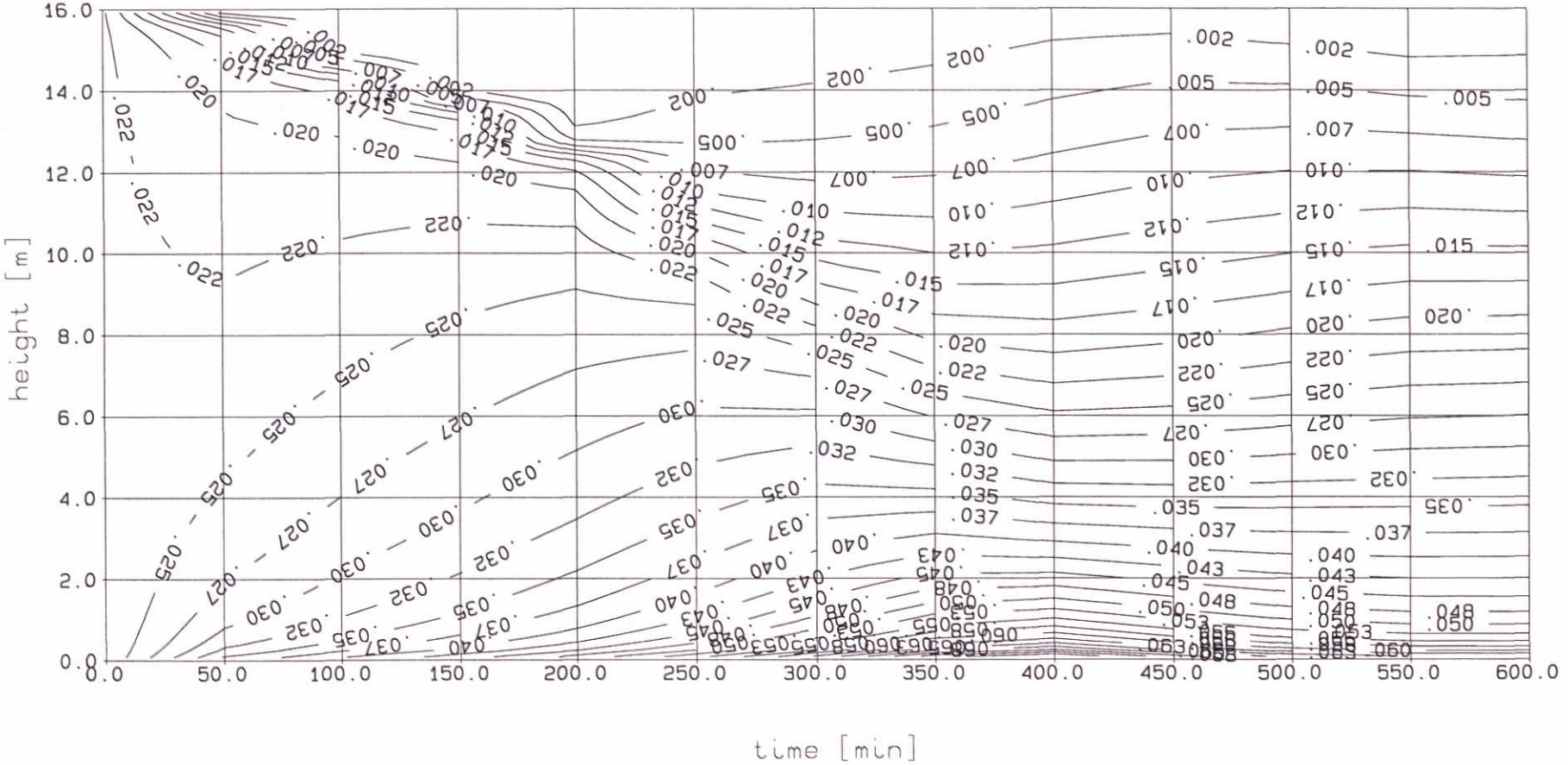

Computed mass concentrations [g/l] - {run s01a} saturation concentration, C_0 = 0.023 g/l h = 16 m, U_m = 0.2 m/s, W_s = 0.5 mm/s, no waves		20-08-97
	steady flow	
DELFT HYDRAULICS - MARINE & COASTAL MANAGEMENT	Proj: Z2263	Fig. 4.1a

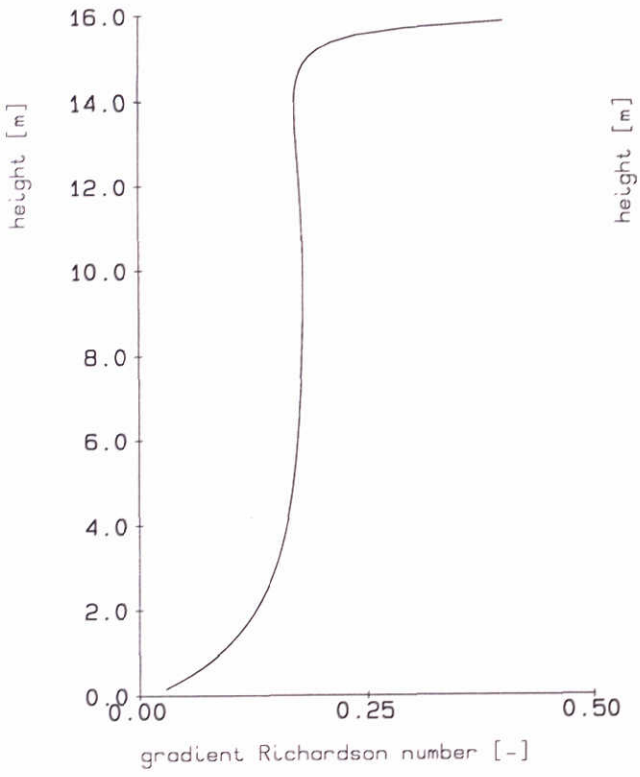

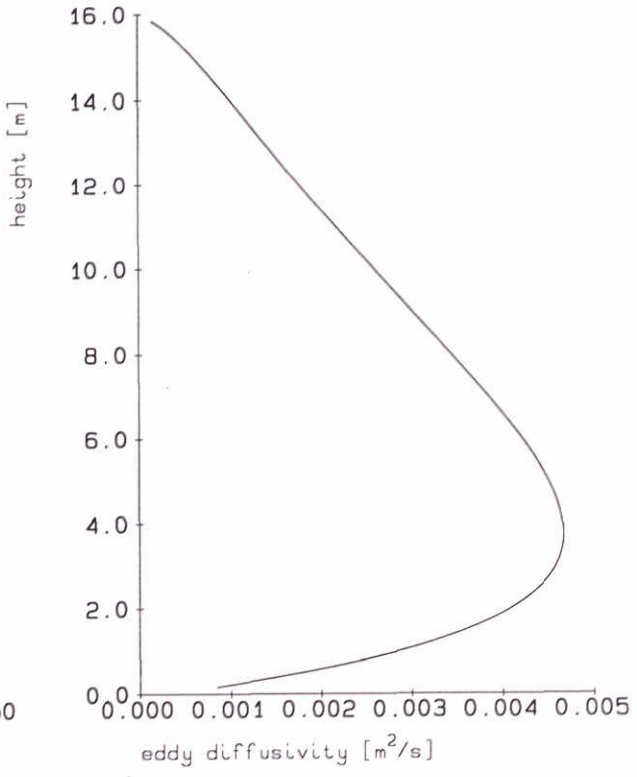

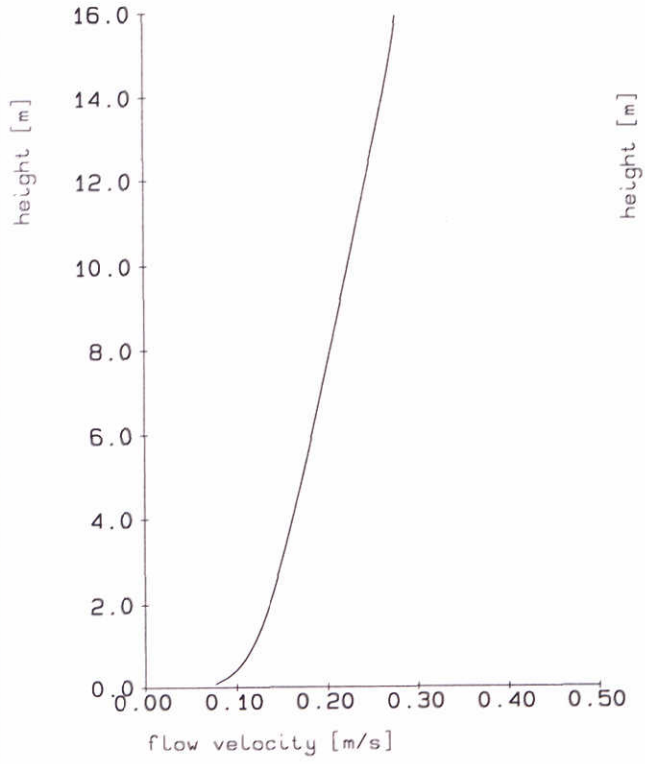

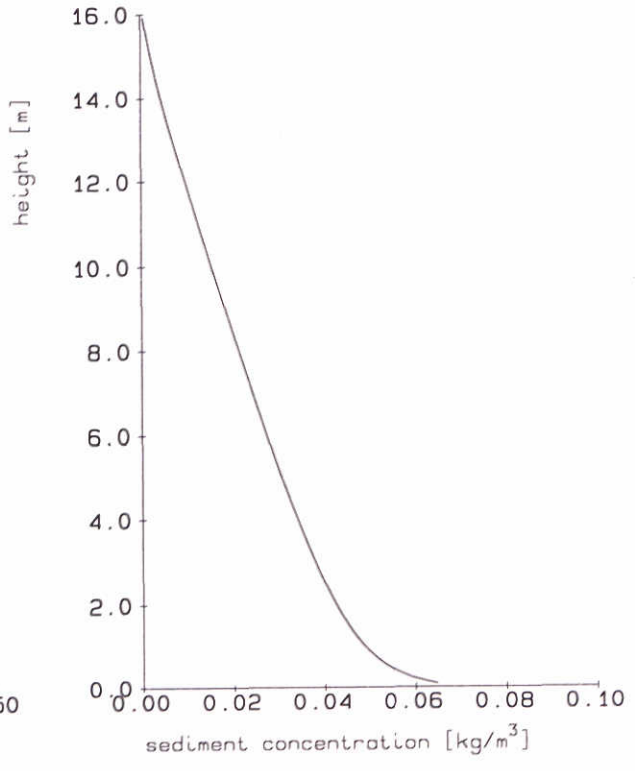

Computed mass concentrations [g/l] - {run s01a} saturation concentration, C_0 = 0.023 g/l h = 16 m, U_m = 0.2 m/s, W_s = 0.5 mm/s, no waves		time : 600
	steady flow	
DELFT HYDRAULICS - MARINE & COASTAL MANAGEMENT	Proj: Z2263	Fig. 4.1b

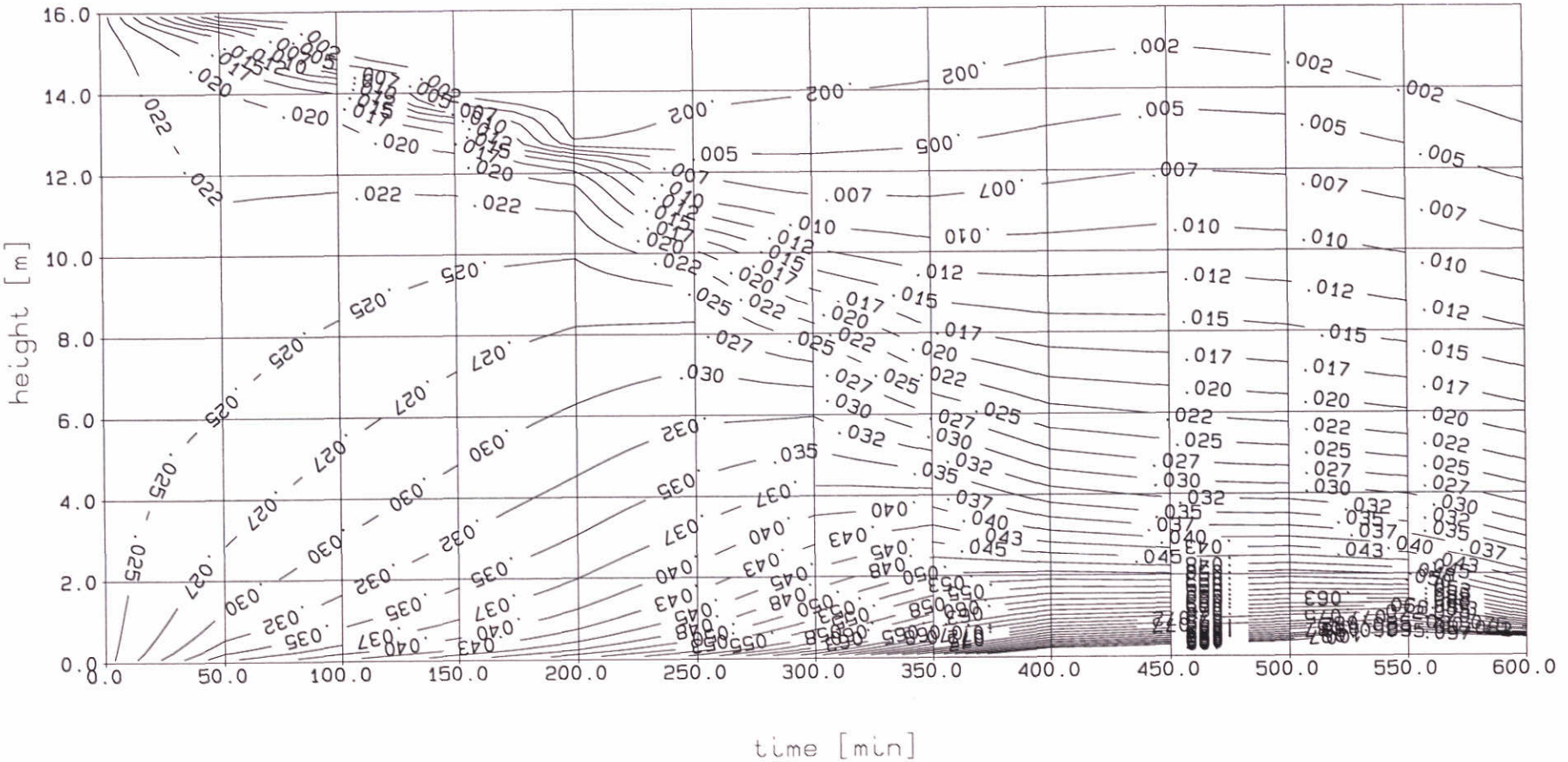

Computed mass concentrations [g/l] - {run s01b} saturation concentration, C_0 = 0.024 g/l h = 16 m, U_m = 0.2 m/s, W_s = 0.5 mm/s, no waves		20-08-97
	steady flow	
DELFT HYDRAULICS - MARINE & COASTAL MANAGEMENT	Proj: Z2263	Fig. 4.2a

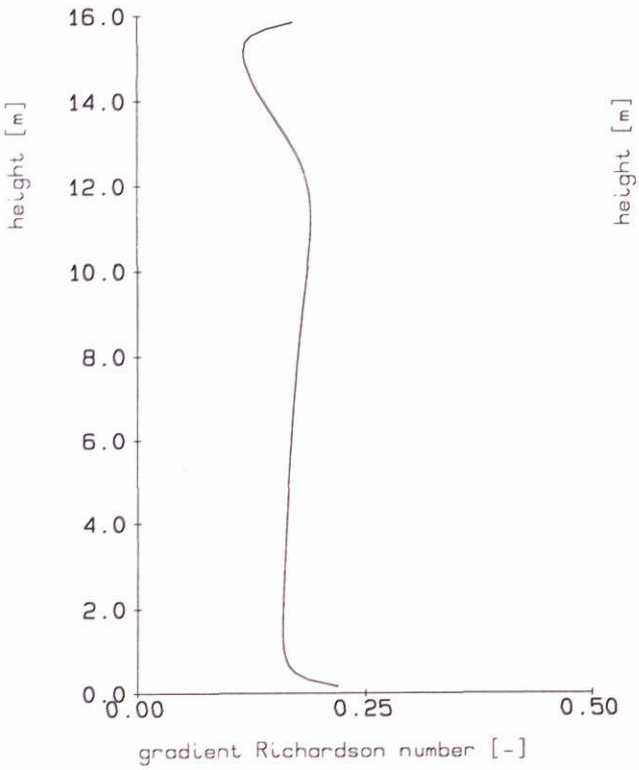

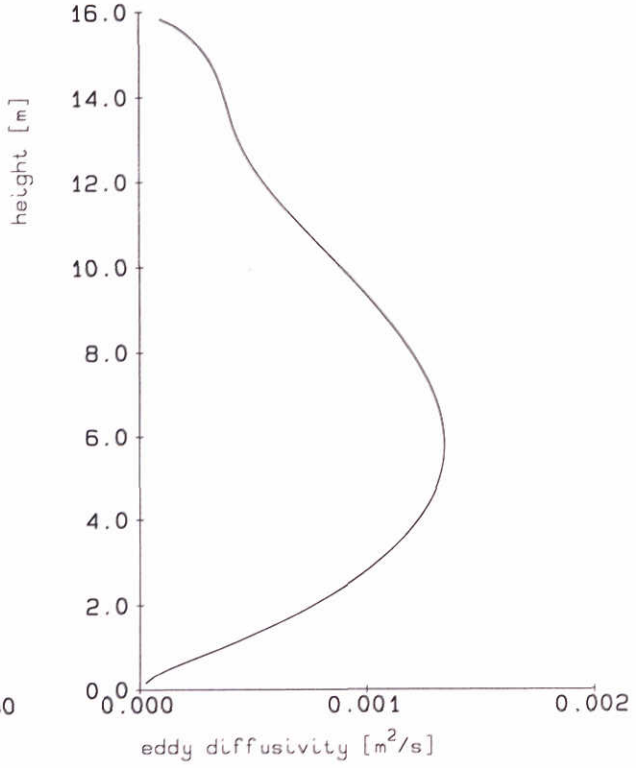

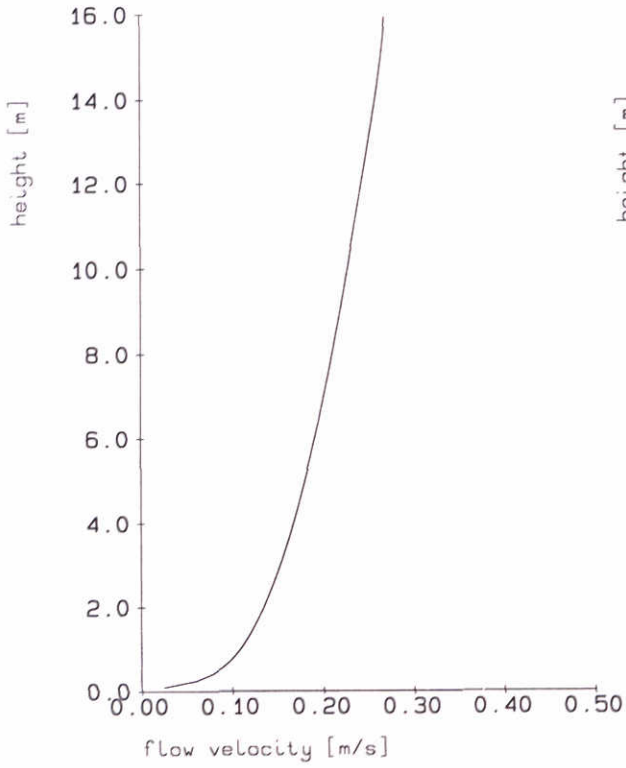

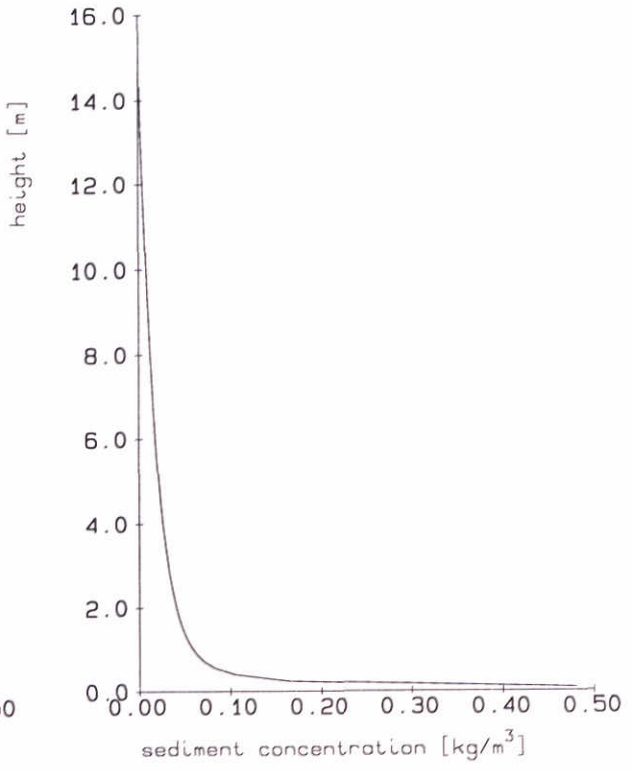

Computed mass concentrations [g/l] - {run s01b} saturation concentration, C_0 = 0.024 g/l h = 16 m, U_m = 0.2 m/s, W_s = 0.5 mm/s, no waves		time : 600
	steady flow	
DELFT HYDRAULICS - MARINE & COASTAL MANAGEMENT	Proj: Z2263	Fig. 4.2b

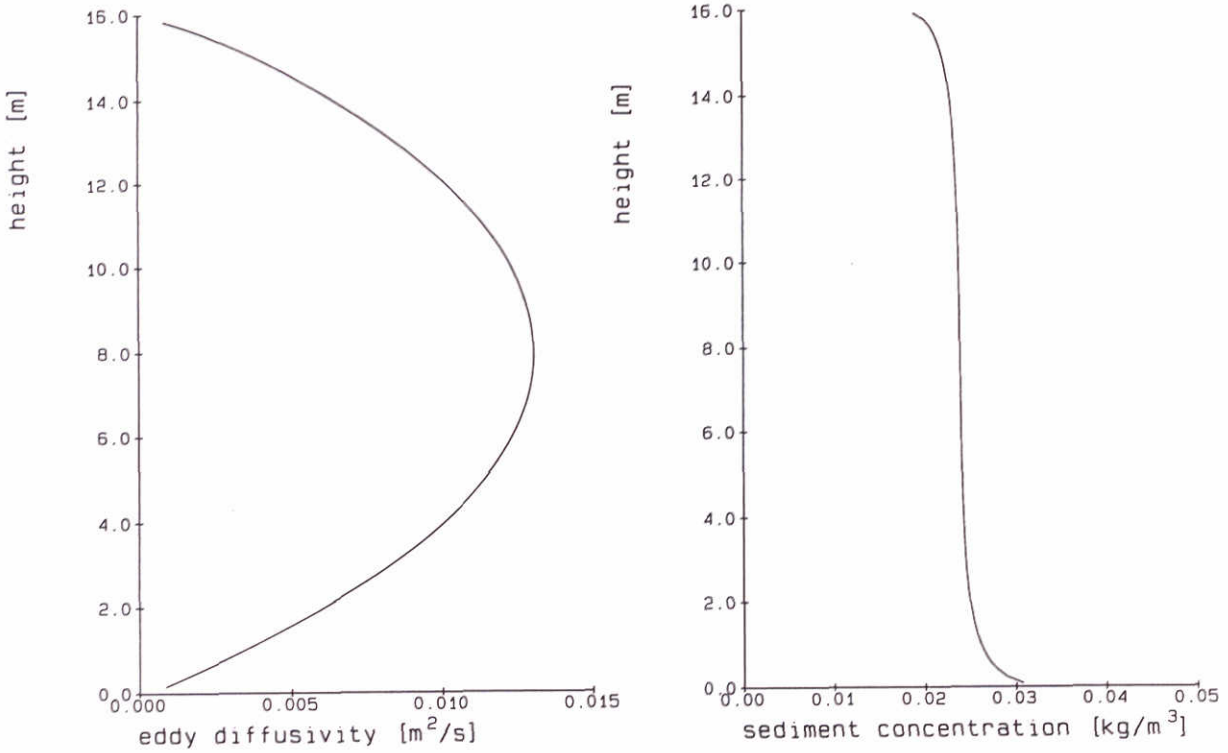

TIME : 10

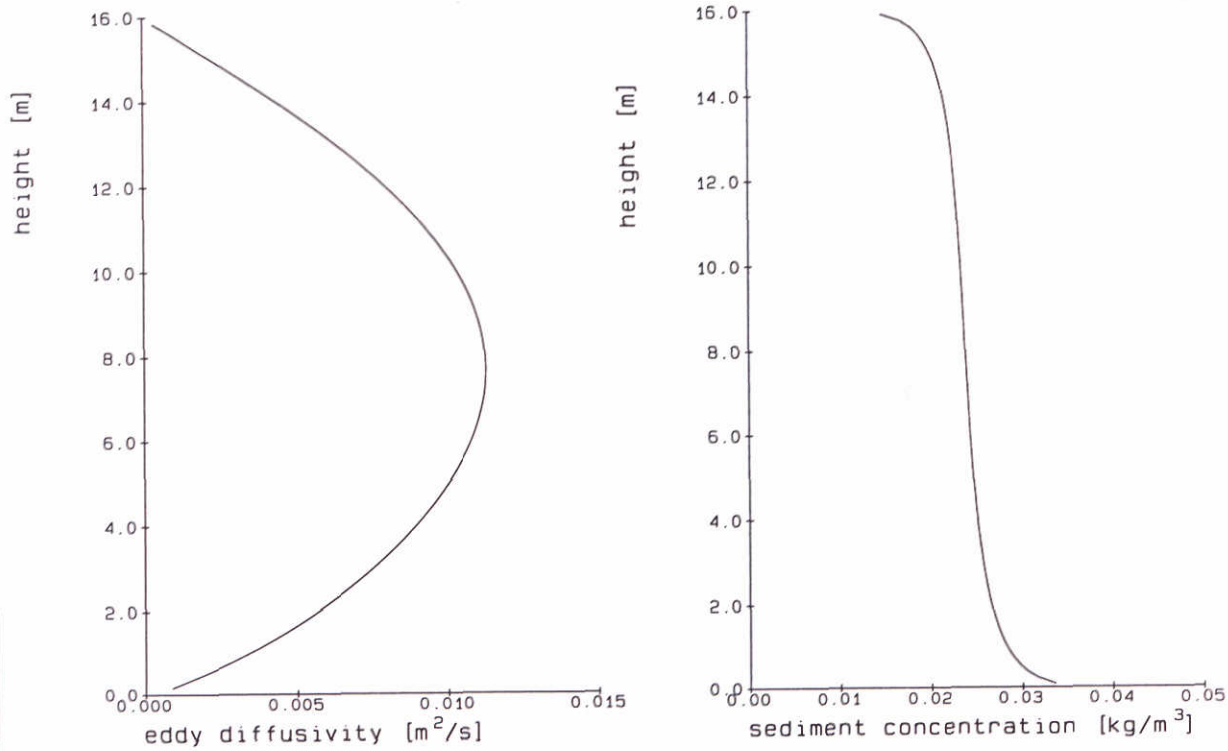

TIME : 25

Computed mass concentrations [g/l] - {run s01} saturation concentration, C_0 = 0.024 g/l h = 16m, U_m = 0.2 m/s, W_s = 0.5 mm/s, no waves		
	steady flow	
DELFT HYDRAULICS - MARINE & COASTAL MANAGEMENT	Proj. Z2263	Fig. 4.2c

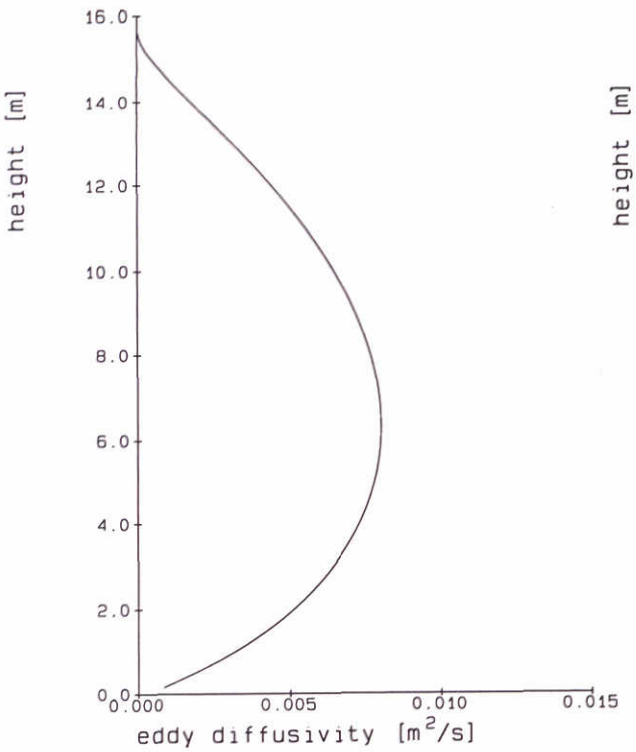

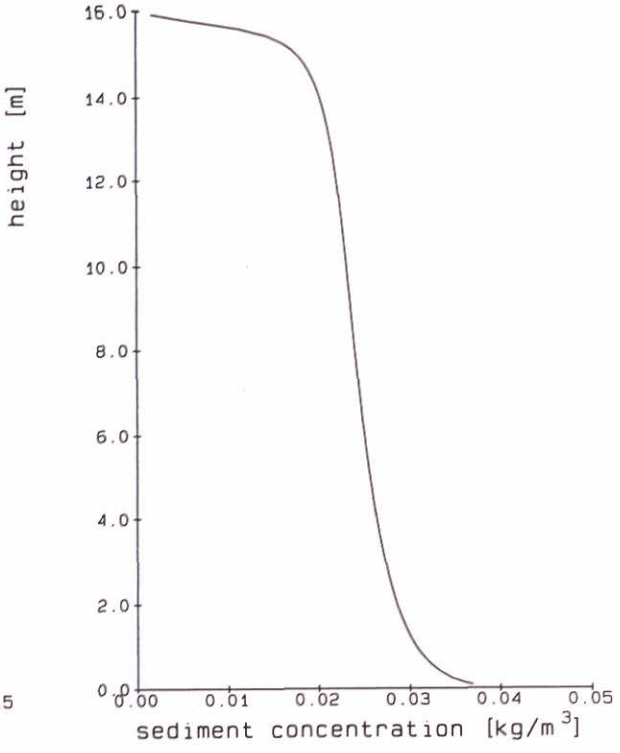

TIME : 50

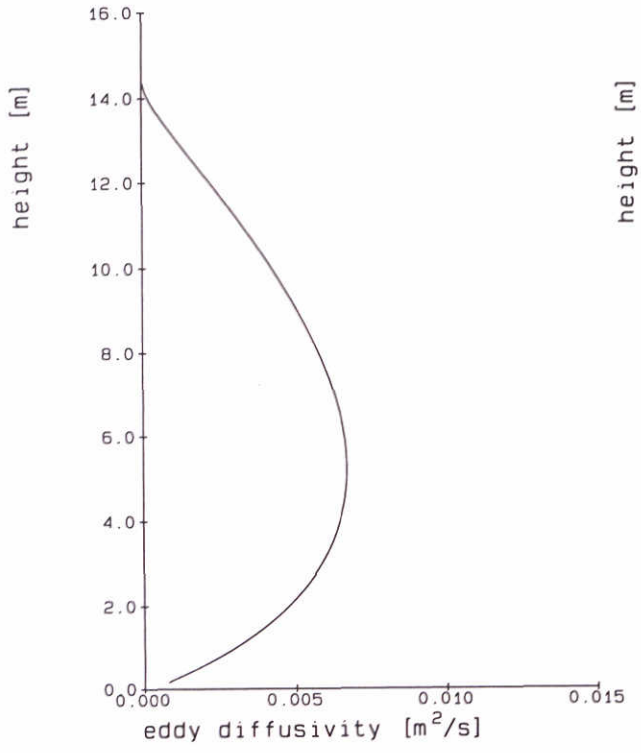

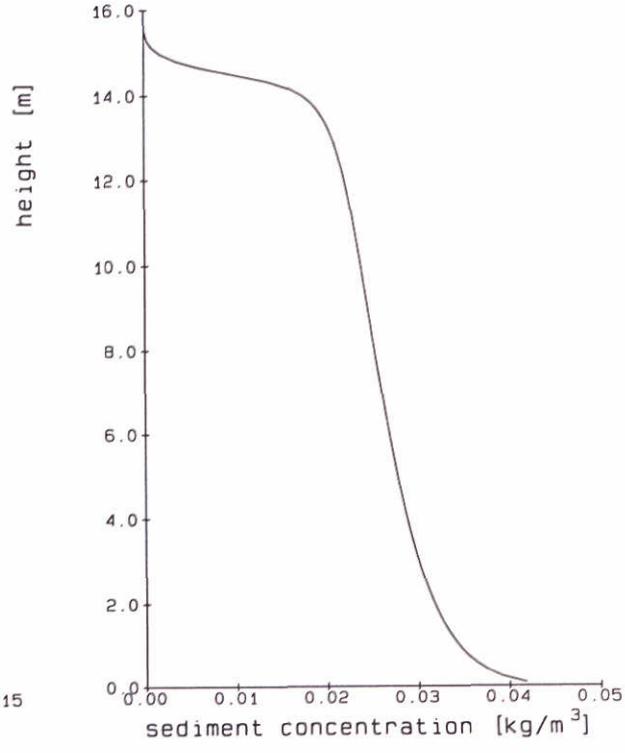

TIME : 100

Computed mass concentrations [g/l] - {run s01} saturation concentration, C_0 = 0.024 g/l h = 16m, U_m = 0.2 m/s, W_s = 0.5 mm/s, no waves		
	steady flow	
DELFT HYDRAULICS - MARINE & COASTAL MANAGEMENT	Proj. Z2263	Fig. 4.2d

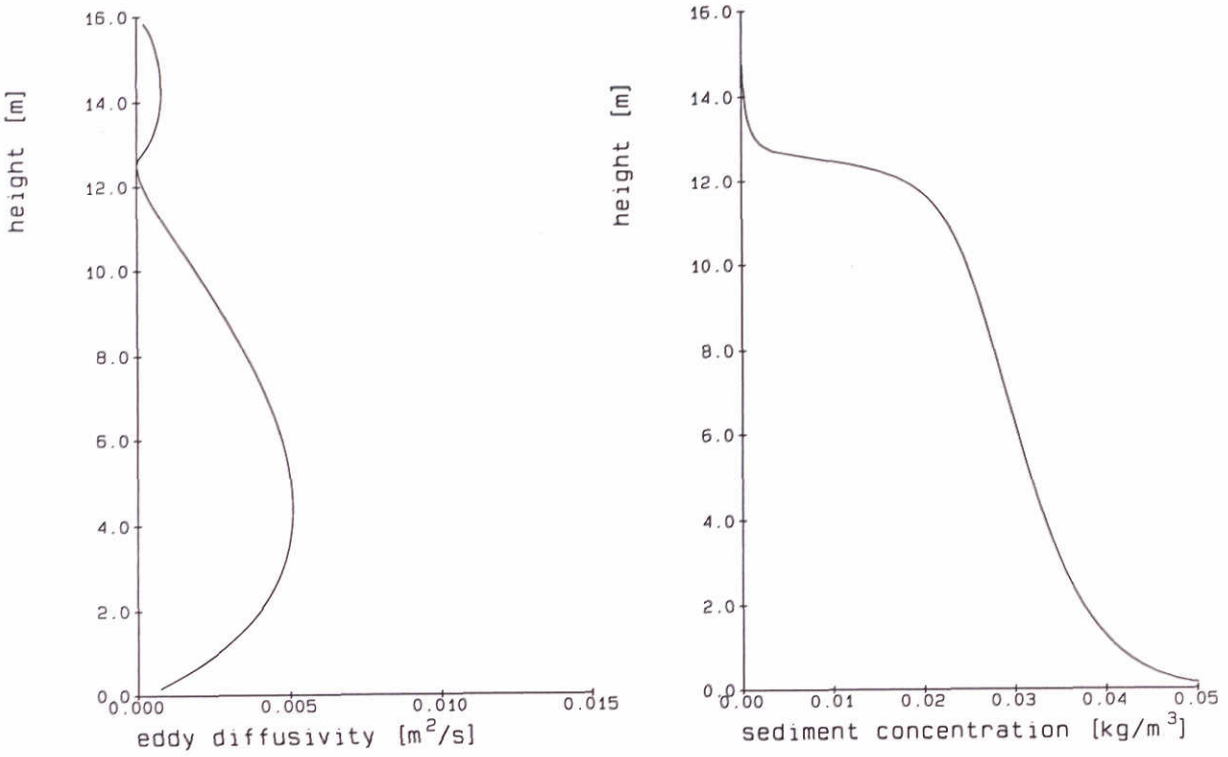

TIME : 200

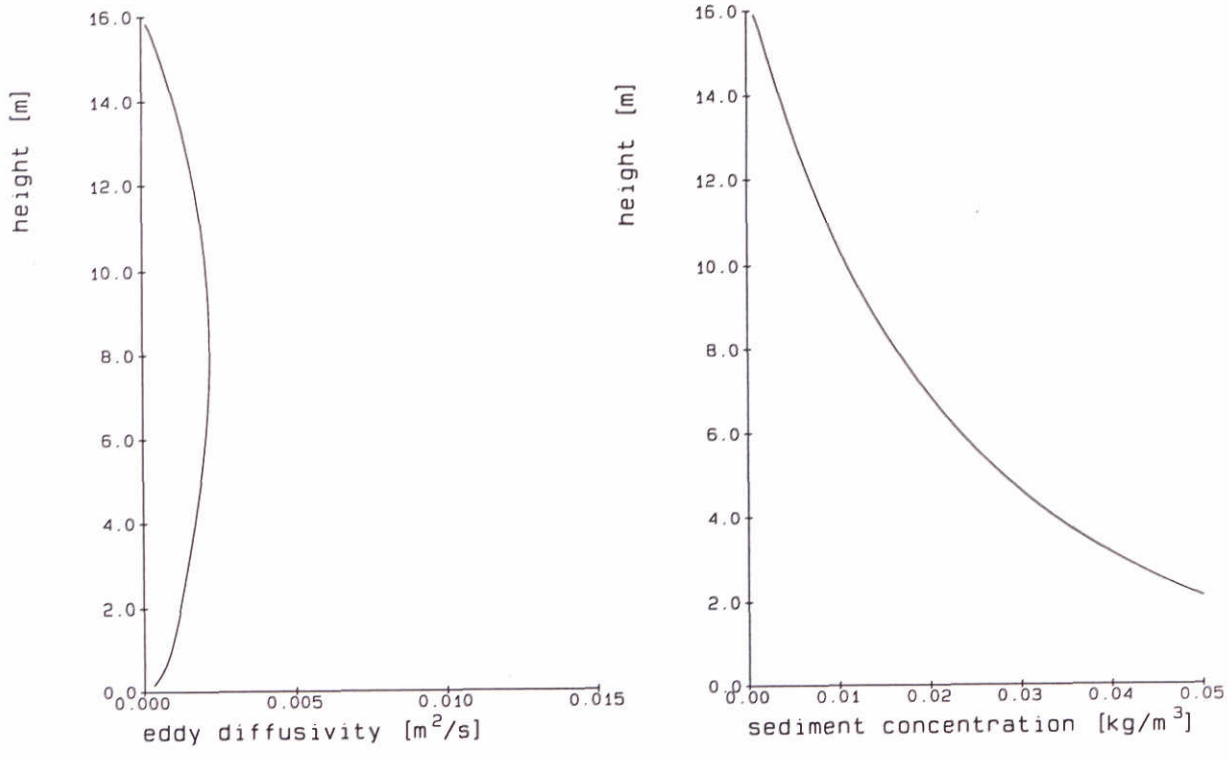

TIME : 400

Computed mass concentrations [g/l] - {run s02} saturation concentration, C_0 = 0.024 g/l h = 16m, U_m = 0.2 m/s, W_s = 0.5 mm/s, no waves		
	steady flow	
DELFT HYDRAULICS - MARINE & COASTAL MANAGEMENT	Proj. Z2263	Fig. 4.2e

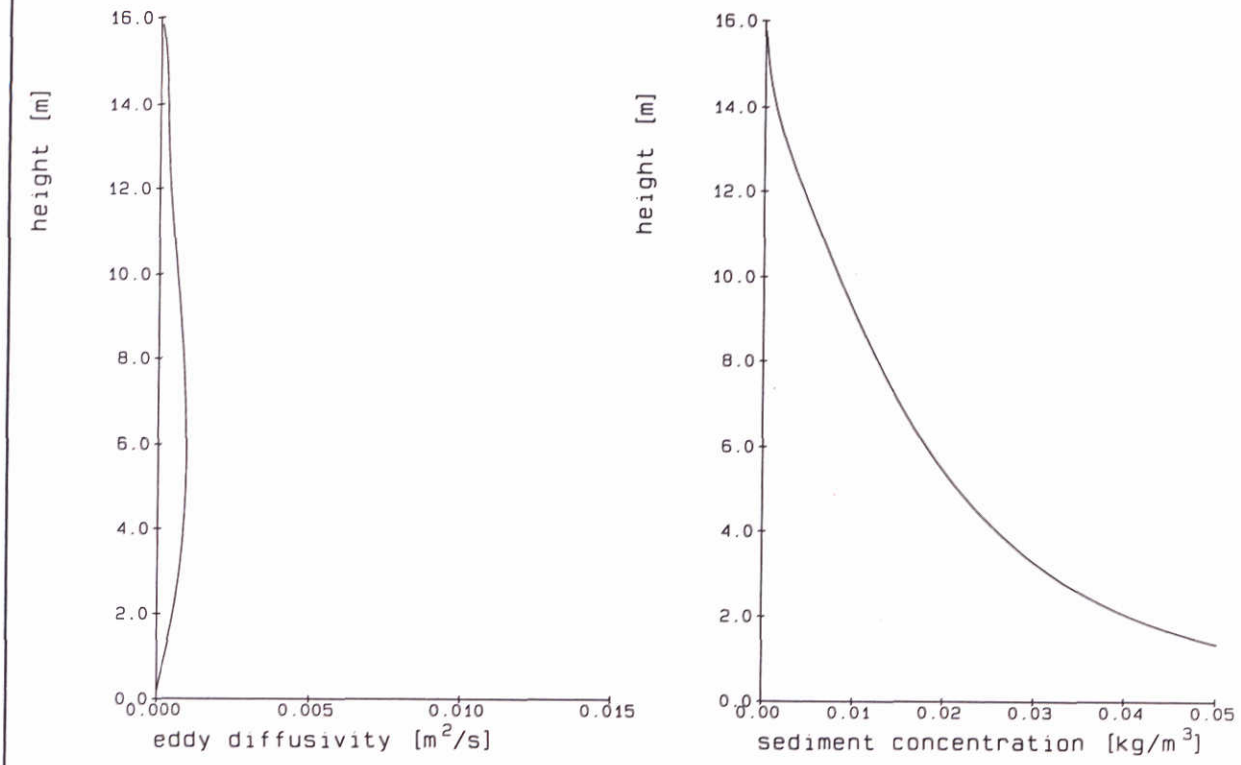

TIME : 600

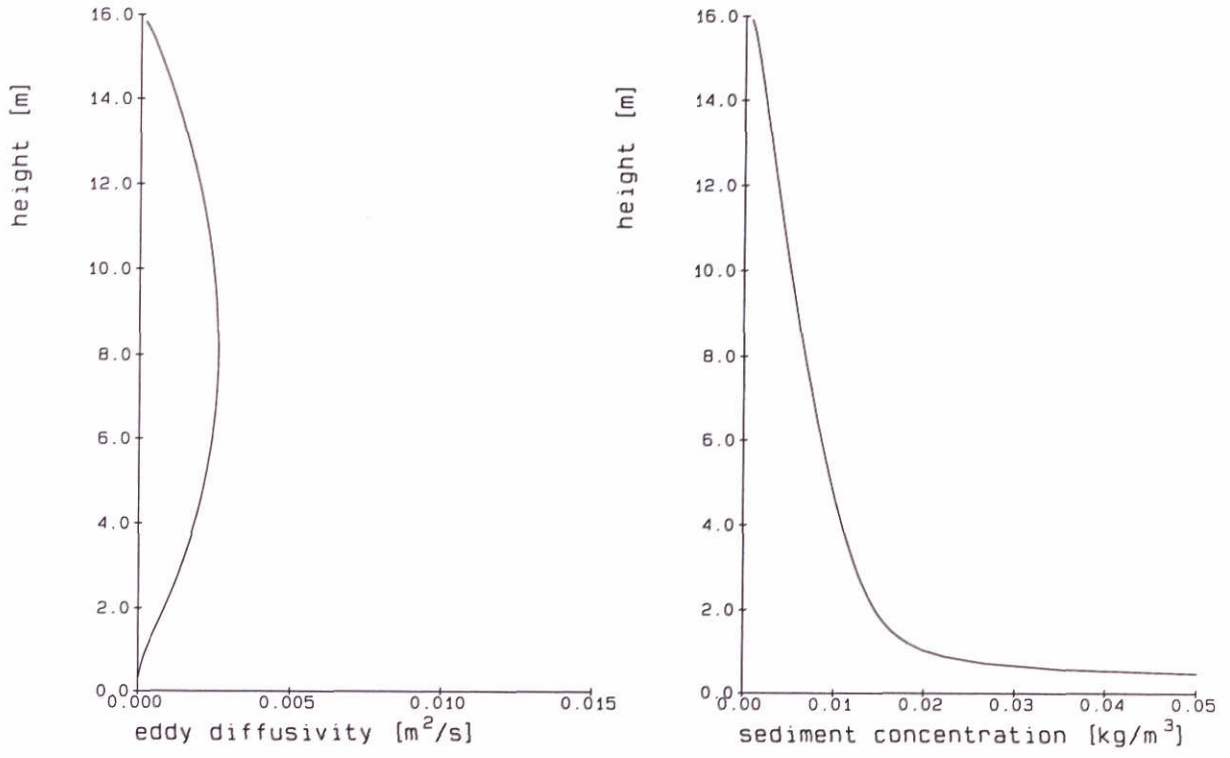

TIME : 800

Computed mass concentrations [g/l] - {run s01} saturation concentration, C_0 = 0.024 g/l h = 16m, U_m = 0.2 m/s, W_s = 0.5 mm/s, no waves		
	steady flow	
DELFT HYDRAULICS - MARINE & COASTAL MANAGEMENT	Proj. Z2263	Fig. 4.2f

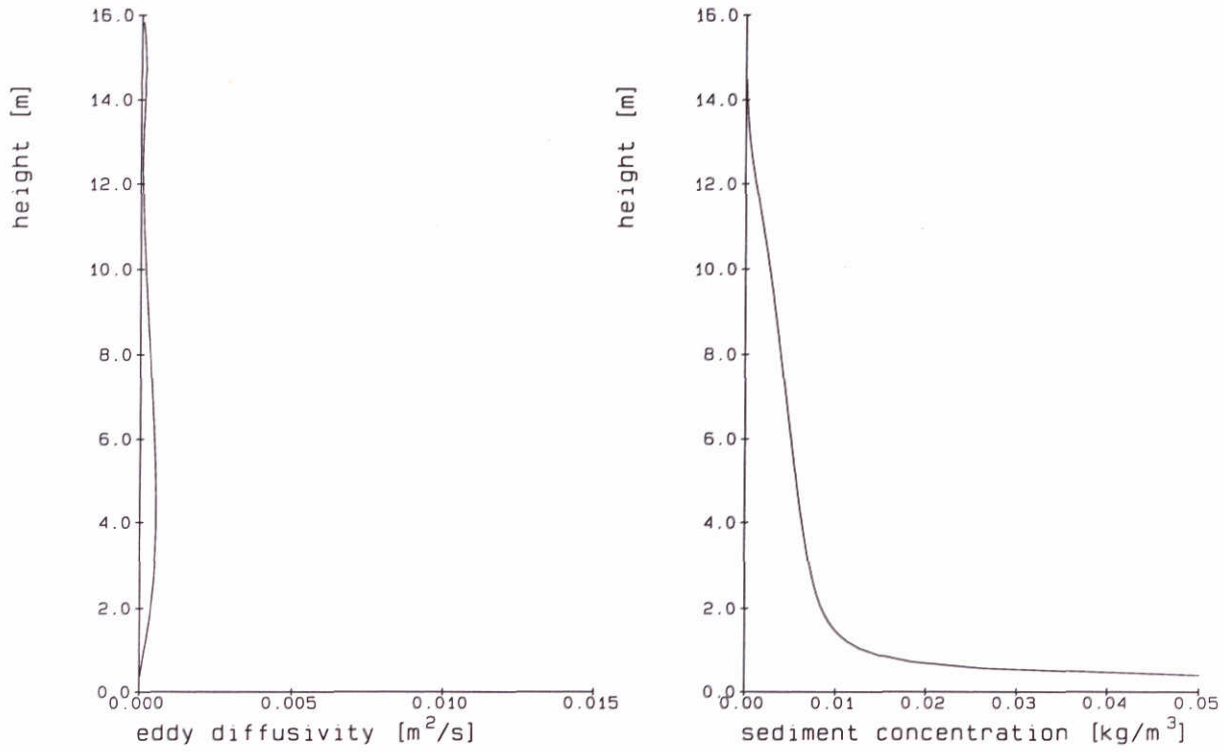

TIME : 1000

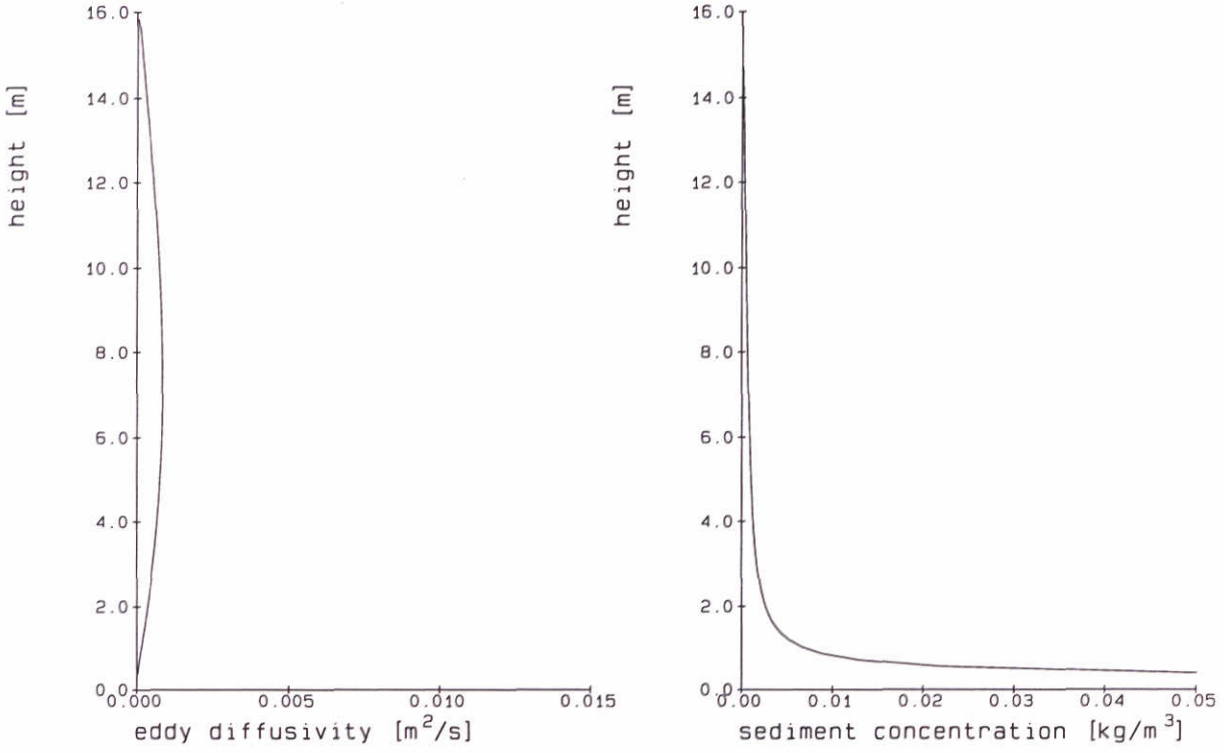

TIME : 1500

Computed mass concentrations [g/l] - {run s01} saturation concentration, C_0 = 0.024 g/l h = 16m, U_m = 0.2 m/s, W_s = 0.5 mm/s, no waves		
	steady flow	
DELFT HYDRAULICS - MARINE & COASTAL MANAGEMENT	Proj. Z2263	Fig. 4.2g

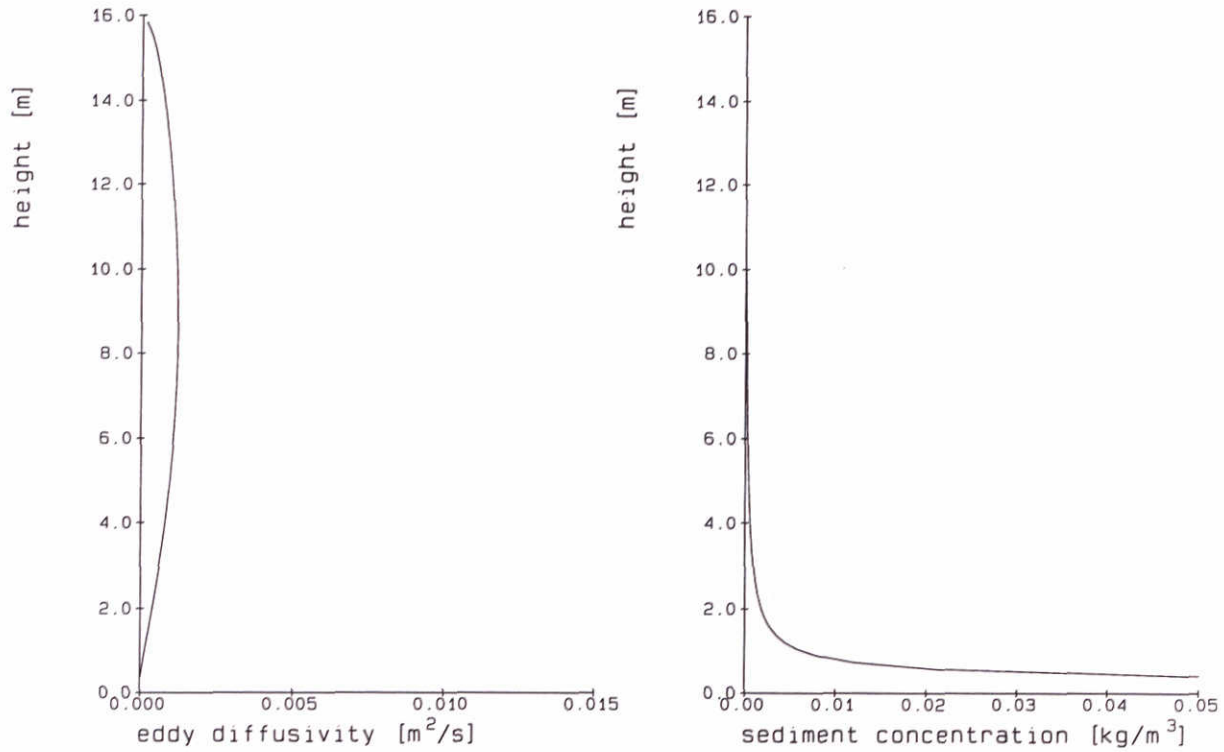

TIME : 3000

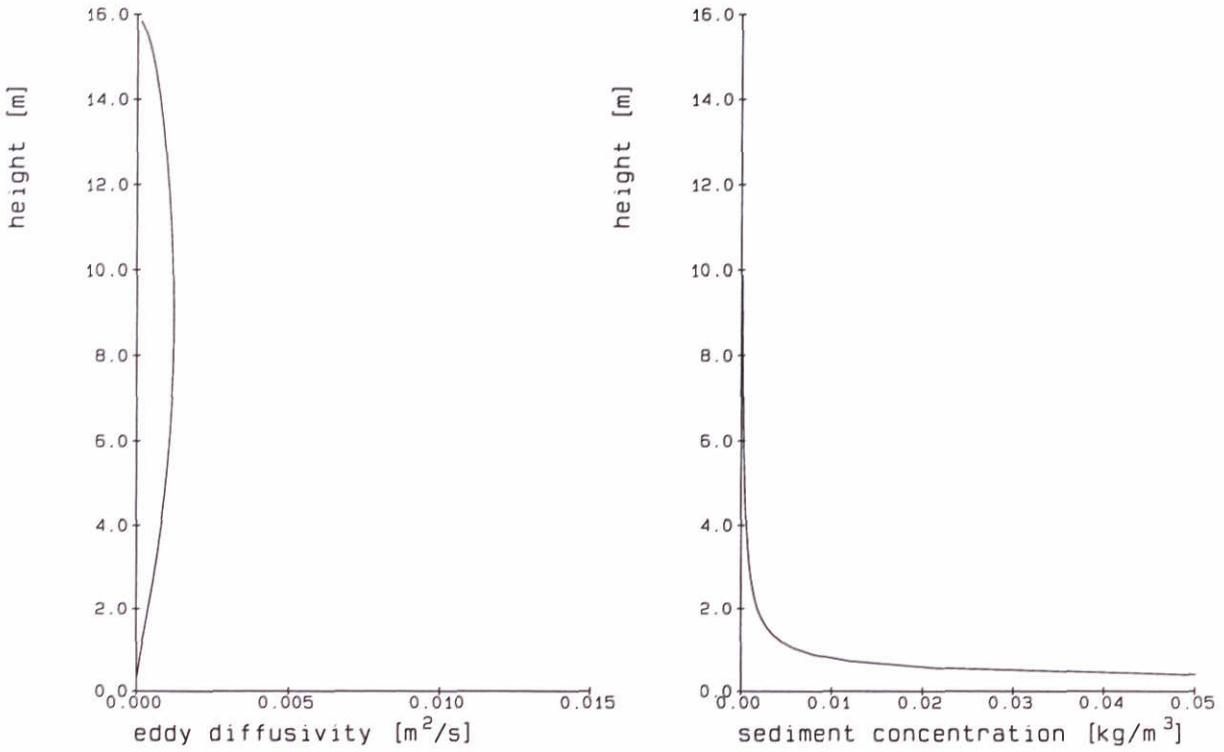

TIME : 6000

Computed mass concentrations [g/l] - {run s01} saturation concentration, C_0 = 0.024 g/l h = 16m, U_m = 0.2 m/s, W_s = 0.5 mm/s, no waves		
	steady flow	
DELFT HYDRAULICS - MARINE & COASTAL MANAGEMENT	Proj. Z2263	Fig. 4.2h

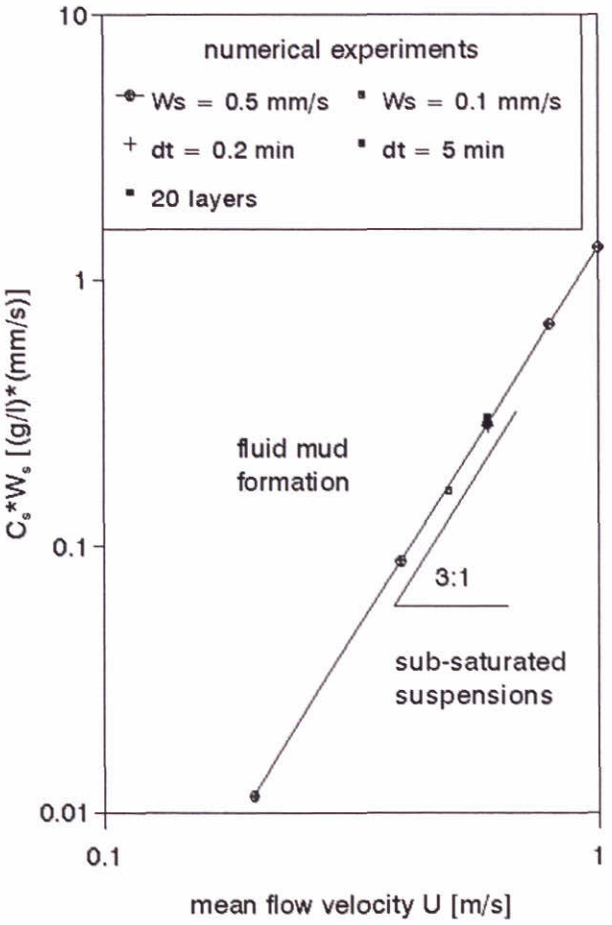

Fig. 4.3a

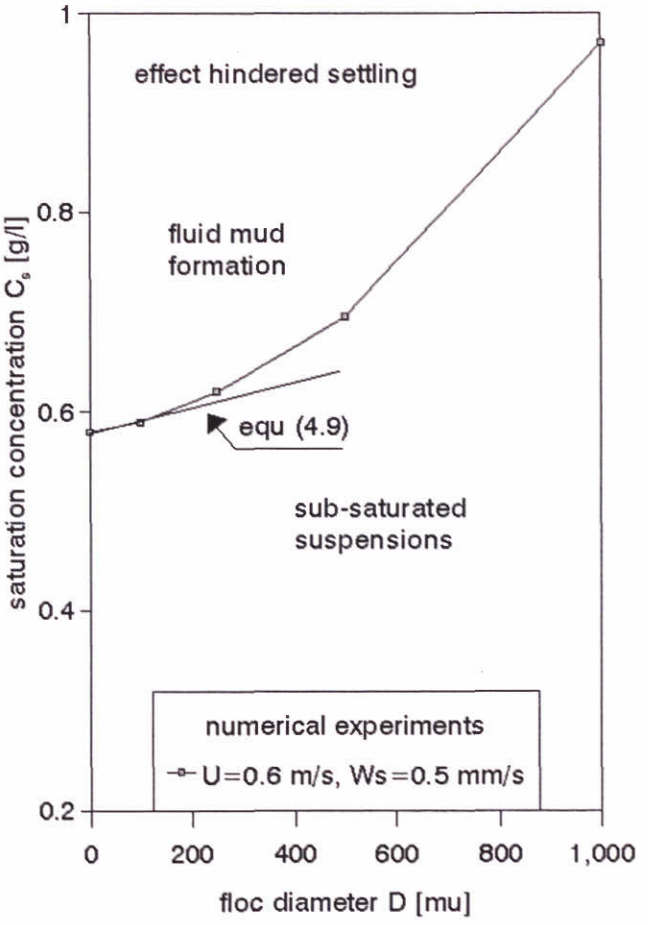

Fig. 4.3b

Saturation concentration as a function of flow velocity (4.3a) and floc diameter (4.3b); steady flow conditions

DELFT HYDRAULICS	
Proj: Z2263	SILTMAN
Fig. 4.3	Sept. 1997

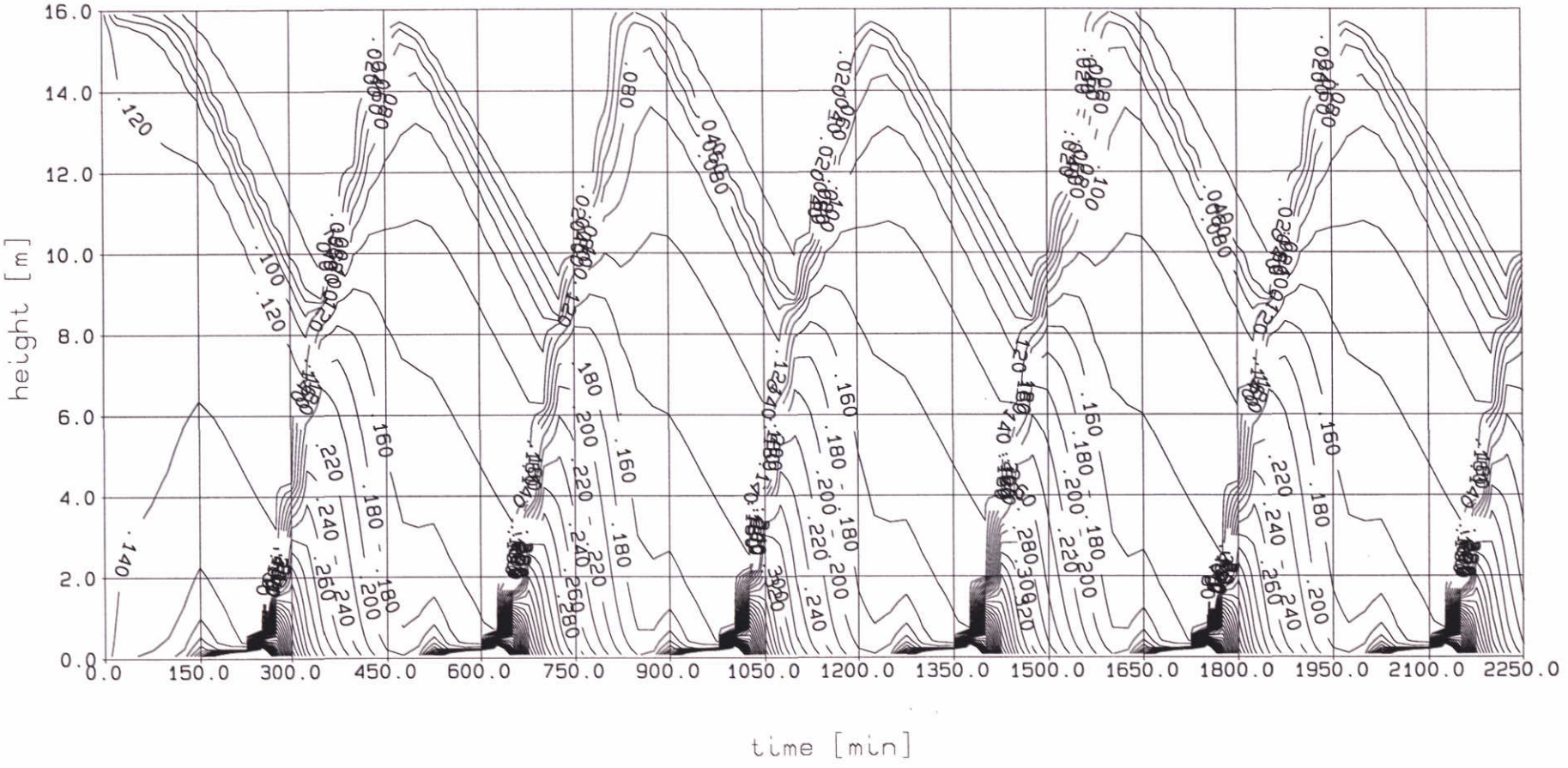

Computed mass concentrations [g/l] - {run s11a} initial concentration, C_0 = 0.13 g/l h = 16 m, U_m = 0.5 m/s, W_s = 0.5 mm/s, no waves		27-08-97
	M_2 tide	
DELFT HYDRAULICS - MARINE & COASTAL MANAGEMENT	Proj: Z2263	Fig. 4.4a

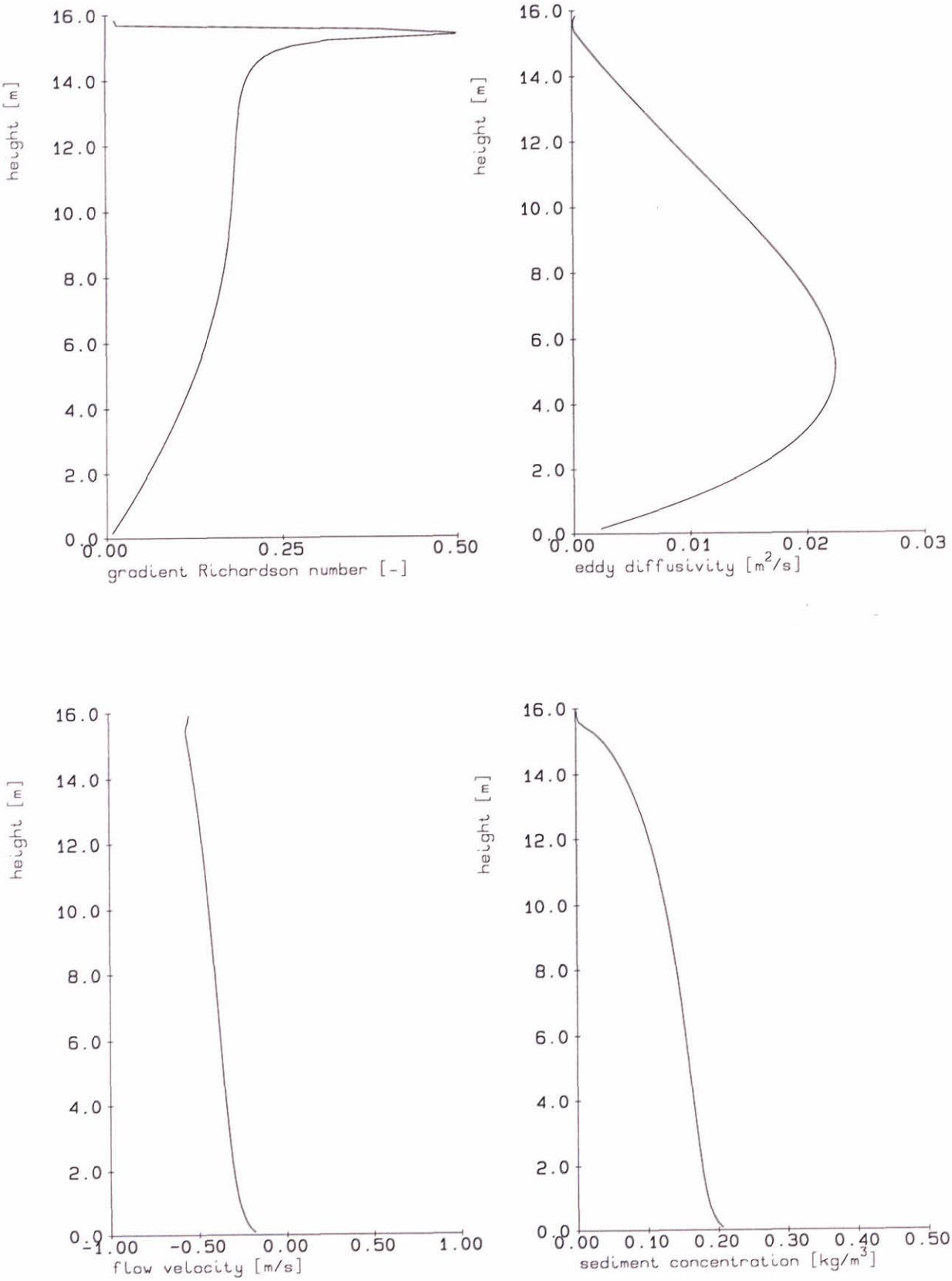

Computed mass concentrations [g/l] - {run s11a} initial concentration, C_0 = 0.13 g/l h = 16 m, U_m = 0.5 m/s, W_s = 0.5 mm/s, no waves	time : 1950	27-08-97
	M_2 tide	
DELFT HYDRAULICS - MARINE & COASTAL MANAGEMENT	Proj: Z2263	Fig. 4.4b

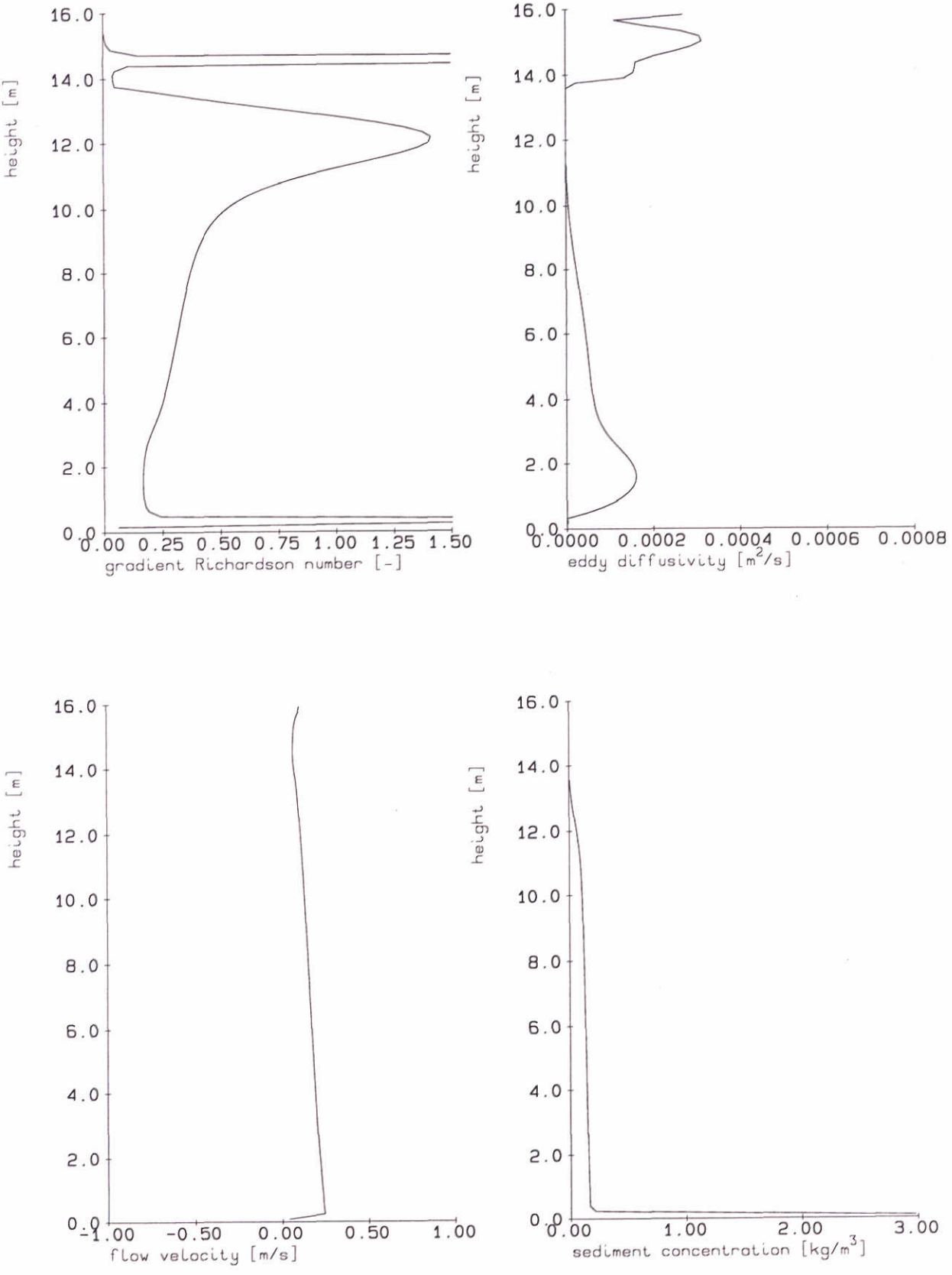

Computed mass concentrations [g/l] - {run s11a} initial concentration, C_0 = 0.13 g/l h = 16 m, U_m = 0.5 m/s, W_s = 0.5 mm/s, no waves	time : 2100 M_2 tide	27-08-97
DELFT HYDRAULICS - MARINE & COASTAL MANAGEMENT	Proj: Z2263	Fig. 4.4c

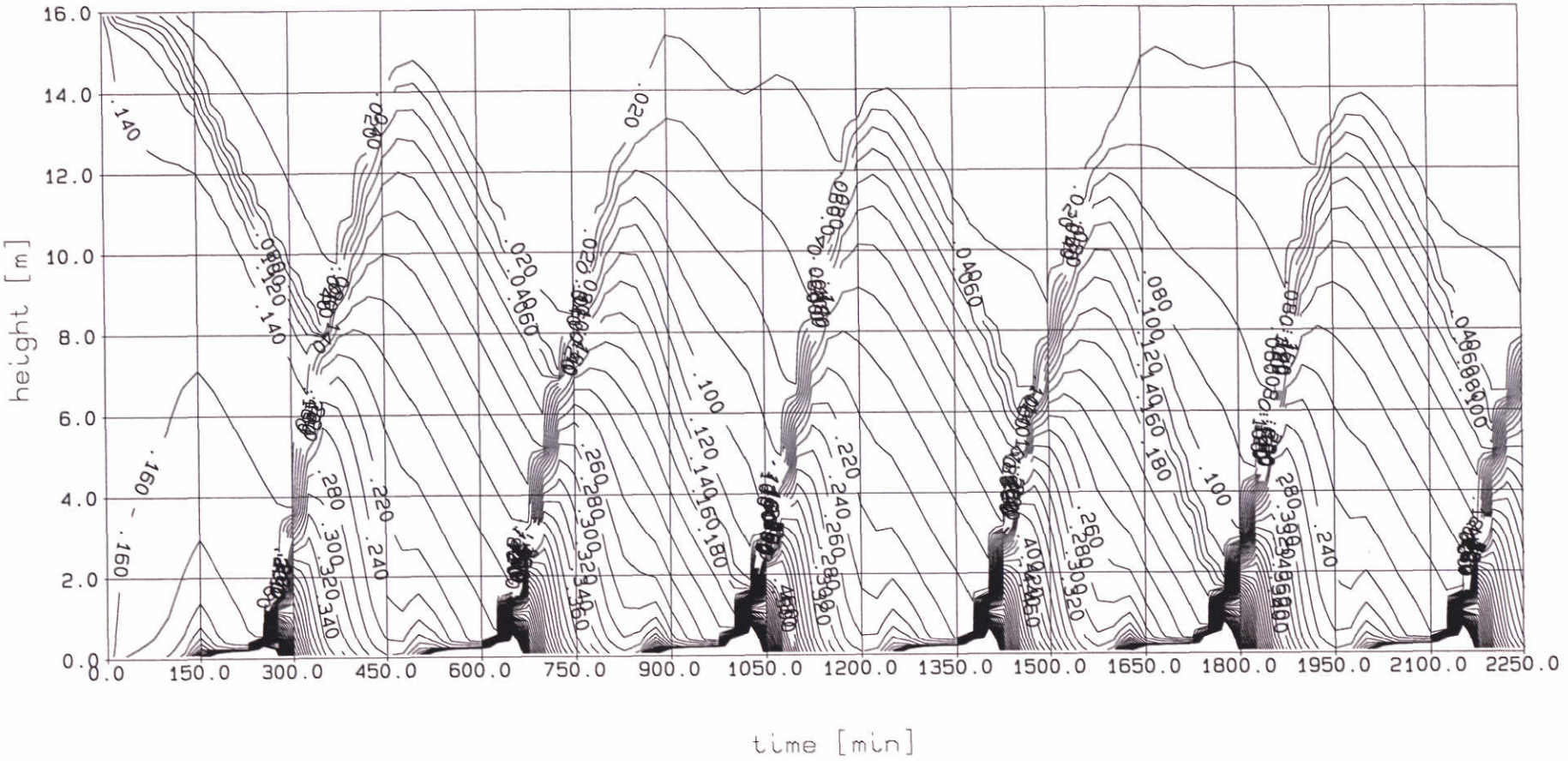

Computed mass concentrations [g/l] - {run s11b} initial concentration, C_0 = 0.15 g/l h = 16 m, U_m = 0.5 m/s, W_s = 0.5 mm/s, no waves		27-08-97
	M_2 tide	
DELFT HYDRAULICS - MARINE & COASTAL MANAGEMENT	Proj: Z2263	Fig. 4.5a

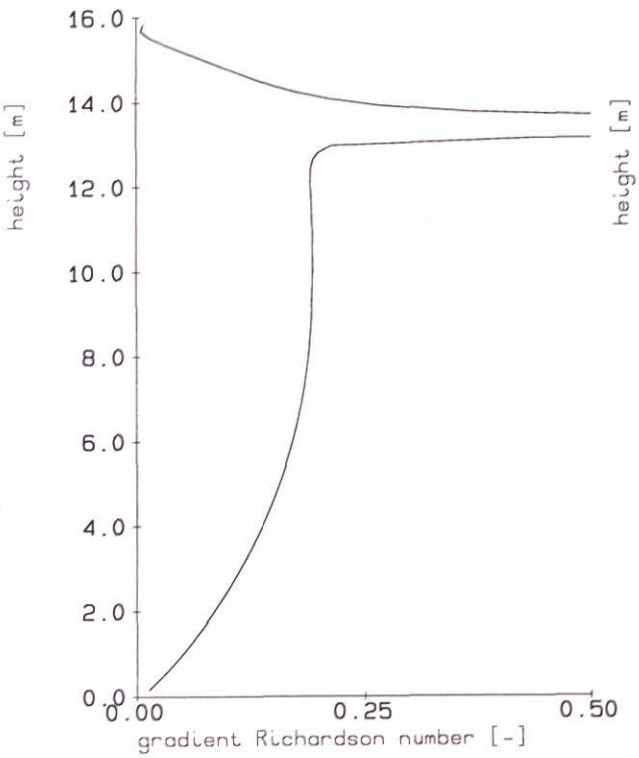

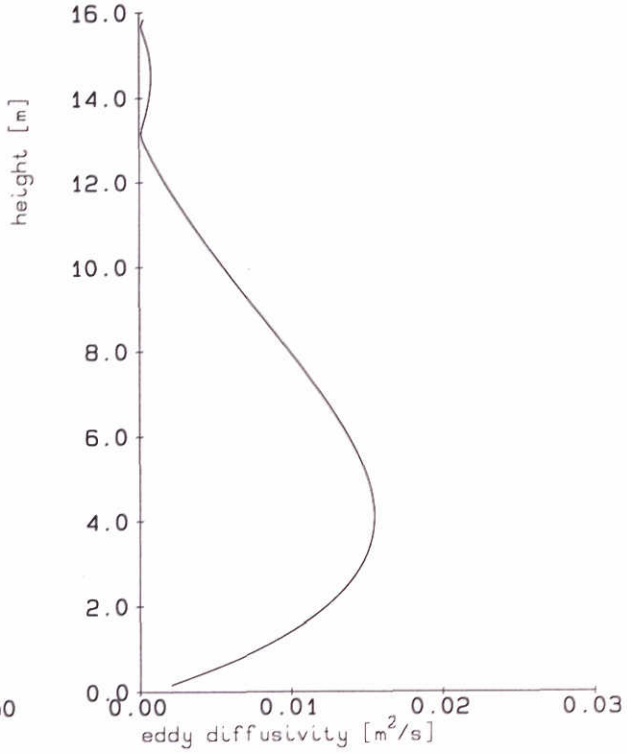

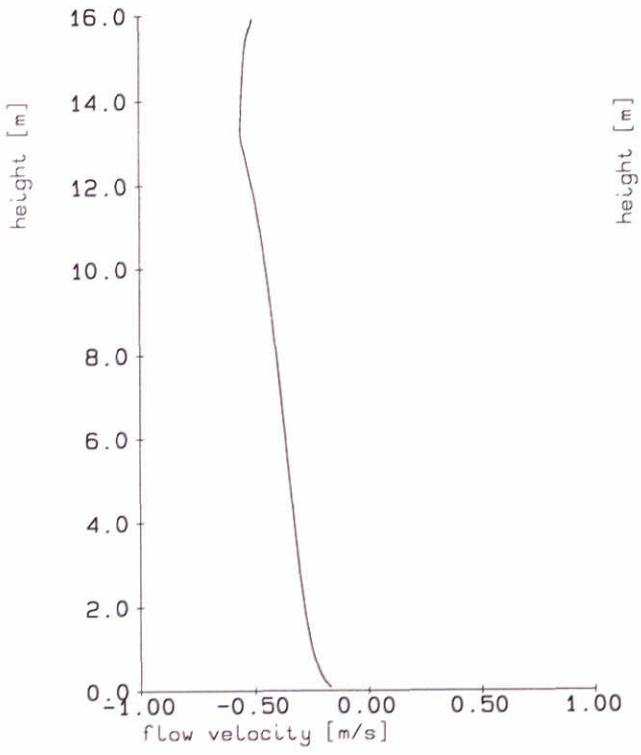

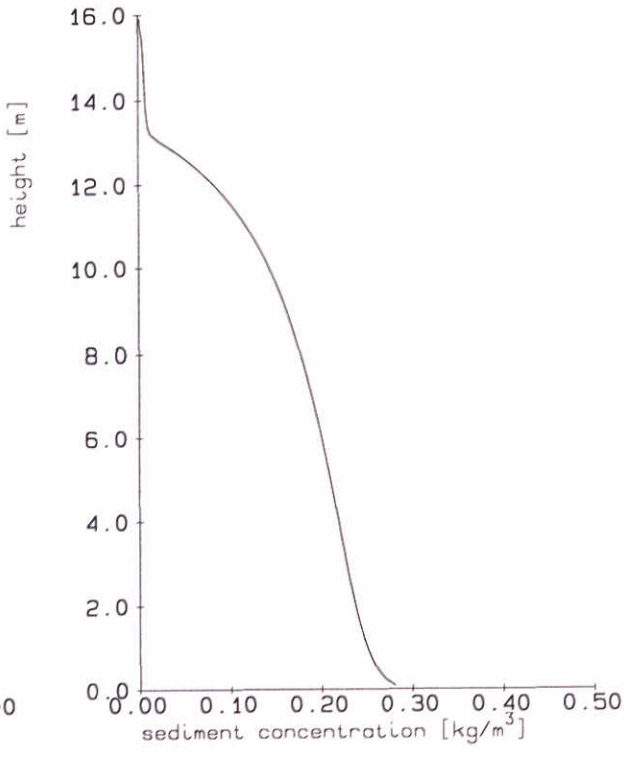

Computed mass concentrations [g/l] - {run s11b} initial concentration, C_0 = 0.15 g/l h = 16m, U_m = 0.5 m/s, W_s = 0.5 mm/s, no waves	time : 1950	27-08-97
	M_2 tide	
DELFT HYDRAULICS - MARINE & COASTAL MANAGEMENT	Proj: Z2263	Fig. 4.5b

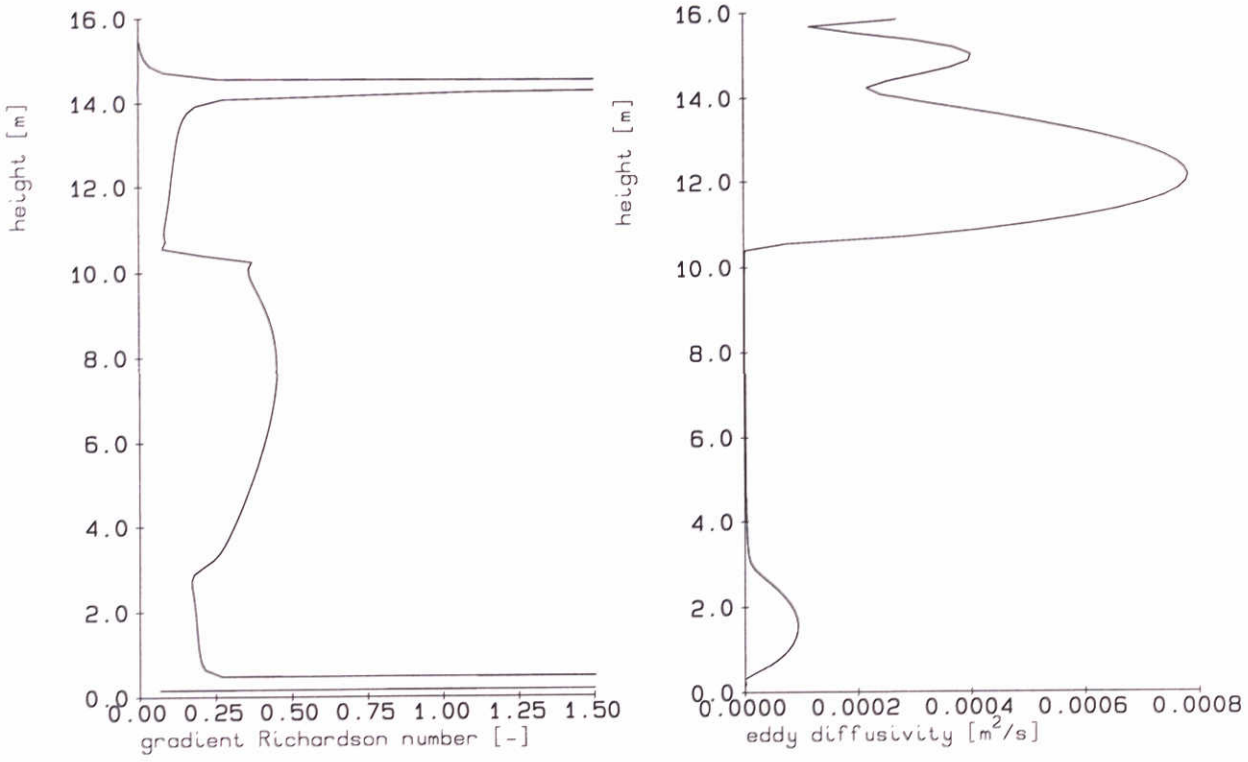

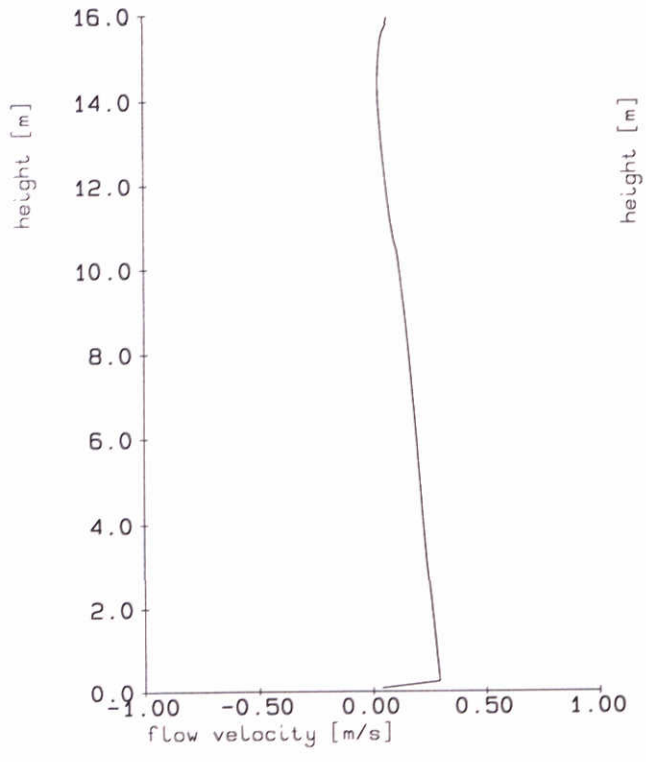

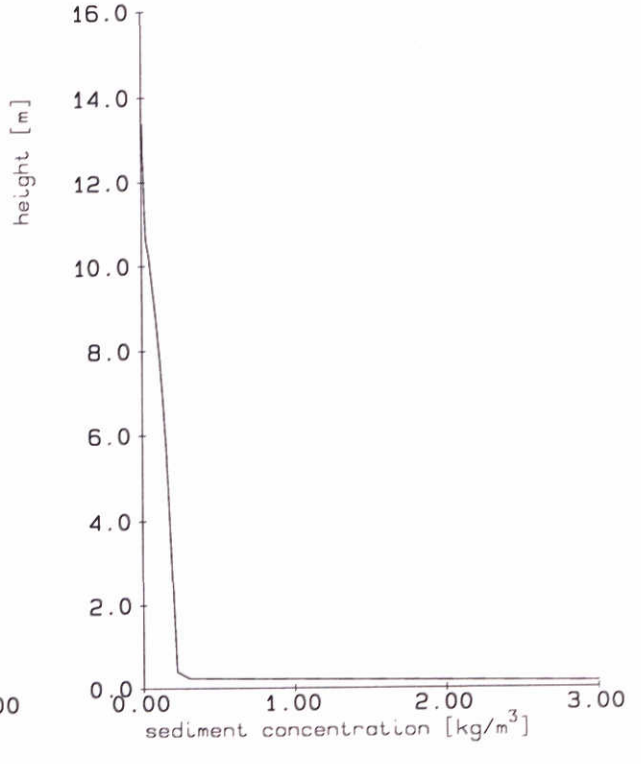

Computed mass concentrations [g/l] - {run s11b} initial concentration, C_0 = 0.15 g/l h = 16m, U_m = 0.5 m/s, W_s = 0.5 mm/s, no waves	time : 2100	27-08-97
	M_2 tide	
DELFT HYDRAULICS - MARINE & COASTAL MANAGEMENT	Proj: Z2263	Fig. 4.5c

Fig. 4.6a

Fig. 4.6b

Saturation concentration as a function of flow velocity and settling velocity (tidal conditions)		Sept.1997
	SILTMAN	
DELFT HYDRAULICS	Proj: Z2263	Fig. 4.6

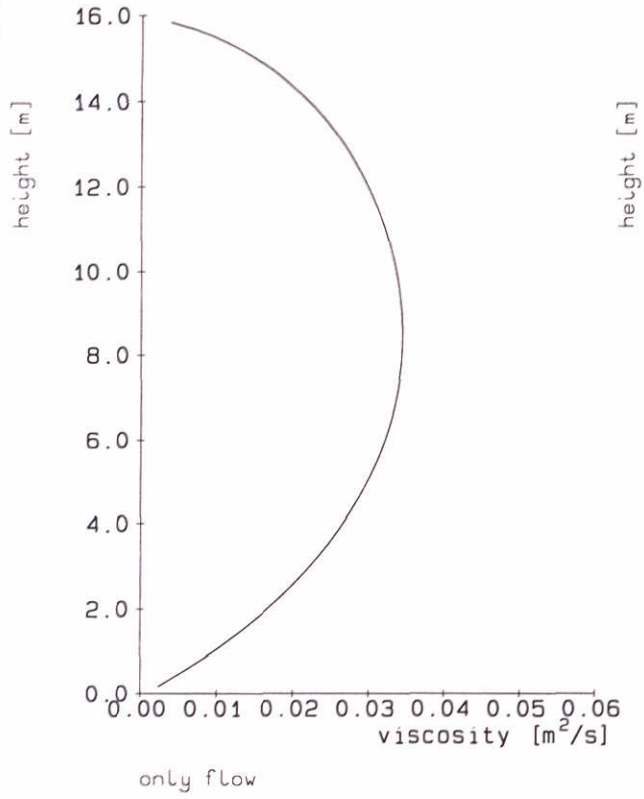

only flow

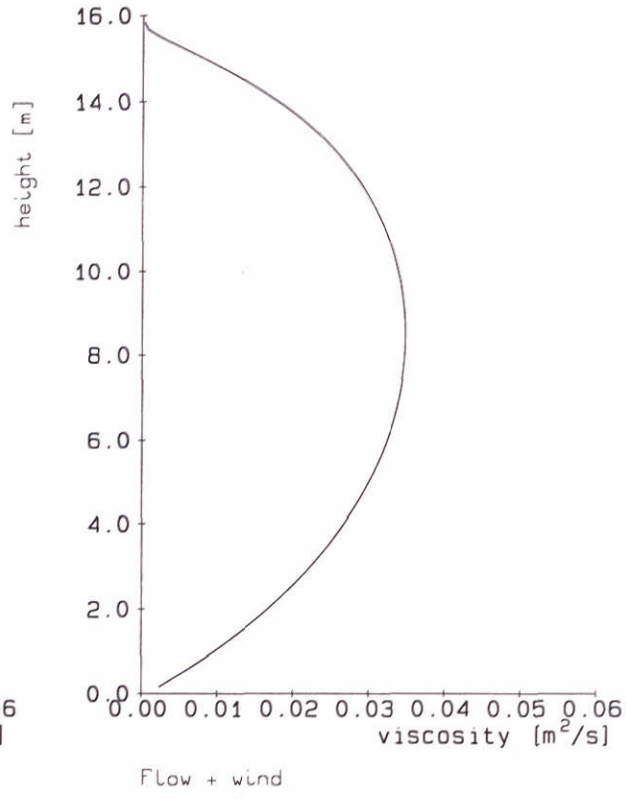

Flow + wind

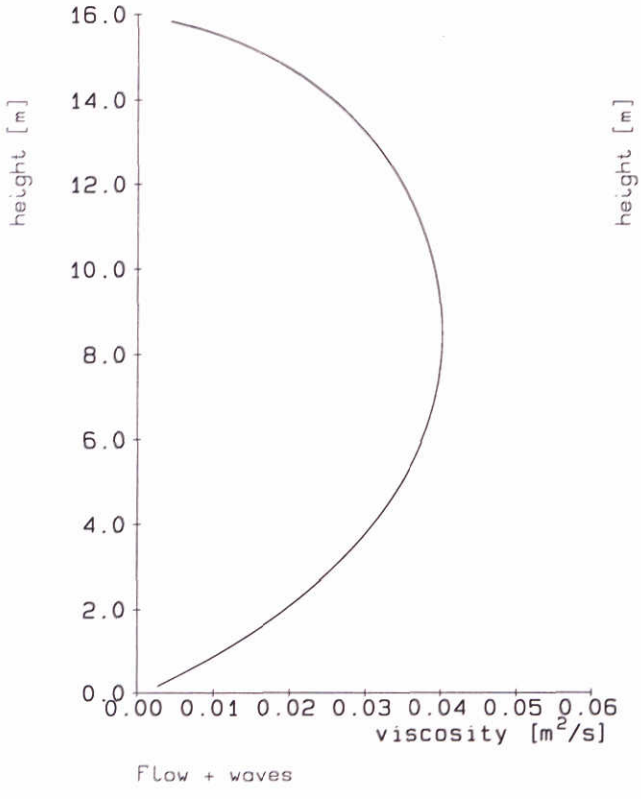

Flow + waves

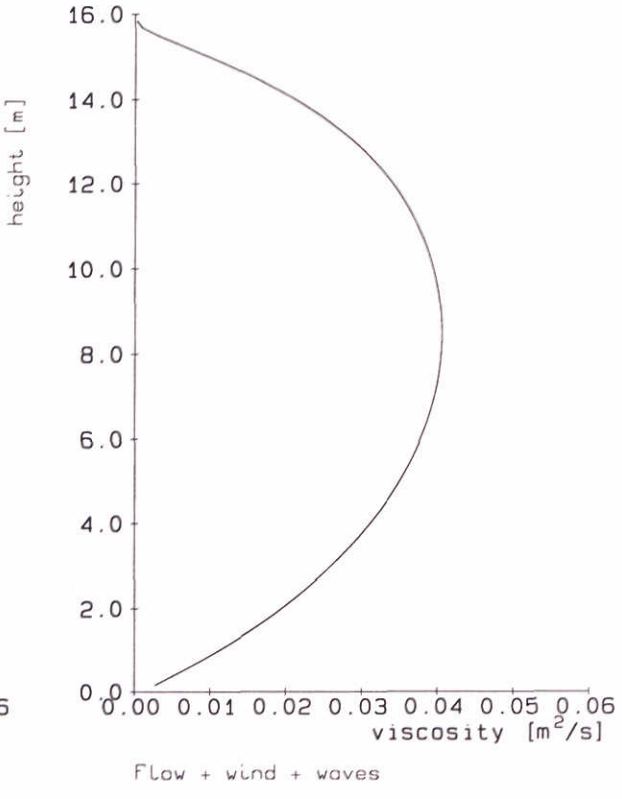

Flow + wind + waves

Eddy viscosity profiles for various flow conditions (run - s18)	U = 0.5 m/s	
DELFT HYDRAULICS - MARINE & COASTAL MANAGEMENT	Proj: Z2263	Fig. 5.1a

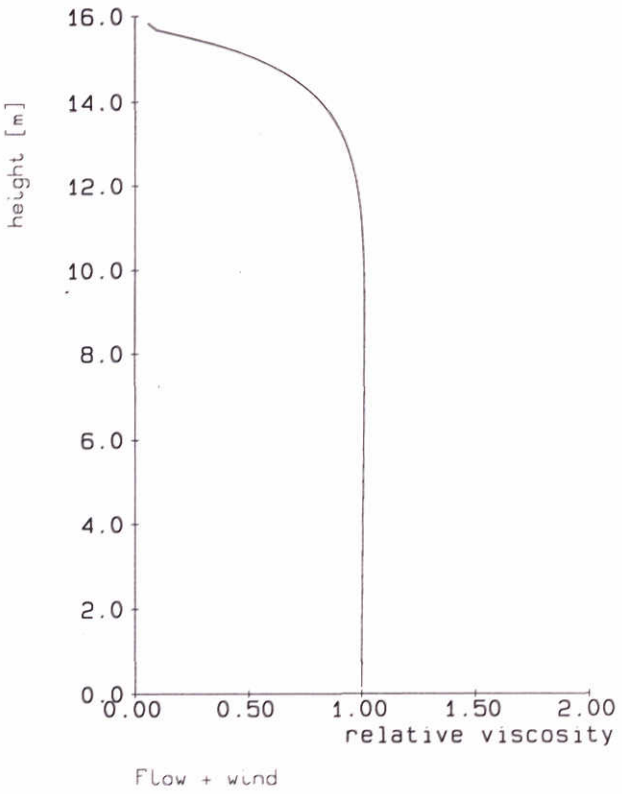

Flow + wind

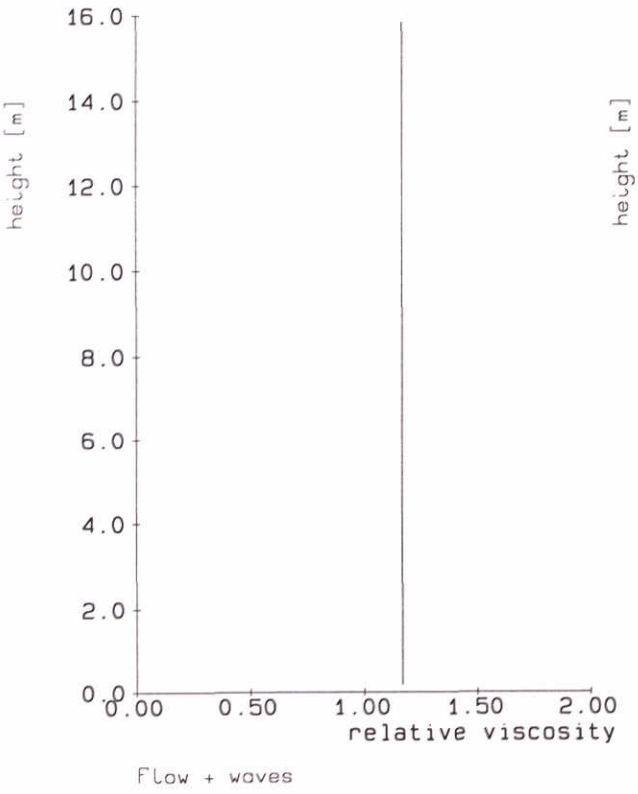

Flow + waves

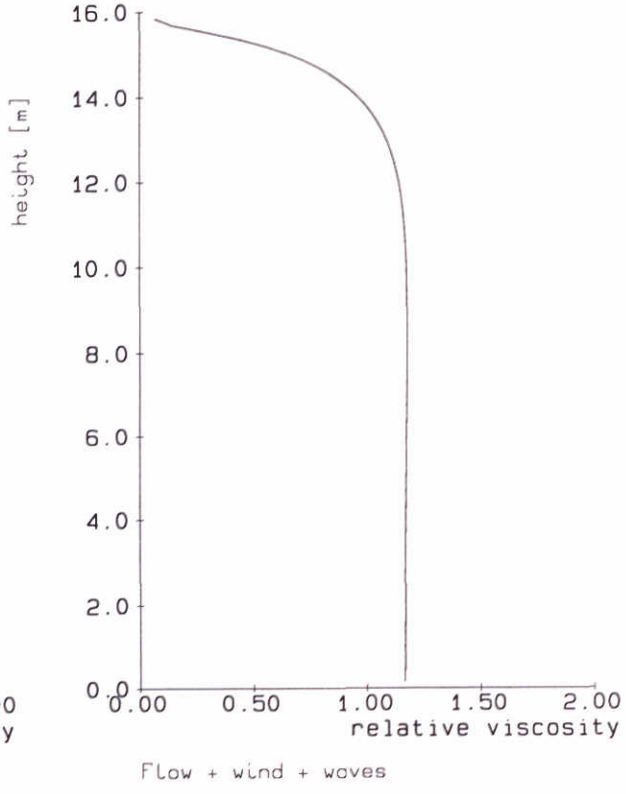

Flow + wind + waves

Relative eddy viscosity profiles for various flow conditions (run - s18)	U = 0.5 m/s	
DELFT HYDRAULICS - MARINE & COASTAL MANAGEMENT	Proj: Z2263	Fig. 5.1b

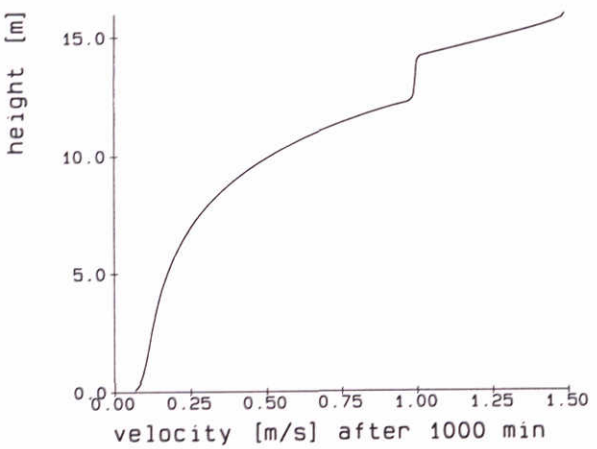

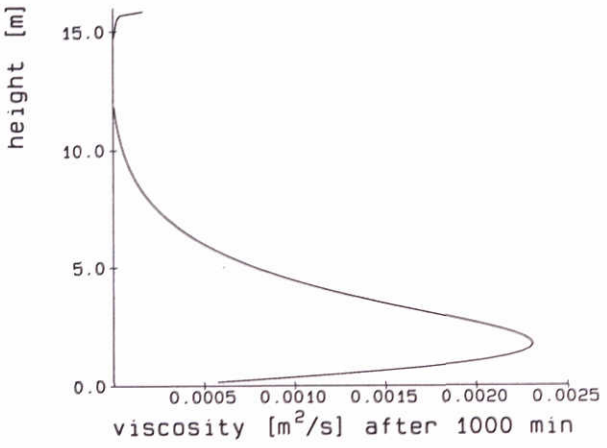

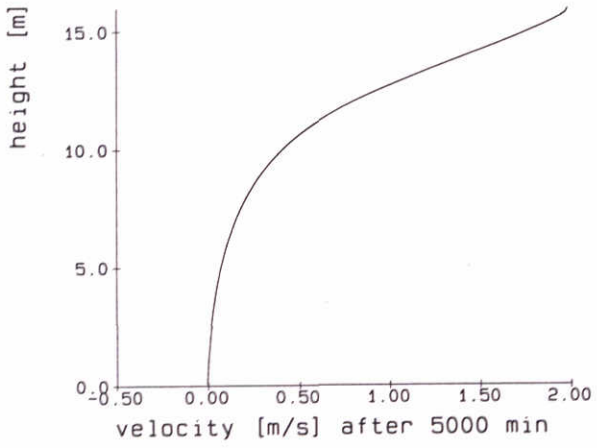

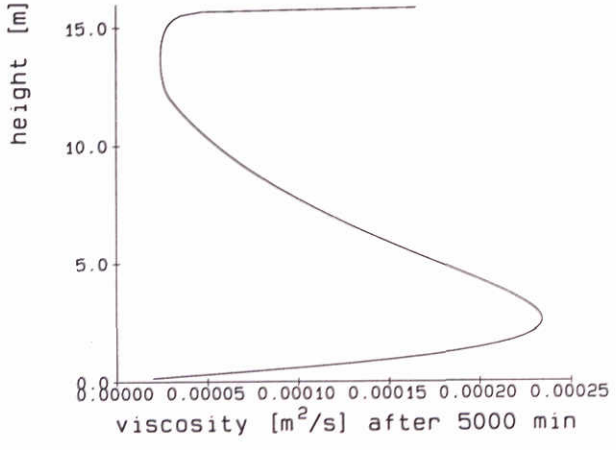

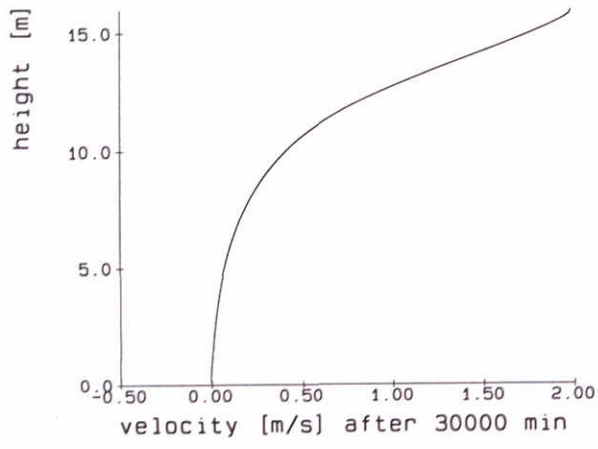

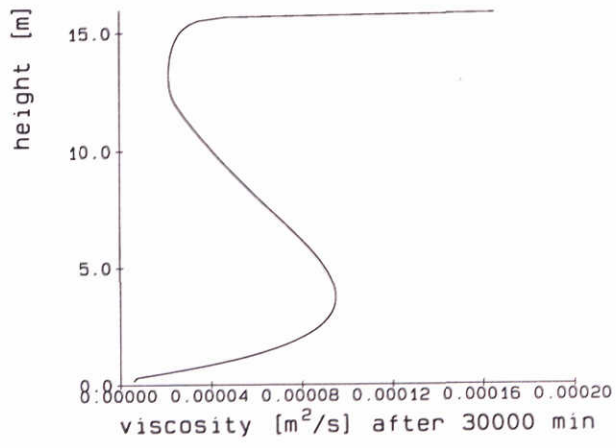

Velocity and eddy viscosity profiles Initial salinity-induced stratification	U = 0.5 m/s	
DELFT HYDRAULICS - MARINE & COASTAL MANAGEMENT	Proj: Z2263	Fig. 5.2

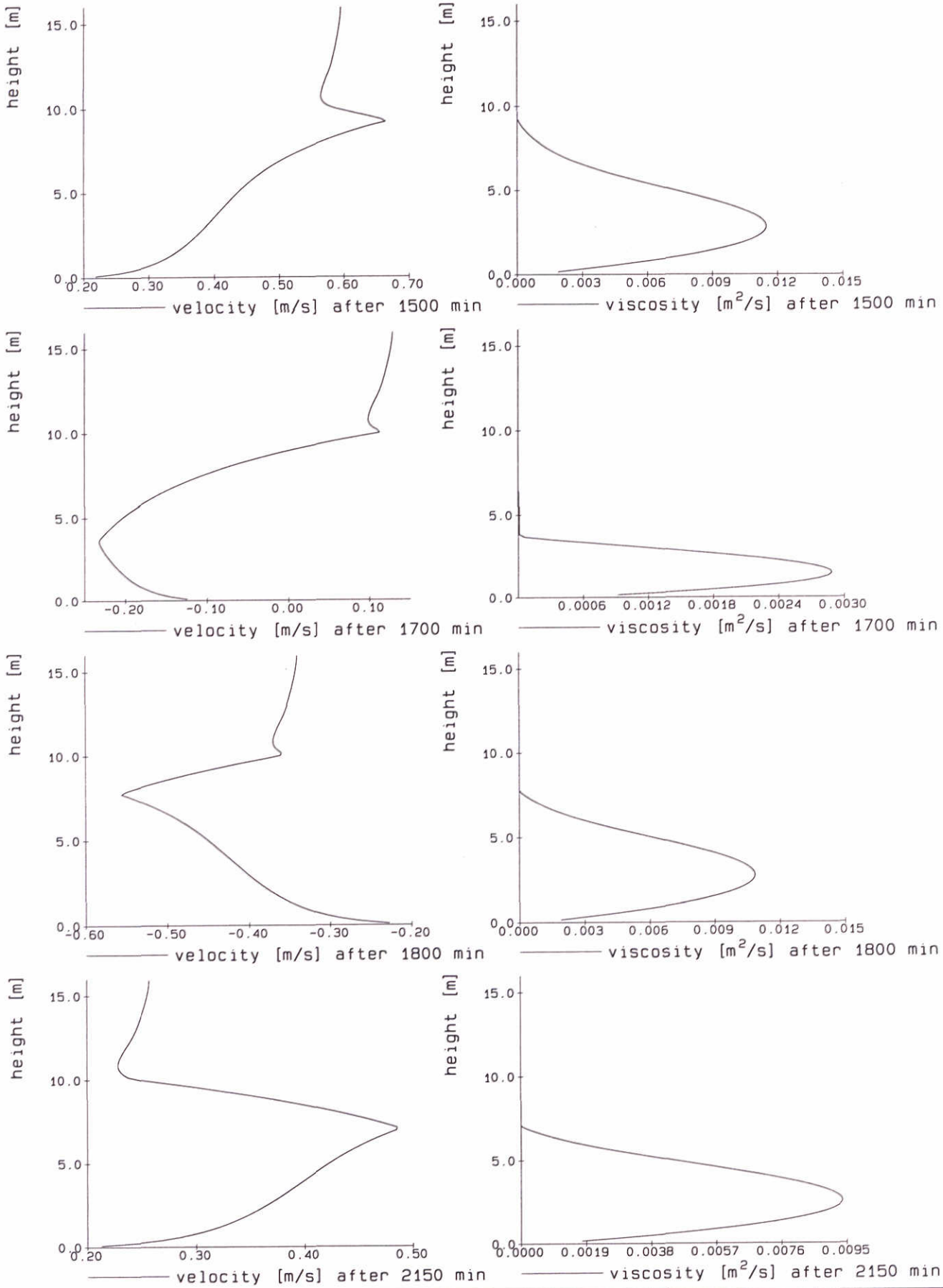

Velocity and eddy viscosity profiles
Initial salinity-induced stratification

U_m = 0.5 m/s

M_2 tide

DELFT HYDRAULICS - MARINE & COASTAL MANAGEMENT

Proj: Z2263

Fig. 5.3

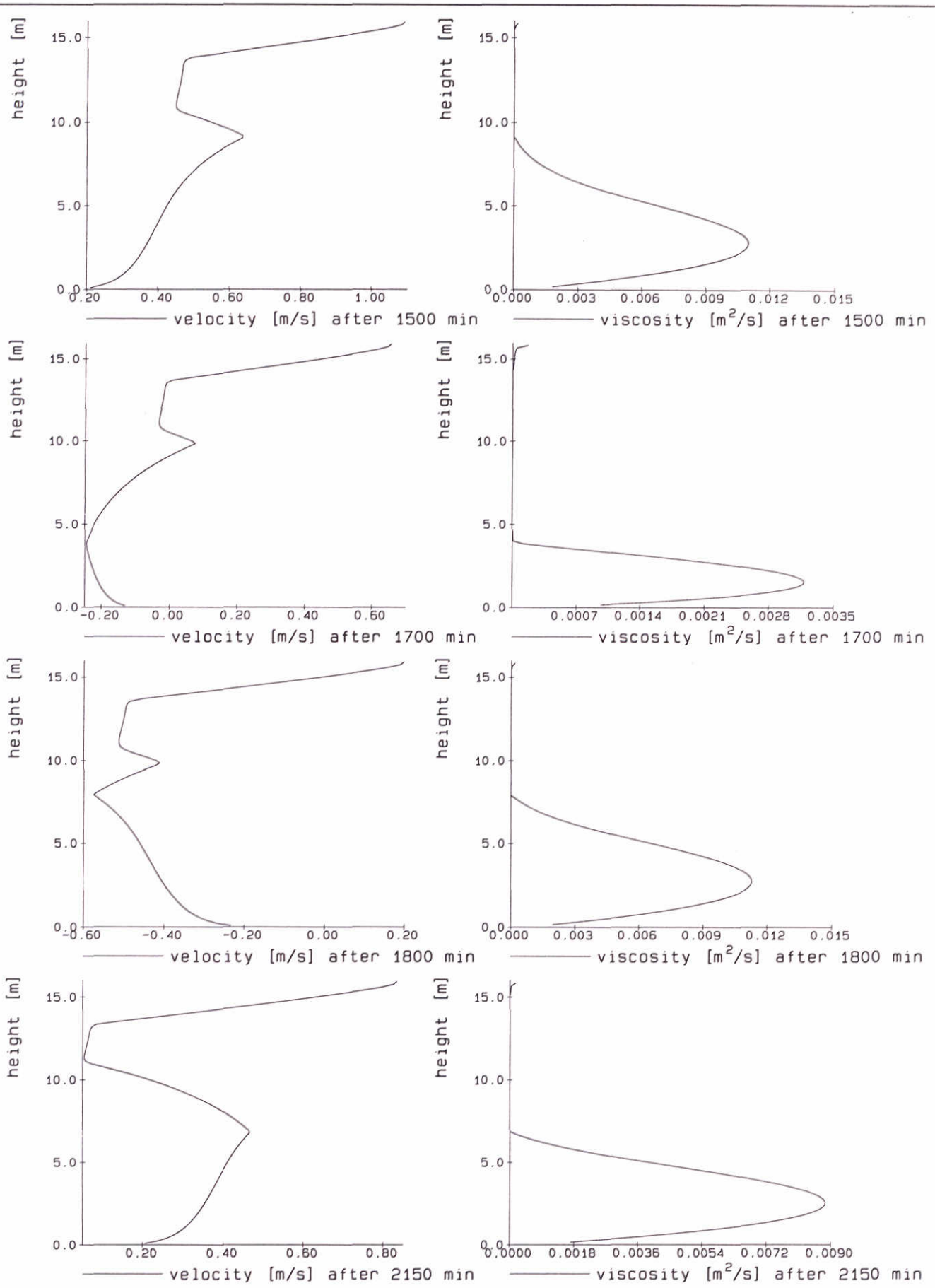

Velocity and eddy viscosity profiles Initial salinity-induced stratification	U_m = 0.5 m/s	
	M_2 tide + wind	
DELFT HYDRAULICS - MARINE & COASTAL MANAGEMENT	Proj: Z2263	Fig. 5.4

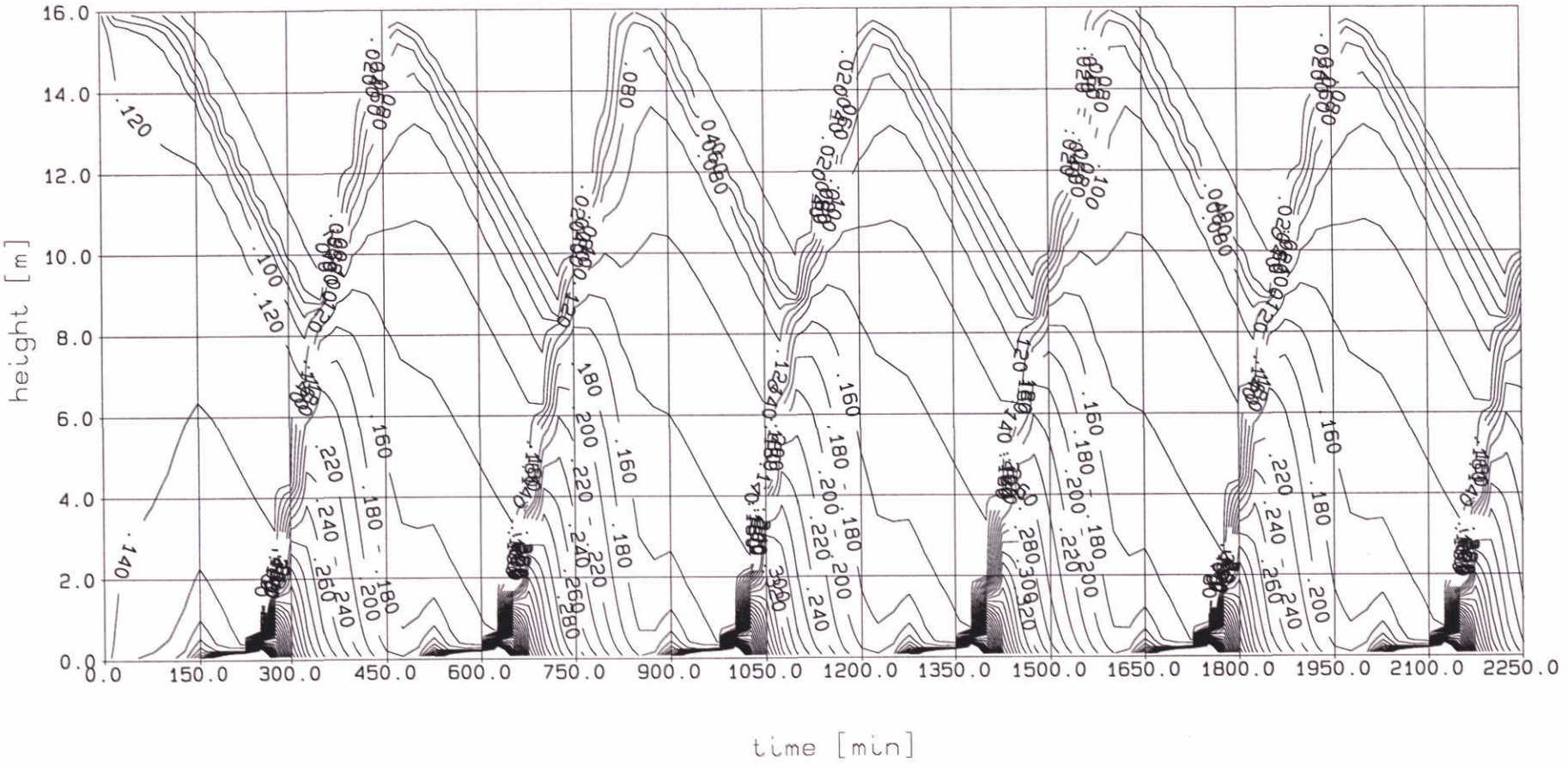

Computed mass concentrations [g/l] - {run s30a} initial concentration, C_0 = 0.013 g/l h = 16 m, U_m = 0.5 m/s, W_s = 0.5 mm/s	M_2 tide	23-09-97
	15 m/s wind	
DELFT HYDRAULICS - MARINE & COASTAL MANAGEMENT	Proj: Z2263	Fig. 5.5a

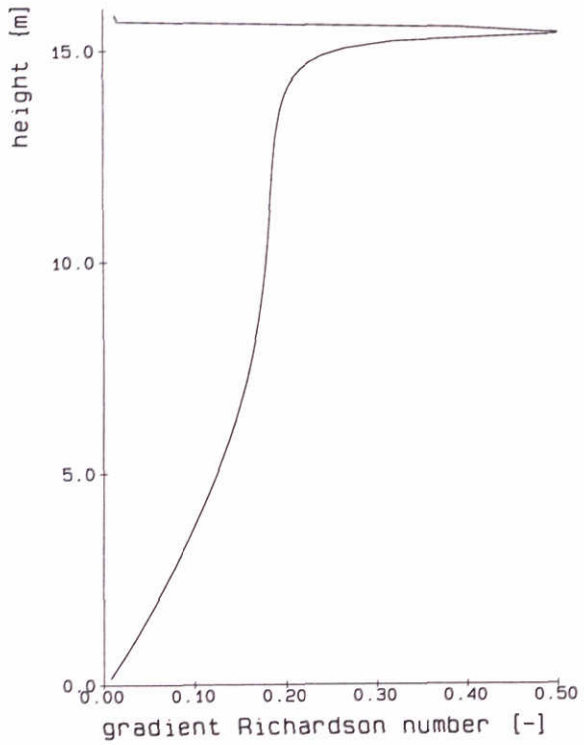

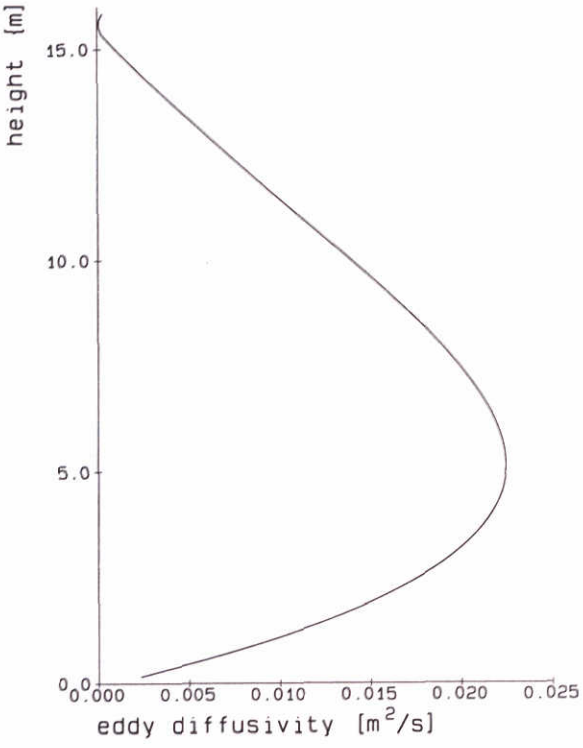

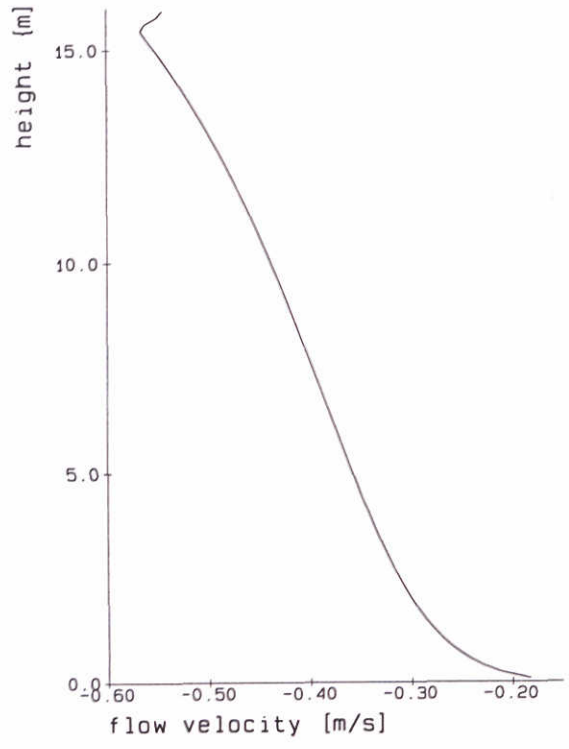

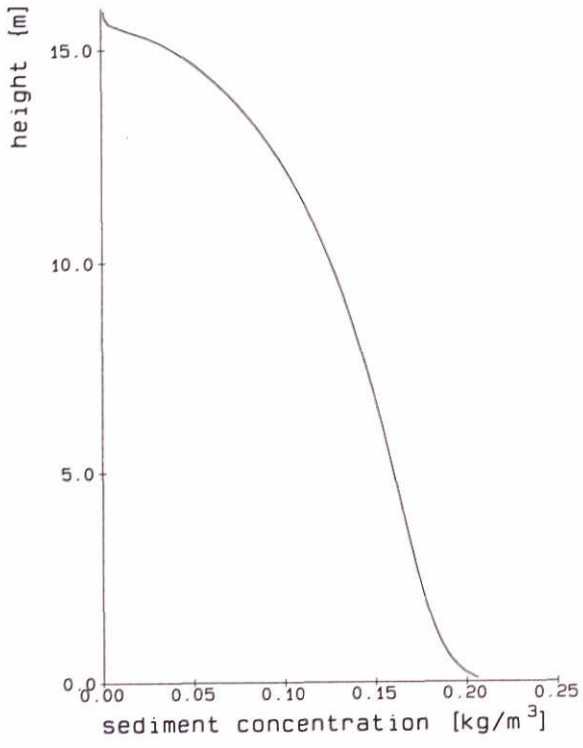

Computed mass concentrations [g/l] - {run s30a} initial concentration, C_0 = 0.013 g/l h = 16 m, U_m = 0.5 m/s, W_s = 0.5 mm/s	M_2 tide	time : 1950
	15 m/s wind	
DELFT HYDRAULICS - MARINE & COASTAL MANAGEMENT	Proj: Z2263	Fig. 5.5b

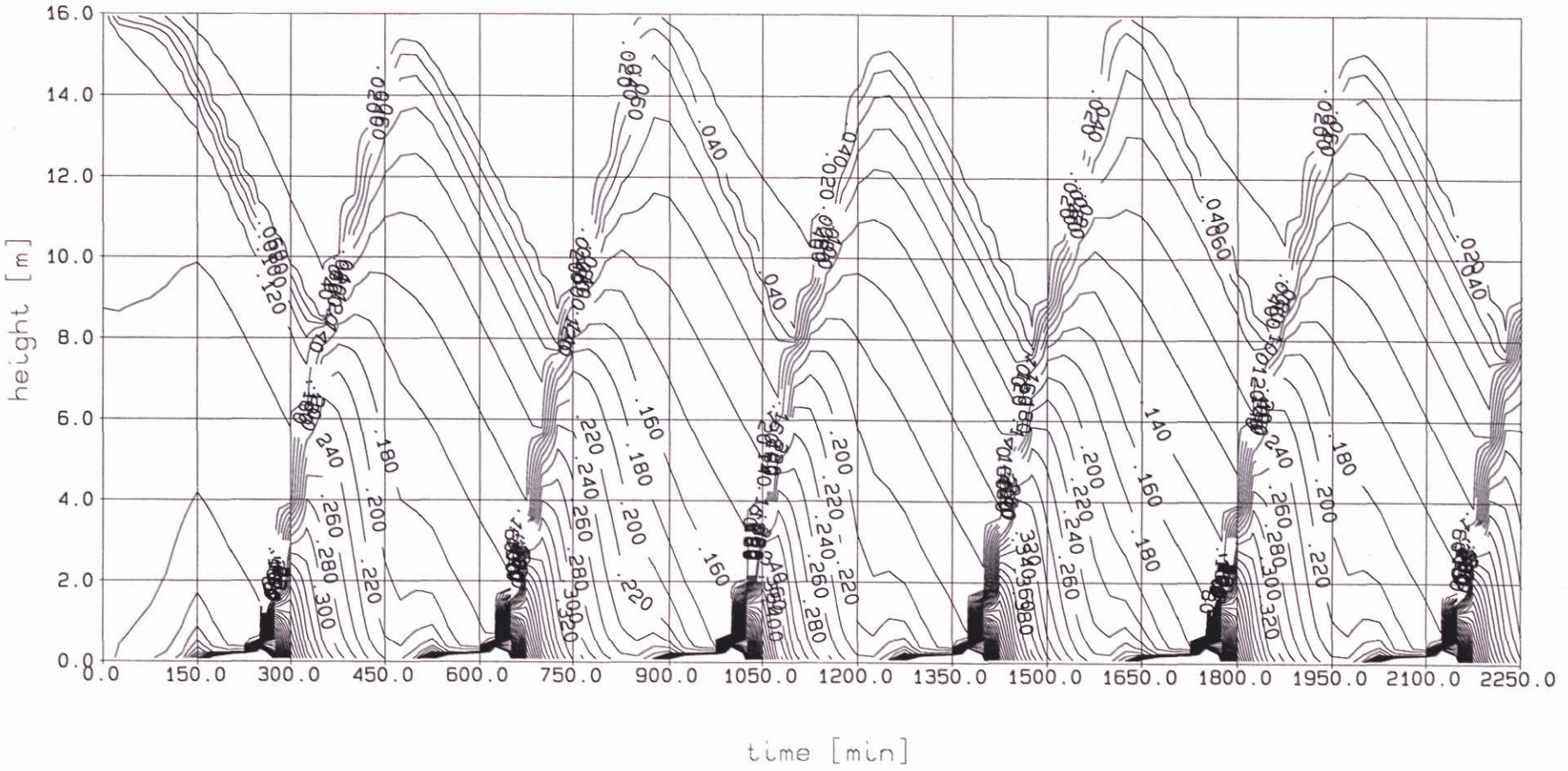

Computed mass concentrations [g/l] - {run s30b} initial concentration, C_0 = 0.014 g/l h = 16 m, U_m = 0.5 m/s, W_s = 0.5 mm/s	M_2 tide	23-09-97
	15 m/s wind	
DELFT HYDRAULICS - MARINE & COASTAL MANAGEMENT	Proj: Z2263	Fig. 5.5c

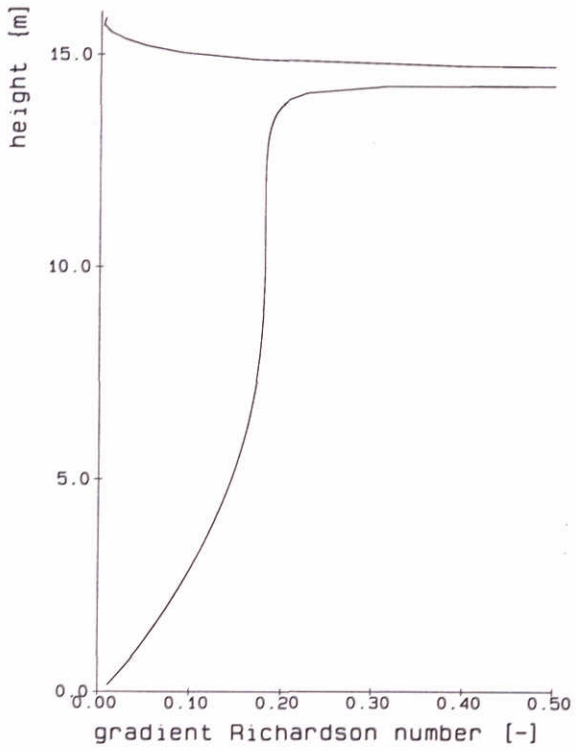

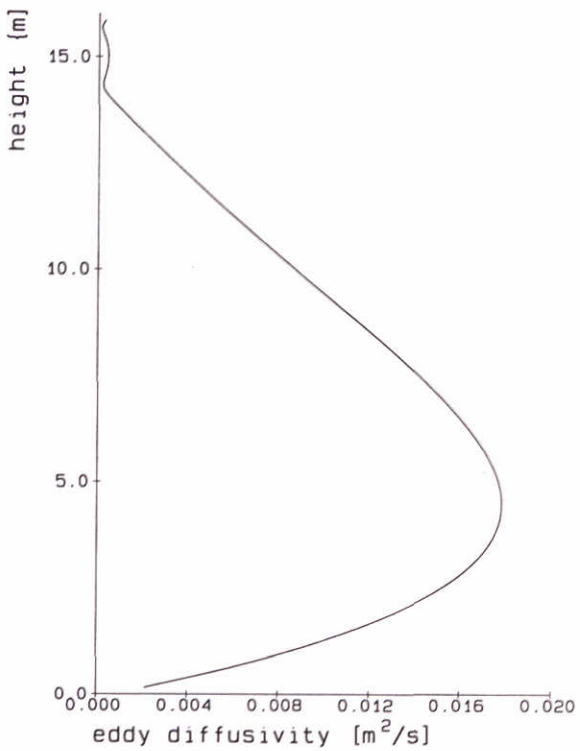

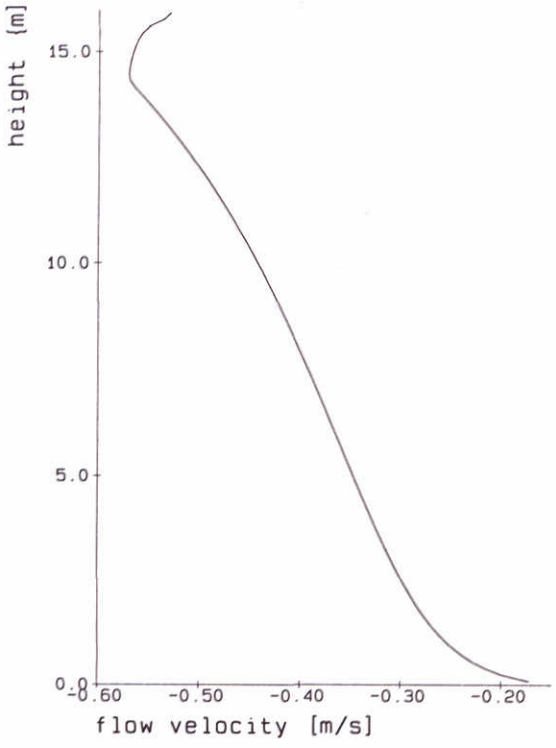

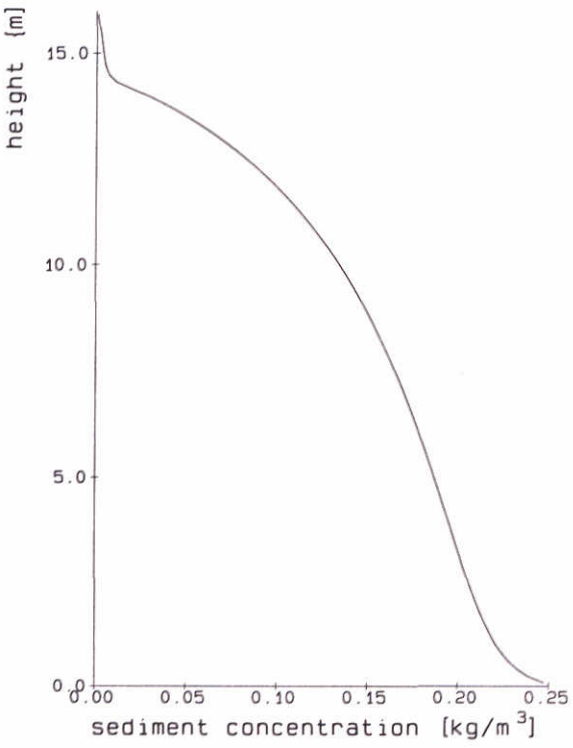

Computed mass concentrations [g/l] - {run s30b} initial concentration, C_0 = 0.014 g/l h = 16 m, U_m = 0.5 m/s, W_s = 0.5 mm/s	M_2 tide	time : 1950
	15 m/s wind	
DELFT HYDRAULICS - MARINE & COASTAL MANAGEMENT	Proj: Z2263	Fig. 5.5d

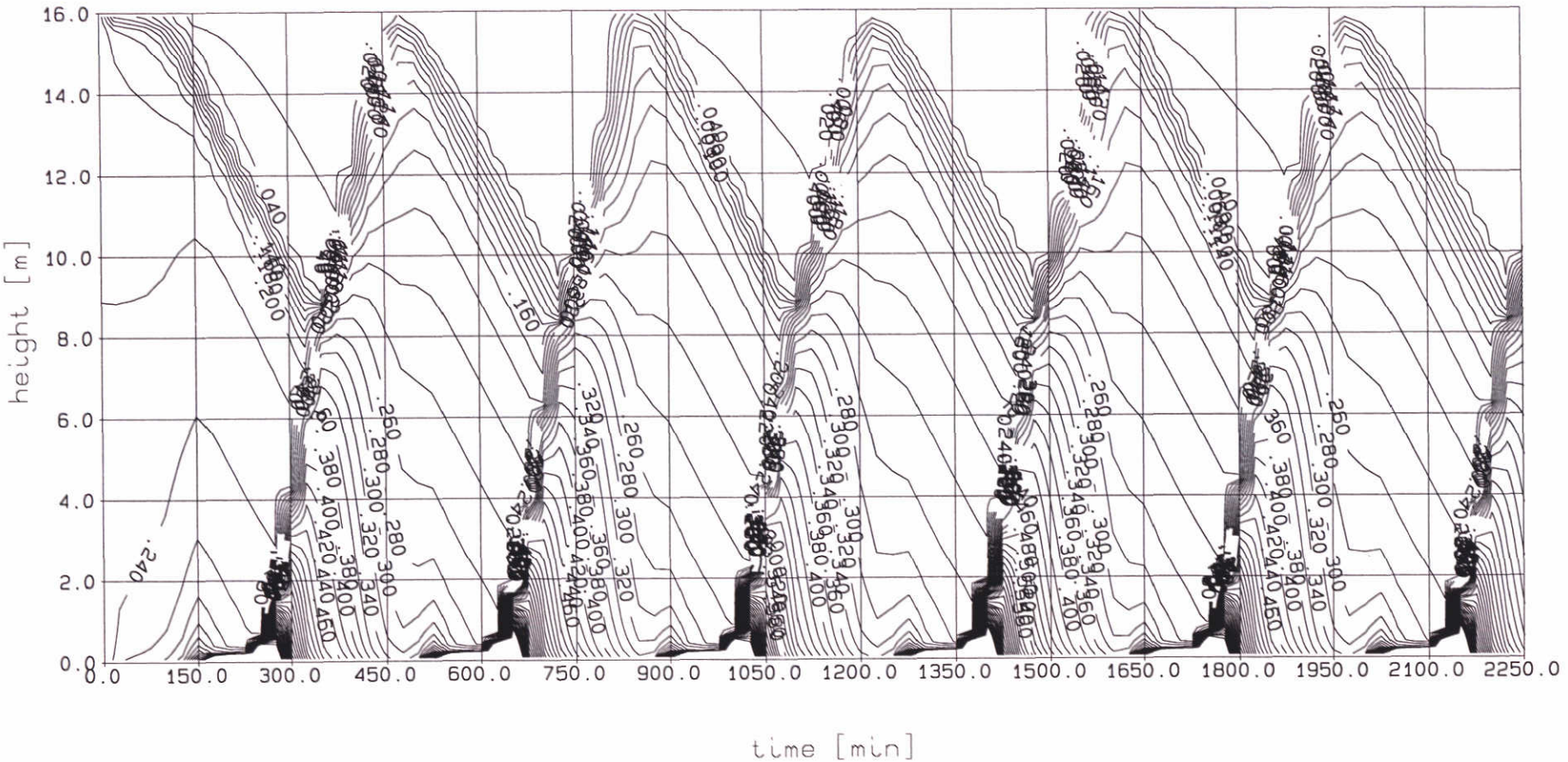

Computed mass concentrations [g/l] - {run s31a} initial concentration, C_0 = 0.22 g/l h = 16 m, U_m = 0.5 m/s, W_s = 0.5 mm/s	M_2 tide	23-09-97
	15 m/s wind 1.3 m wa	
DELFT HYDRAULICS - MARINE & COASTAL MANAGEMENT	Proj: Z2263	Fig. 5.6a

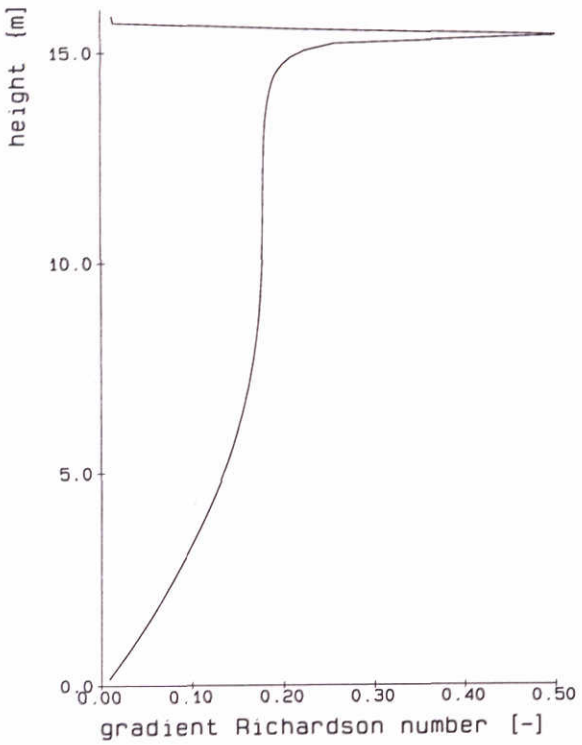

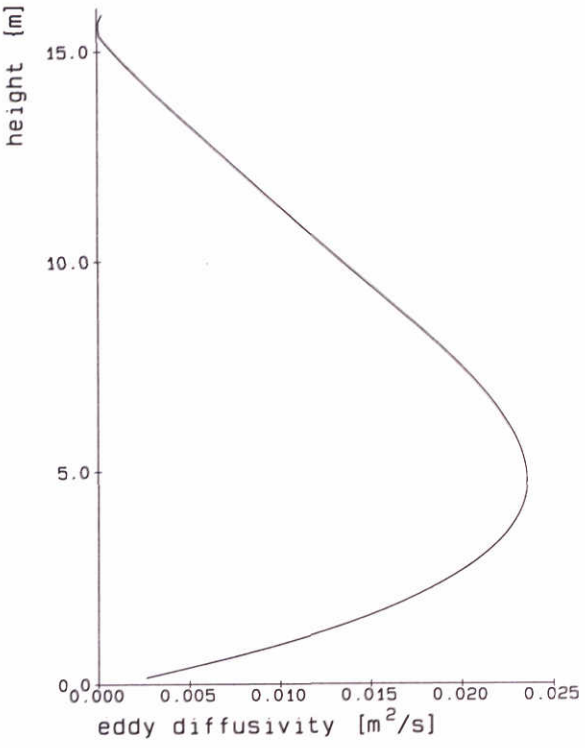

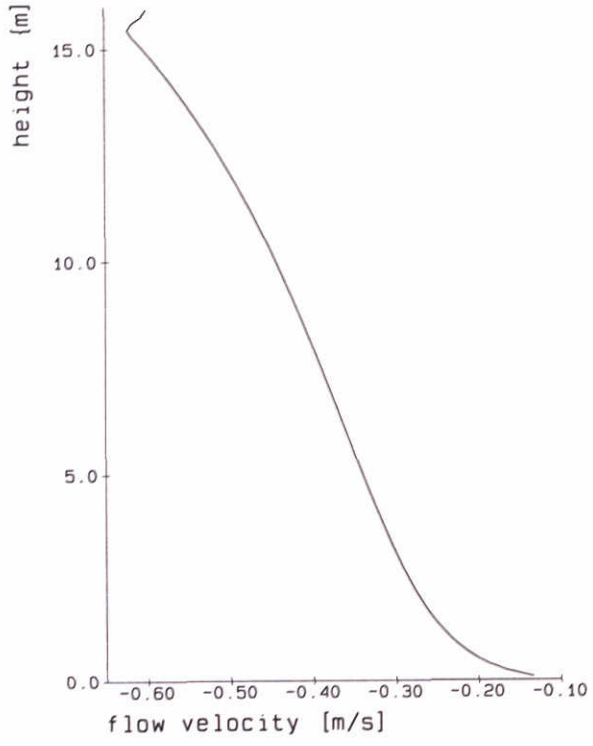

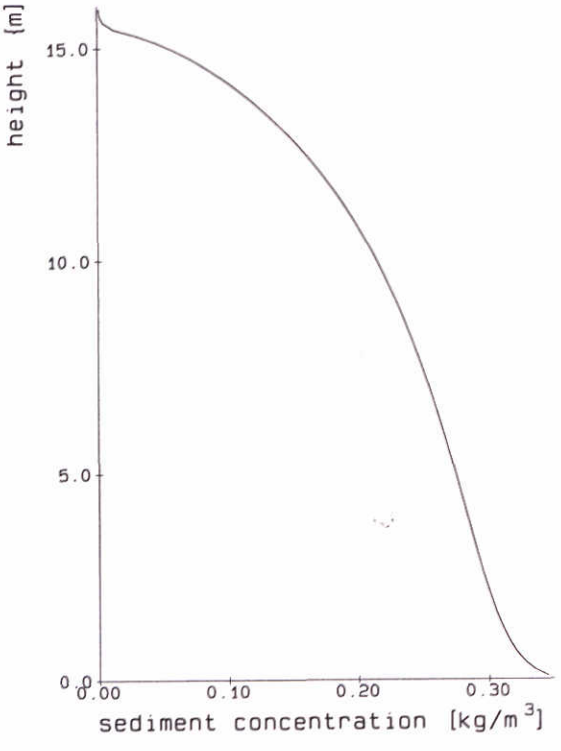

Computed mass concentrations [g/l] - {run s31a} initial concentration, C_0 = 0.22 g/l h = 16 m, U_m = 0.5 m/s, W_s = 0.5 mm/s	M_2 tide	time : 1950
	15 m/s wind 1.3 m wave	
DELFT HYDRAULICS - MARINE & COASTAL MANAGEMENT	Proj: Z2263	Fig. 5.6b

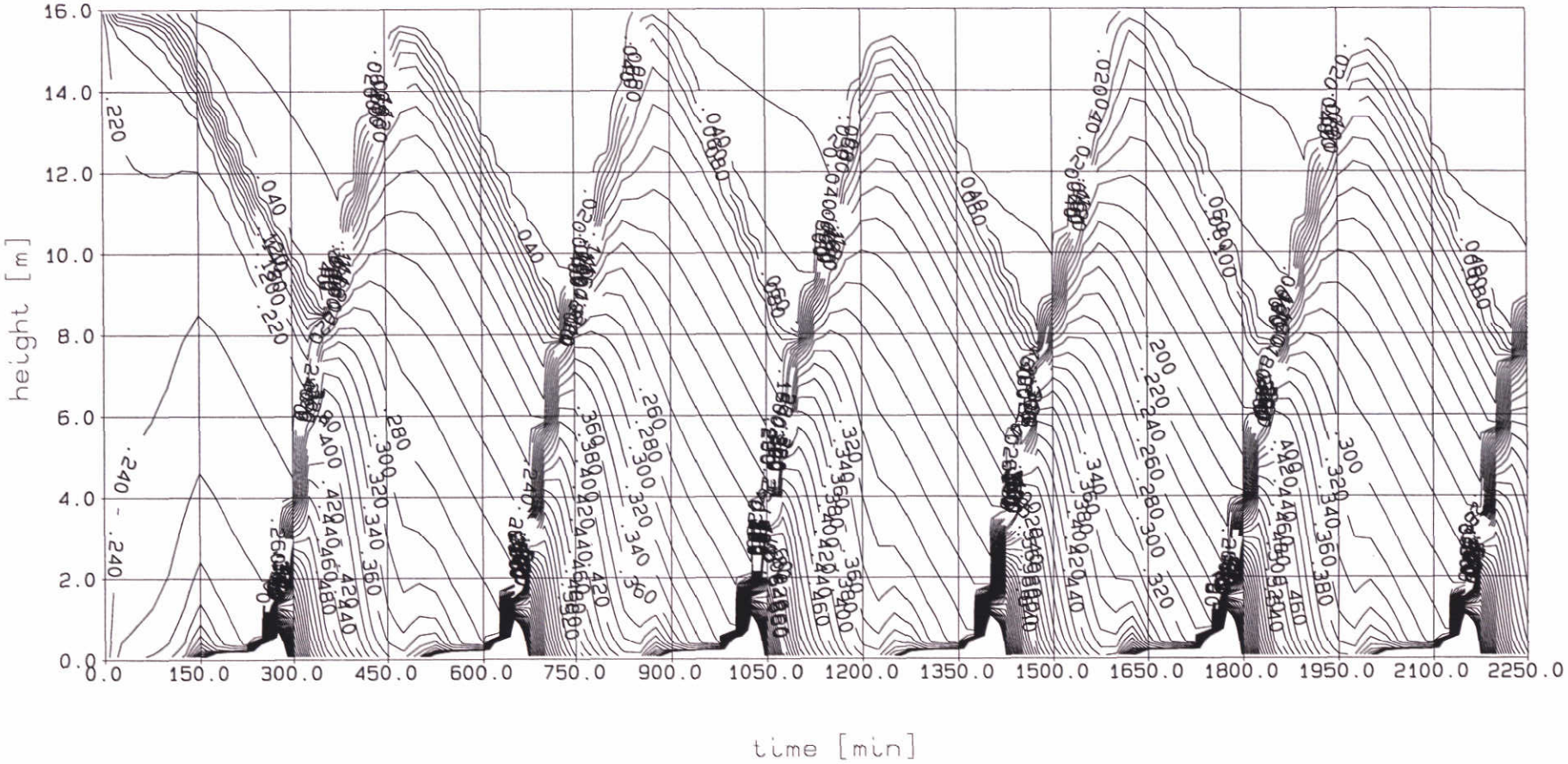

Computed mass concentrations [g/l] - {run s31b} initial concentration, C_0 = 0.23 g/l h = 16 m, U_m = 0.5 m/s, W_s = 0.5 mm/s	M_2 tide	23-09-97
	15 m/s wind 1.3 m wa	
DELFT HYDRAULICS - MARINE & COASTAL MANAGEMENT	Proj: Z2263	Fig. 5.6c

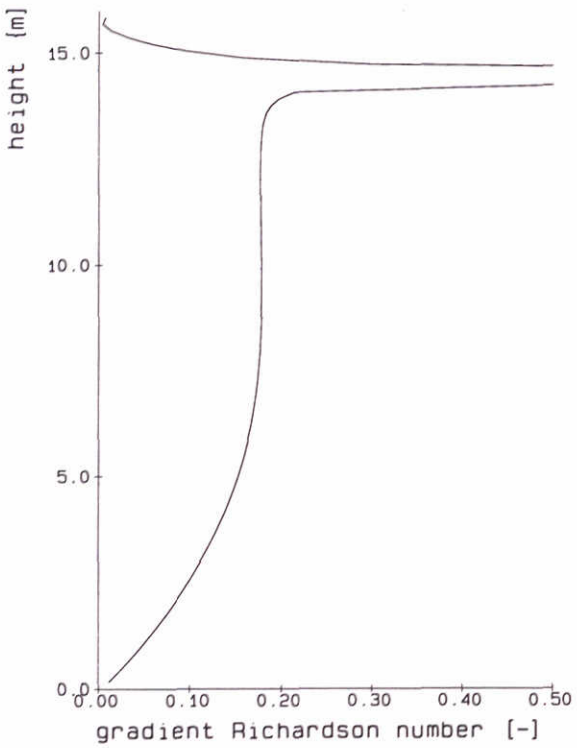

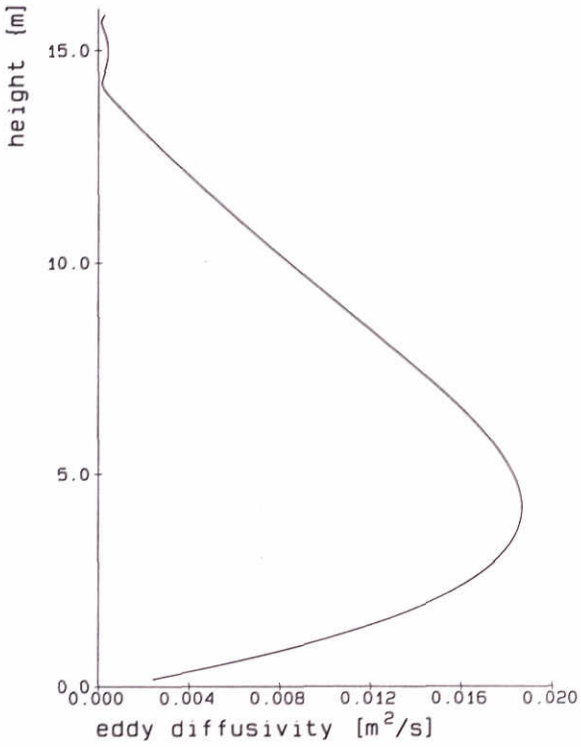

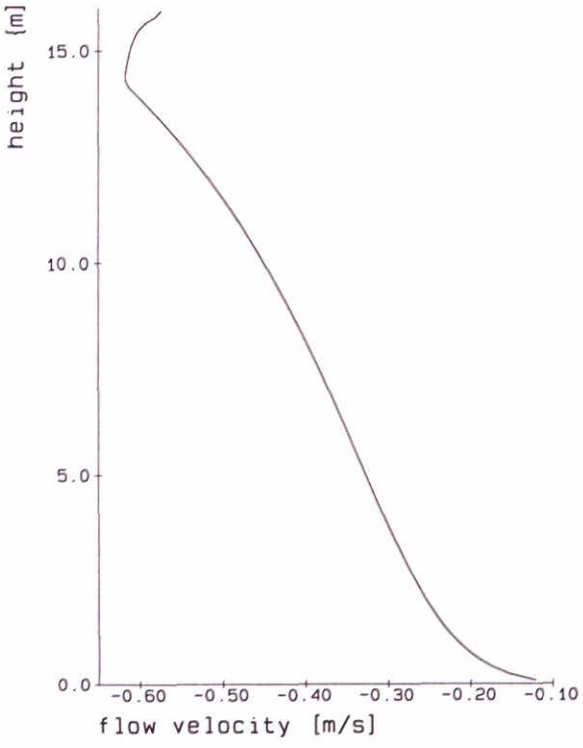

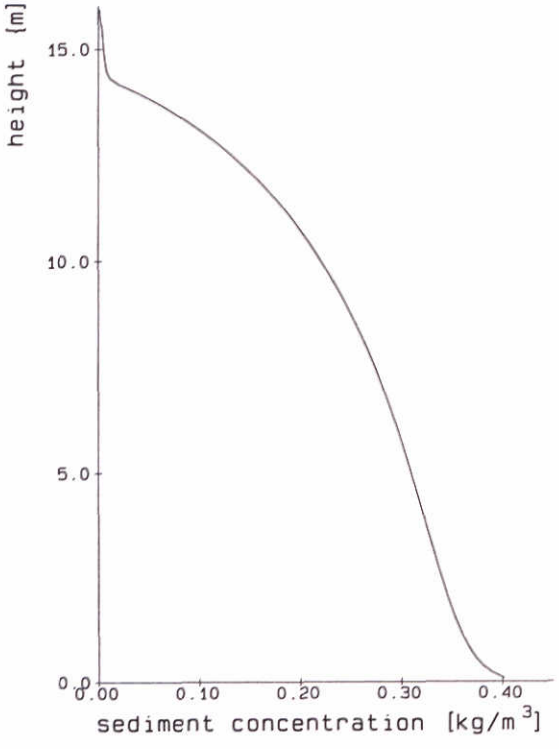

Computed mass concentrations [g/l] - {run s30b} initial concentration, C_0 = 0.23 g/l h = 16 m, U_m = 0.5 m/s, W_s = 0.5 mm/s	M_2 tide	time : 1950
	15 m/s wind 1.3 m wave	
DELFT HYDRAULICS - MARINE & COASTAL MANAGEMENT	Proj: Z2263	Fig. 5.6d

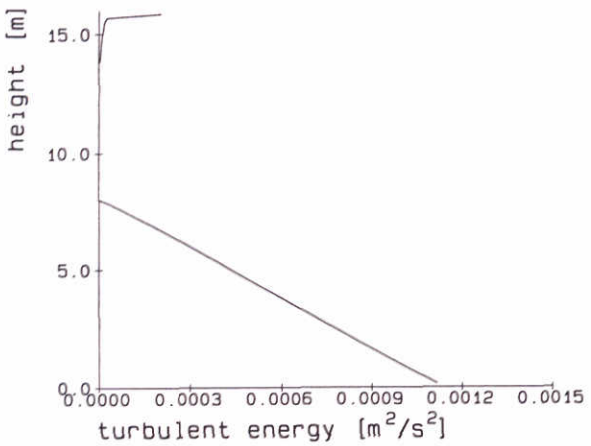

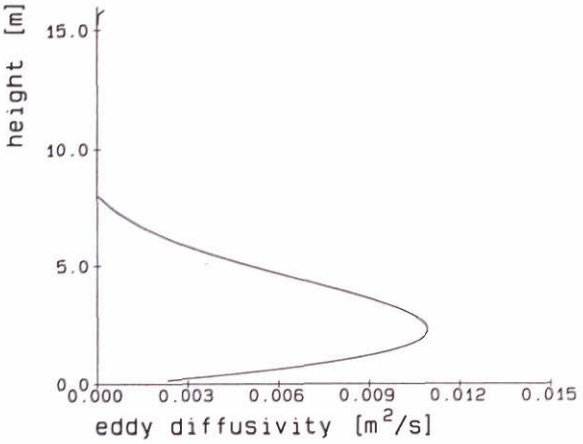

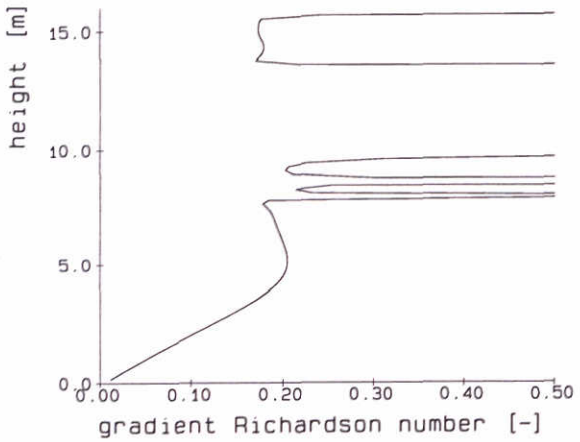

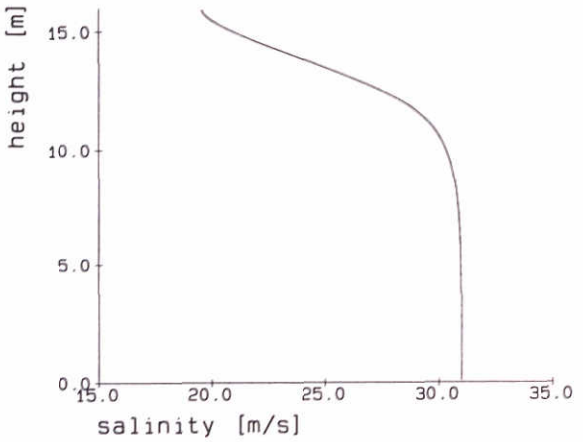

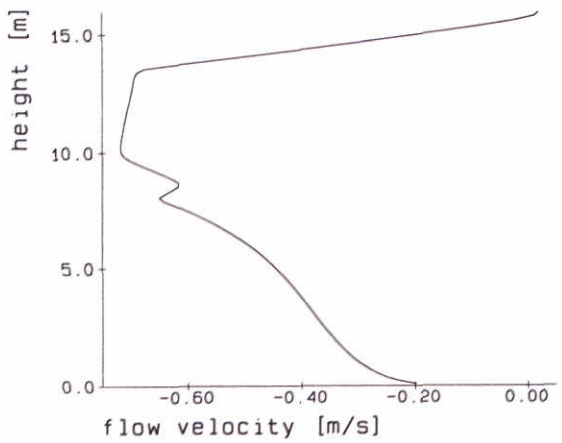

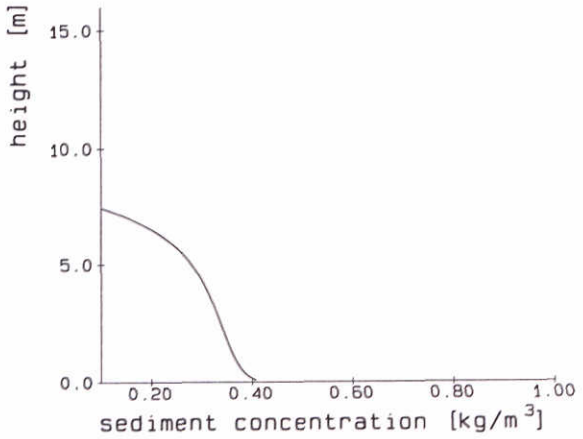

Computed mass concentrations [g/l] (run s32a) Initial conventration, C_0 = 0.14 g/l h = 16 m, U_m = 0.5 m/s, W_s = 0.5 mm/s, no waves	M_2 tide	time : 1900
	salinity gradient	
DELFT HYDRAULICS - MARINE & COASTAL MANAGEMENT	Proj: Z2263	Fig. 5.7b

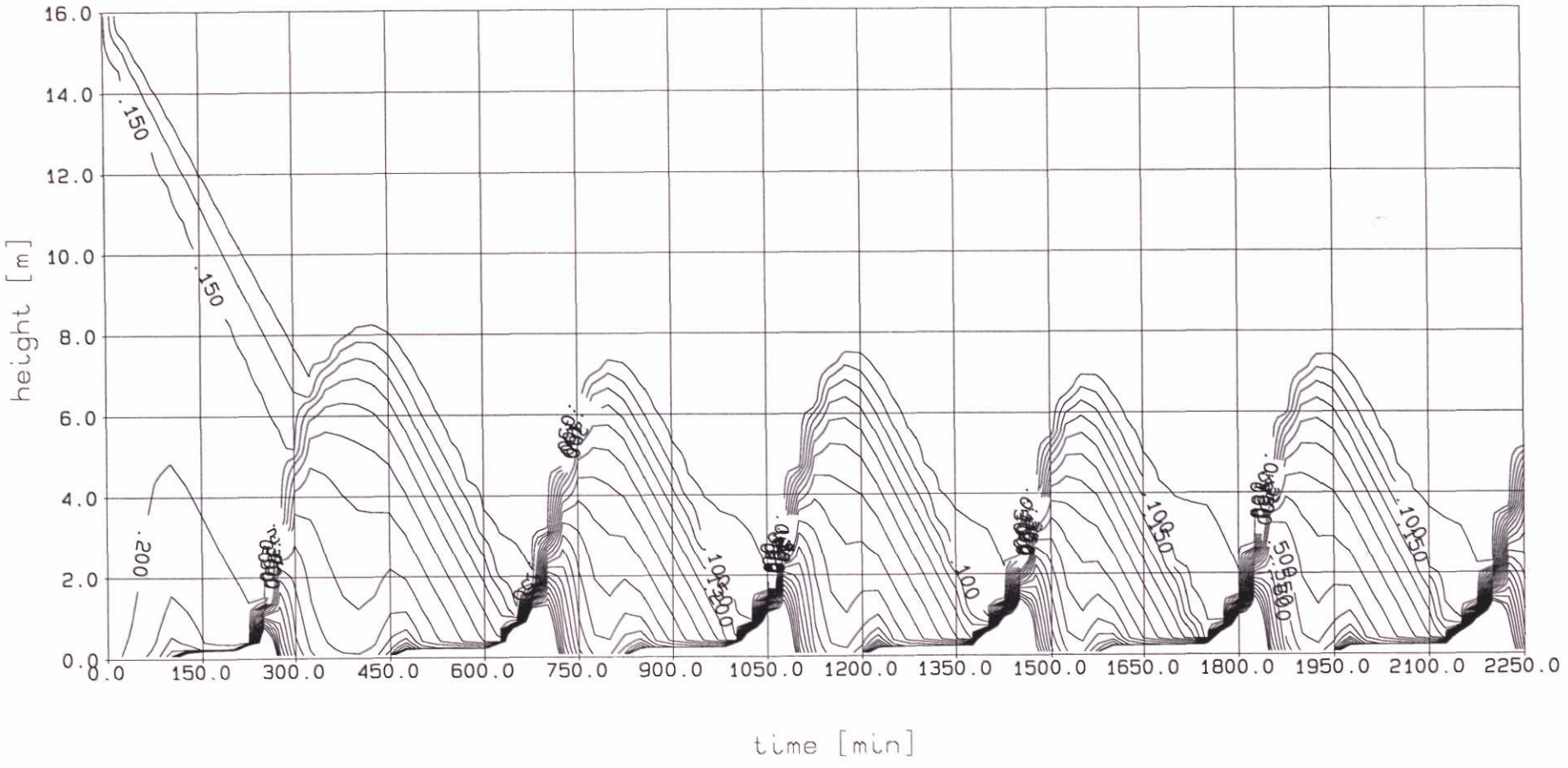

Computed mass concentrations [g/l] (run s32b) initial concentration, C_0 = 0.16 g/l h = 16 m, U_m = 0.5 m/s, W_s = 0.5 mm/s, no waves	M_2 tide	24-09-97
	salinity gradient	
DELFT HYDRAULICS - MARINE & COASTAL MANAGEMENT	Proj: Z2263	Fig. 5.7c

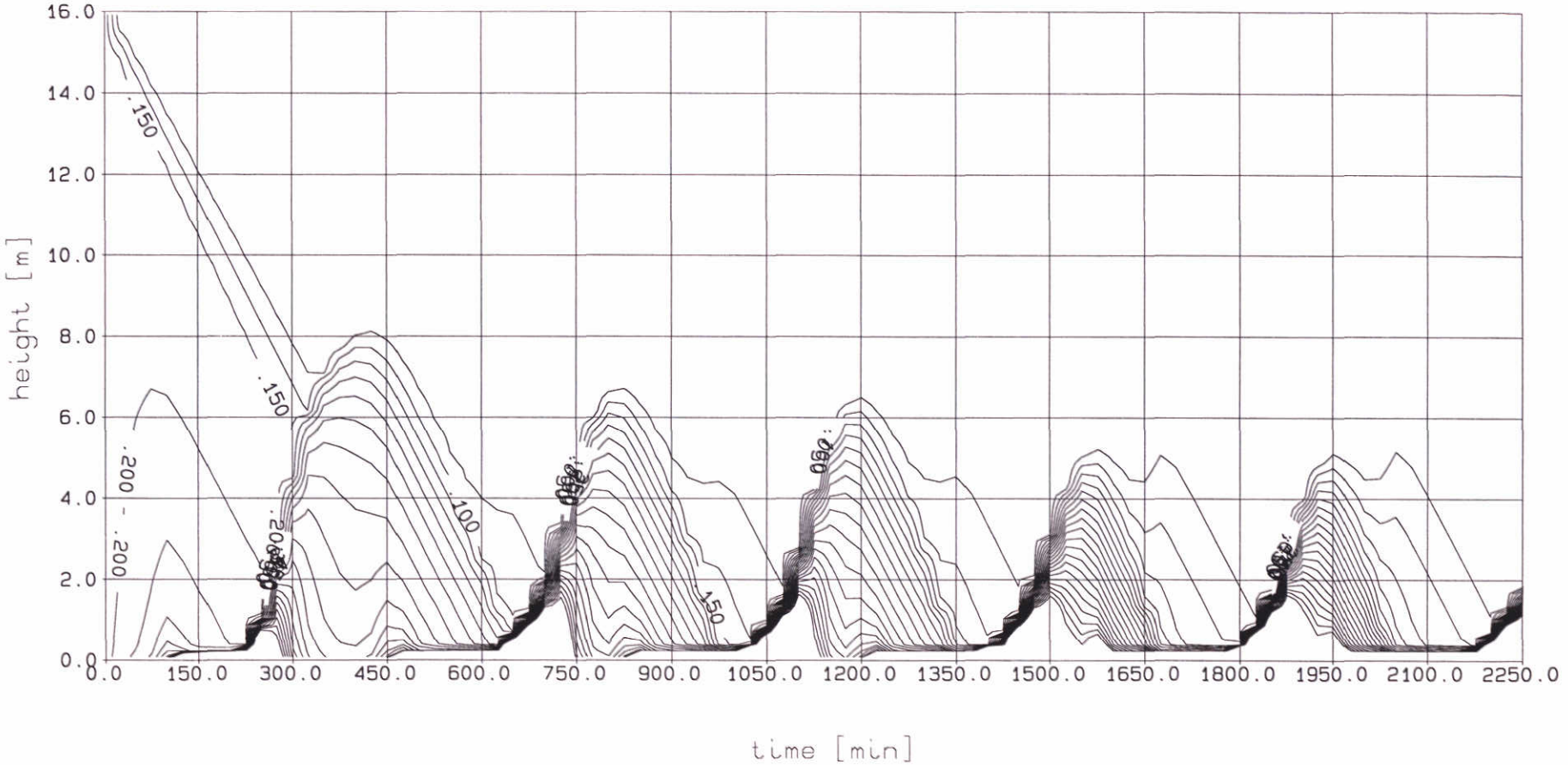

Computed mass concentrations [g/l] {run s32c} initial concentration, C_0 = 0.18 g/l h = 16 m, U_m = 0.5 m/s, W_s = 0.5 mm/s, no waves	M_2 tide	24-09-97
	salinity gradient	
DELFT HYDRAULICS - MARINE & COASTAL MANAGEMENT	Proj: Z2263	Fig. 5.7d

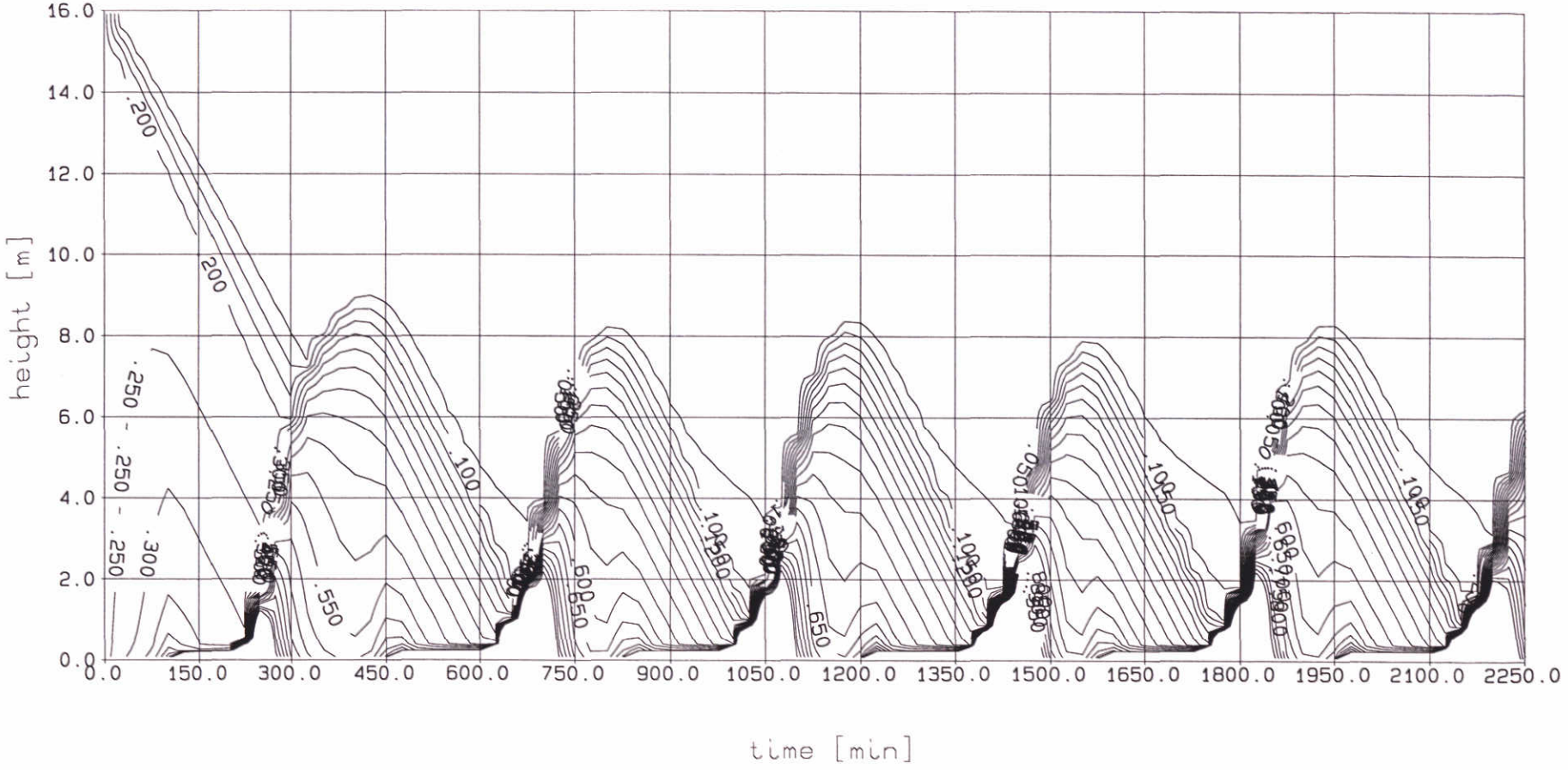

Computed mass concentrations [g/l] {run t33b} initial concentration, C_0 = 0.23 g/l h = 16 m, U_m = 0.5 m/s, W_s = 0.5 mm/s, H_{rms} = 1.3 m	M_2 tide	24-09-97
	salinity gradient	
DELFT HYDRAULICS - MARINE & COASTAL MANAGEMENT	Proj: Z2263	Fig. 5.8a

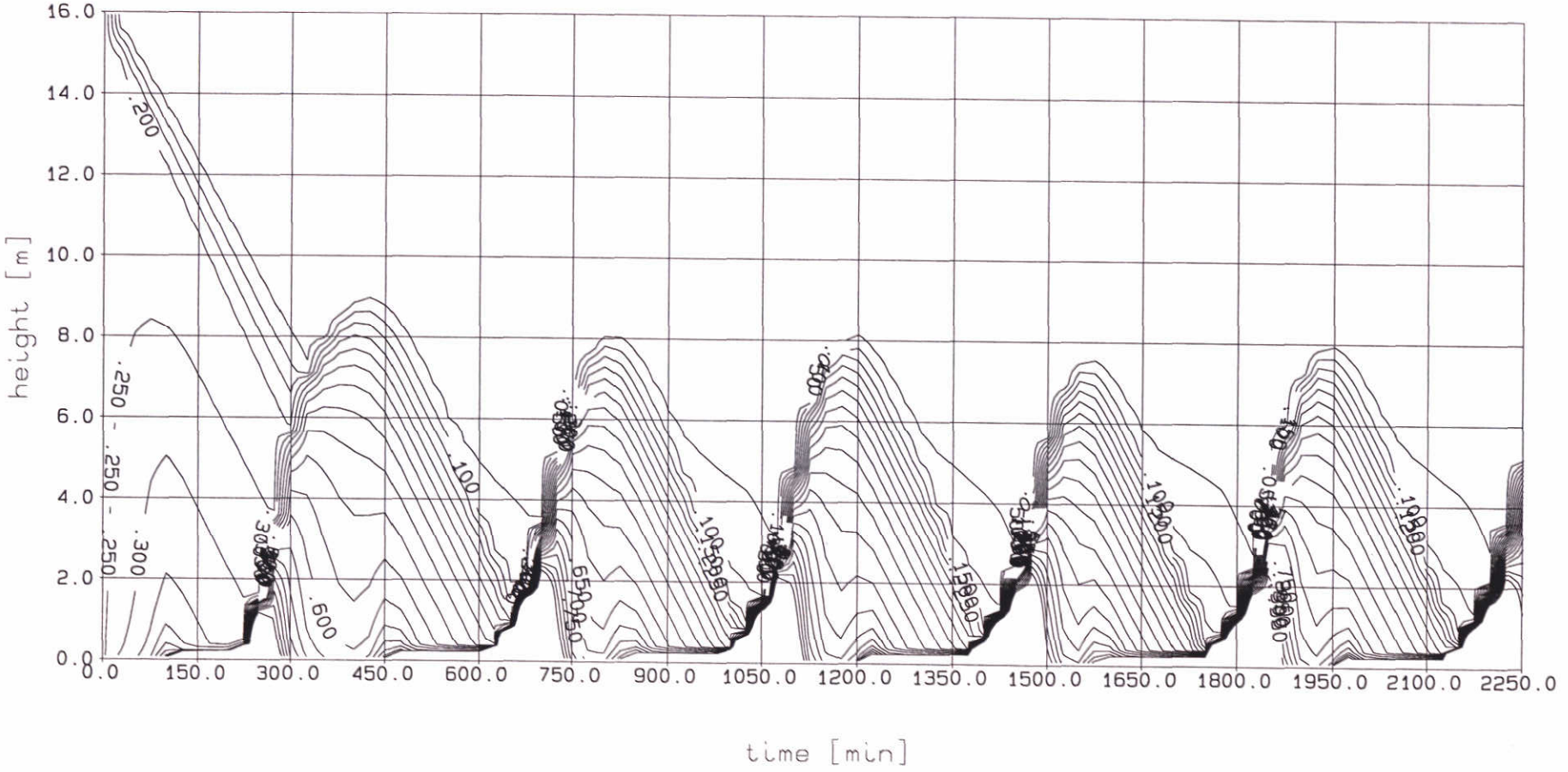

Computed mass concentrations [g/l] {run s33a} initial concentration, C_0 = 0.24 g/l h = 16 m, U_m = 0.5 m/s, W_s = 0.5 mm/s, H_{rms} = 1.3 m	M_2 tide	24-09-97
	salinity gradient	
DELFT HYDRAULICS - MARINE & COASTAL MANAGEMENT	Proj: Z2263	Fig. 5.8b

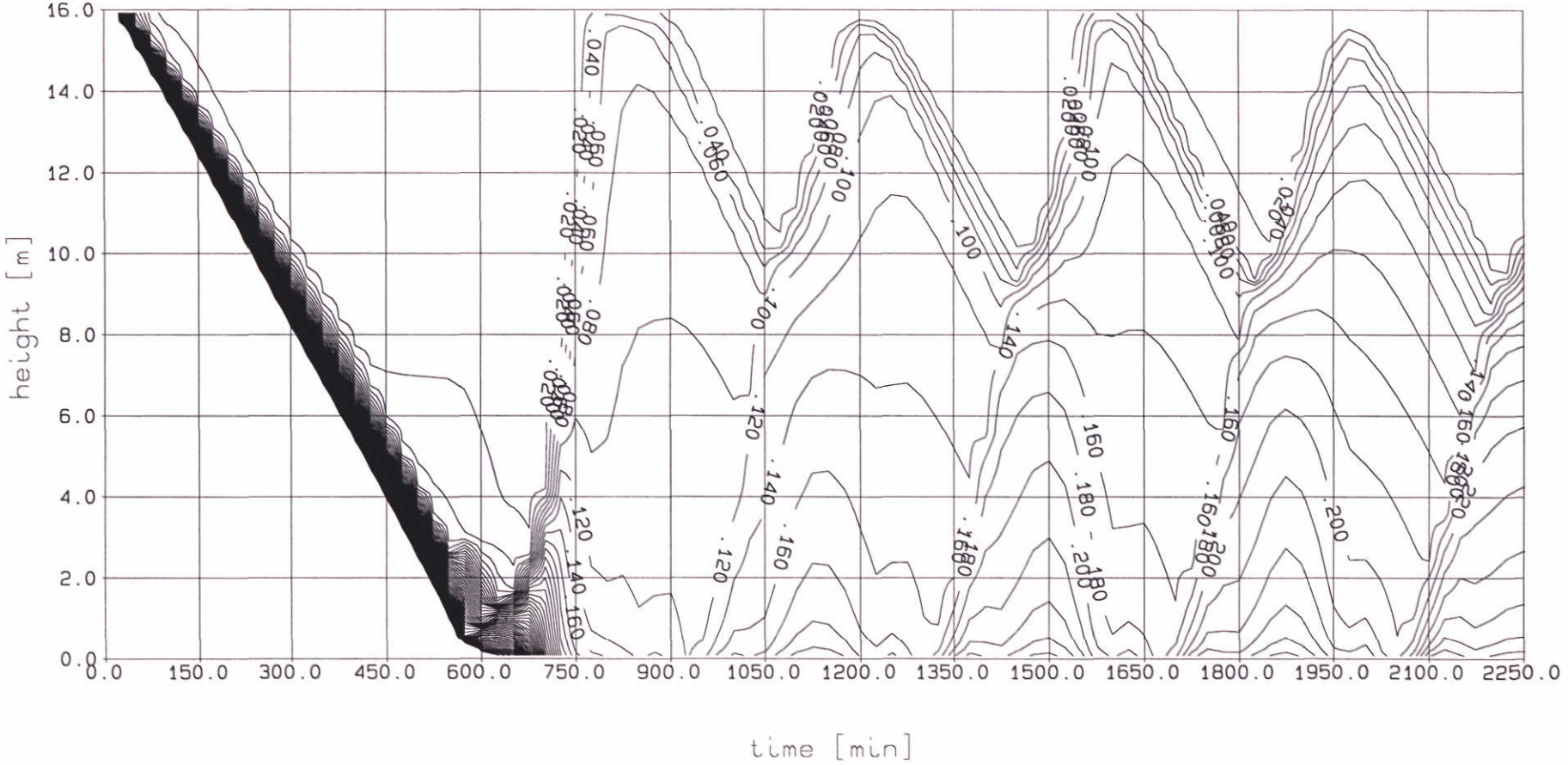

Computed mass concentrations [g/l] - {run s34a} initial concentration, c_0 = 5.0 g/l h = 16 m, U_m = 0.5 m/s, W_s = 0.5 mm/s, no waves	M_2 tide	24-09-97
	incl bed exchange	
DELFT HYDRAULICS - MARINE & COASTAL MANAGEMENT	Proj: Z2263	Fig. 5.9

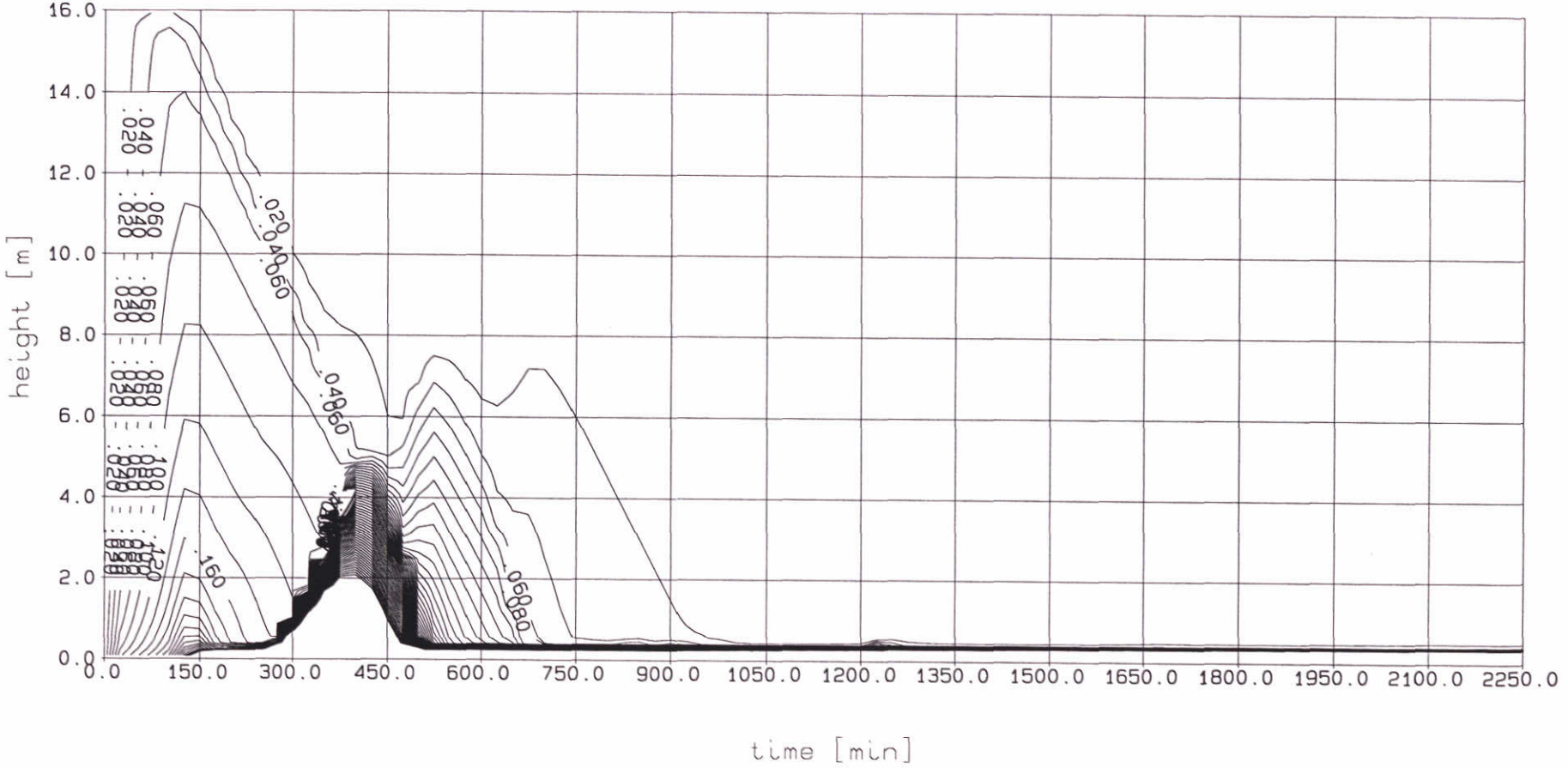

Computed mass concentrations [g/l] - {run s35} initial concentration, c_0 = 0.0 g/l h = 16 m, U_m = 0.5 m/s, W_s = 0.5 mm/s, H_{rms} = 1.3 m	M_2 tide	24-09-97
	incl bed exchange	
DELFT HYDRAULICS - MARINE & COASTAL MANAGEMENT	Proj: Z2263	Fig. 5.10

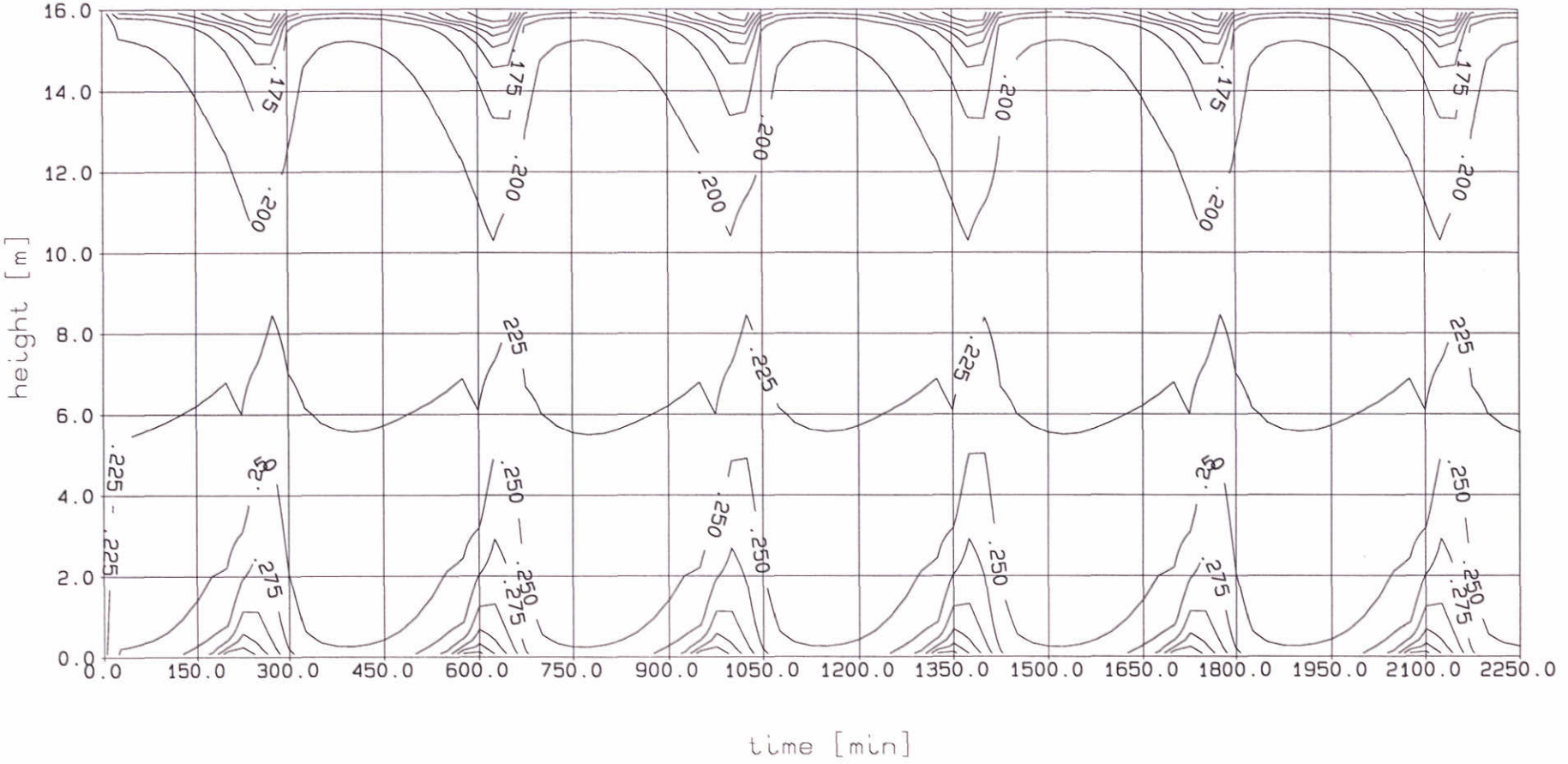

Computed mass concentrations [g/l] - {run s36} initial concentration, c_0 = 0.22 g/l h = 16 m, U_m = 0.5 m/s, W_s = 0.5 mm/s, H_{rms} = 1.3 m	M_2 tide	25-09-97
	no buoyancy effects	
DELFT HYDRAULICS - MARINE & COASTAL MANAGEMENT	Proj: Z2263	Fig. 5.11a

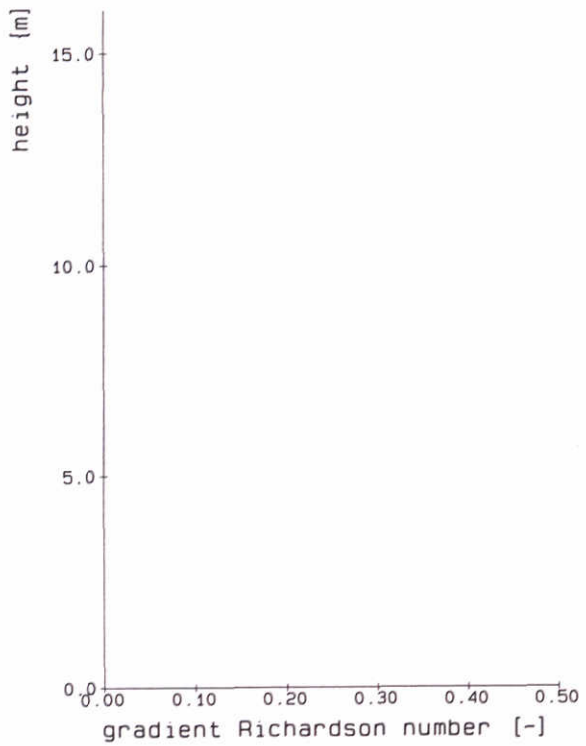

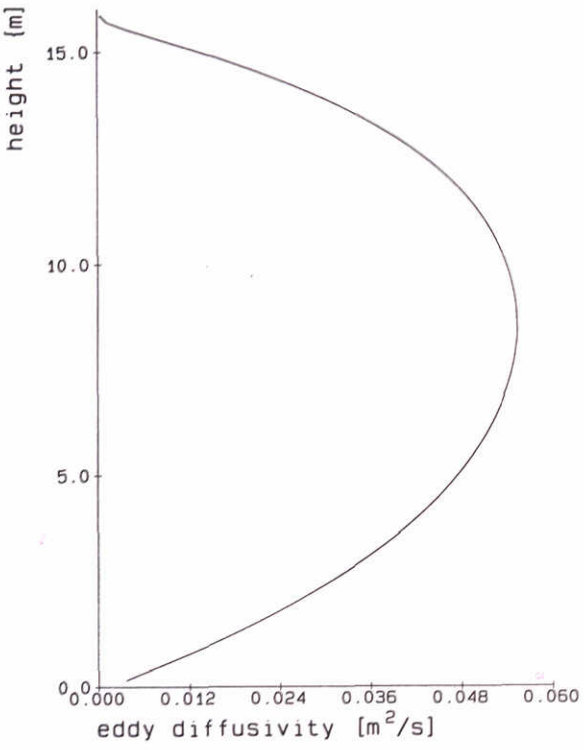

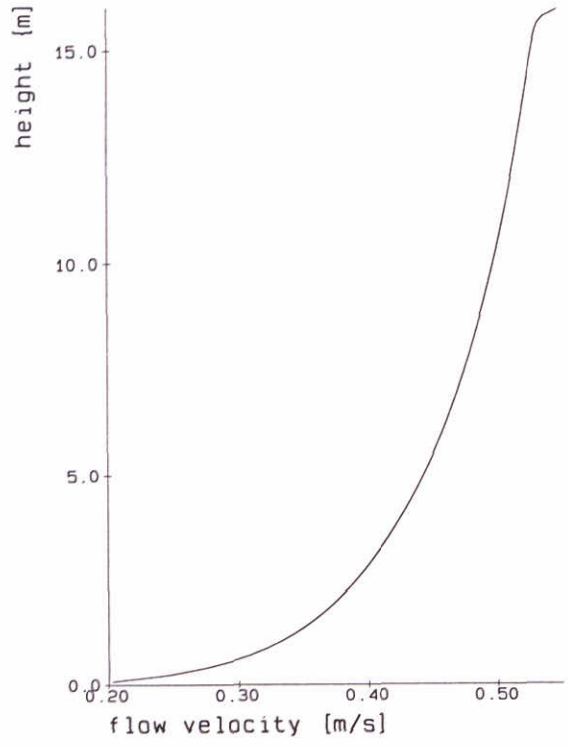

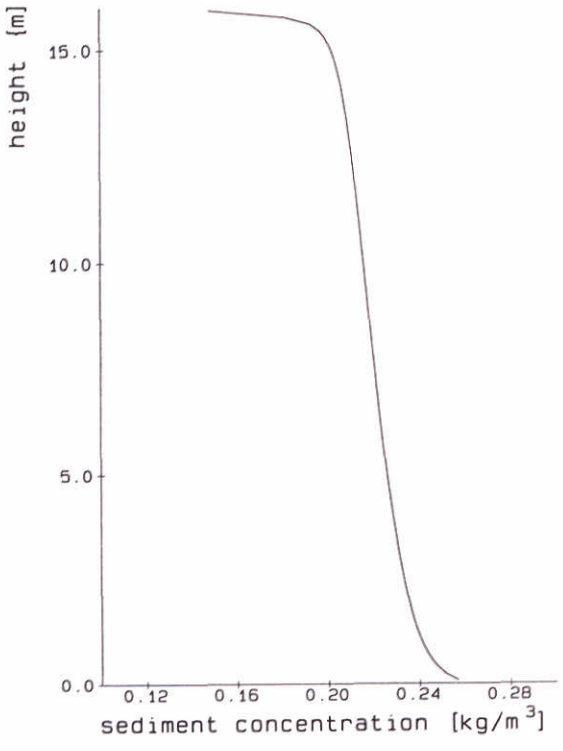

Computed mass concentrations [g/l] - (run s36a) initial concentration, C_0 = 0.22 g/l h = 16 m, U_m = 0.5 m/s, W_s = 0.5 mm/s, H_{rms} = 1.3 m	M_2 tide	time : 1550
	incl bed exchange	
DELFT HYDRAULICS - MARINE & COASTAL MANAGEMENT	Proj: Z2263	Fig. 5.11b

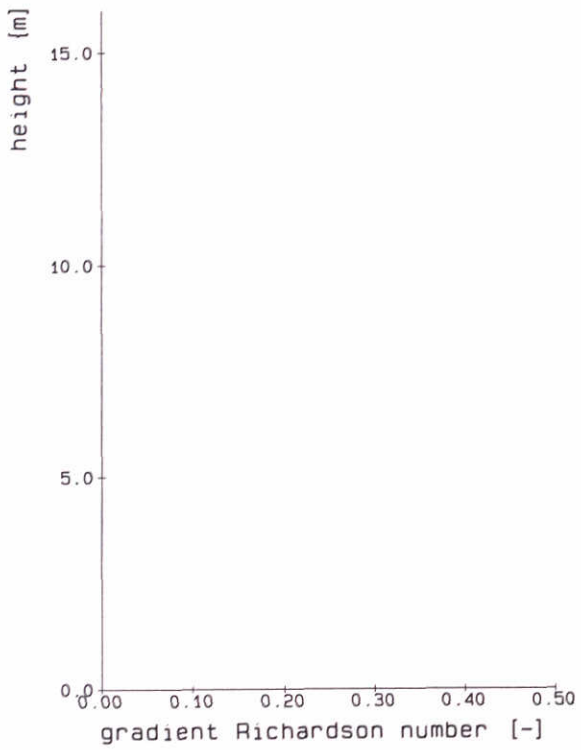

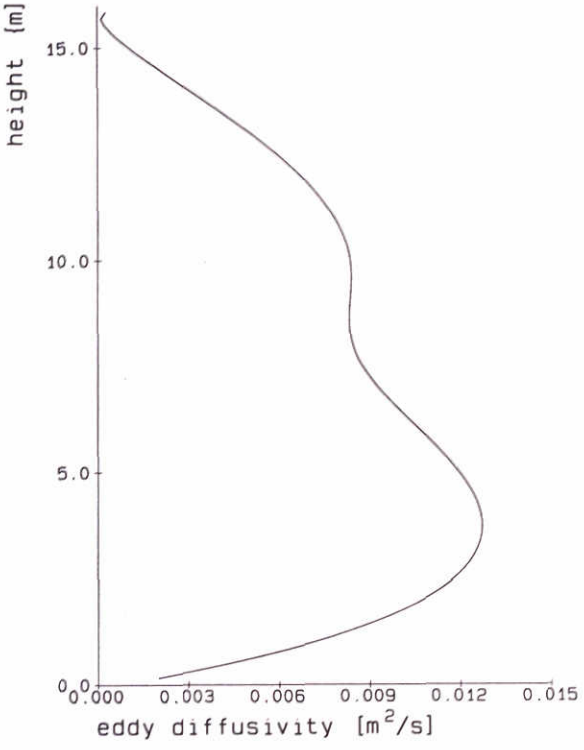

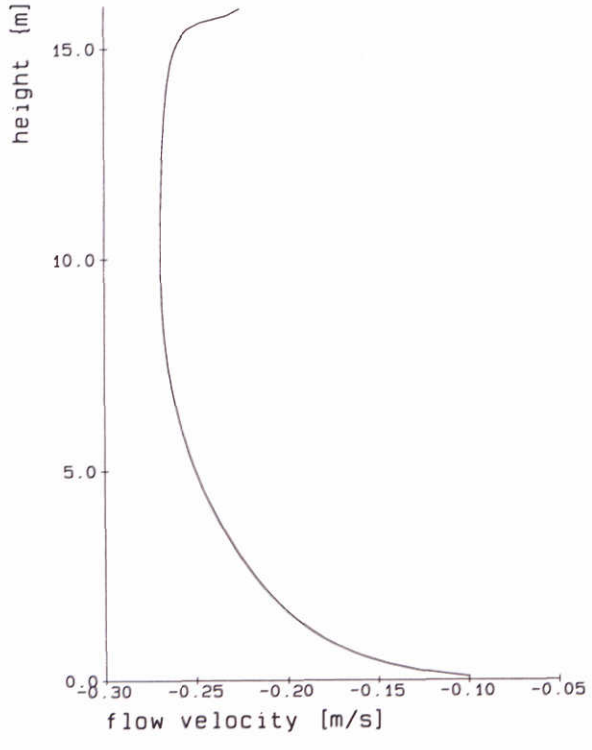

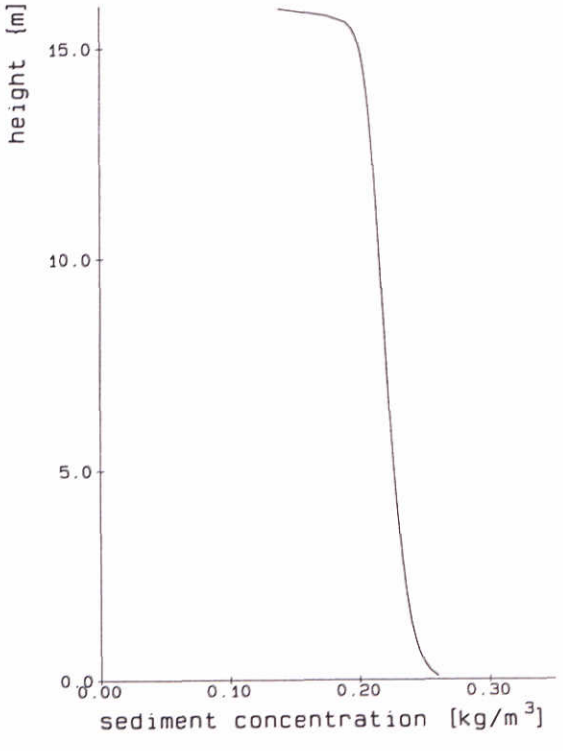

Computed mass concentrations [g/l] - (run s36a) initial concentration, C_0 = 0.22 g/l h = 16 m, U_m = 0.5 m/s, W_s = 0.5 mm/s, H_{rms} = 1.3 m	M_2 tide	time : 1750
	incl bed exchange	
DELFT HYDRAULICS - MARINE & COASTAL MANAGEMENT	Proj: Z2263	Fig. 5.11c

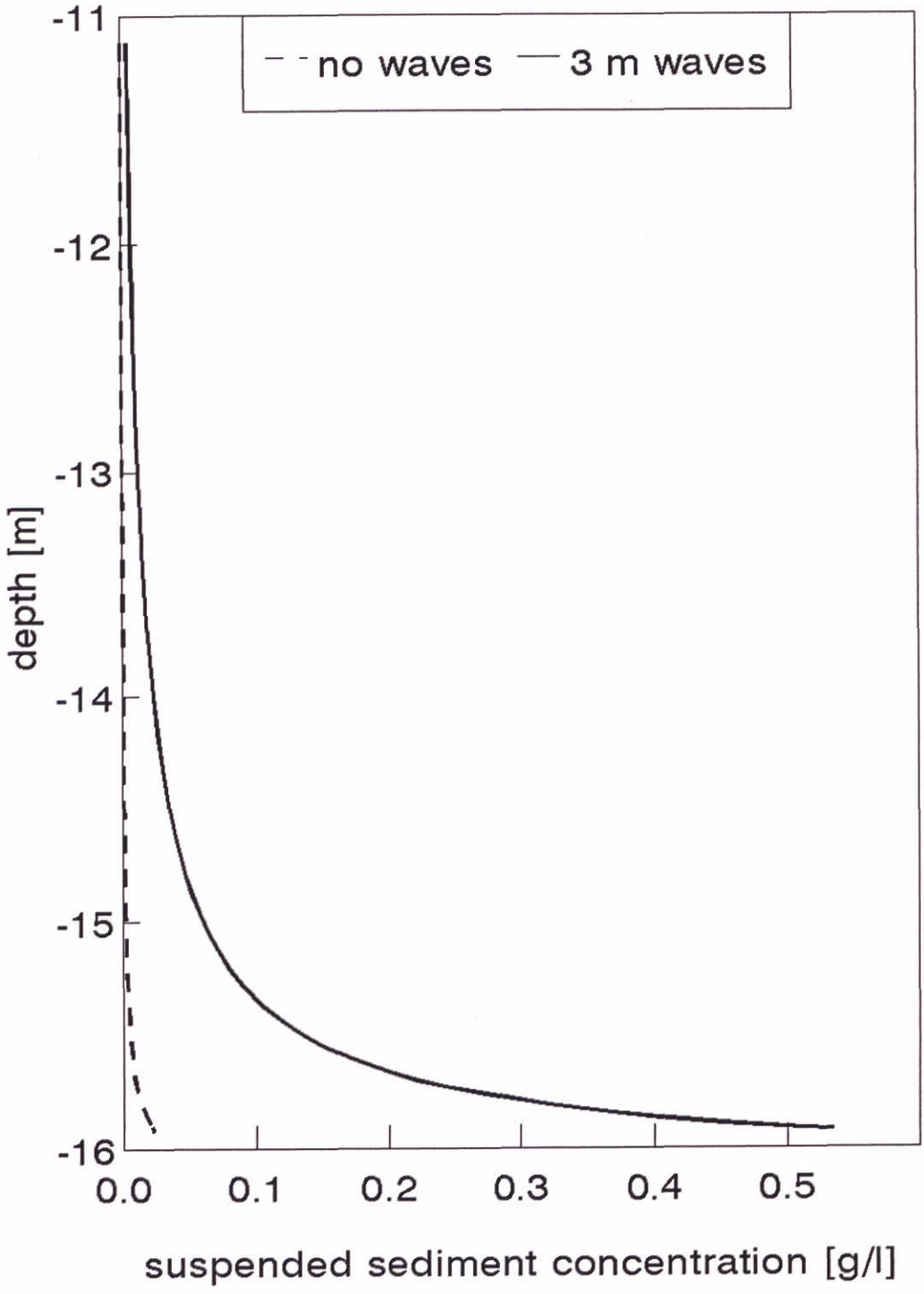

computed suspended sand concentration for steady flow (U = 0.6 m/s, $H_{1/3}$ = 3 m)		Jan. 1998
	SILTMAN	
D E L F T H Y D R A U L I C S	Proj: Z2263	Fig. 5.12

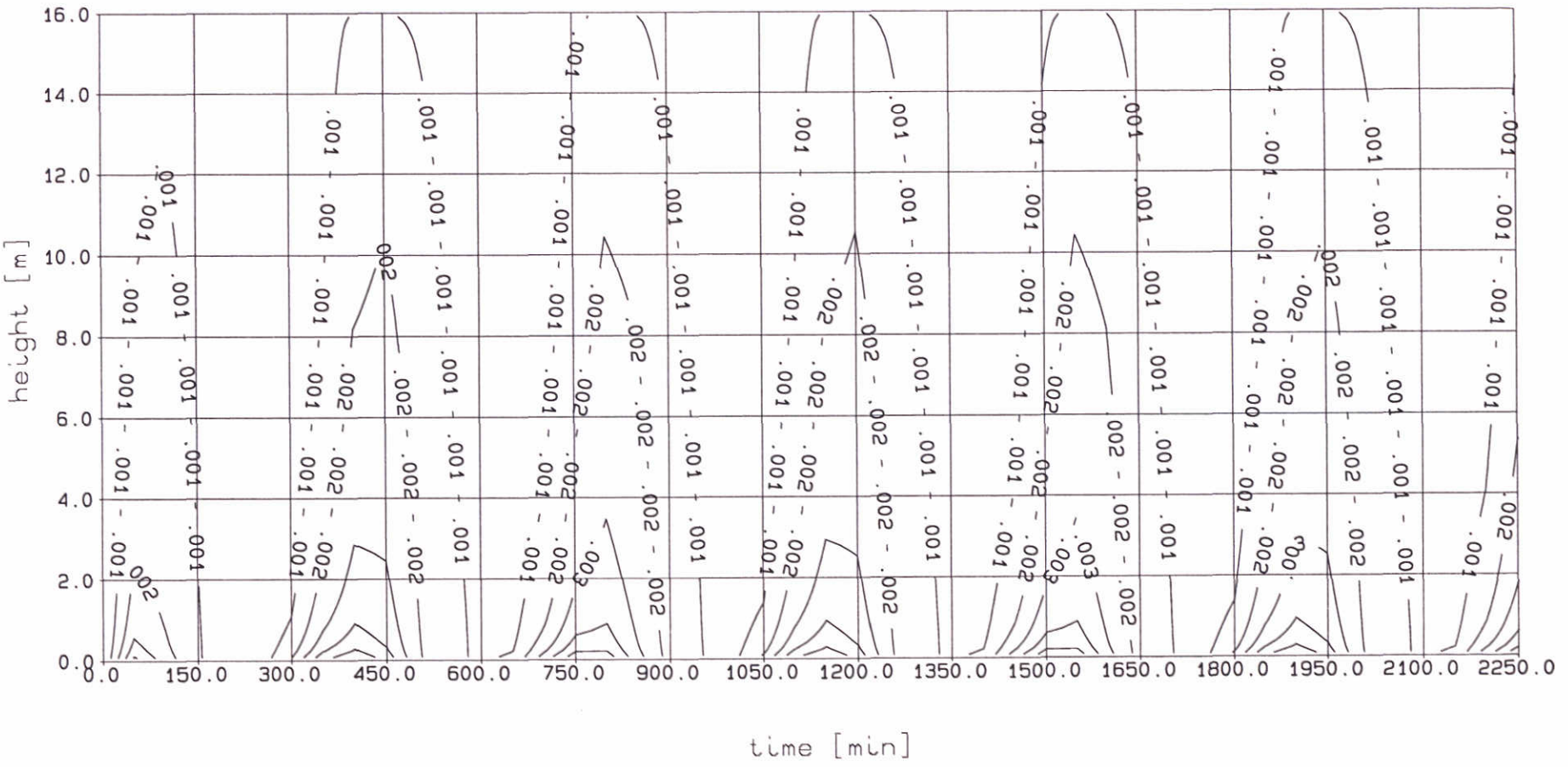

Computed mass concentrations [g/l] - {run Z05} initial concentration, c_0 = 0 g/l h = 16 m, U_m = 0.5 m/s, D_m = 0.05 mm, no waves	M_2 tide	14-01-1998
	run with sand particles	
DELFT HYDRAULICS - MARINE & COASTAL MANAGEMENT	Proj: Z2263	Fig. 5.13

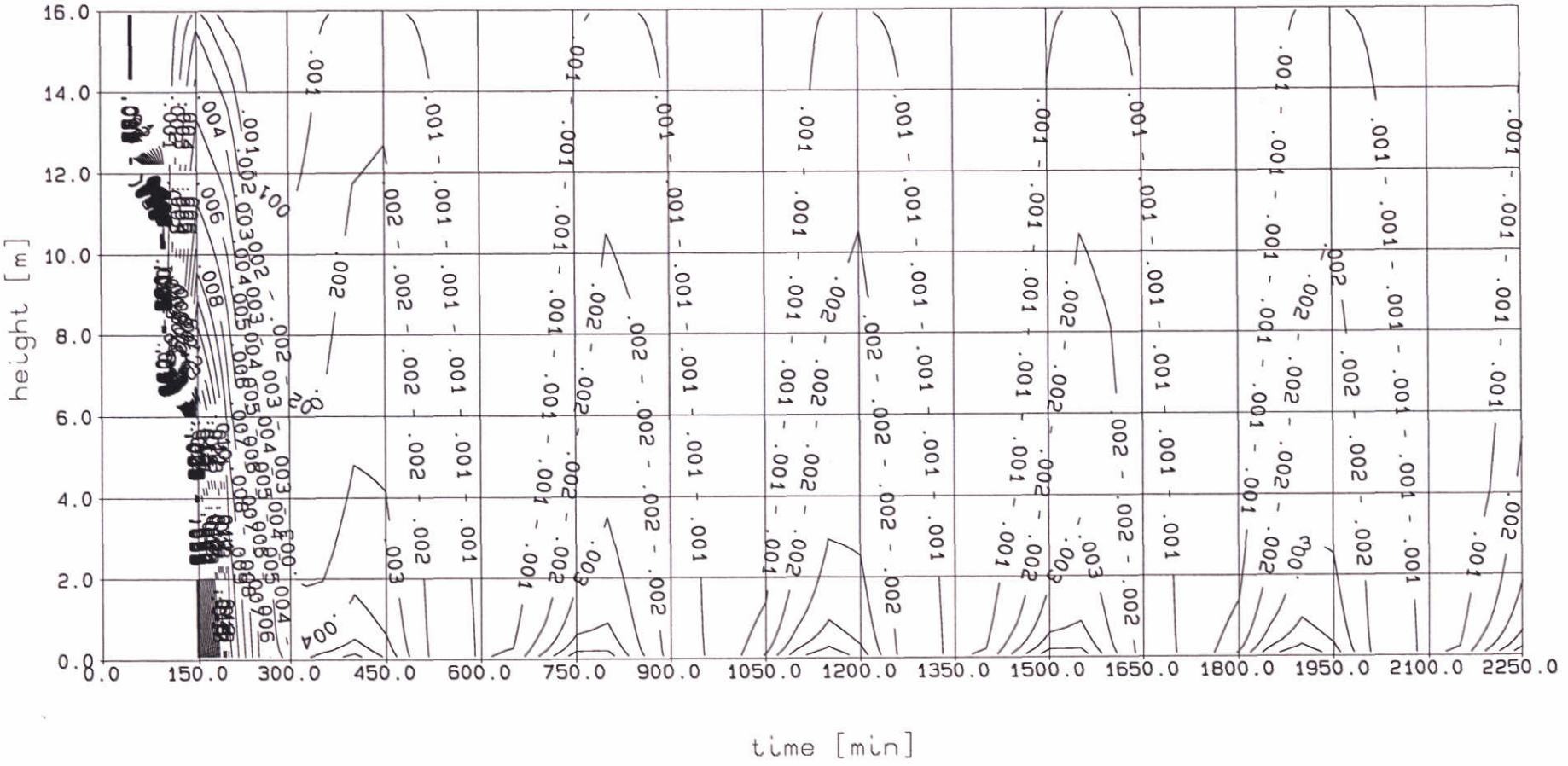

Computed mass concentrations [g/l] - {run Z04} initial concentration, c_0 = 0.5 g/l h = 16 m, U_m = 0.5 m/s, D_m = 0.05 mm, no waves	M_2 tide	14-01-1998
	run with sand particles	
DELFT HYDRAULICS - MARINE & COASTAL MANAGEMENT	Proj: Z2263	Fig. 5.14

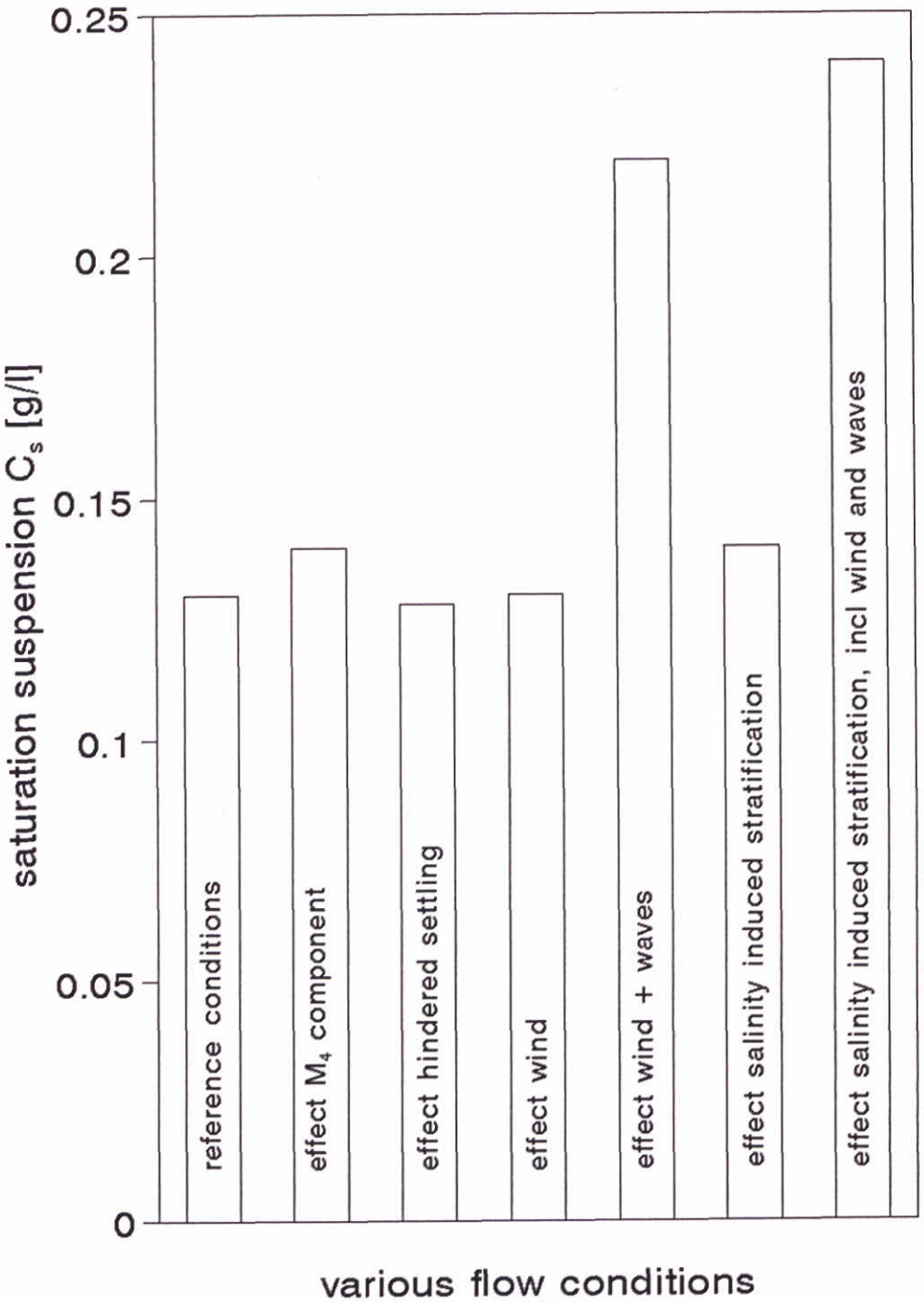

Summary of saturation concentration for various conditions		Sept. 1997
	SILTMAN	
DELFT HYDRAULICS	Proj: Z2263	Fig. 5.15

DELFT HYDRAULICS

Observed and schematisized wave height at Maasgeul station.

Z-2263

SILTMAN

Fig. 6.1

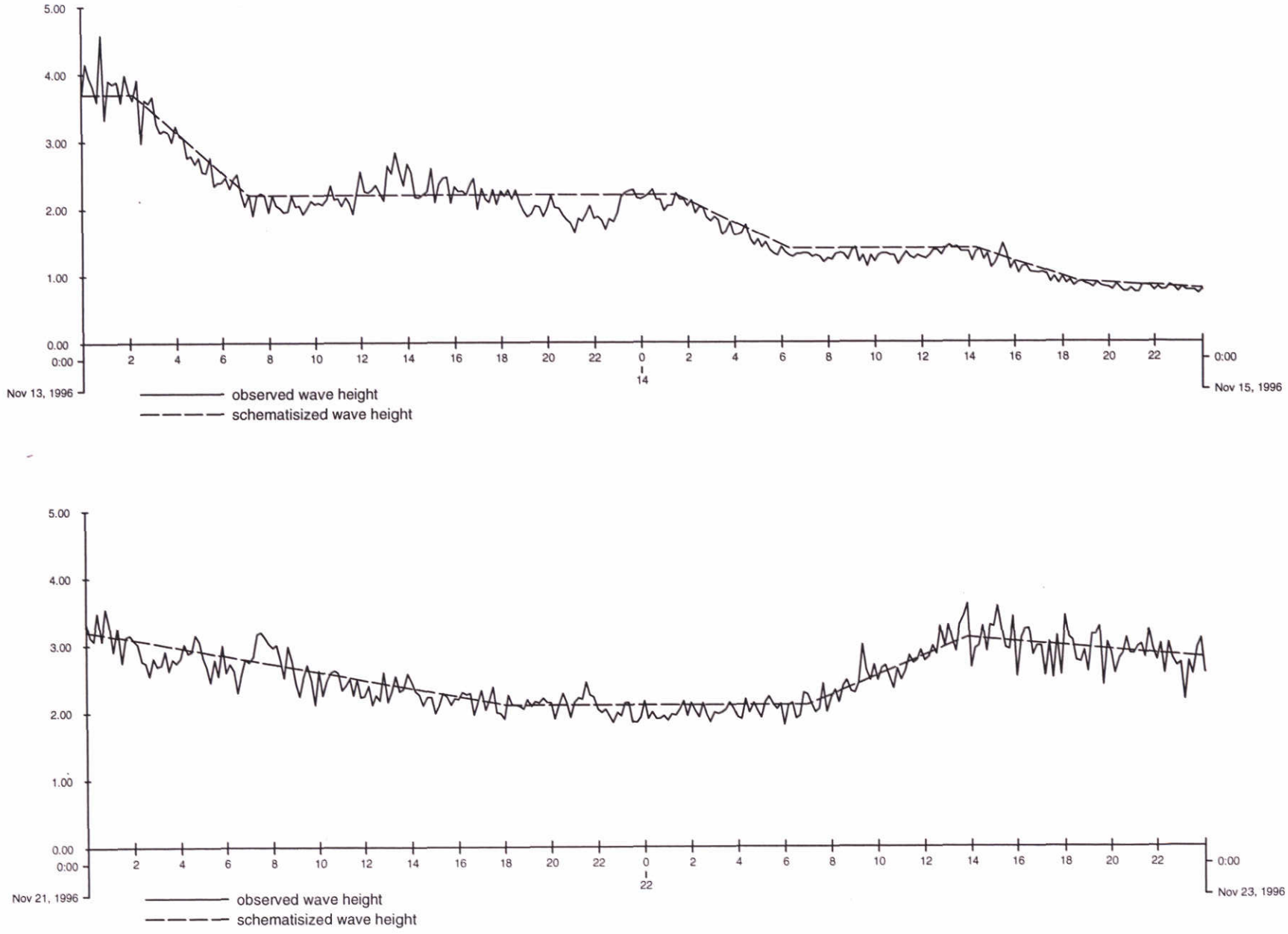

DELFT HYDRAULICS

Filtered velocities for November 1996

Z-2263

Station : B

Fig.6.2

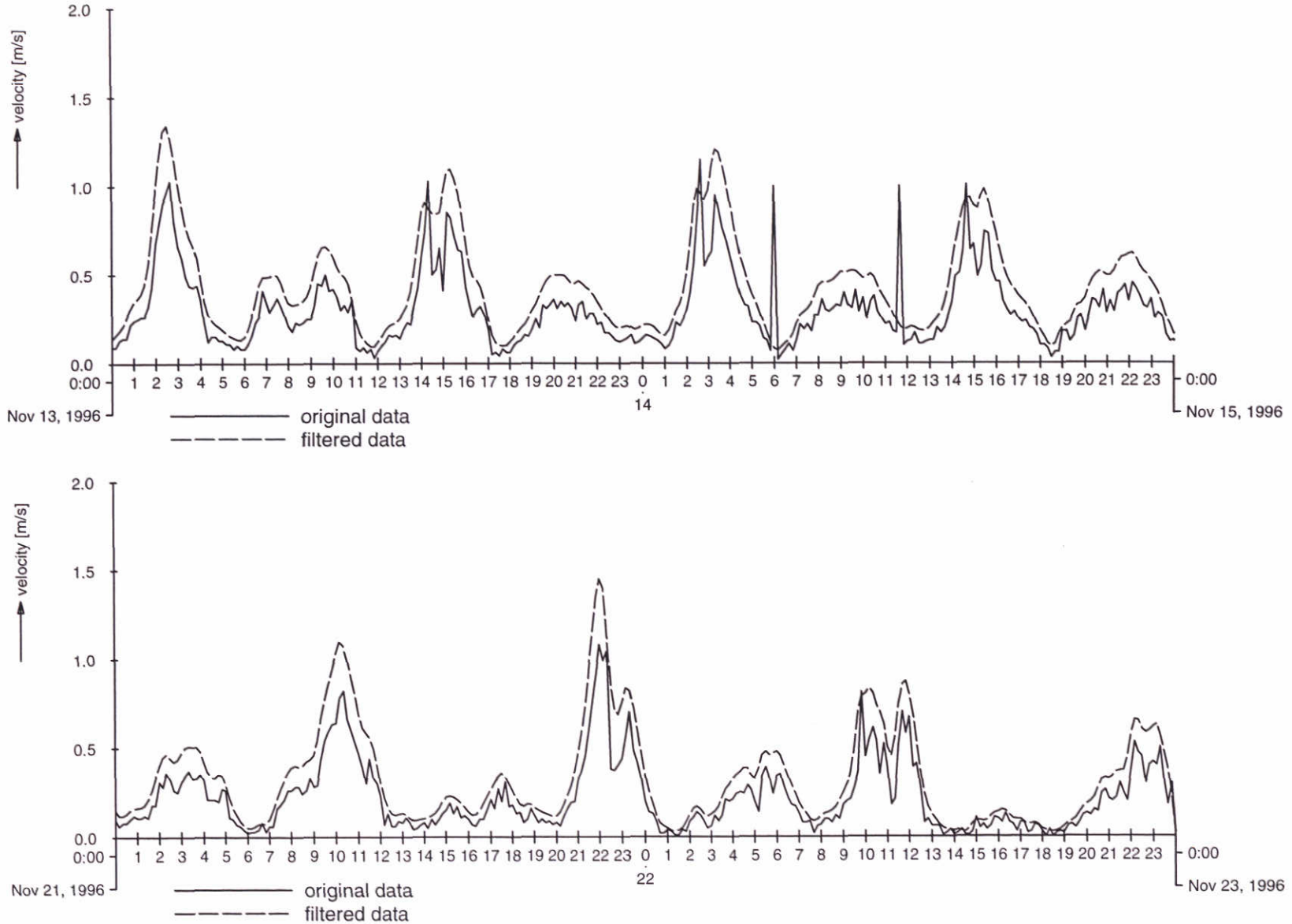

Time variation of depth mean velocity and computed bed shear stress (inc. waves)	Station B	Nov. 1997
	Nov. 21 & 22	
DELFT HYDRAULICS	Proj: Z2263	Fig.6.5

Time variation of depth mean velocity and computed bed shear stress (inc. waves) - Maasgeul outside	Station B	Nov. 1997
	Nov. 13 & 14	
DELFT HYDRAULICS	Proj: Z2263	Fig.6.6

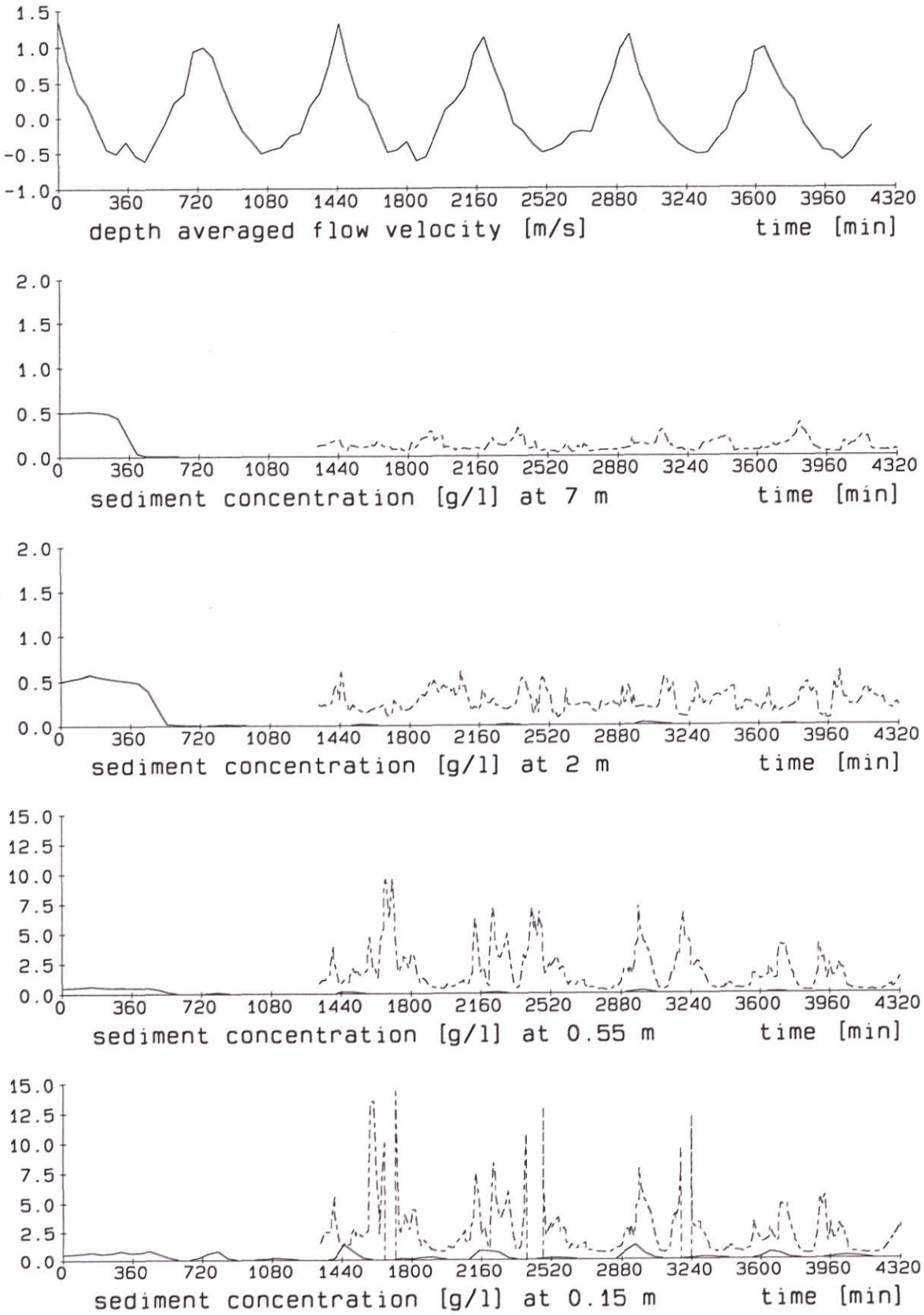

Simulation suspended sediment concentration initial concentration C_0 = 0.5 g/l, W_s = 0.6 mm/s incl. effects waves and no flocculation	Run P02	Station B
	Nov. 13 and 14, 1996	
DELFT HYDRAULICS - MARINE and COASTAL MANAGEMENT	Proj: Z2263	Fig. 6.7

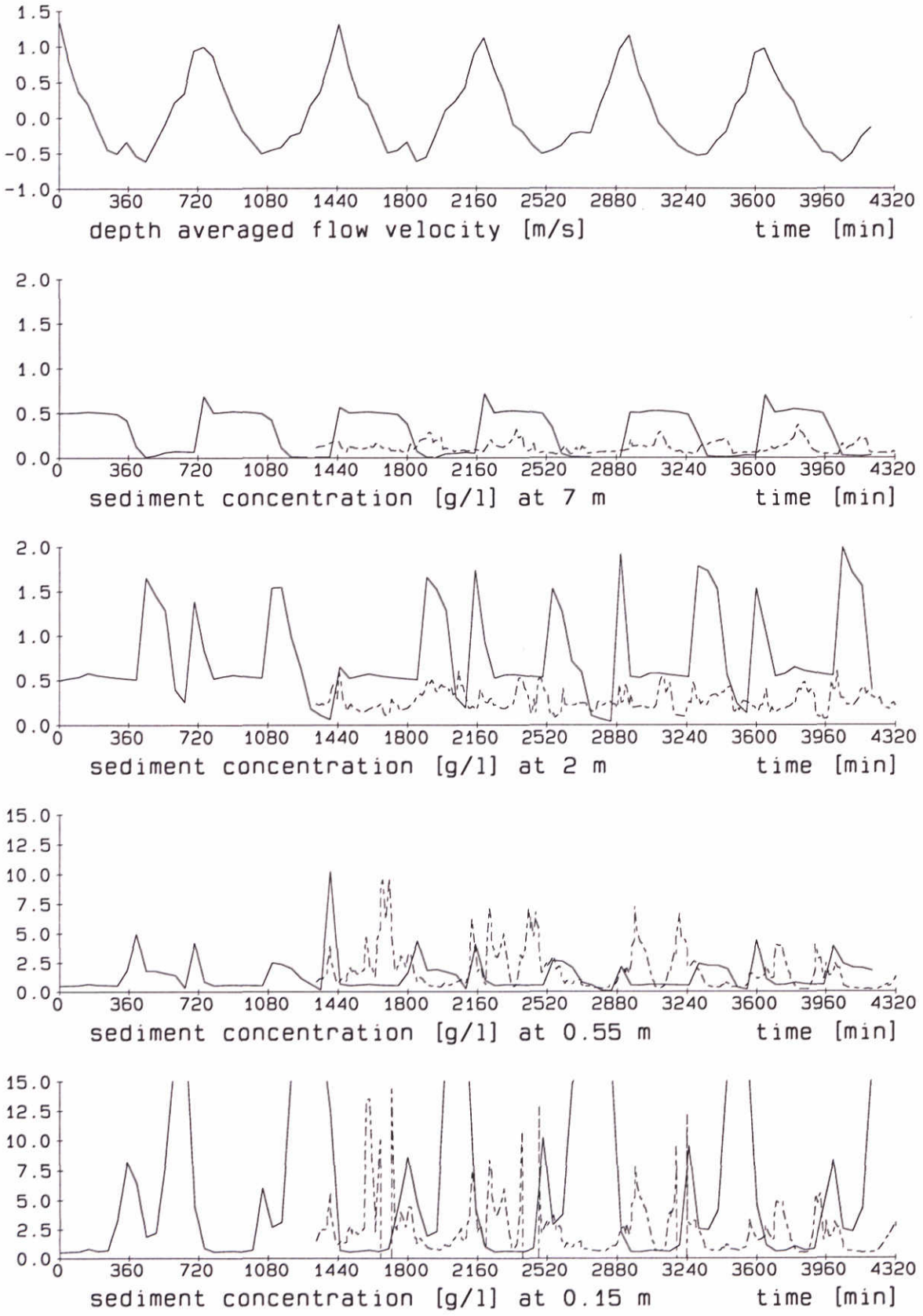

Simulation suspended sediment concentration initial concentration C_0 = 0.5 g/l, W_s = 0.6 mm/s incl. effects waves and floc.model A	Run P18	Station B
	Nov. 13 and 14, 1996	
DELFT HYDRAULICS - MARINE and COASTAL MANAGEMENT	Proj: Z2263	Fig. 6.8

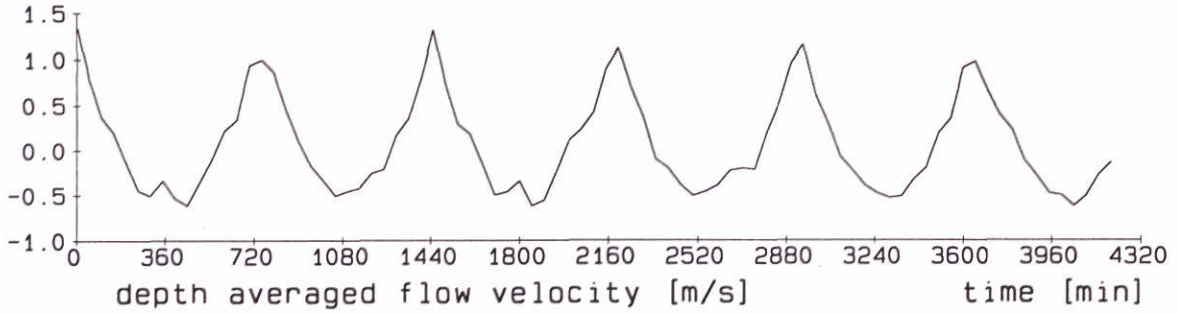

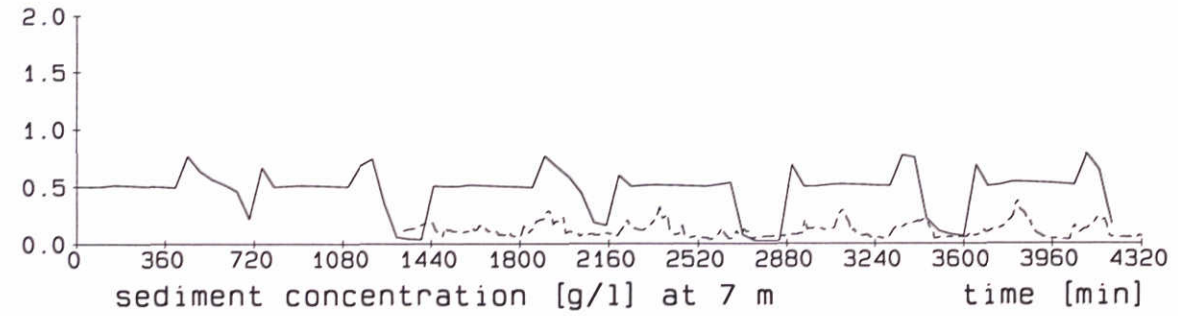

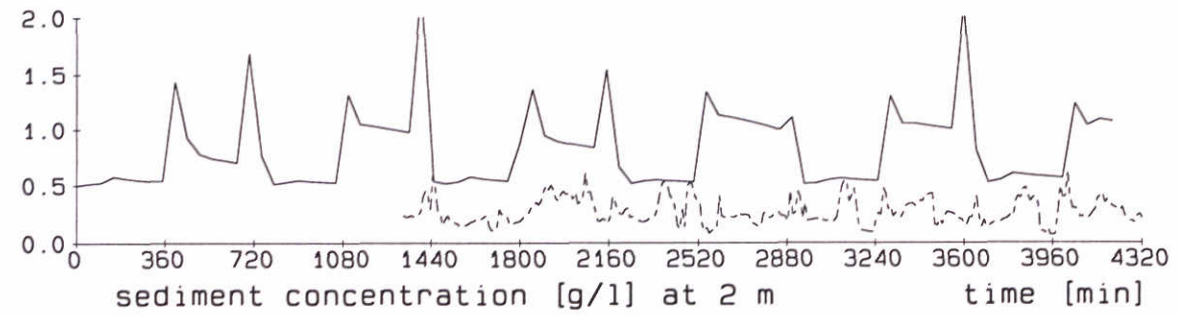

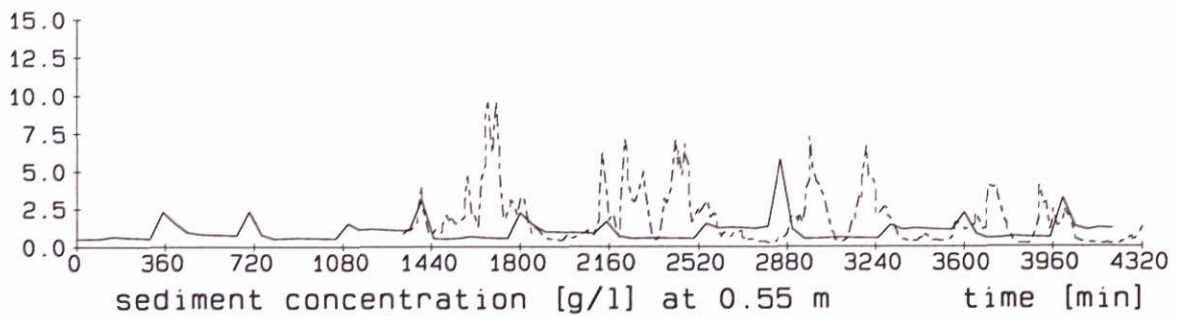

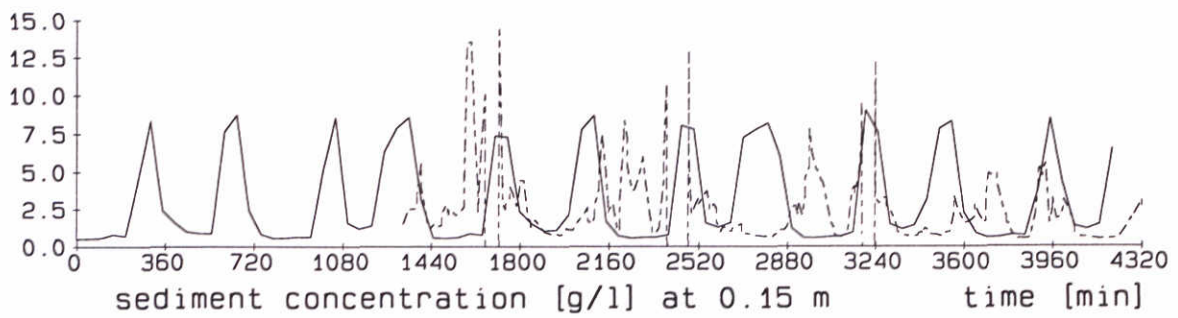

——— Simulations - - - - - - - - - Observations (z = 2 and 7 m for Station H)

Simulation suspended sediment concentration initial concentration C_0 = 0.5 g/l, W_s = 0.5 mm/s incl. effects waves and floc.model B	Run P04	Station B
	Nov. 13 and 14, 1996	
DELFT HYDRAULICS - MARINE and COASTAL MANAGEMENT	Proj: Z2263	Fig. 6.9

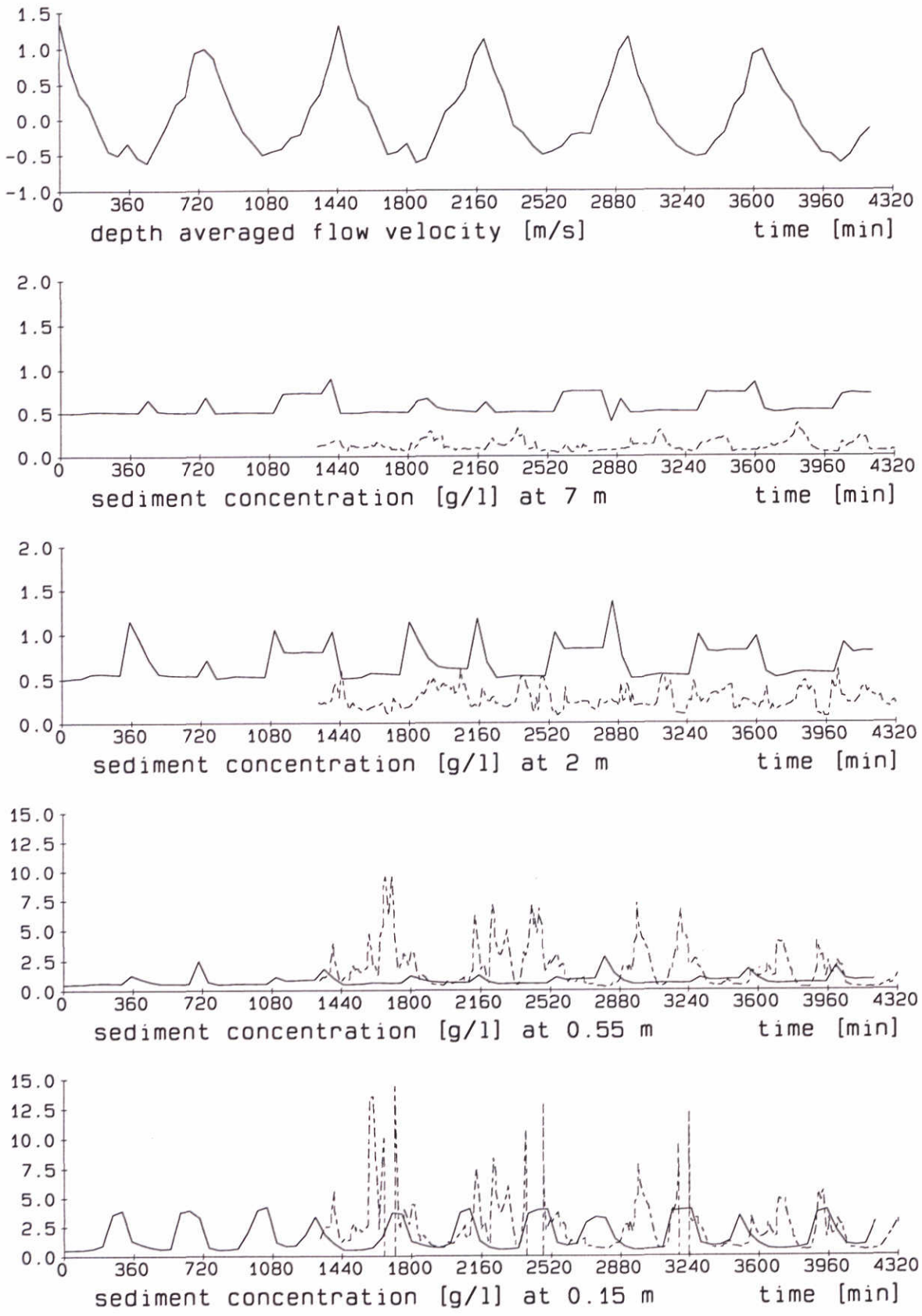

Simulation suspended sediment concentration initial concentration C_0 = 0.5 g/l, W_s = 0.5 mm/s incl. effects waves and floc.model C	Run P05	Station B
	Nov. 13 and 14, 1996	
DELFT HYDRAULICS - MARINE and COASTAL MANAGEMENT	Proj: Z2263	Fig. 6.10

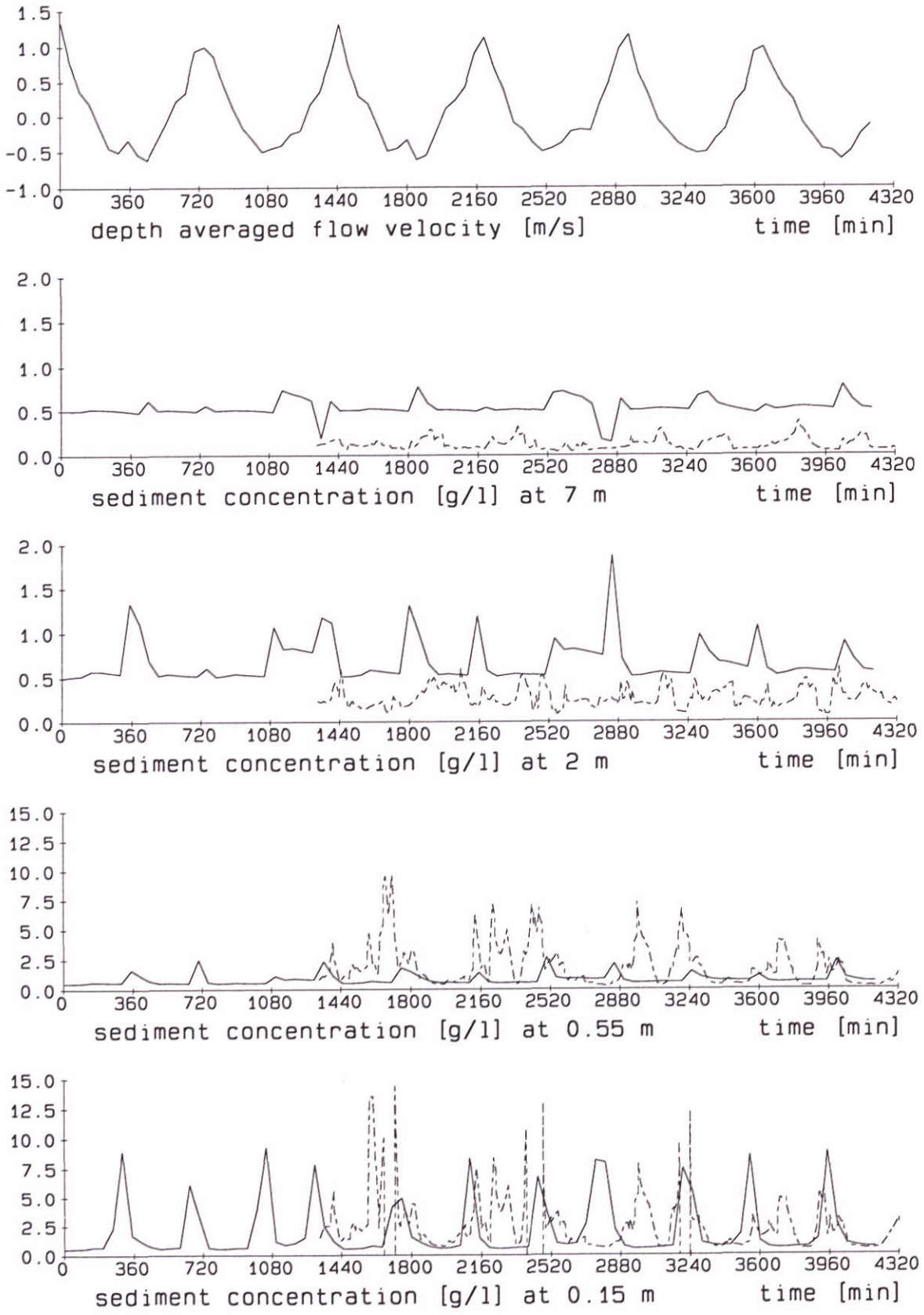

Simulation suspended sediment concentration initial concentration C_0 = 0.5 g/l, W_s = 0.5 mm/s incl. surf. and int. waves and floc.model B	Run P12	Station B
	Nov. 13 and 14, 1996	
DELFT HYDRAULICS - MARINE and COASTAL MANAGEMENT	Proj: Z2263	Fig. 6.11

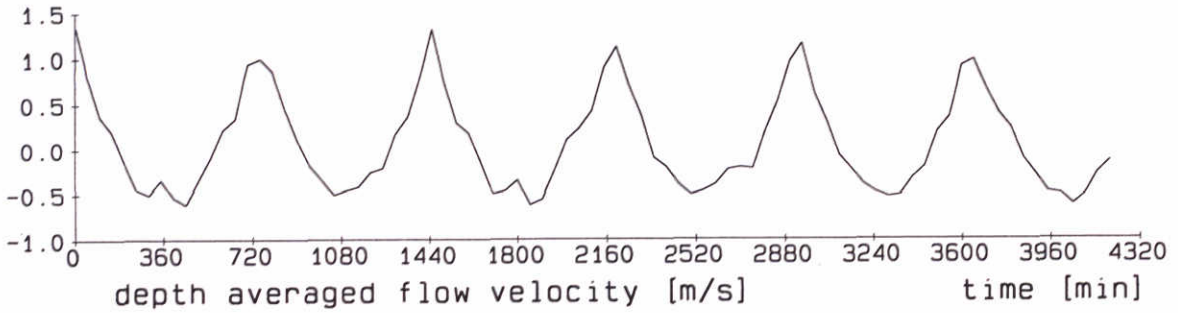

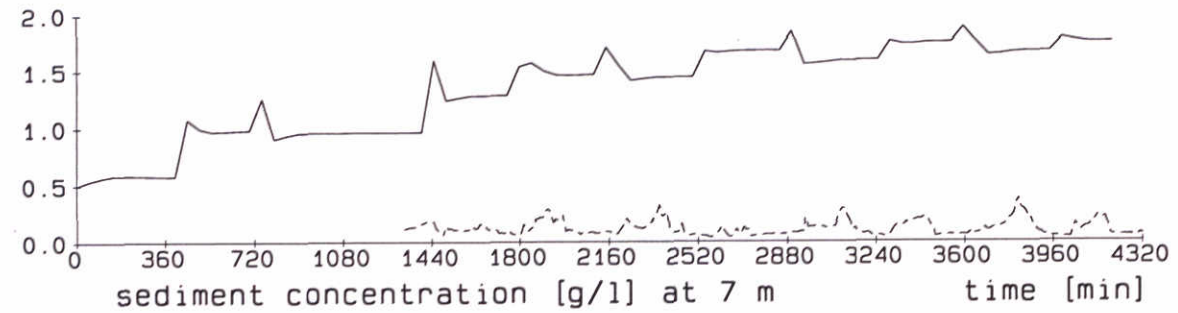

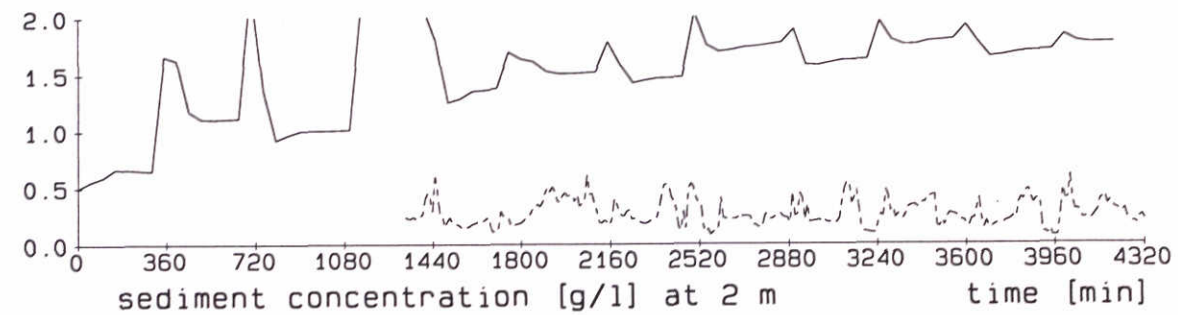

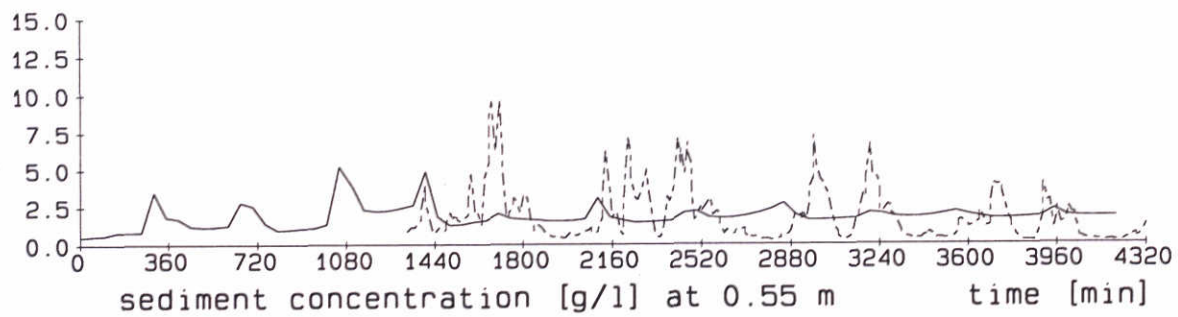

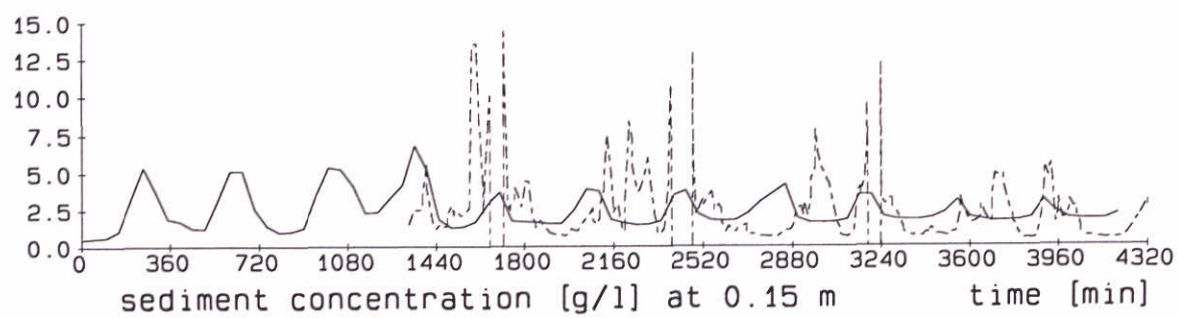

——— Simulations ---------- Observations (z = 2 and 7 m for Station H)

Simulation suspended sediment concentration initial concentration C_0 = 0.5 g/l, W_s = 0.5 mm/s incl. waves, floc.model B and erosion	Run P11	Station B
	Nov. 13 and 14, 1996	
DELFT HYDRAULICS - MARINE and COASTAL MANAGEMENT	Proj: Z2263	Fig. 6.12

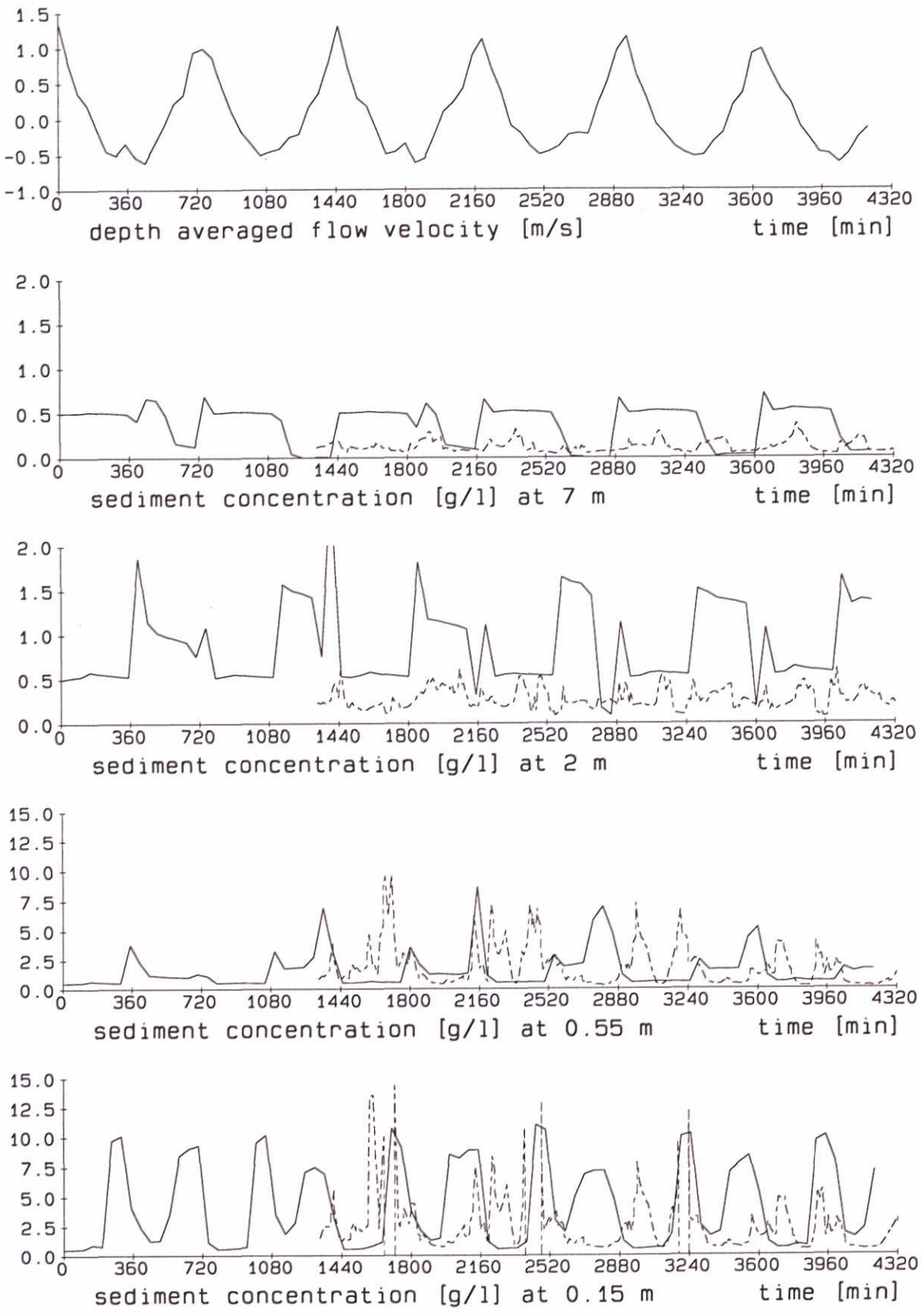

Simulation suspended sediment concentration initial concentration C_0 = 0.5 g/l, W_s = 0.6 mm/s incl. effects waves and floc.model B	Run P13	Station B
	Nov. 13 and 14, 1996	
DELFT HYDRAULICS - MARINE and COASTAL MANAGEMENT	Proj: Z2263	Fig.6.13

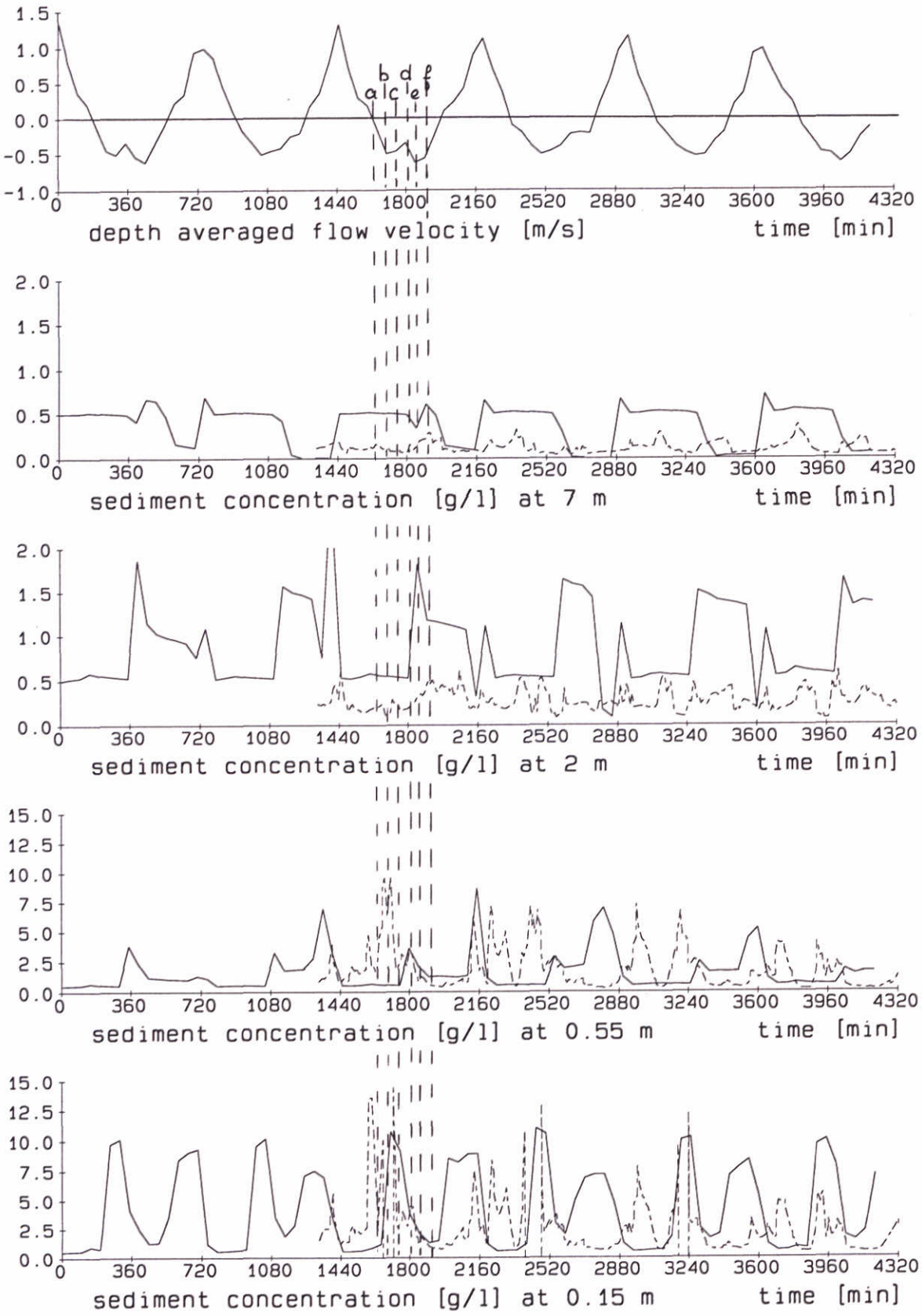

Simulation suspended sediment concentration initial concentration C_0 = 0.5 g/l, W_s = 0.6 mm/s incl. effects waves and floc.model B	Run P13	Station B
	Nov. 13 and 14, 1996	
DELFT HYDRAULICS - MARINE and COASTAL MANAGEMENT	Proj: Z2263	Fig.6.13*

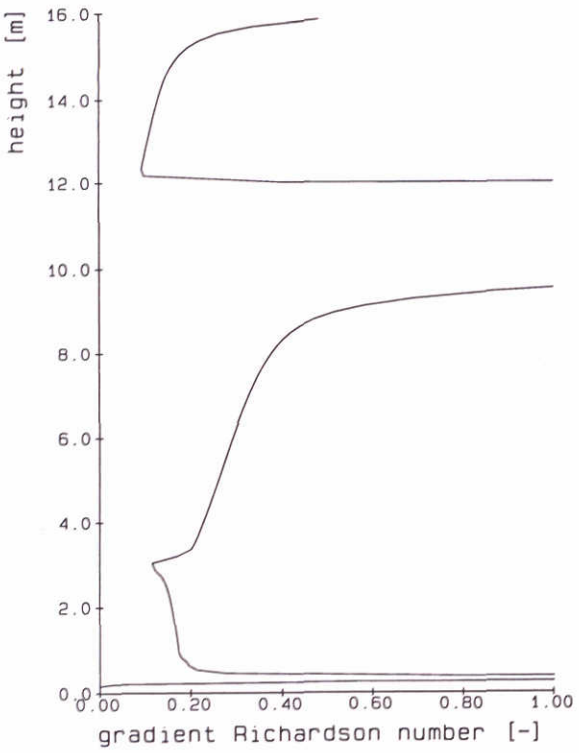

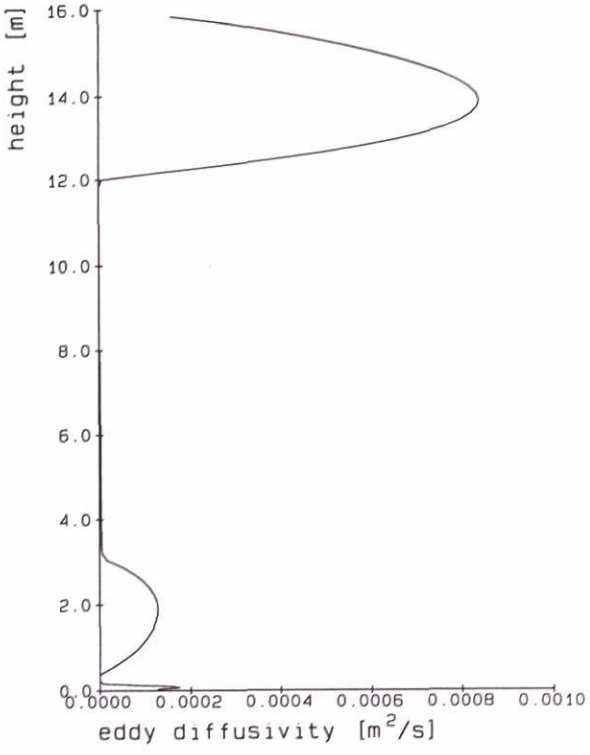

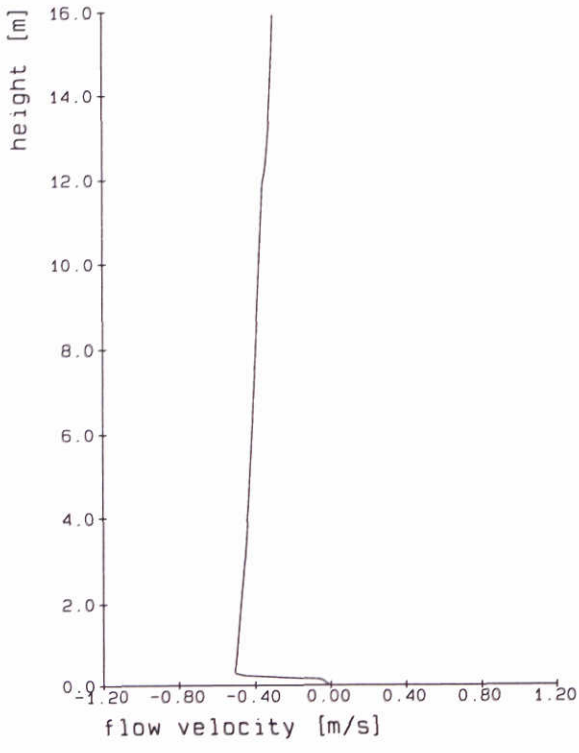

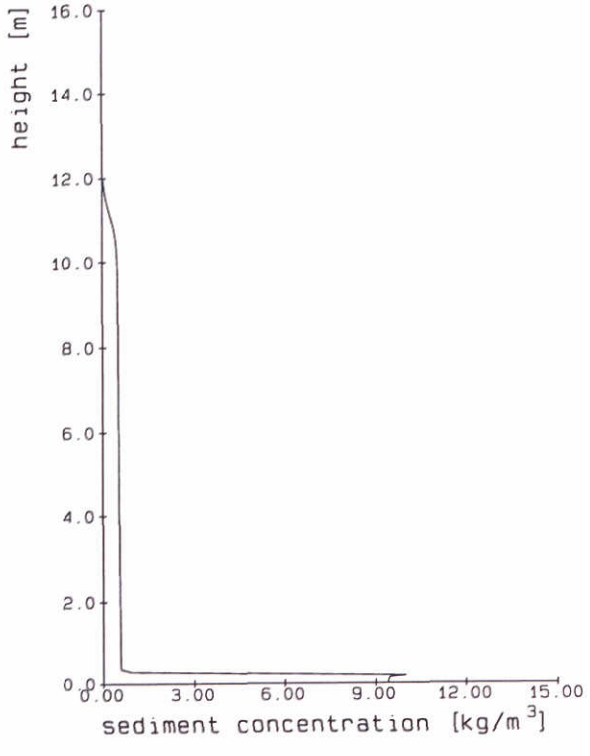

Vertical flow and concentration profiles initial concentration, C_0 = 0.5 g/l, W_s = 0.6 mm/s incl. effects waves and some flocculation	Run : P13	time : 3200
	Station B	
DELFT HYDRAULICS - MARINE & COASTAL MANAGEMENT	Proj: Z2263	Fig. 6.13b

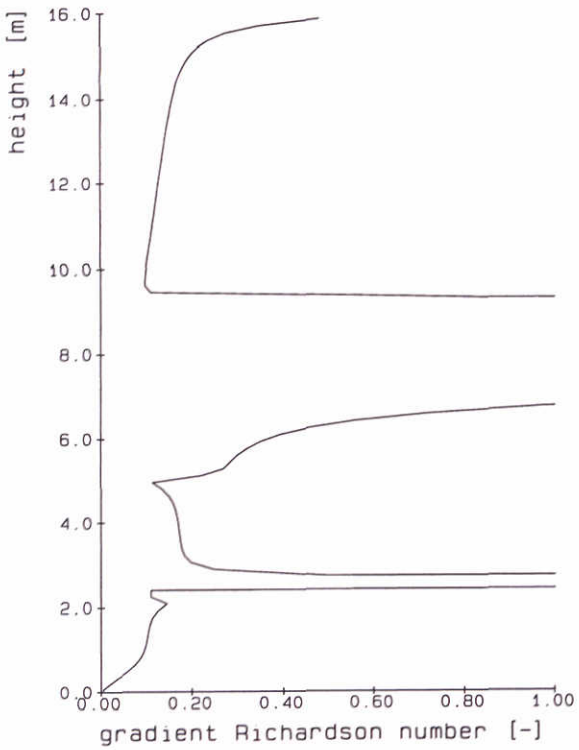

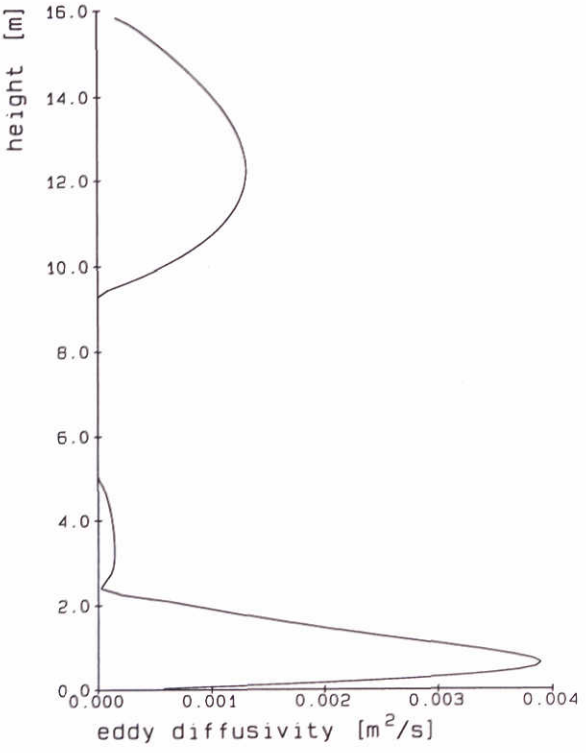

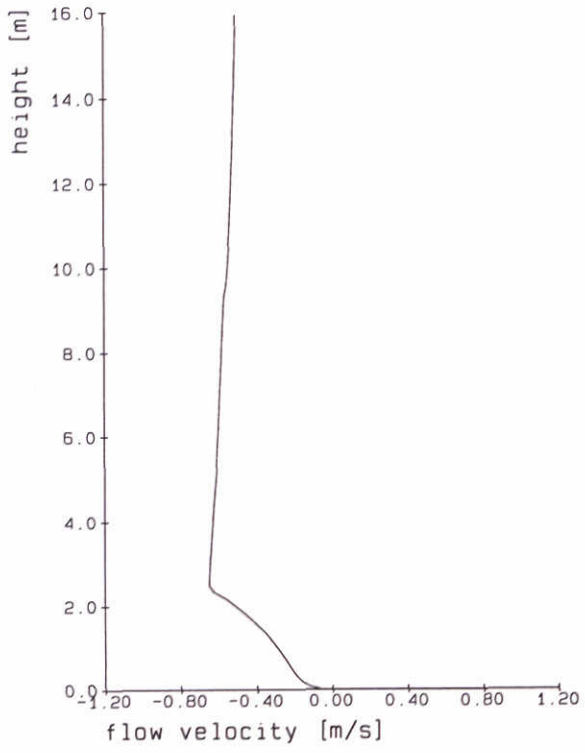

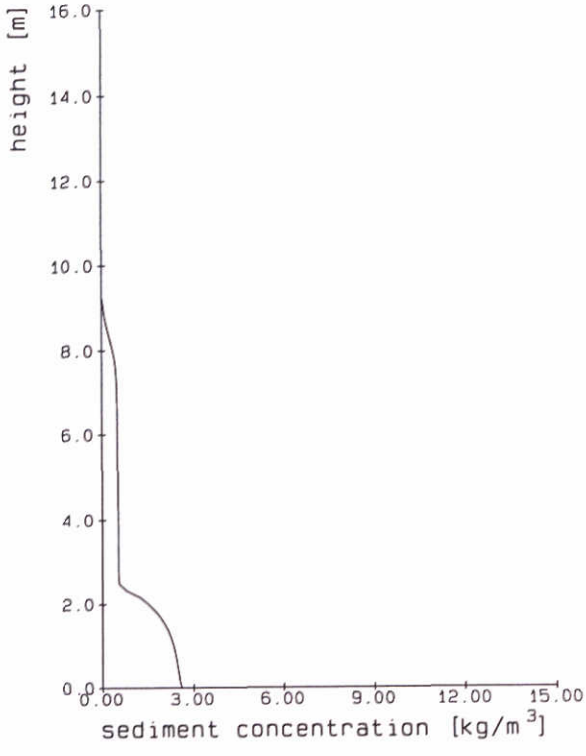

Vertical flow and concentration profiles initial concentration, C_0 = 0.5 g/l, W_s = 0.6 mm/s incl. effects waves and some flocculation	Run : P13	time : 3300
	Station B	
DELFT HYDRAULICS - MARINE & COASTAL MANAGEMENT	Proj: Z2263	Fig. 6.13c

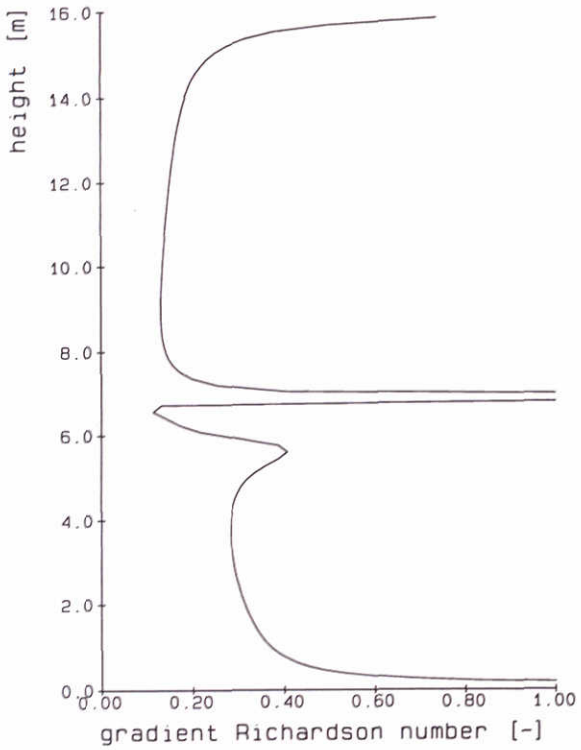

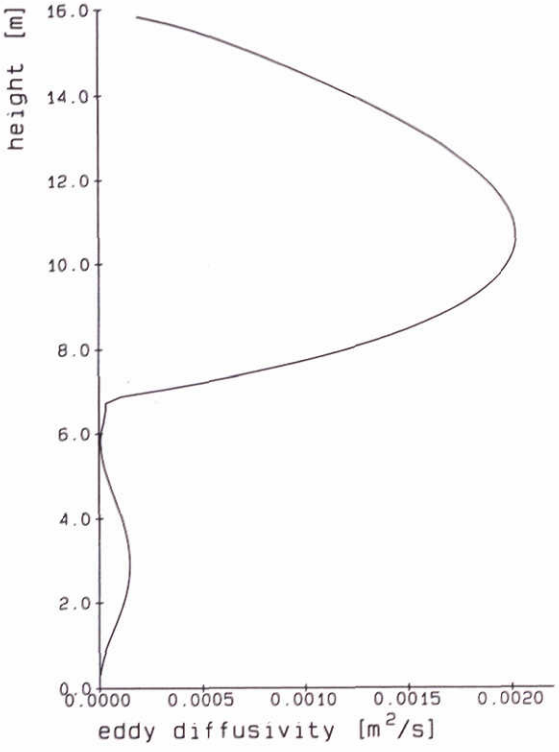

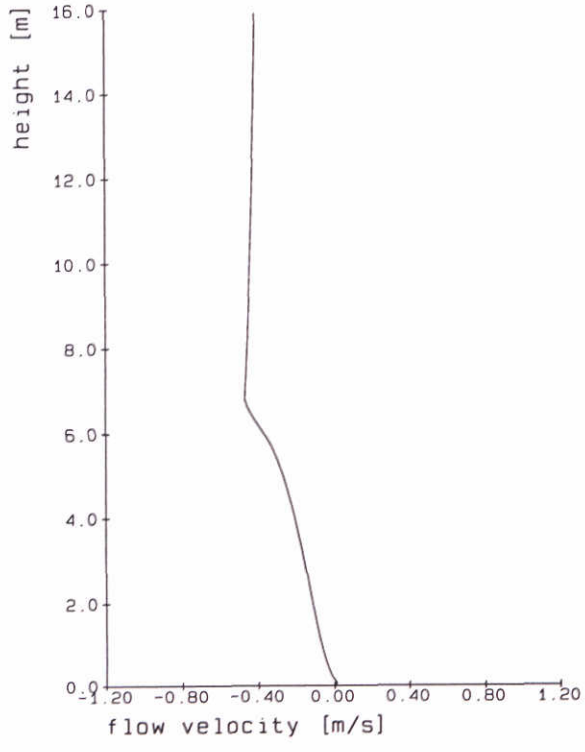

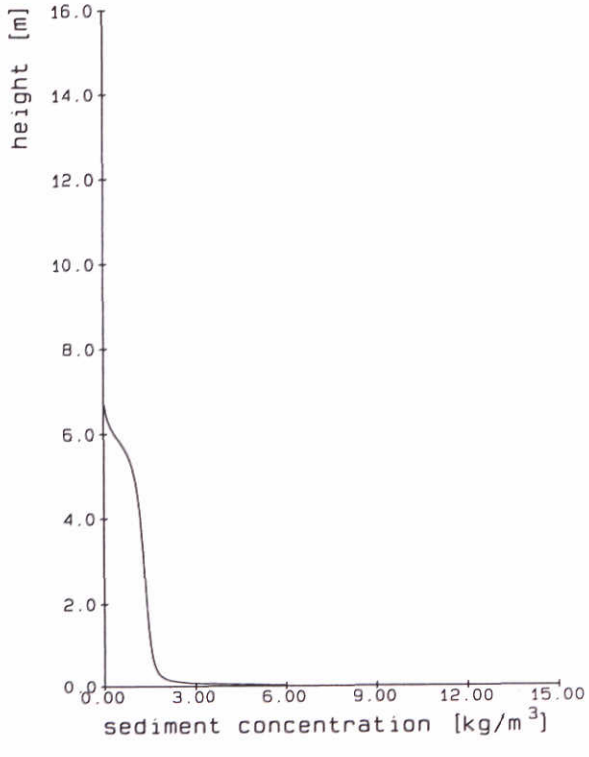

Vertical flow and concentration profiles initial concentration, C_0 = 0.5 g/l, W_s = 0.6 mm/s incl. effects waves and some flocculation	Run : P13	time : 3400
	Station B	
DELFT HYDRAULICS - MARINE & COASTAL MANAGEMENT	Proj: Z2263	Fig. 6.13d

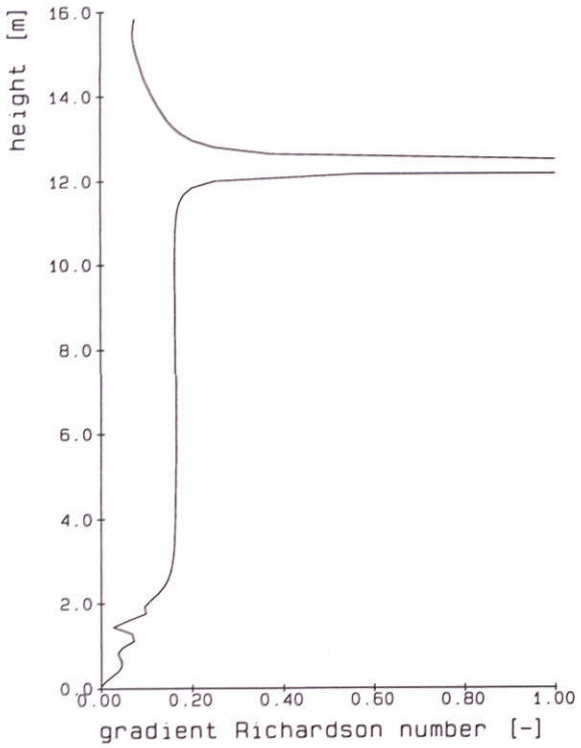

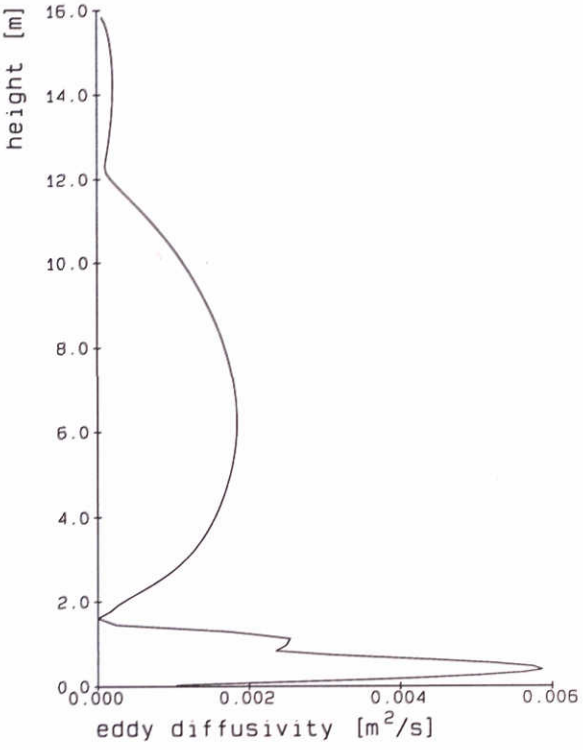

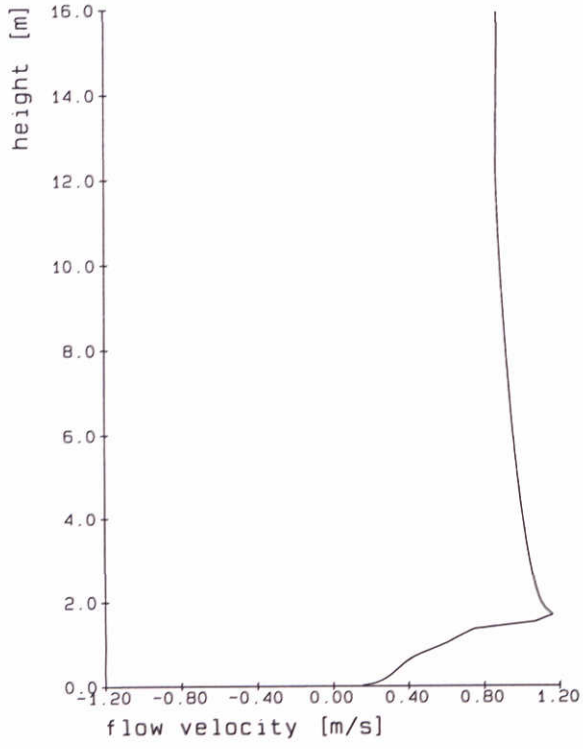

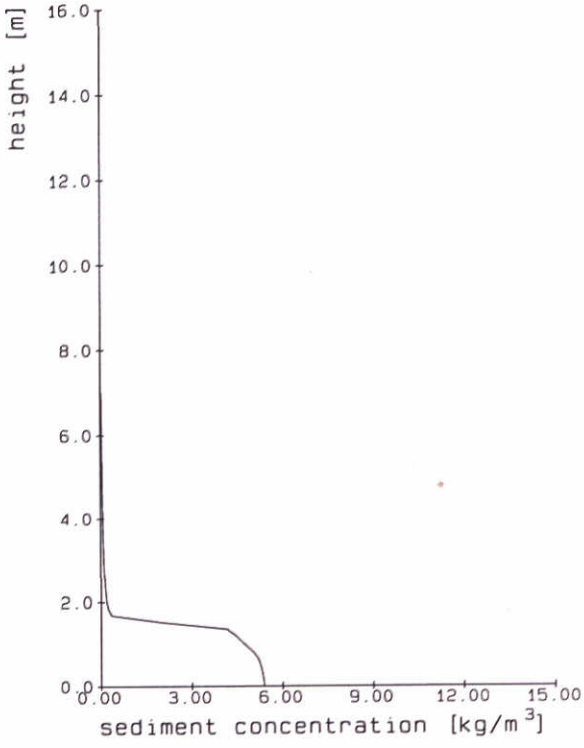

Vertical flow and concentration profiles initial concentration, C_0 = 0.5 g/l, W_s = 0.6 mm/s incl. effects waves and some flocculation	Run : P13	time : 3600
	Station B	
DELFT HYDRAULICS - MARINE & COASTAL MANAGEMENT	Proj: Z2263	Fig. 6.13e

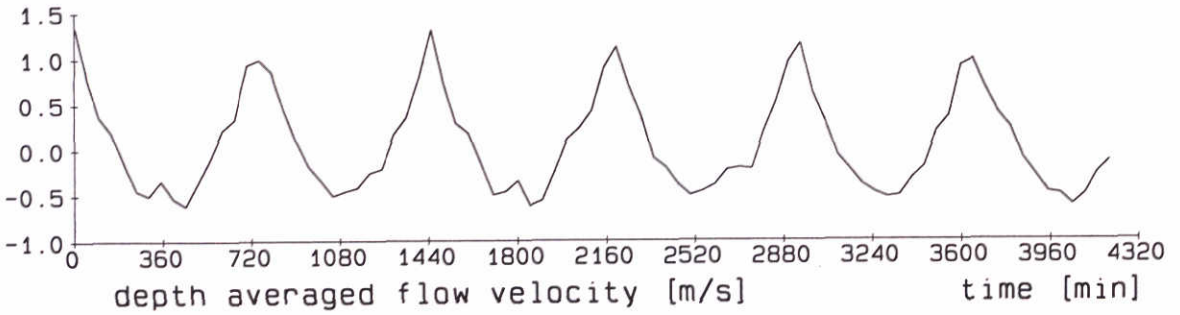

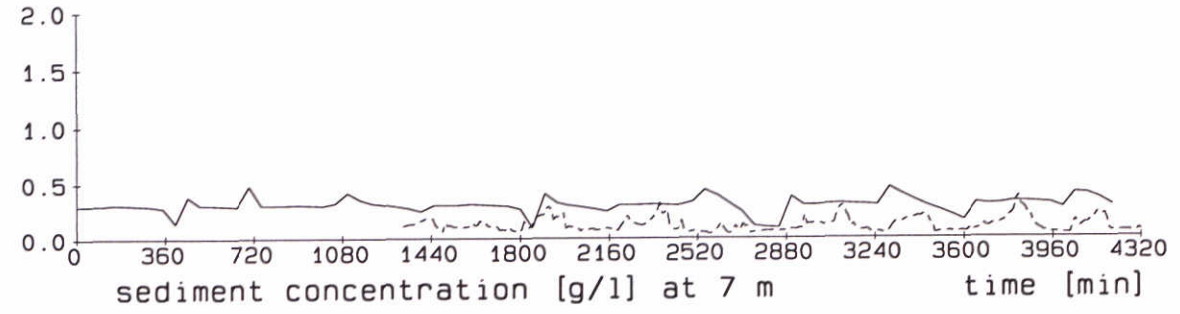

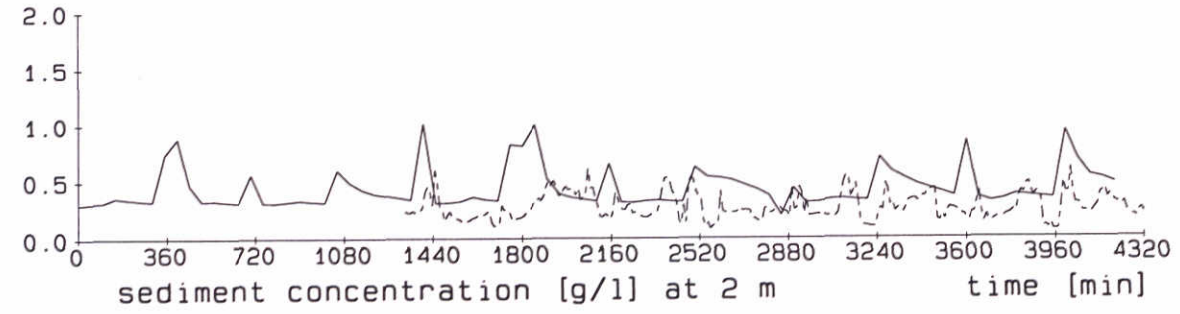

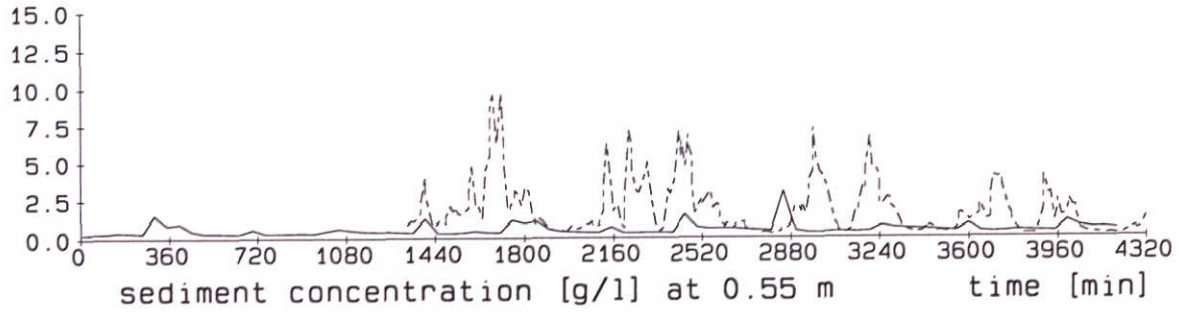

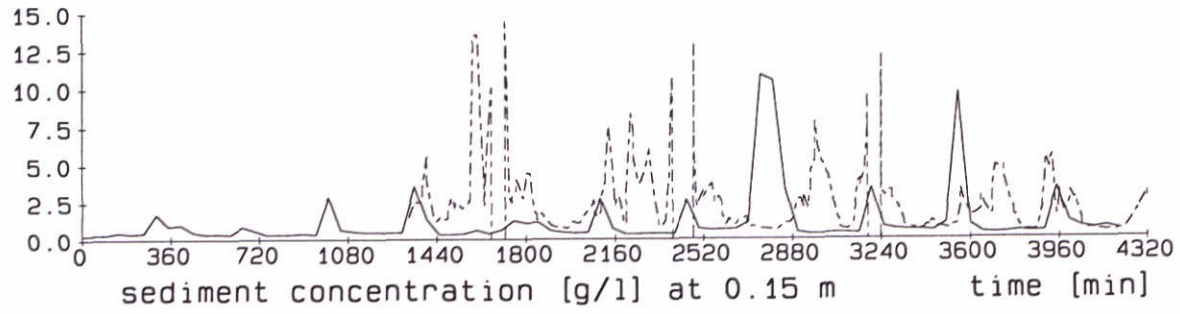

——— Simulations ---------- Observations (z = 2 and 7 m for Station H)

Simulation suspended sediment concentration initial concentration C_0 = 0.3 g/l, W_s = 0.6 mm/s incl. effects waves and floc.model B	Run P16	Station B
	Nov. 13 and 14, 1996	
DELFT HYDRAULICS - MARINE and COASTAL MANAGEMENT	Proj: Z2263	Fig. 6.14

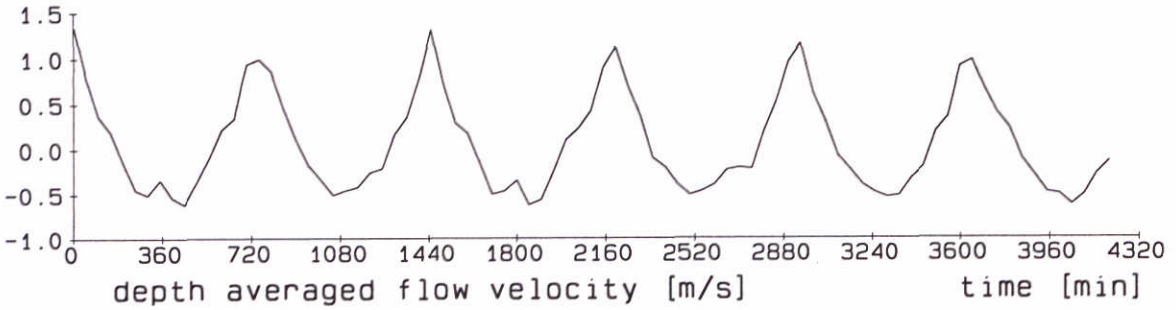

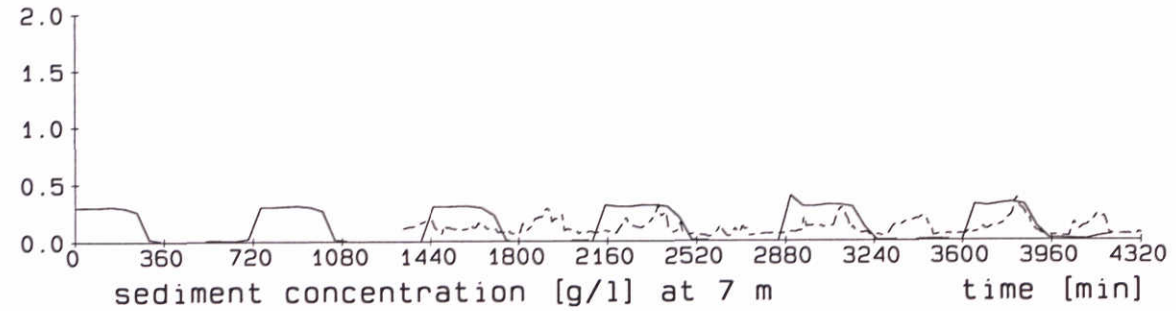

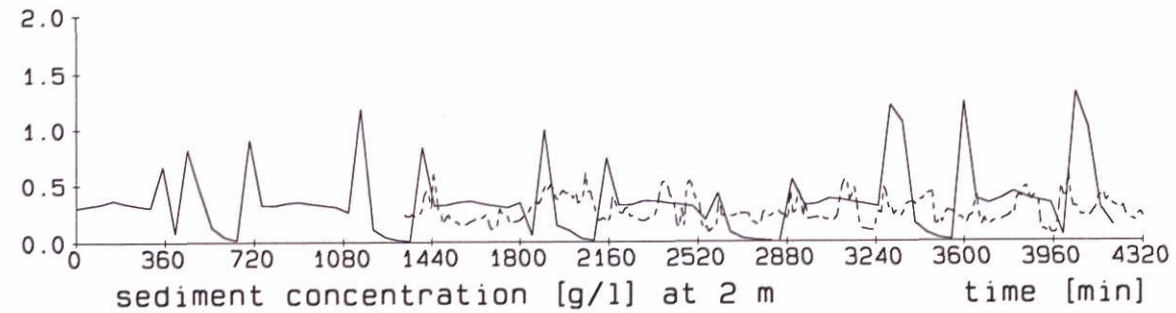

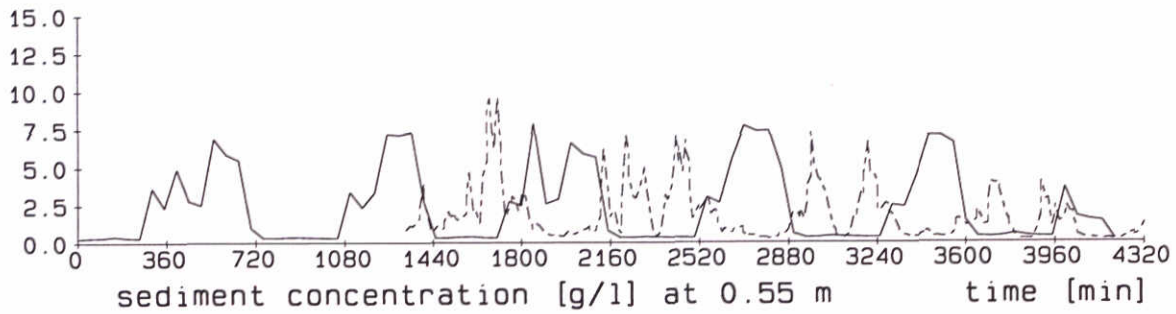

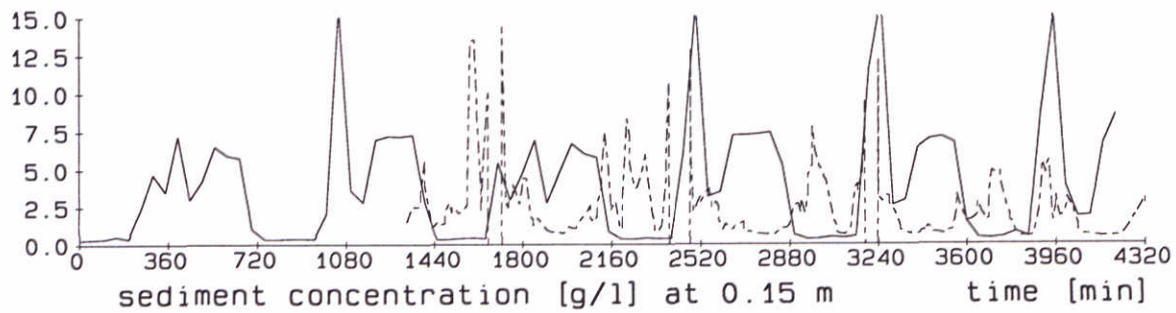

——— Simulations ---------- Observations (z = 2 and 7 m for Station H)

Simulation suspended sediment concentration initial concentration C_0 = 0.3 g/l, W_s = 1.0 mm/s incl. effects waves and floc.model B	Run P14	Station B
	Nov. 13 and 14, 1996	
DELFT HYDRAULICS - MARINE and COASTAL MANAGEMENT	Proj: Z2263	Fig. 6.15

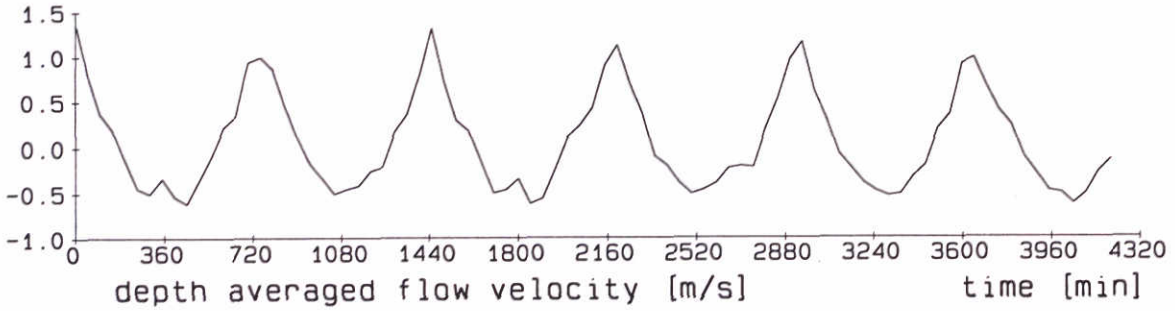

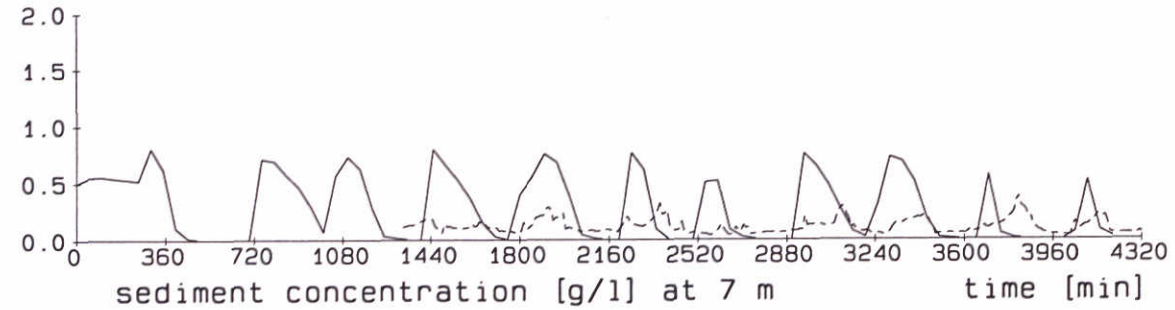

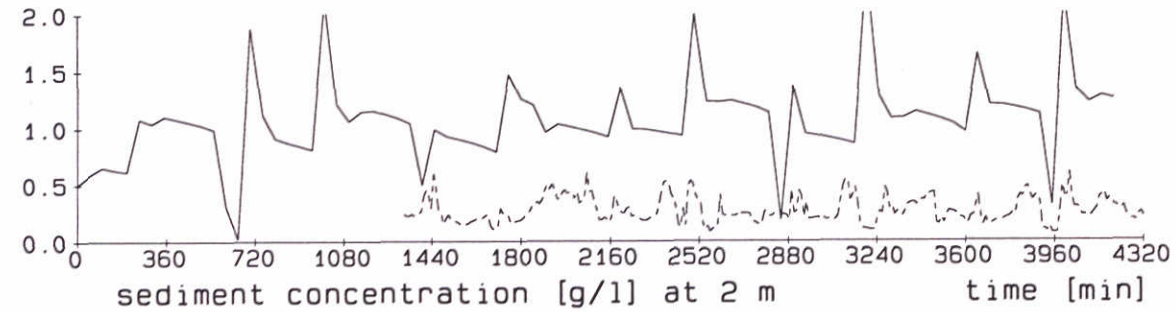

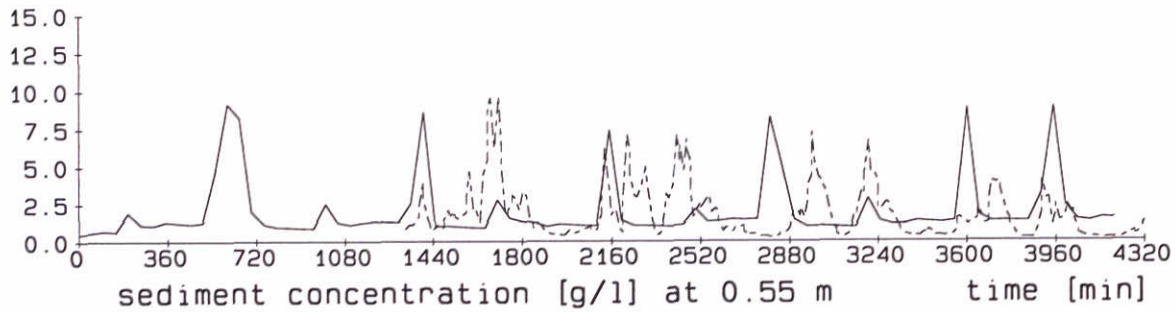

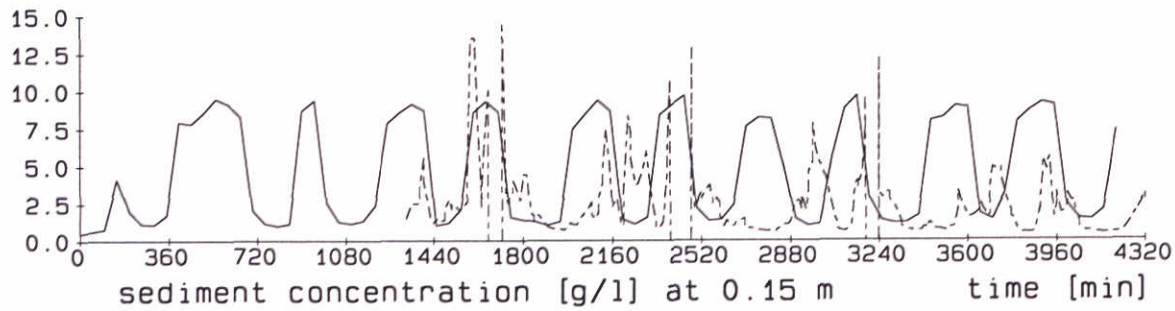

——— Simulations ---------- Observations (z = 2 and 7 m for Station H)

Simulation suspended sediment concentration initial concentration C_0 = 0.5 g/l, W_s = 0.6 mm/s incl. effects waves, salinity and floc.model B	Run P15	Station B
	Nov. 13 and 14, 1996	
DELFT HYDRAULICS - MARINE and COASTAL MANAGEMENT	Proj: Z2263	Fig. 6.16

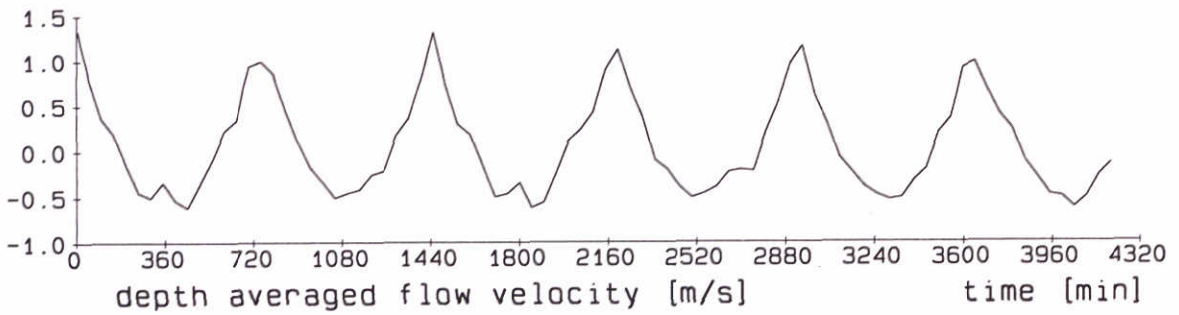

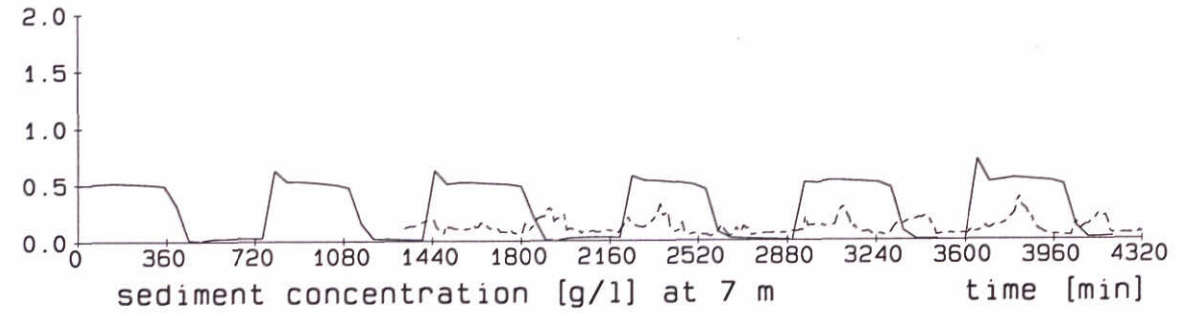

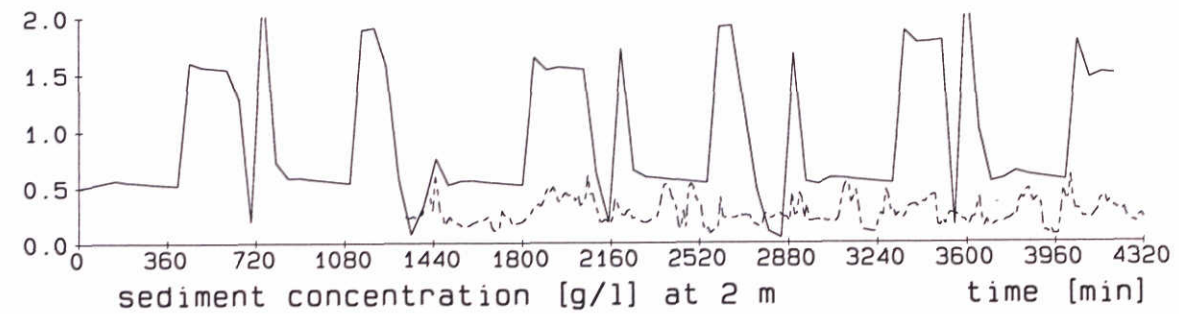

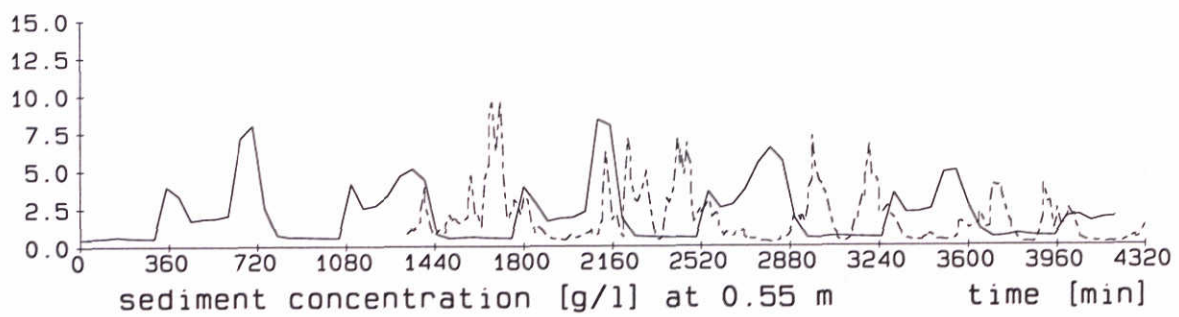

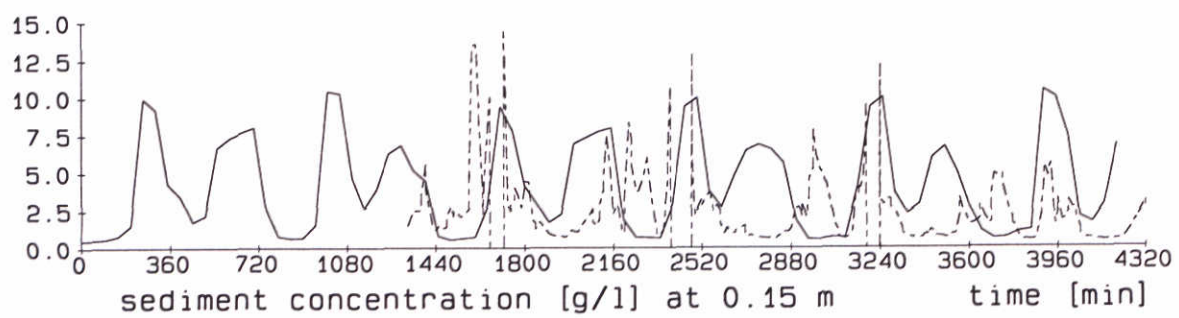

——— Simulations ---------- Observations (z = 2 and 7 m for Station H)

Simulation suspended sediment concentration initial concentration C_0 = 0.5 g/l, W_s = 0.6 mm/s incl. effects floc.model B; no waves	Run P17	Station B
	Nov. 13 and 14, 1996	
DELFT HYDRAULICS - MARINE and COASTAL MANAGEMENT	Proj: Z2263	Fig. 6.17

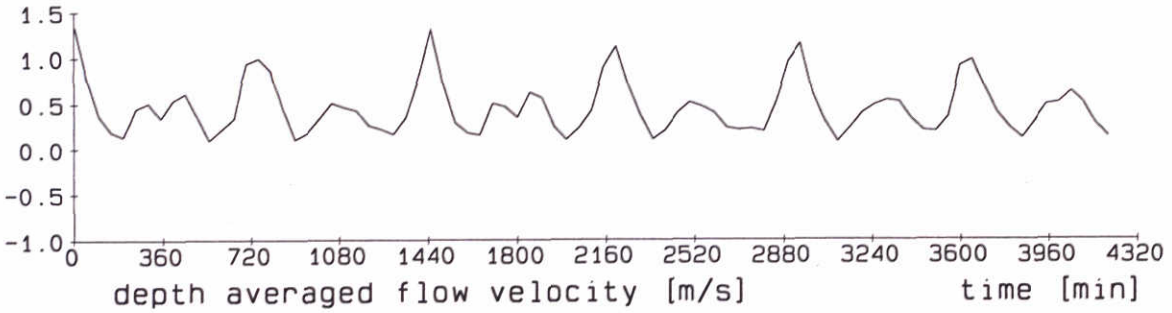

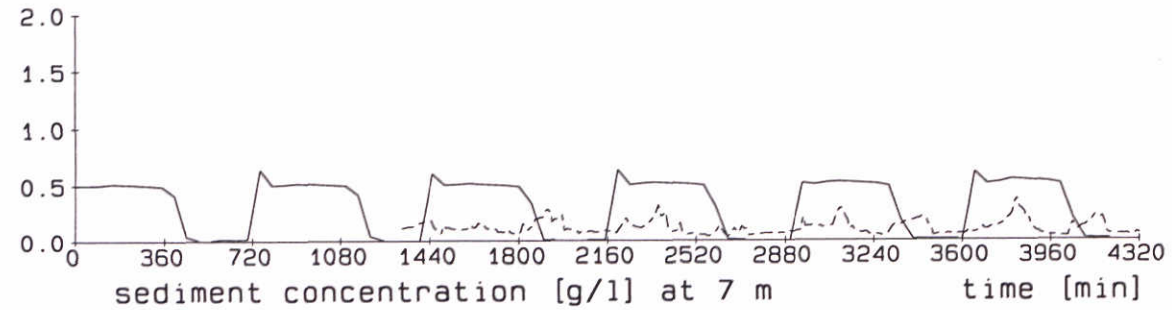

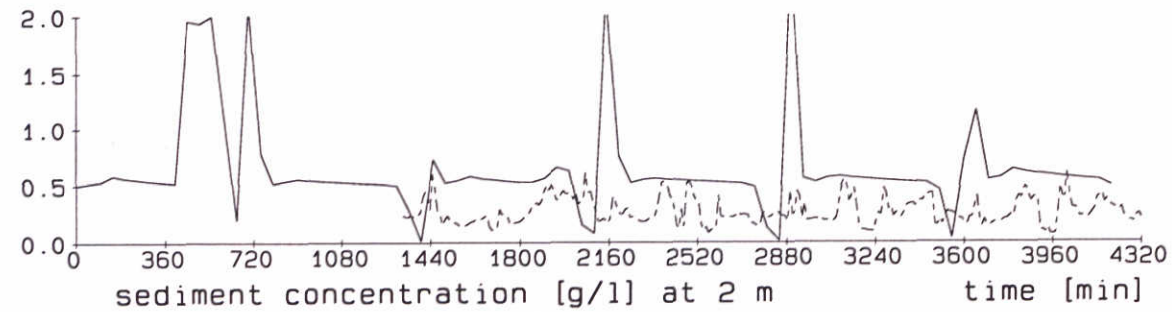

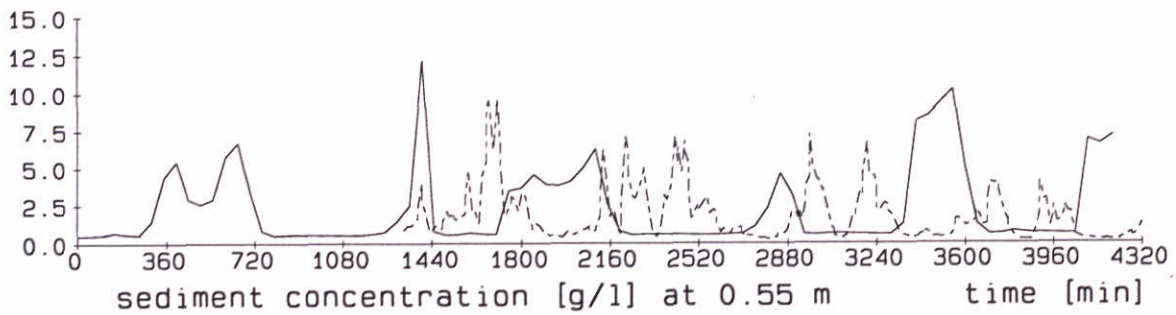

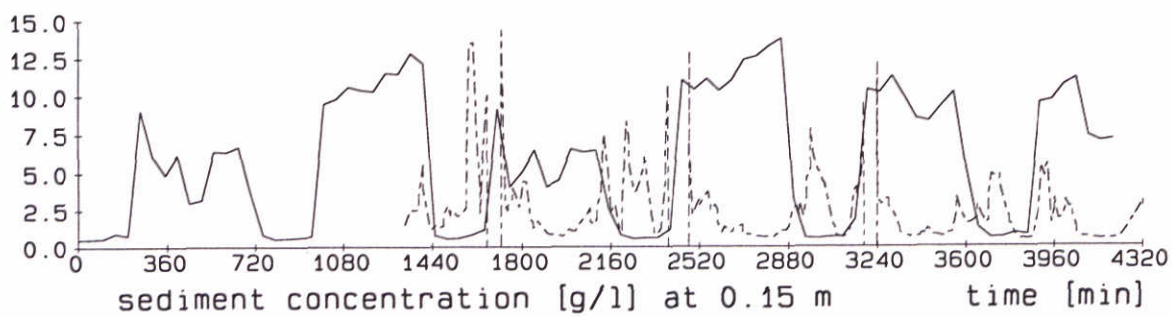

——— Simulations ---------- Observations (z = 2 and 7 m for Station H)

Simulation suspended sediment concentration initial concentration C_0 = 0.5 g/l, W_s = 0.6 mm/s incl. effects waves, floc.model B and pos. U only	Run P21	Station B
	Nov. 13 and 14, 1996	
DELFT HYDRAULICS - MARINE and COASTAL MANAGEMENT	Proj: Z2263	Fig.6.19

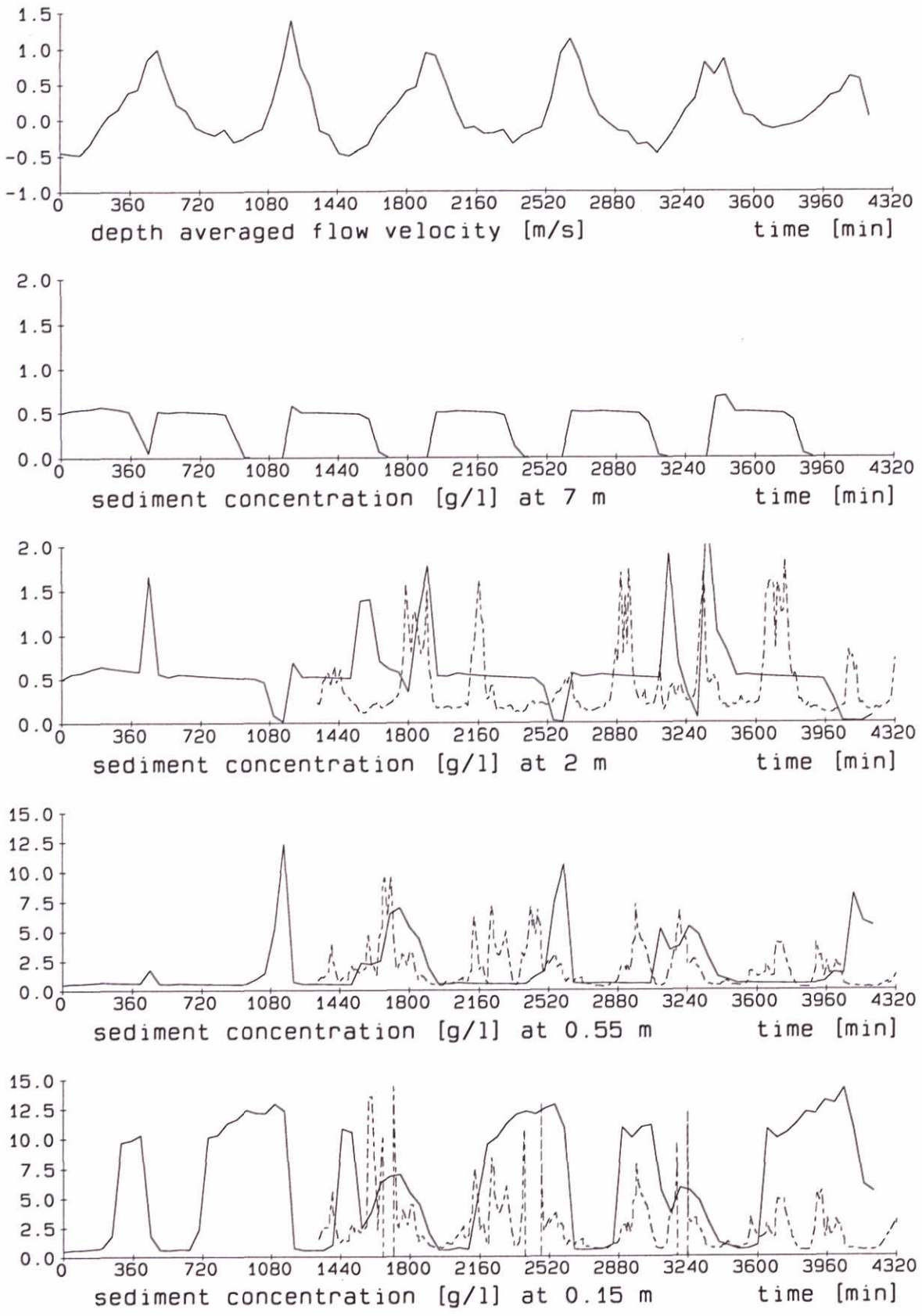

Simulation suspended sediment concentration initial concentration C_0 = 0.5 g/l, W_s = 0.6 mm/s incl. effects waves and floc.model B	Run P19	Station B
	Nov. 21 and 22, 1996	
DELFT HYDRAULICS - MARINE and COASTAL MANAGEMENT	Proj: Z2263	Fig. 6.20

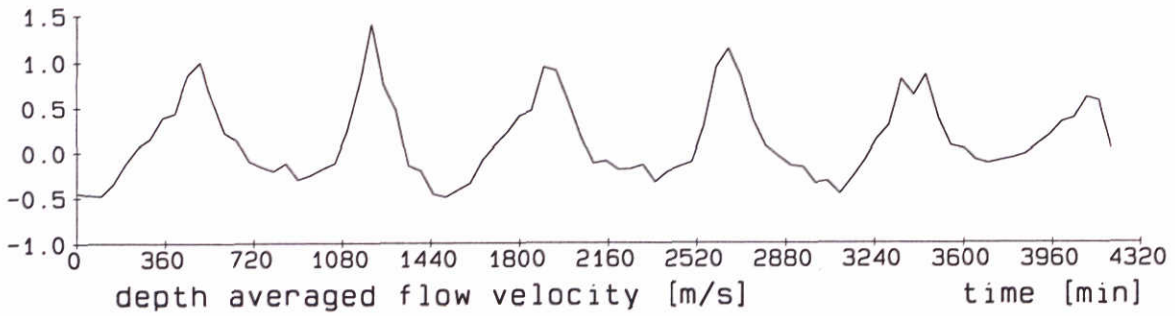

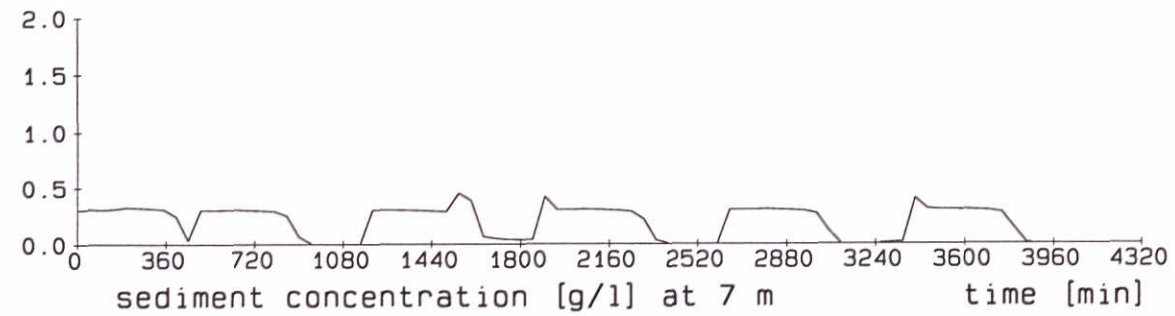

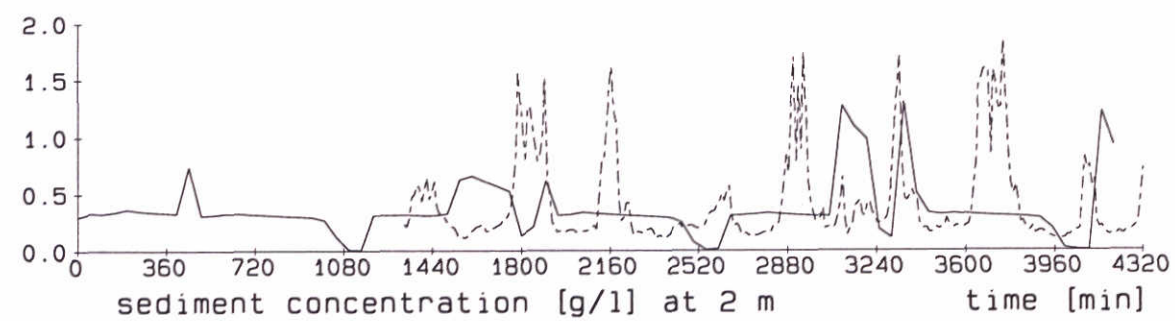

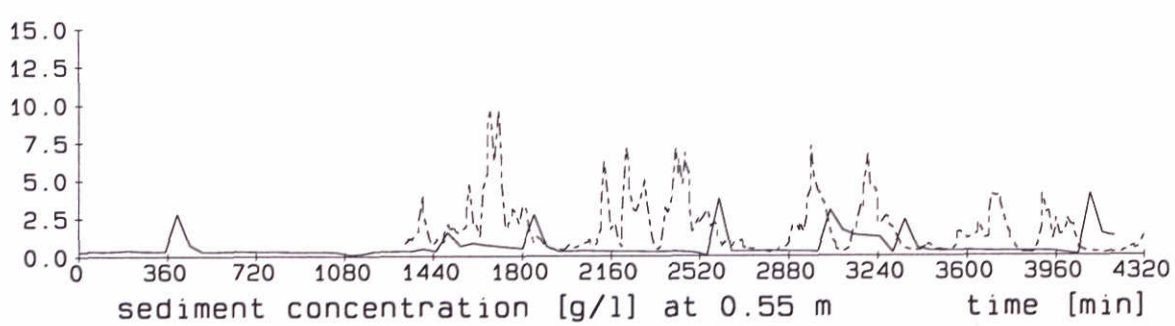

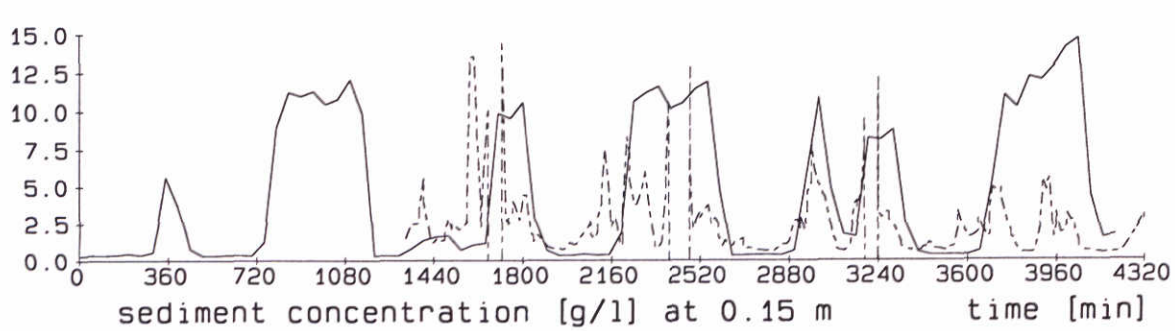

Simulations ---------- Observations (z = 2 and 7 m for Station H)

Simulation suspended sediment concentration initial concentration C_0 = 0.3 g/l, W_s = 0.6 mm/s incl. effects waves and floc.model B	Run P20	Station B
	Nov. 21 and 22, 1996	
DELFT HYDRAULICS - MARINE and COASTAL MANAGEMENT	Proj: Z2263	Fig. 6.21

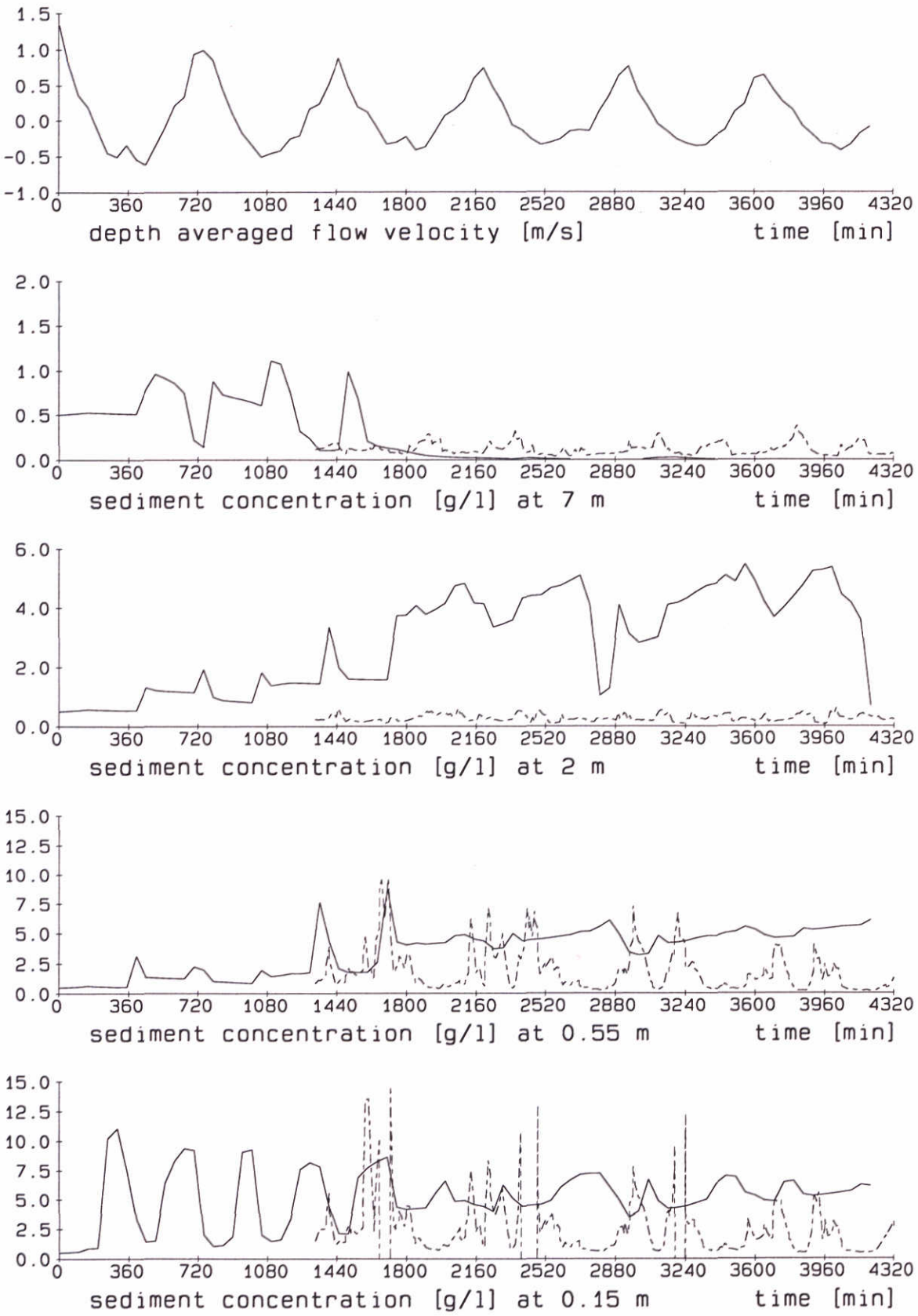

Simulation suspended sediment concentration initial concentration C_0 = 0.5 g/l, W_s = 0.6 mm/s idem P13, in Eurogeul off shore	Run D02	Station B
	Nov. 13 and 14, 1996	
DELFT HYDRAULICS - MARINE and COASTAL MANAGEMENT	Proj: Z2263	Fig. 6.22

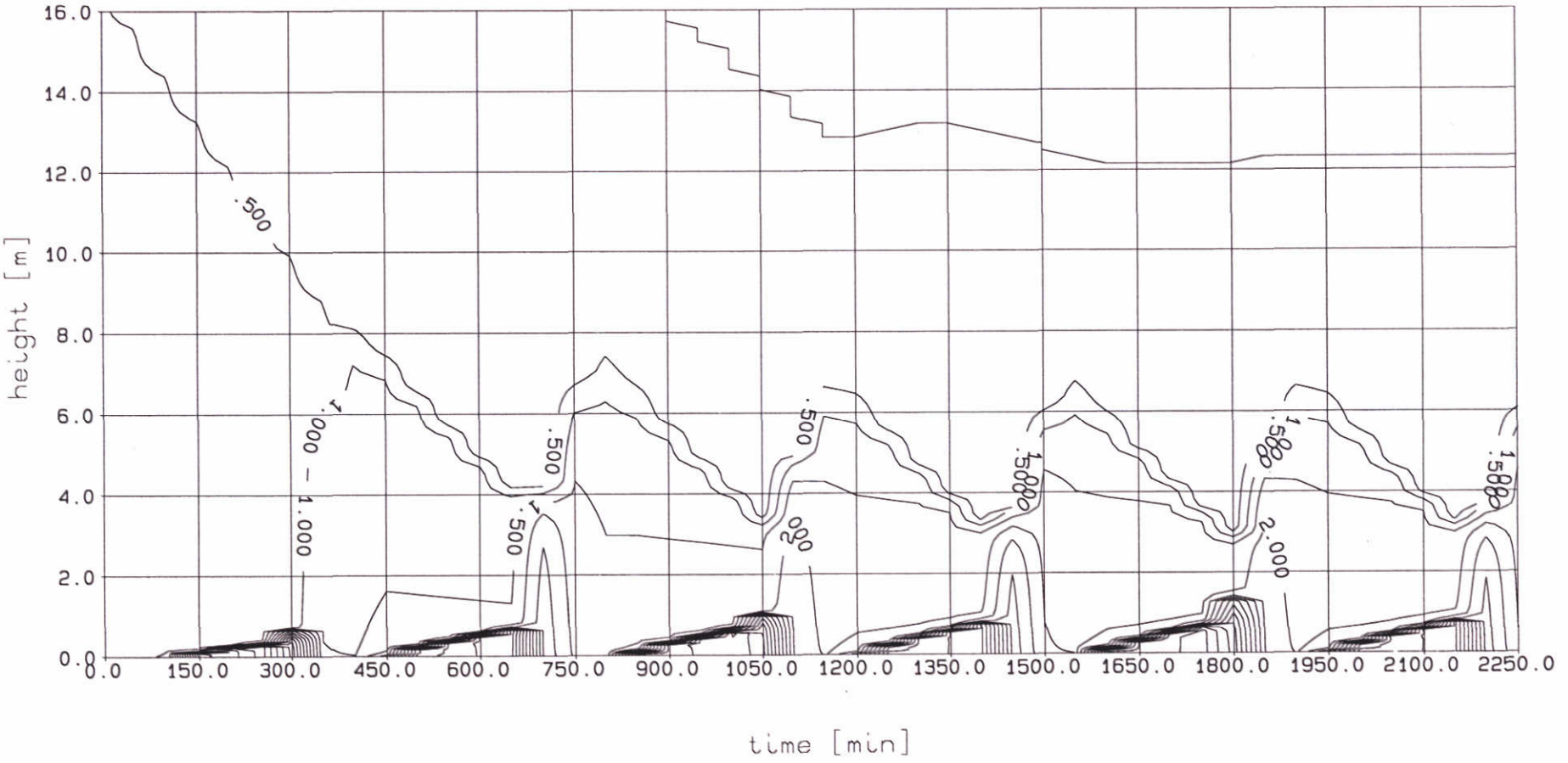

Computed mass concentrations [g/l] - {run Q04} C_0 = 0.6 g/l, W_s = 0.5 mm/s, U = 0.5/0.8 m/s h = 17 m, $H_{1/3}$ = 3 m, initial salinity profile	tidal run	20-01-1998
	prognostic simulations	
DELFT HYDRAULICS - MARINE & COASTAL MANAGEMENT	Proj: Z2263	Fig.6.23a

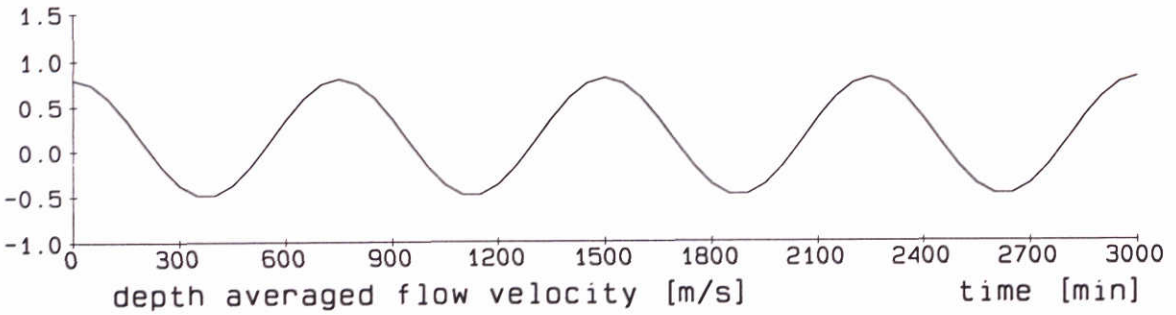

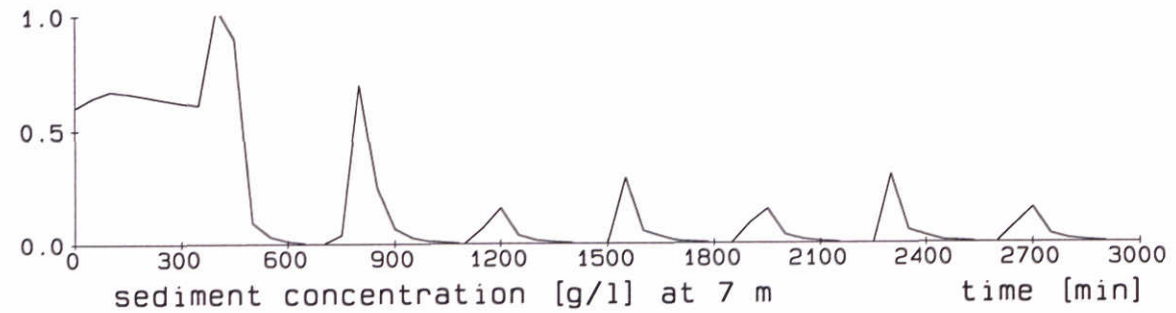

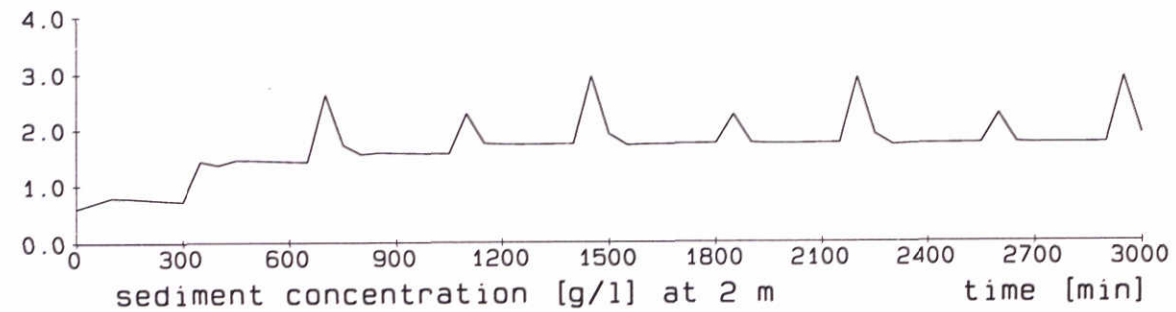

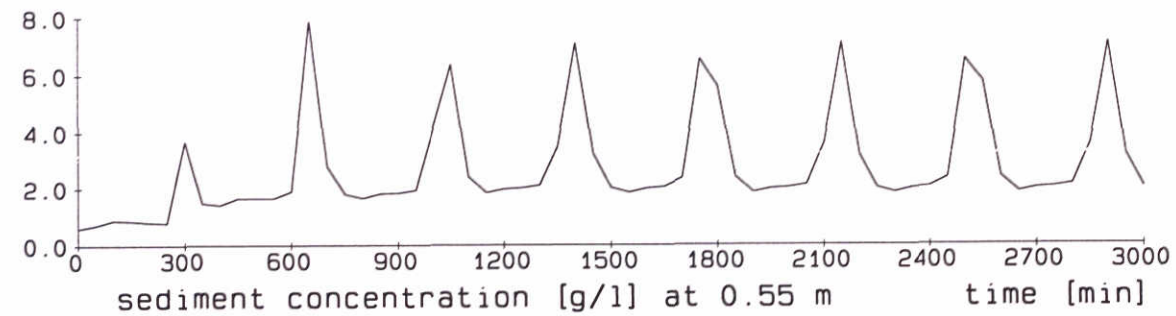

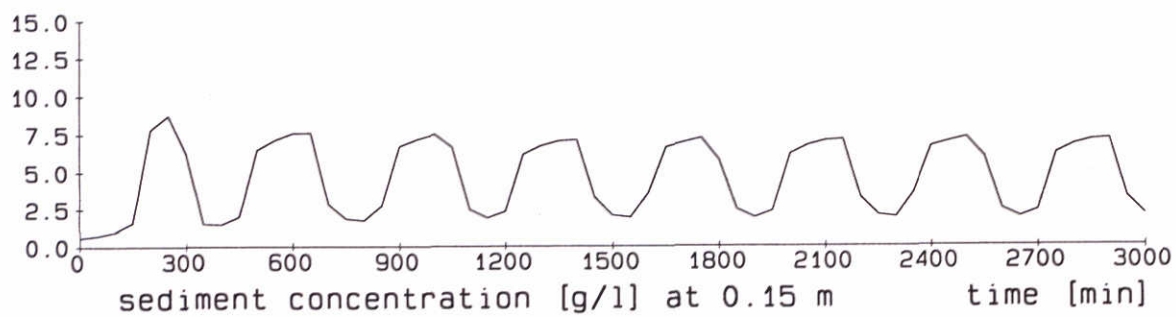

Simulations

Computed mass concentrations [g/l] - {run Q04} C_0 = 0.5 g/l, W_s = 0.5 mm/s, U = 0.5/0.8 m/s h = 17 m, $H_{1/3}$ = 3 m, initial salinity profile	tidal run	20-01-1998
	prognostic simulations	
DELFT HYDRAULICS - MARINE & COASTAL MANAGEMENT	Proj: Z2263	Fig.6.23b

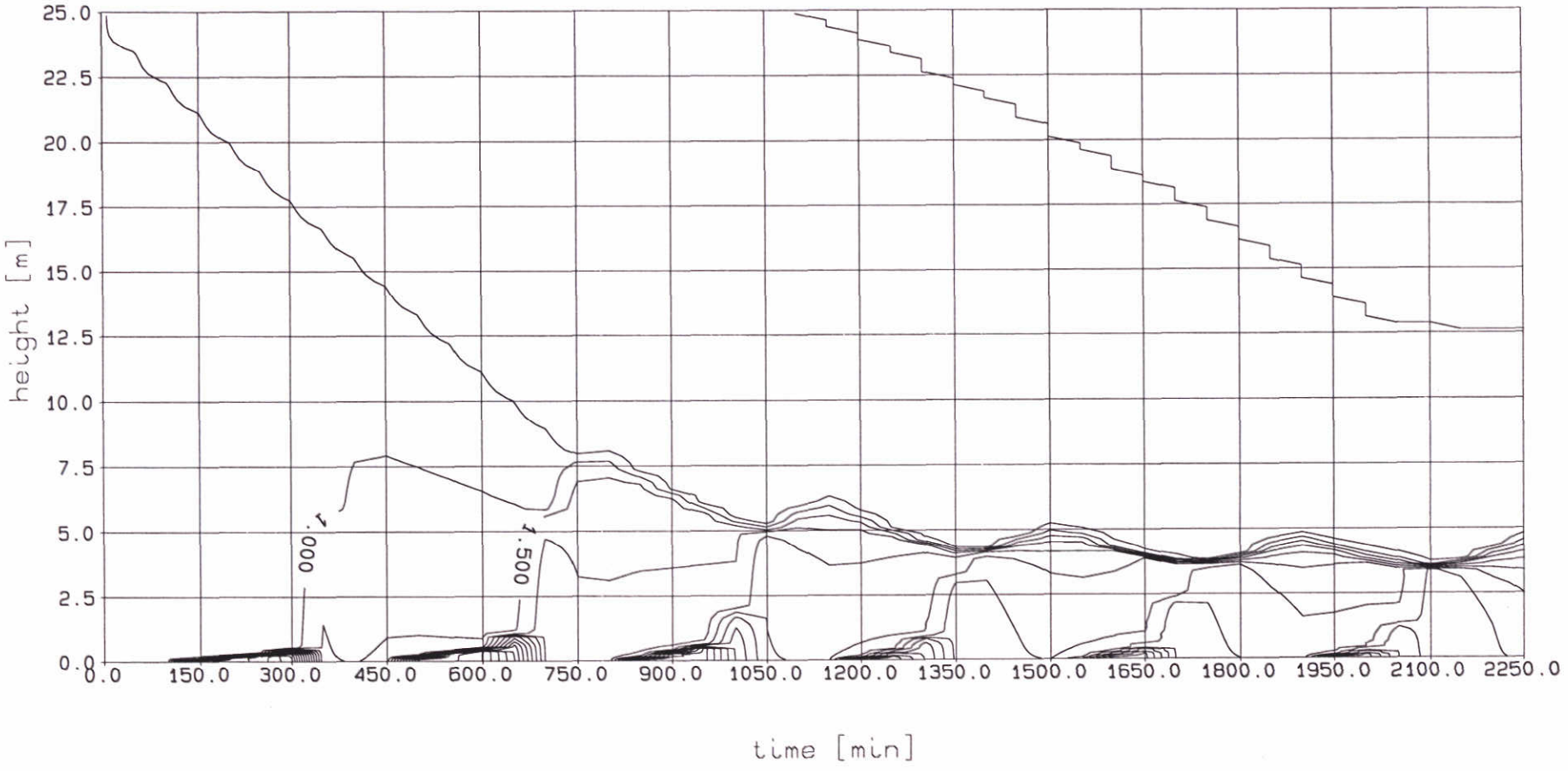

Computed mass concentrations [g/l] - {run Q05} C_0 = 0.6 g/l, W_s = 0.5 mm/s, U = 0.5/0.8 m/s h = 25 m, $H_{1/3}$ = 3 m, initial salinity profile	tidal run	20-01-1998
	prognostic simulations	
DELFT HYDRAULICS - MARINE & COASTAL MANAGEMENT	Proj: Z2263	Fig.6.24a

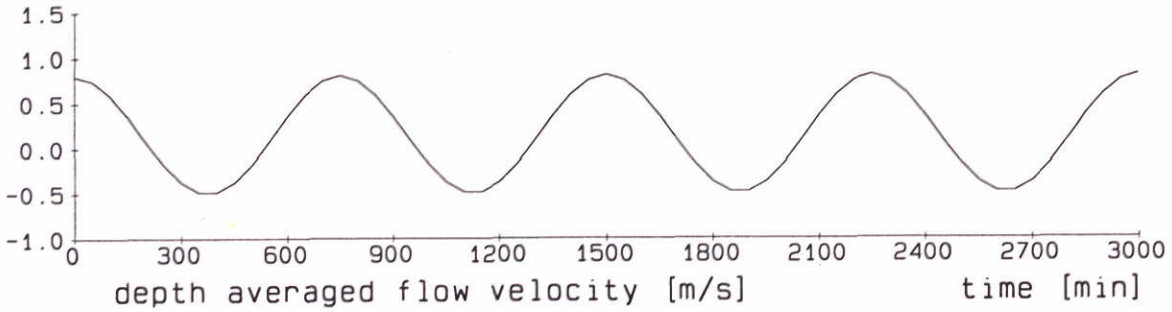

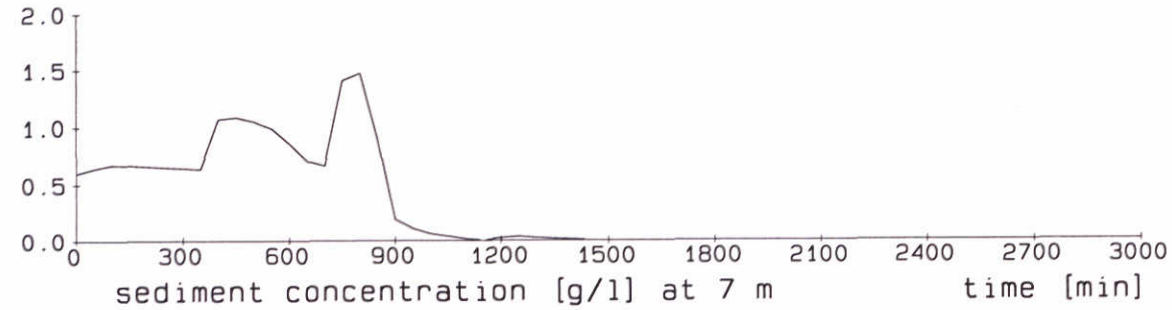

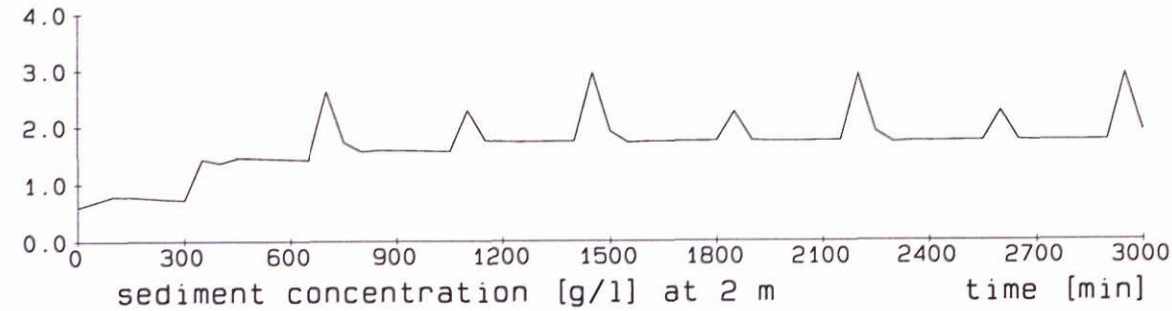

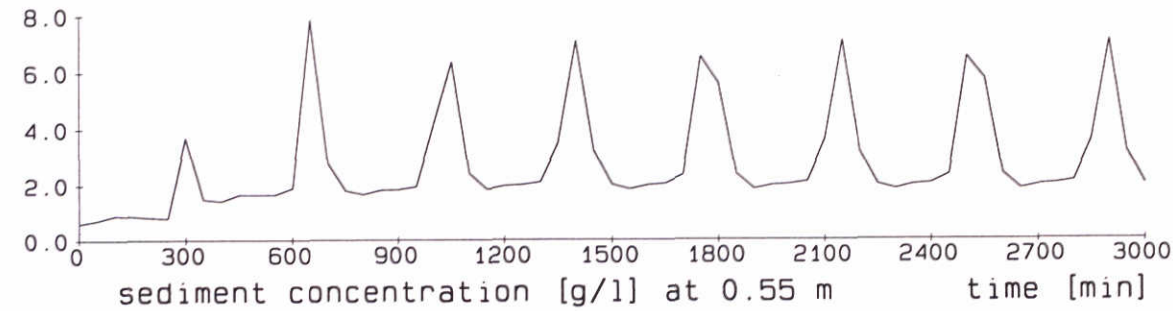

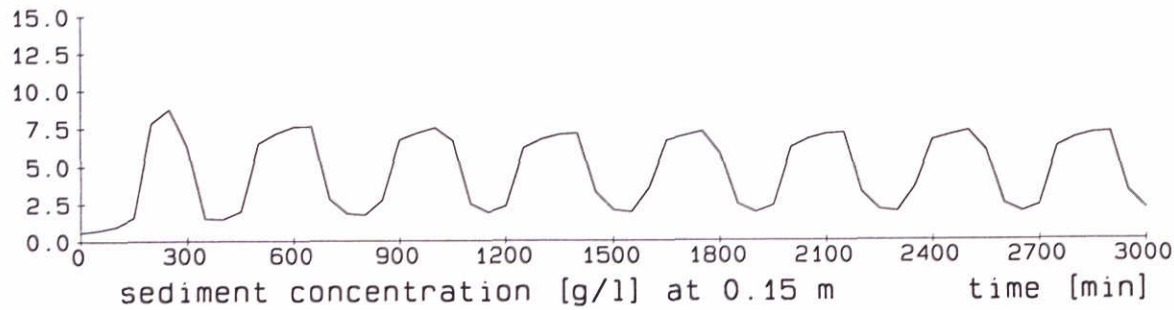

Simulations

Computed mass concentrations [g/l] - {run Q05} C_0 = 0.5 g/l, W_s = 0.5 mm/s, U = 0.5/0.8 m/s h = 25 m, $H_{1/3}$ = 3 m, initial salinity profile	tidal run	20-01-1998
	prognostic simulations	
DELFT HYDRAULICS - MARINE & COASTAL MANAGEMENT	Proj: Z2263	Fig.6.24b

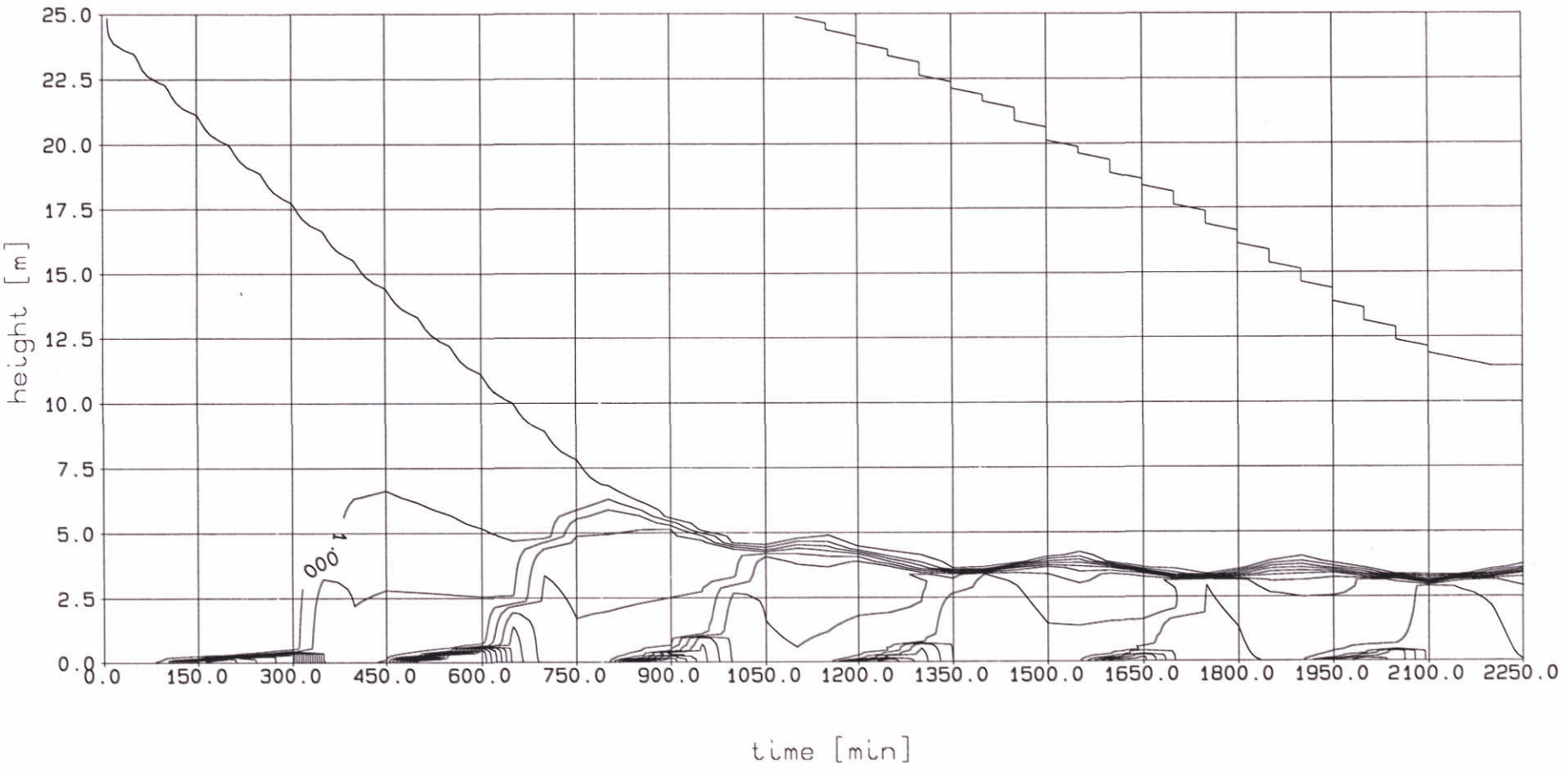

Computed mass concentrations [g/l] - {run Q06} C_0 = 0.6 g/l, W_s = 0.5 mm/s, U = 0.5/0.8 m/s h = 25 m, no waves, initial salinity profile	tidal run	20-01-1998
	prognostic simulations	
DELFT HYDRAULICS - MARINE & COASTAL MANAGEMENT	Proj: Z2263	Fig.6.25a

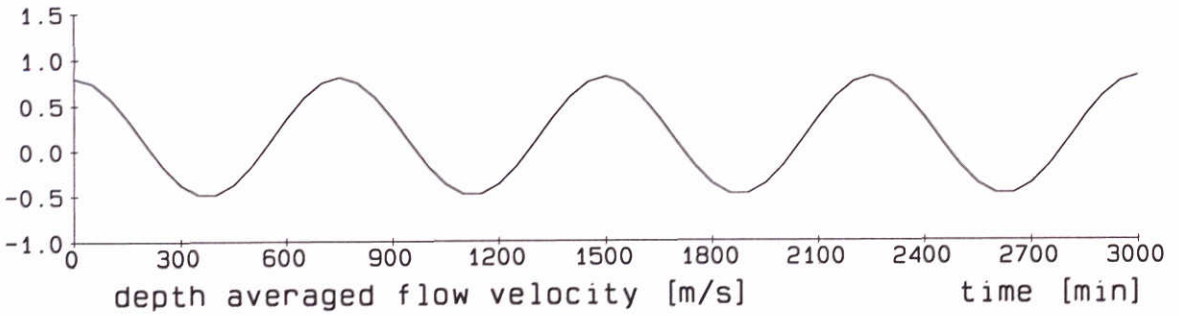

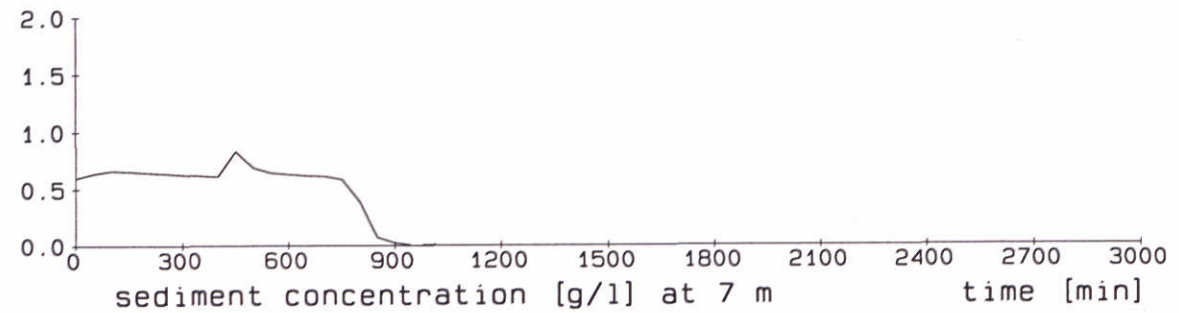

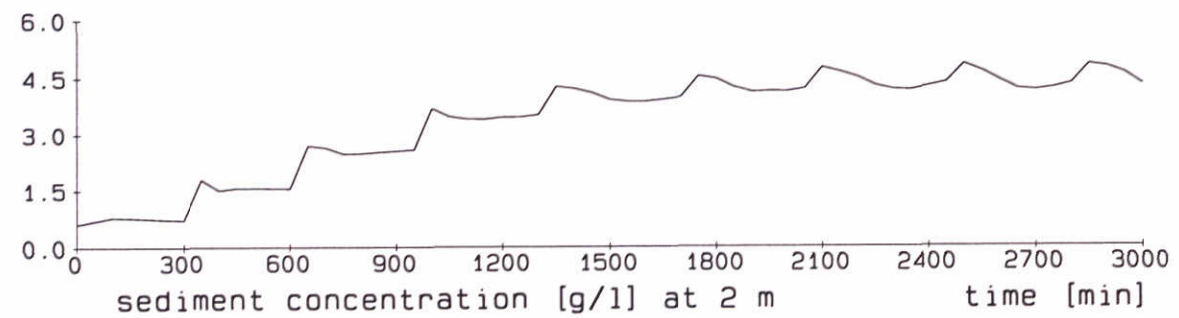

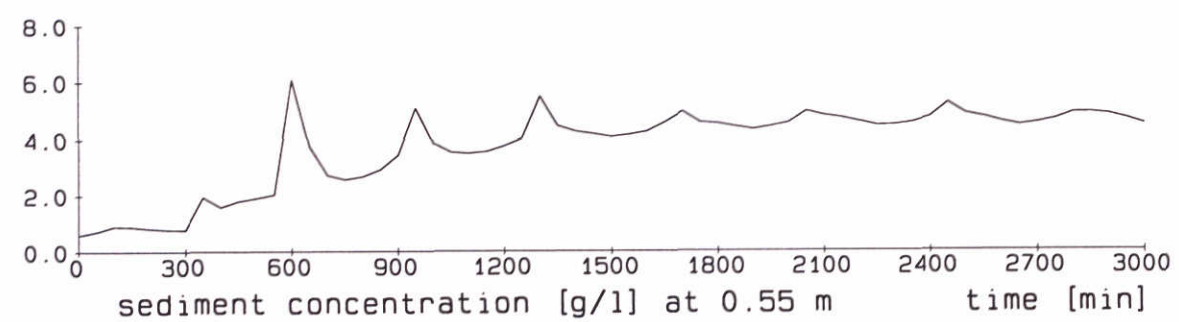

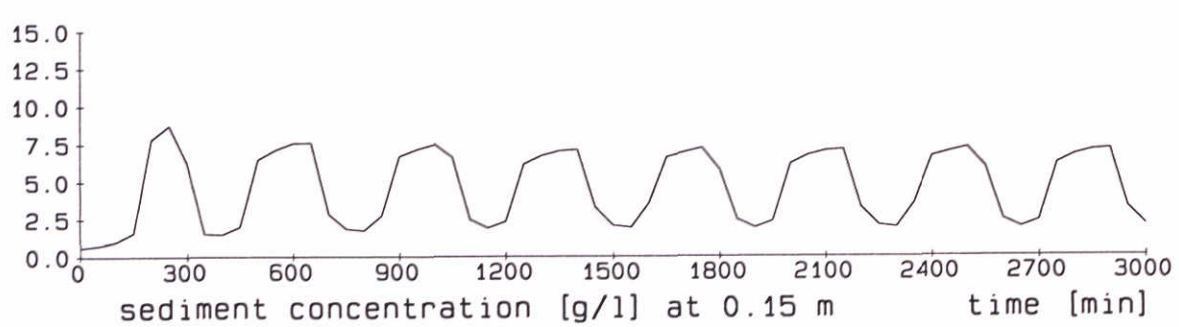

Simulations

Computed mass concentrations [g/l] - {run Q06} C_0 = 0.5 g/l, W_s = 0.5 mm/s, U = 0.5/0.8 m/s h = 25 m, no waves, initial salinity profile	tidal run	20-01-1998
	prognostic simulations	
DELFT HYDRAULICS - MARINE & COASTAL MANAGEMENT	Proj: Z2263	Fig.6.25b

Appendix A:

Detailed derivation of dimensionless numbers

Appendix A: Detailed derivation of dimensionless numbers

A.1 Dimensional analysis - Π-theorem

As discussed in Section 4.1, seven parameters can be identified that govern the vertical suspended sediment concentration distribution, if horizontal advection effects are negligible. By means of applying the classical Π-theorem, these parameters are ordered to obtain four dimensionless parameters, using the three dimensional units M [kg], L [m] and T [s].

The primary parameter matrix is given in Table A.1:

	k_1 C_s	k_2 h	k_3 u_*	k_4 T/4	k_5 W_s	k_6 ρ	k_7 g
M [kg]	1					1	
L [m]	-3	1	1		1	-3	1
T [s]			-1	1	-1		-2

Table A.1: Parameter dimensions.

This matrix yields the following three equations for the seven dimension-parameters k_1 through k_7:

$$k_5 = -2k_2 - k_3 - k_4$$
$$k_6 = -k_1 \qquad (A.1)$$
$$k_7 = k_2 + k_4$$

It is convenient to establish the four dimensionless parameters Π_1 through Π_4 from equ (A.1) with the use of a second table:

	k_1 C_s	k_2 h	k_3 u_*	k_4 T	k_5 W_s	k_6 ρ	k_7 g	
Π_1	1	0	0	0	0	-1	0	$\Pi_1 = C_s/\rho$
Π_2	0	1	0	0	-2	0	1	$\Pi_2 = hg/W_s^2$
Π_3	0	0	1	0	-1	0	0	$\Pi_3 = u_*/W_s$
Π_4	0	0	0	1	-1	0	1	$\Pi_4 = gT/W_s$

Table A.2: Dimensionless parameters.

Π_1 is the dimensionless form of the saturation concentration. Combination of the other dimension-

less parameters through $\Pi_5 = \Pi_2/\Pi_4$, $\Pi_6 = \Pi_5/\Pi_3$ and $\Pi_7 = \Pi_1\Pi_2/\Pi_3^2$, yields the following dimensionless physical parameters:

$$\Pi_5 = T_s = \frac{h}{W_s T} \quad = \text{relative time scale for settling}$$

$$\Pi_6 = T_m = \frac{h}{u_* T} \quad = \text{relative time scale for vertical mixing}$$

$$\Pi_7 = Ri_* = \frac{hgC_s}{\rho u_*^2} \quad = \text{bulk Richardson number (buoyancy effects).}$$

Hence, the following functional relationship can be formulated for tidal flow conditions:

$$\frac{C_s}{\rho} = f(T_s, T_m, Ri_*) \tag{A.2}$$

Note that for steady flow conditions, the tidal period is no longer a parameter in Table A.1, and the number of dimensionless parameters reduces by one. In fact it can be shown that Π_5 and Π_6 merge to become $\Pi_8 = W_s/u_*$, yielding the following functional relationship for steady flow conditions:

$$\frac{C_s}{\rho} = f\left(\frac{W_s}{u_*}, Ri_*\right) \tag{A.3}$$

This relation was found earlier by Galland et al. (1997).

On the basis of this relationship, the flow conditions can be classified with respect to the vertical profile of the suspended sediment concentration.

A.2 Classification flow conditions

For tidal conditions, the three dimensionless parameters T_s, T_m and Ri_* yield 27 combinations. The case $T_s << 1$ corresponds to (quasi-)steady flow conditions.
Note that for Ri-values beyond a critical value, turbulence will collapse, and the flow will not be able to keep the sediment in suspension. As mentioned before, the depth-averaged concentration just prior to this collapse is called the saturation concentration C_s.

The 27 combinations are given in Table A.3, and a classification scheme for tidal flow conditions with respect to the suspended sediment concentration profile is proposed. If mixing is rapid ($T_m \leq 1$) we anticipate that the collapse of the concentration profile will be slow, and that a range of C_s-values will be found where the concentration profile is close to collapse.

Note that the combination $T_m << 1$ and $Ri_* >> Ri_{*,cr}$ is not likely to occur: if for stratified conditions Ri_* exceeds its critical value, vertical mixing will become very small, hence $T_m >> 1$.

settling	mixing	buoyancy	classification
$T_s << 1$	$T_m << 1$	$Ri_* < Ri_{*,cr}$	well mixed, stagnant water conditions
		$Ri_* \approx Ri_{*,cr}$	saturated if $T_s \approx T_m$
		$Ri_* > Ri_{*,cr}$	not likely
	$T_m \approx 1$	$Ri_* < Ri_{*,cr}$	well mixed
		$Ri_* \approx Ri_{*,cr}$	saturated; rapid collapse
		$Ri_* > Ri_{*,cr}$	fluid mud formation
	$T_m >> 1$	$Ri_* < Ri_{*,cr}$	poorly mixed
		$Ri_* \approx Ri_{*,cr}$	saturated; rapid collapse
		$Ri_* > Ri_{*,cr}$	fluid mud formation
$T_s \approx 1$	$T_m << 1$	$Ri_* < Ri_{*,cr}$	well mixed
		$Ri_* \approx Ri_{*,cr}$	saturated; slow collapse
		$Ri_* > Ri_{*,cr}$	not likely
	$T_m \approx 1$	$Ri_* < Ri_{*,cr}$	well mixed
		$Ri_* \approx Ri_{*,cr}$	saturated
		$Ri_* > Ri_{*,cr}$	fluid mud formation
	$T_m >> 1$	$Ri_* < Ri_{*,cr}$	poorly mixed
		$Ri_* \approx Ri_{*,cr}$	saturated; rapid collapse
		$Ri_* > Ri_{*,cr}$	fluid mud formation
$T_s >> 1$	$T_m << 1$	$Ri_* < Ri_{*,cr}$	well mixed
		$Ri_* \approx Ri_{*,cr}$	saturated; slow collapse
		$Ri_* > Ri_{*,cr}$	not likely
	$T_m \approx 1$	$Ri_* < Ri_{*,cr}$	well mixed
		$Ri_* \approx Ri_{*,cr}$	saturated; slow collapse
		$Ri_* > Ri_{*,cr}$	fluid mud formation
	$T_m >> 1$	$Ri_* < Ri_{*,cr}$	poorly mixed
		$Ri_* \approx Ri_{*,cr}$	saturated; rapid collapse
		$Ri_* > Ri_{*,cr}$	fluid mud formation

Table A.3: Classification of flow conditions with respect to saturation concentration.

Appendix B:

Bagnolds' transport formula for sand

Appendix B: Bagnolds' transport formula for sand

Multiplying (4.5) with the local flow velocity and integrating over the water depth h yields a transport formula for saturated suspensions of (cohesive) sediment per unit width:

$$T_{max} = \int_0^h u c_s dz = \int_0^h \left(\frac{0.15\rho}{\alpha g \kappa} \frac{u_*^3}{h w_s} u(z) \left(\frac{h}{z} - 1 \right) \right) dz \propto \frac{\tau_b u_* U}{g W_s} \qquad (B.1)$$

T_{max} is the maximal load of sediment that can be carried in suspension by the flow, before turbulence collapses. It is remarkable that this formula is almost identical to the transport formula by Bagnold (1966) for a flat, horizontal bed, but for some coefficients:

$$T_{bag} = \frac{e_s (1 - e_b) \tau_b U^2}{(\rho_s - \rho) g W_s} \qquad (B.2)$$

in which e_b and e_s are efficiencies.

Because of this similarity, it is worth while to summarize the underlying analyses and assumptions by Bagnold. Bagnolds' transport formula is derived for the transport of non-cohesive sediment, i.e. sand. He claims that it is only possible to arrive at a sound transport formula from dynamic considerations, and he introduces the physical quantity "stream power" ω per unit flow width:

$$\omega = \frac{\rho g Q S}{B} = \rho g h S U = \tau_b U \qquad (B.3)$$

in which S is the energy slope and B the flow width. Bagnold makes the following assumptions:

1. steady open-channel flow by gravity,
2. unlimited availability of transportable solids,
3. the concentration of transportable solids is sufficiently small that the contribution of the tangential gravity pull on the solids to the applied tractive stress can be neglected,
4. the system considered is defined as statistically steady and as representative for the average conditions for a certain stretch of the channel, and
5. the bed is flat and horizontal.

The last assumption is not Bagnolds', but is included here to facilitate comparison. Next, Bagnold states that the solids can only be suspended by the shearing fluid (e.g. turbulence), and that the power required to keep the particles in suspension is at the cost of the available stream power. Part of this available stream power is used for bed load transport, as a result of which only the fraction $(1-e_b)\omega$ is available for the "suspension work", at the efficiency e_s. The work W_r required to keep the particles in suspension is:

$$W_r = \frac{\rho_s - \rho}{\rho_s} \frac{W_s}{U} g I \qquad (B.4)$$

The efficiency e_b follows from considerations of internal friction due to particle-particle interaction, and amounts to about 0.13 to 0.15, depending on the flow velocity and grain size. The efficiency e_s follows from considerations on the anisotropy of turbulence near the bed, resulting in

an upward mass flux, and e_s is estimated at about 0.016. Note that Bagnold assumes a priori and explicitly non-stratified conditions, whereas (B.1) is developed for stratified conditions. However, stratification effects may have slipped in implicitly in the final formula (B.2) through calibration of the coefficients against experimental data.

The reason, of course, that Bagnolds' transport formula, nor any other formula for the transport of loose, non-cohesive sediment, is not applicable in general to describe the transport of fine grained cohesive sediment, is the availability of transportable cohesive sediment particles, which is **limited** in general. In fact, the time scale for the erosion of a muddy bed is much larger than for a sand bed. For sub-saturated suspensions the flow is able to carry all available sediment, and the transport rate is governed by the supply of sediment.
The second major difference between the transport processes of non-cohesive and cohesive sediment is the variability of the settling velocity of the latter, complicating the actual transport formula considerably.
A third difference is found in the condition of the bed. Deposition of a loose material like sand will generate immediately a hard bed, at which turbulence can be produced. Fine grained cohesive sediment though does form a soft bed, which can gain strength through gelling and consolidation effects. Only after a certain strength has been attained, turbulence production is possible again. However, the process takes time (time scales for thixotropy and consolidation), which is another difference from the behaviour of sand.

WL | delft hydraulics

Rotterdamseweg 185
postbus 177
2600 MH Delft
telefoon 015 285 85 85
telefax 015 285 85 82
e-mail info@wldelft.nl
internet www.wldelft.nl

Rotterdamseweg 185
p.o. box 177
2600 MH Delft
The Netherlands
telephone +31 15 285 85 85
telefax +31 15 285 85 82
e-mail info@wldelft.nl
internet www.wldelft.nl